Studies and Modelling of High Temperature Diffusion Processes in Selected High Performance Structural Coating Systems

Haifa Ghanim Ahmad

A thesis submitted in partial fulfilment
of the requirements of the
University of Northumbria at Newcastle
for the degree of
Doctor of Philosophy

Research undertaken in the
School of Computing, Engineering and Information Sciences

February 2010

ABSTRACT

The central theme of the work undertaken in this thesis involved modelling of diffusion – numerical and microstructural – occurring during high temperature exposure of selected materials and coatings.

The materials and coatings and their high temperature treatments included carburization of steel (nonsteady-state diffusion of iron carburized at 950^{o} C after 7.1 hours), a two component Cu-Ni diffusion couple subjected to diffusion anneal at 1054^{o}C for 300 hours, a three component Pt-Ni-Al solid alloy subjected to oxidation and diffusion anneal, Multicomponent Ni -aluminide and Pt-aluminide coatings on MAR M002 subjected to 150 hours of diffusion treatment at temperature 1273K, a Ir and Ir/Pt Low-activity aluminide / MAR M002 system at 1100^{o}C after 100 hours, aluminise coating on low alloy steels at 650^{o}C, Innovatial coatings- Ti45Al8Nb coated with Al_2Au subjected to air oxidation at 750^{o}C for 1000 hours, and Ti45Al8Nb coated with TiAlCrY subjected to air oxidation at 750^{o}C for 500 hours.

Such coatings are being increasingly used to protect materials against high temperature (600-1000^{o}C) degradation by oxidation. The demands for using such coatings have arisen because of the need to increase the efficiency by increasing the operation temperature in many areas of technological applications such as power operation, aero engines, and energy conversion systems and in processing industries. However the one of the major obstacles to use these coatings to prevent high temperature oxidation of materials is the degradation of the coatings due to the coating/substrate interdiffusion. Interdiffusion of critical elements from the coating to the substrate will deplete the protective scale forming elements in the coating.

Equally the diffusion of rogue elements from the substrate to the coating will undermine the coatings efficacy by initiating precipitation of the critical elements and by promoting stress generation within the coatings.

Such considerations clearly show the need for modelling of interdiffusion in order to predict the changes in composition and to calculate the coating life time.

Numerical modelling (main part of this thesis) was done by RK method with GAs method applied to optimise diffusion coefficients allowing prediction of composition profiles following coating substrate interdiffusion during diffusion anneals, oxidation treatments and coating fabrications. Microstructural modelling was constructed from the information on changes in morphologies, composition profiles and phase contents. Microstructural modelling aided the interpretation of the results produced by numerical modelling.

Finally it is important to note that in general the model prediction improved when all the terms in the diffusion matrix and their composition dependence were taken into account in calculation.

CONTENTS

DEDICATION

To the memory of my father Mr. Ghanim Ahmad Altaee.

I would also like to dedicate this to my darling mother Mrs Suriaa Mohammad Husain.

ACKNOWLEDGEMENTS

I would like to thank Dr. Ken Leung and Prof. Santu Datta, my supervisors for their continued guidance, technical advice and encouragement throughout this thesis.

I would also like to take the opportunity to thank the staff and research students for their support throughout my PhD studies.

In particular I would like to express my sincere thanks to my close friend Mrs. Ihab Salman and her family, and Dr. Lynne Henry for proof reading this thesis and her commitment to help and advise me throughout the process of this thesis.

I specially thank my family, specially my husband Dr. Belal Aljibouri for his constant support, patience, understanding and encouragement throughout the duration of this work, and my children: Aya, Abdullah, Abdurahman, Tasneem and Omar Al-Farooq.

DECLARATION

I declare that the work contained in this thesis is entirely mine and that no portion has been submitted in support of an application for another degree or qualification in this, or any other university, or institute of learning, or industrial organisation.

Ahmad, Haifa Ghanim

February 2010

CHAPTER ONE

Introduction

CHAPTER ONE

1.1. Introduction

Diffusion occurs in most areas of the physical and chemical world. Most processes in this universe involve diffusion.

A simple example of diffusion is observed when or droplet of ink is placed without stirring at the bottom of a container filled with water, the colour will slowly spread through the container. At the beginning, it will be concentrated near the bottom. After certain time it will spread and the solution will be coloured homogeneously. The process responsible for the movement of the coloured material is diffusion. Here diffusion is caused by the Brownian motion of atoms or molecules leading to the mixing process. In gases, diffusion progresses at a rate of centimetres per second; in liquids, its rate is typically fractions of millimetres per second; in solids, diffusion is a fairly slow process and the rate of diffusion decreases strongly with reducing the temperature: near the melting temperature of a metal a typical rate is about one micrometer per second; near half of the melting temperature it is only of the order of nanometres per second.

In solids diffusion occurs by vacancy, interstitial and substitutional exchanges.

1.2. Vacancy Diffusion

This mechanism involves the exchange of an atom from the normal lattice location to an adjacent vacant lattice site or a vacancy, as represented schematically in Figure 1.1.

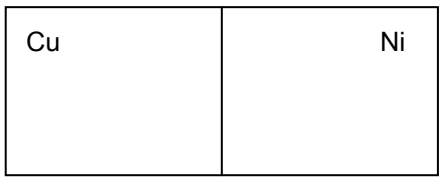

(a)

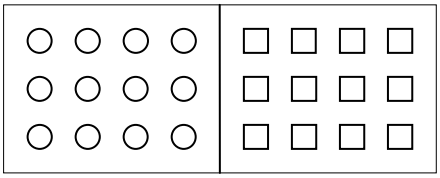

(b)

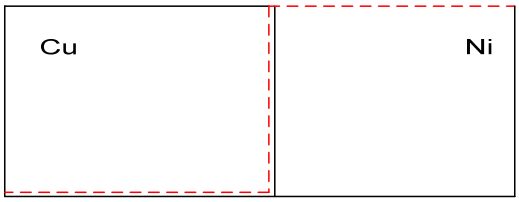

(c)

Figure 1.1 a) Shows a copper-nickel diffusion couple before it is subjected to the high-temperature heat treatment, b) Shows a schematic representation of Cu (circles) and Ni (squares) atoms sites inside the diffusion couple, c) Explains the copper and nickel concentrations as a function of position across the couple (step function) at time t=0

Since diffusing atoms and vacancies exchange positions, the diffusion of atoms in one direction corresponds to the motion of vacancies in the opposite direction. This mechanism can be explained in the following Figure:

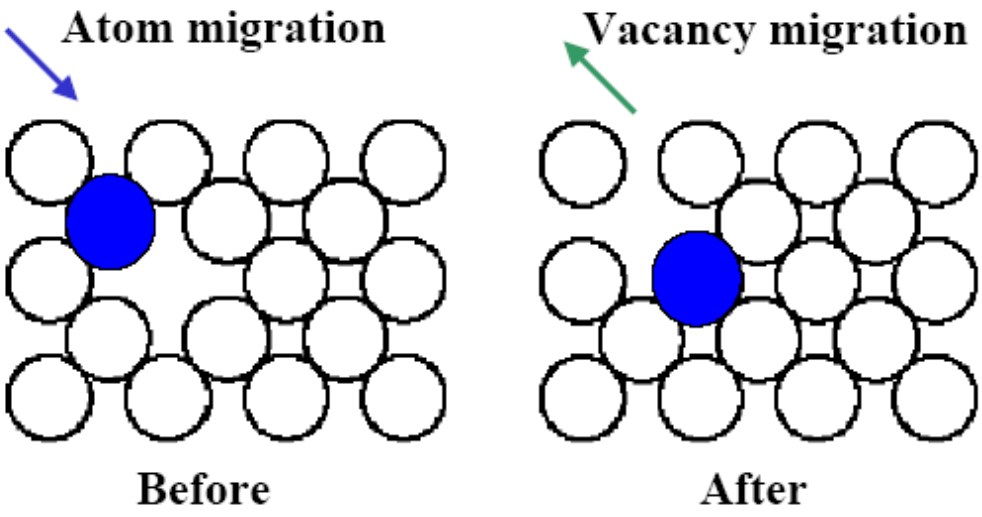

Figure 1.2 Vacancy diffusion [1]

1.3. Interstitial Diffusion

The other type of diffusion involves atoms that migrate from an interstitial position to a neighbouring one that is vacant. This mechanism is found for interdiffusion of impurities such as hydrogen, carbon, nitrogen, and oxygen, which have atoms that are small enough to fit into the interstitial positions as described in the following Figure:

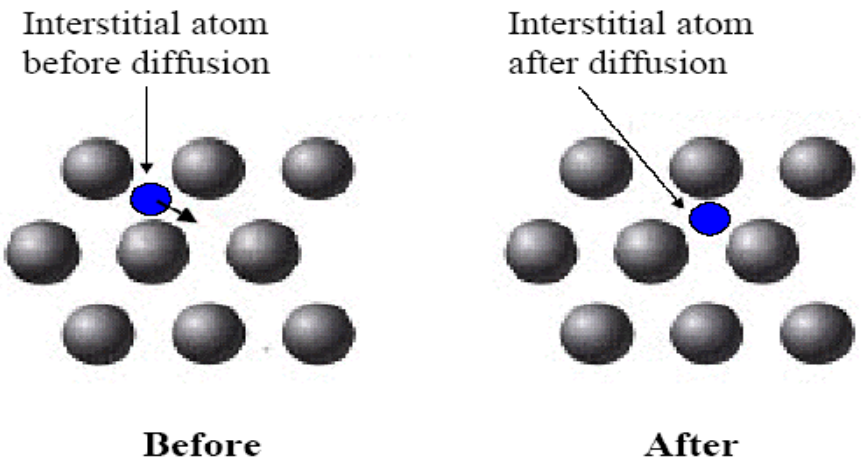

Figure 1.3 Interstitial diffusion [1]

1.4. Substitutional Diffusion

Substitutional diffusion applies to substitutional impurities. Atoms exchange with vacancies and the rate depends on the number of vacancies and on the activation energy to exchange

The following Figure shows this mechanism:

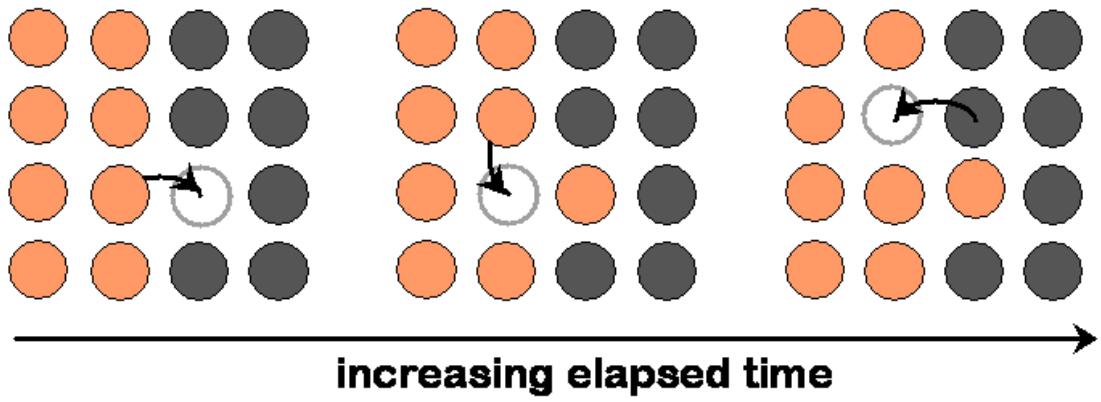

Figure 1.4 Substitutional diffusion [1]

Therefore diffusion involves mass transport of materials from one part of the system to another part as a result of random molecular motion. Many reactions and processes that are significant in the treatment of materials rely on the transfer of mass either within a solid or from a liquid, a gas, or another solid phase. Diffusion is the movement of particles from an area of high concentration to an area of low concentration in a given volume.

This thesis is concerned with studies of diffusion in solids:

- Diffusion simply to take place between two points in a stepwise manner (transport of material by moving atoms);
- Two conditions need to be satisfied:
    1) The presence of an empty adjacent site;

2) The atom has a sufficient energy (heat and concentration gradient) in order to break the bonds with its neighbour atoms to produce some lattice distortion during the movement.

Consequently mechanical properties are the primary attention of the physical metallurgist. Most chemical, physical and mechanical changes in materials take place by diffusion. So diffusion plays a critical role in

- alloying metals, bronze, silver, and gold;
- strengthening and heat treatment processes, (hardening the surfaces of steel);
- high temperature mechanical behaviour;
- phase transformations, (mass transport during FCC to BCC);
- environment degradation, (corrosion, etc.).

1.5. Self Diffusion

Self-diffusion coefficient is the diffusion coefficient of species when the chemical potential gradient equals zero, i.e. in elemental solid, atoms also migrate. Diffusion is a function of time temperature and concentration gradient.

1.6. Interdiffusion

In the alloy the atoms tend to migrate from regions of large concentration as shown below:

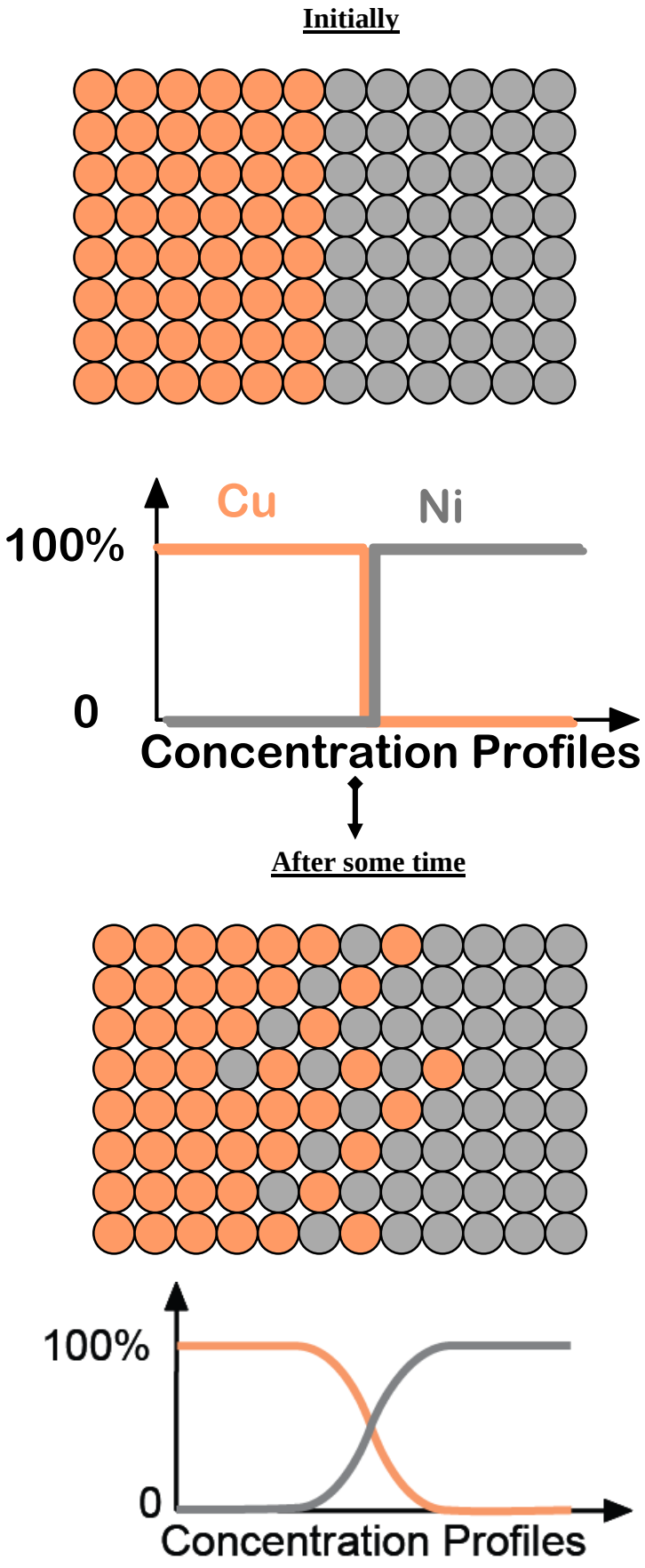

Figure 1.5 Interdiffusion phenomena

At a specific time not all the atoms vibrate at the same frequency and amplitude, or have the same energy. For a given temperature there will be a distribution of energies for the constituent atoms about an average energy. This average energy will increase with temperature.

The main theme of this thesis is to model quantitatively diffusion processes in solids at elevated temperature. Progress in the area of materials science has been hampered due to the lack of application of numerical modelling. In recent years computational materials science (CMC) has gained much attention. The work undertaken in this research falls under this CMC.

1.7. Aims and Objectives

This work addresses more specifically diffusion studies and modelling in various coating systems, in both closed (diffusion annealing) and open systems (oxidation).
The main objectives of this work are to:

- study diffusion in selected materials and coating systems;
- understand the processes of diffusion (in the selected system) in terms their microstructural description / modelling;
- provide explanation of scale formation through consideration of kinetic (diffusion) and thermodynamic factors(free energy);
- the key objective has been to model quantitatively the diffusion processes involved using numerical technique.

In the area of diffusion modelling it is important to note that most of the work in the area of diffusion has so far been concerned with single or two component systems. However in real situations most materials and coating systems are multicomponent. Until recently [1] not many studies of diffusion have been undertaken in

multicomponent systems. Until now, even in multicomponent systems diffusion equations have been solved using Darken's method. There are various limitations of Darken's method;

- Darken's method does not allow the consideration of the cross terms in a diffusion matrix;
- It also can not take into account the concentration dependence of *D*;
- Darken method uses only the diagonal terms in the diffusion matrix.

The numerical method used here overcomes these limitations.

The systems studied included: 1) Carburization of iron (at 950^{o}C). 2) Cu-Ni alloys. 3) Three component $Pt-Ni$- aluminide system.4) Multicomponent $Pt-Ni$- aluminide coatings on MAR M002. 5) Studies of Ir low-activity aluminide / MAR M002 system: assessment of the oxidation resistance and microstructural of diffusion process involved at 1100^{o}C. 6) Formation of aluminised coatings on low alloy steels at 650^{o}C. 7) Four component $TiAlCrY/TiAl$ system (subjected to oxidation at 850^{o}C), $Al_2Au/TiAl$ (subjected to oxidation at 750^{o}C).

This thesis has been structured in nine chapters. Chapter 1 gives the introduction to the thesis background knowledge on diffusion behaviour and reported diffusion behaviour in metallic alloys is presented in chapter 2. Design, development, preparation and microstructure analysis of the coating systems considered is shown in chapter 3. Mathematics of diffusion, relevant laws to Runge-Kutta method are given in chapter 4. In chapter 5 outlines of Genetic Algorithms method (GAs), fminbnd, and Simplex search method are presented. The results, (the diffusion coefficients and the numerical concentration profiles), for all the components contained in the systems are included in chapter 6. General discussion, which outlines the advantage of using GAs method, including all the diffusion matrix terms, and concentration dependent diffusion

coefficients are integrated in chapter 7. Chapter 8 includes conclusions from the present work and future areas of research based on the outcomes derived from this thesis.

CHAPTER TWO

Literature Review

CHAPTER TWO

The literature Review is presented in two sections:

In the first section a review of some of the background information on diffusion in solids is discussed. The contents of this section illustrate the development of theories of diffusion. The second section deals with some reported work on diffusion problems and analyses to the present work.

2.1. Background knowledge on Diffusion behaviour

2.2. History and Bibliography of Diffusion

The science of diffusion in solids had its beginnings in the 19th century. Diffusion science is based on several points. The most important ones are [1]:

- The continuum theory of diffusion originated from work of the German scientist Adolf Fick, who was inspired by elegant experiments on diffusion in gases and of salt in water carried out by Thomas Graham in Scotland;
- Brownian motion was detected by the Scotish botanist Robert Brown. This phenomenon was interpreted many decades later by Albert Einstein. His theory provided the statistical keystone of diffusion and bridged the gap between mechanics and thermodynamics.

Diffusion experimental studies were performed the first time by Thomas Graham (1805–1869). In one of his articles he clearly stated what we now call Graham's law: 'The diffusion or spontaneous intermixture of two gases is effected by an interchange in position of indefinitely tiny volumes of the gases, where volumes are not of equal magnitude, in the case of each gas, which is inversely proportional to the square root of the density of that gas.' The crucial point about Graham's work on diffusion in gases

was that it could be understood by the kinetic theory of gases developed by Maxwell and Clausius shortly after the middle of the 19th century. Graham's law can be attributed to the equipartition of kinetic energies between molecules with different molecular masses. In this way diffusion was connected with the thermal motion of atoms or molecules, and the idea of the mean free path entered into science. Graham also extended his studies to diffusion of salts in liquids [2] and to the uptake of hydrogen in metals. He showed that diffusion in liquids was at least several thousand times slower than in gases. The next major advance in the field of diffusion came from the work done by Adolf Eugen Fick (1829–1901).

2.3. Introduction to Interdiffusion Theory

In an ionic lattice, such as that of Ag_2S or FeO, the migration velocity of the anion may differ clearly from that of the cation, the cation being more mobile [2]. Also investigation of solid solutions of various salts shows that there is usually considerable difference in the mobility of the different cations. Measurements of the mobility of various metals in liquid mercury show that various metals move at different rates relative to the mercury. Therefore in any single phase solution, the atoms of different elements react in different ways. In particular the force arising from a particular concentration gradient in a binary alloy would cause the atoms of one component to move with a drift velocity different from that of the atoms of the other component.

2.4. Continuum Theory of Diffusion

The equations leading diffusion processes are Fick's laws. These laws correspond to a continuum description and are purely phenomenological. The original work of Adolf

Fick was completed in 1855 [3] and explained a salt-water system undergoing diffusion. Fick set up the idea of the diffusion coefficient and suggested a linear response between the concentration gradient and the mixing of salt and water. Previously, in 1807 Josef Fourier had developed a similar relation between the flow of heat and the temperature gradient [4]. Fick's laws describe the diffusive transport of matter as an experimental fact without stating that it derives from basic concepts. It is, however, indicative of the power of Fick's continuum description that all subsequent developments have in no way affected the validity of his approach. Diffusion in solids is based on random walk theory and on the atomic mechanisms of diffusion.

2.5. Interdiffusion

In multi-component solid solutions (single phase alloys) the atoms of a particular element can migrate from one position to another according to the concentration gradients of the elements. Diffusing atoms have different chemical environments and therefore have different diffusion coefficients. The composition-dependent diffusivity is usually denoted as the interdiffusion coefficient. Therefore the phenomenon of interdiffusion between dissimilar materials in contact with each other is of interest to materials scientists. The symbol $\tilde{D}$ indicates that the diffusion coefficient is concentration-dependent (interdiffusion or chemical diffusion coefficient). Fick's second law applies when D depends on concentration;

$$\frac{\partial C}{\partial t} = \nabla \bullet (D \nabla C) \qquad (2.1)$$

Then

$$\frac{\partial C}{\partial t} = \frac{\partial}{\partial x}\left[\tilde{D}(C)\frac{\partial C}{\partial x}\right] = \tilde{D}(C)\frac{\partial^2 C}{\partial x^2} \tag{2.2}$$

The symbol $\tilde{D}$ indicates that the diffusion coefficient is concentration-dependent (interdiffusion or chemical diffusion coefficient).

2.6. Boltzmann Transformation

In 1894 Ludwig Boltzmann [3] showed that the nonlinear partial differential equation (equation 2.2) can be transformed to a nonlinear but ordinary differential equation if $\tilde{D}$ is a function of $C(x)$ alone. He introduced the variable

$$\eta \equiv \frac{x - x_M}{2\sqrt{t}} \tag{2.3}$$

which is a mixture of the space and time variables x and t, respectively. x_M corresponds to a special position plane-the so called Matano plane – to be defined below. Applying chain-rule differentiation to equation (2.2), we obtain the following identity:

$$\frac{\partial}{\partial x} \equiv \frac{d}{d\eta}\cdot\frac{\partial \eta}{\partial x} = \frac{1}{2\sqrt{t}}\cdot\frac{d}{d\eta} \tag{2.4}$$

The operative on the left-hand side of equation 2.2 is:

$$\frac{\partial}{\partial t} \equiv \frac{d}{d\eta} \cdot \frac{\partial \eta}{\partial t} = -\frac{x - xM}{4t^{3/2}} \cdot \frac{d}{d\eta} = -\frac{\eta}{2t} \cdot \frac{d}{d\eta} \tag{2.5}$$

and on the right-hand side of equation 2.2 in terms of η is:

$$\frac{\partial}{\partial x}(\tilde{D}(C)\frac{\partial C}{\partial x}) = \frac{d}{d\eta} \cdot \frac{\partial \eta}{dx}\left[\frac{\tilde{D(C)}}{2\sqrt{t}} \cdot \frac{dC}{d\eta}\right] \tag{2.6}$$

$$= \frac{1}{4t} \cdot \frac{d}{d\eta}\left[\tilde{D}(C) \cdot \frac{dC}{d\eta}\right] \tag{2.7}$$

By recombining left- and right-hand sides and using the Boltzmann variable, Fick's second law as an ordinary differential equation for $C(\eta)$ becomes as follows:

$$-2\eta \frac{dC}{d\eta} = \frac{d}{d\eta}\left[\tilde{D}(C)\frac{dC}{d\eta}\right] \tag{2.8}$$

Some authors omit the factor 2 in the definition equation 2.3 of η. Then, a factor of 1/2 instead of 2 appears in the equation corresponding to equation 2.8.

2.6.1. Boltzmann-Matano Method

The Boltzmann-transformed description of Fick's second law equation 2.8 is a nonlinear ordinary differential equation. This equation led us to assume the concentration-dependent interdiffusion coefficient from an experimental concentration-

depth profile $C(x)$. The suitable boundary conditions for an interdiffusion experiment have been recommended by the Japanese scientist Matano in 1933 [5]. He measured a binary diffusion couple, consisting of two semi-infinite bars joined at time t = 0. The initial conditions are:

$$C = C_L \text{ for } (x < 0, t = 0)$$
$$C = C_R \text{ for } (x > 0, t = 0) \qquad (2.9)$$

for the duration of a diffusion anneal of time t, a concentration profile $C(x)$ is constructed. This profile can be calculated on a cross section of the diffusion zone, for example by electron microprobe analysis (EMPA). This profile is schematically illustrated in Figure 2.1. Carrying out the integration between C_L and a fixed concentration C^*, we obtain from equation 2.7;

$$-2\int_{C_L}^{C^*} \eta \, dC = D\left(\frac{dC}{d\eta}\right)_{C^*} - D\left(\frac{dC}{d\eta}\right)_{C_L} \qquad (2.10)$$

Matano's geometry guarantees the gradients $\left(\frac{dC}{d\eta}\right)$ will vanish as C^* approaches to C_L (or C_R).

i.e. $\left(\frac{dC}{d\eta}\right) = 0$

So solving equation 2.10 for D

$$D(C^*) = -2\frac{\int_{C_L}^{C^*} \eta \, dC}{(dC/d\eta)_{C=C^*}} \qquad (2.11)$$

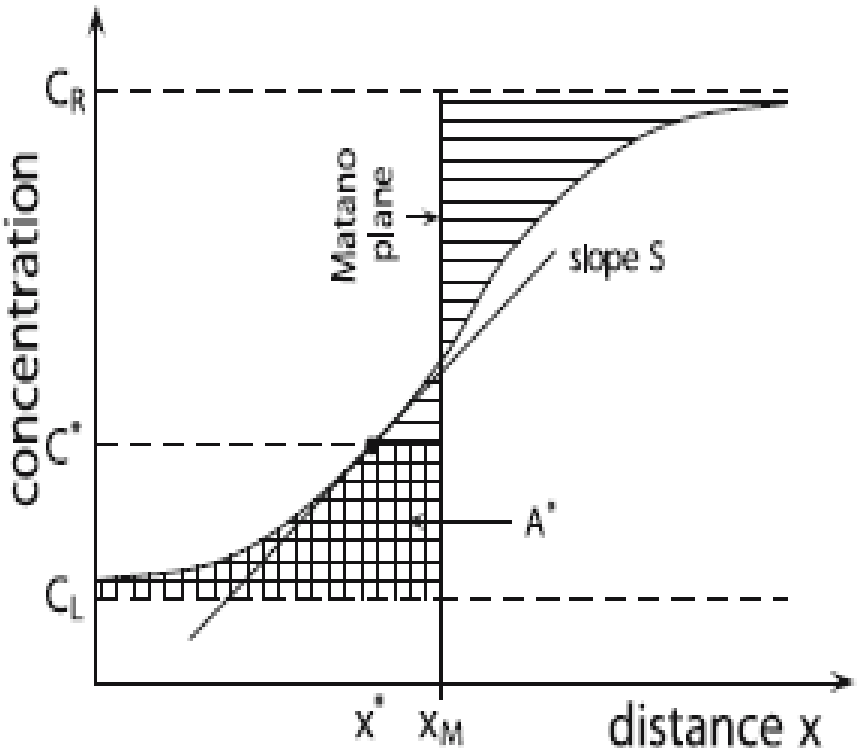

Figure 2.1 Schematic illustration of the Boltzman-Matano method for a binary diffusion couple with starting compositions C_L and C_R

Equation 2.11 has been changed to space and time coordinates using Boltzmann variable (equation 2.3) and thus,

$$\tilde{D}(C^*) = -\frac{1}{2t}\frac{\int_{C_L}^{C^*}(x - x_M)}{(dC/dx)_{C^*}} \tag{2.12}$$

Equation 2.12 is called the Boltzmann-Matano equation. It allows us to conclude $\tilde{D}$ for any C^* from an experimental concentration-distance profile. The position of the Matano plane x_M must be known for the analysis. Carrying out the integration between the limits C_L and C_R, we obtain from equation 2.8;

$$\int_{C_L}^{C_R} \eta \, dC = 0 \tag{2.13}$$

So equation 2.13 can be measured as the definition of the Matano plane. x_M have to be selected in such a way that equation 2.13 is satisfied.

In order to find out the Matano plane, we have to keep in mind that to start the experiment the concentration of the diffusing species was C_L (C_R) on the left-hand (right-hand) side. For example, if $C_L < C_R$ then, at the conclusion of the experiment, the species that is remains (or left) of the diffusing species found on the left-hand side must have arrived by diffusion from the right-hand side. The location of the Matano plane can be determined from the mass conservation condition:

$$\underbrace{\int_{-\infty}^{x_M} [C(x) - C_L]\, dx}_{\text{gain}} = \underbrace{\int_{x_M}^{\infty} [C_R - C(x)]\, dx}_{\text{loss}} \tag{2.14}$$

Using integration by parts, so the integrals in equation 2.14 change to the integrals with C instead of x. From the Matano boundary conditions, equation 2.9, we obtain:

$$(C_L - C_R)x_M + \int_{C_L}^{C_M} x\, dC + \int_{C_M}^{C_R} x\, dC = 0 \tag{2.15}$$

where C_M indicates to the concentration at the Matano plane.

If we have the Matano plane as origin of the x-axis $x_M = 0$, the first term in equation 2.15 disappears. Then equation 2.14 becomes:

$$\int_{C_L}^{C_M} x\, dC + \int_{C_M}^{C_R} x\, dC = 0 \tag{2.16}$$

In summary, the determination of interdiffusion coefficients from an experimental concentration-distance profile via the Boltzmann-Matano method needs the following steps:

- Determine the position of the Matano plane from equation 2.13 and utilize this position as the origin of the *x*-axis;
- Choose C^* and conclude the integral $\int_{C_L}^{C^*} x\, dC$ from the experimental concentration-distance data. The integral indicates the double hatched area A^* in Figure 2.1;
- Conclude the concentration gradient $S = (\frac{dC}{dx})_{C^*}$. S corresponds to the slope of the concentration-distance curve at the position x^*;
- Conclude the interdiffusion coefficient $\tilde{D}$ for $C = C^*$ from the Boltzmann-Metano equation 2.12 as:

$$\tilde{D}(C^*) = -A^*(2tS).$$

The initial interface of a diffusion couple can be labelled by inert diffusion markers (for example ThO_2 particles, thin *Mo* or *W* wires). The plane of the markers in the diffusion couple is represented as the Kirkendall plane. Usually, for $t = 0$ the positions of the Matano plane and of the Kirkendall plane will be different, this is called the Kirkendall effect and is discussed in section 2.4.4.

2.6.2. Intrinsic Diffusion and Kirkendall Effect

So far, the diffusion of a two-component system has described by a single interdiffusion coefficient, which depends on composition. In general, the rate of transfer

of A atoms is greater/smaller than that of B atoms. Thus, there are two diffusion coefficients, D^I_A and $D^I_{B,}$ which are denoted as the intrinsic diffusion coefficients of the components. They are concentration dependent as well. Fick's first law can be shown for the diffusion fluxes relative to a frame fixed in the local crystal lattice (intrinsic diffusion fluxes):

$$J_A = -D^{\mathrm{I}}{}_{\mathrm{A}} \frac{\partial C_A}{\partial x}, \qquad J_B = -D^{\mathrm{I}}{}_{\mathrm{B}} \frac{\partial C_B}{\partial x} \tag{2.17}$$

The inequality of these fluxes leads to a net mass flow accompanying the interdiffusion process, which causes the diffusion couple to shrink on one side and to swell on the other side. This observation is called the Kirkendall effect. It was discovered by Kirkendall and Co-workers in a copper-brass diffusion couple in the 1940s [6]. The Kirkendall shift can be observed by adding in inert inclusions, called markers (for example *Mo* or *W* wires, ThO_2 particles), at the interface where the diffusion couple is initially connected. Figure 2.2 is a schematic representation of a Kirkendall diffusion couple. In the plane of the weld, in the centre of Figure 2.2, a number of fine wires are incorporated in the diffusion couple. The metals separated by the plane of the weld are pure metal A and pure metal B. Then it is necessarily for this couple to be heated close to the melting point of the metals comprising the bar, forward cooling the specimen to room temperature, it is placed in the lathe and thin layers parallel to the weld interface are removed from the bar. Each layer is analyzed chemically and the results plotted to give a curve showing the composition as a function of distance along the bar Figure 2.3;

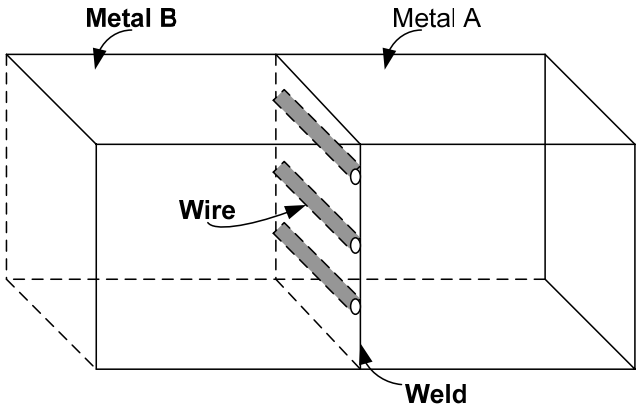

Figure 2.2 Kirkendall diffusion couple

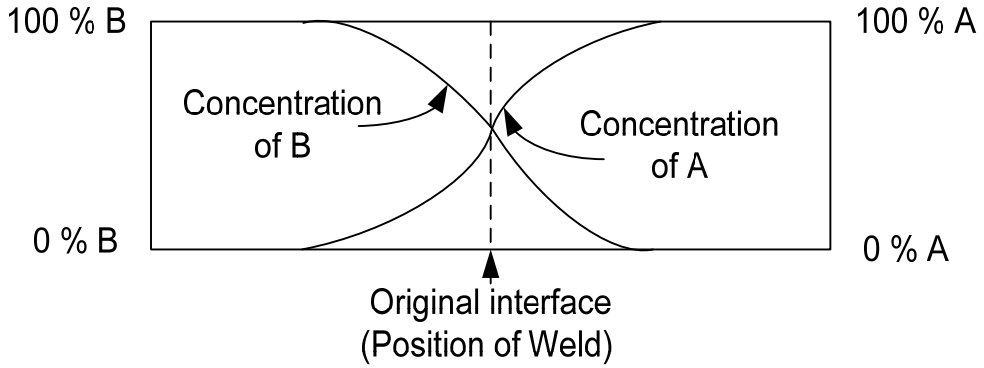

Figure 2.3 Curves showing concentration as a function of distance along a diffusion couple

The motivating result was that the wires moved during the diffusion process. The nature of this movement is shown in Figure 2.4, where the left Figure indicates the diffusion couple before the isothermal treatment, and the right, the same bar after diffusion happened.

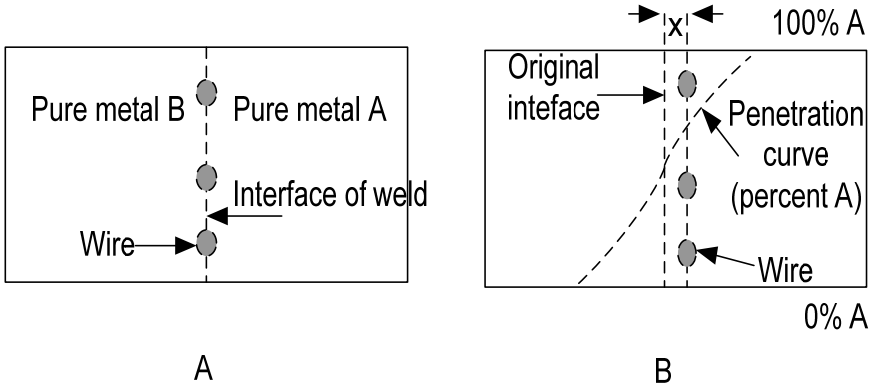

Figure 2.4 Marker movements in a Kirkendall diffusion couple

Figure 2.4 shows that the wires have moved to the right through the distance *x* which is small, is measurable. This distance has been found to vary as the square root of the time during diffusion.

The only way to explain the movement of the wires in Figure 2.4 is for A atoms to diffuse faster than the B atoms, i.e. more A atoms than B atoms must pass through the cross-section (defined by the wire) per unit time. This hypothesis is supported by the experiment of Smigelskes and Kirkendall [6]; the specimen consisted of a long 18-cm brass bar (70 wt % *Cu*-30 wt % *Zn*) on which were placed 12 parallel, molybdenum wires (six on top and six below), as shown in Figure 2.6.

The original Kirkendall experiment is illustrated in Figure 2.5. It showed that Zn atoms diffused faster outwards than *Cu* atoms inward ($D^I_{Zn} > D^I_{Cu}$) causing the inner brass core to shrink. This in turn resulted in the movement of the inert Mo wires. More recently, it has been demonstrated that the Kirkendall effect is a general phenomenon of interdiffusion in substitutional alloys Figure 2.5. Presented below is a schematic illustration of a cross section of a diffusion couple composed of pure Cu and brass (*Cu-Zn*) prepared by Smigelskas and Kirkendall [6] before and after heat treatment. The *Mo* markers placed at the original contact surface moved towards each other. It was

concluded that Zn atoms diffused faster outwards than *Cu* atoms move inwards ($D^I_{Zn} > D^I_{Cu}$).

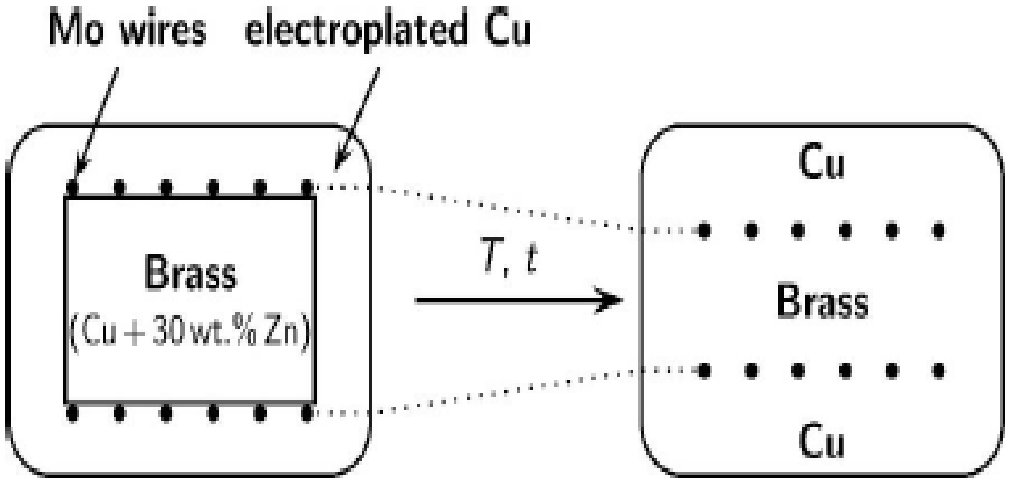

Figure 2.5 Schematic design of a cross section of a diffusion couple composed of pure *Cu* and brass (*Cu-Zn*) prepared by Smigelskas and Kirkendall [6] before and after diffusion treatment

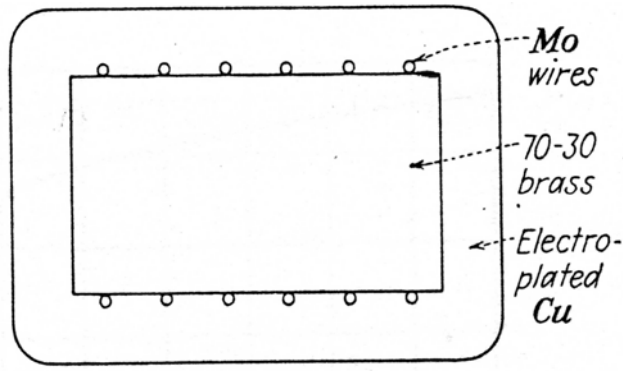

Figure 2.6 Cross section of original bar

The wires were plated with a thick layer of pure *Cu* electrodeposited to a final thickness of about 2.5 mm. This assembly was heated at 400°C for 3 hours to removes the hydrogen. Then a diffusion experiment was carried at 785°C, it was found that

during diffusion, according to the fact that the solute atoms might cross the diffusion interface without an equal number of solvent atoms diffusing across the interface in the opposite direction, the zinc atoms in alpha Brass diffuse across the interface more rapidly in one direction than the copper atoms diffuse across the interface in the opposite direction, this means that the rate of diffusion of *Zn* in α-brass (composition) is much greater than *Cu*, *Zn* diffuses faster than *Cu*, and the interface shifts to compensate for the required lattice motion.

This phenomenon forced the interface to move in the opposite direction of the diffusion of the zinc atoms to provide space for the additional zinc atoms dissolved in the alpha brass. Figure 2.6 is a sketch of the cross section of the bar. Molybdenum wires have been chosen because of their very low solubility in copper and alpha brass. The wires and the interface moved together toward the centre of the bar as the zinc diffused out. The movement of the insoluble molybdenum wires was conclusive evidence that the alpha brass was being forced back as a whole as a result of the diffusing out of the zinc atoms.

The Mo markers were placed at the original contact surface. It was concluded that *Zn* atoms diffused faster outwards than *Cu* atoms moved inwards.

2.6.3. Determination of the Intrinsic Diffusivities

The determination of the intrinsic diffusivities has been demonstrated with the use of the assumed data of Table 2.1. First an expression for the marker velocity v in terms of the marker displacement and the time of diffusion t is required to be derived. Experimentally, it has been determined that the markers move in such a way that the ratio of their displacement squared to the time of diffusion is a constant, thus [7]:

$$\frac{x^2}{t} = k \tag{2.18}$$

where k is a constant. Therefore the marker velocity is,

$$v = \frac{\partial x}{\partial t} = \frac{k}{2x} \tag{2.19}$$

$$\Rightarrow v = \frac{x}{2t} \tag{2.20}$$

In Figure 2.7, an arbitrarily assumed position of the marker interface was shown at a distance $x = 0.0001$ m from the Matano interface. The diffusion time t taken for the data was 50 hours, or 180,000 s. These numbers correspond to a marker velocity;

$$v = \frac{0.0001}{2(180{,}000)} = 2.78 \times 10^{-10}\, m/s \tag{2.21}$$

At the position of the markers, the atom fractions of the A and B atoms were $N_A = 0.65$ and $N_B = 0.35$ respectively, and

$$\tilde{D}_M = 5.5 \times 10^{-12}; \qquad \frac{\partial N_A}{\partial x} = 144 m^{-1}$$

The value of $\tilde{D}_M$ is obtained from Figure 2.8, while $\frac{\partial N_A}{\partial x}$ is the slope of the penetration curve in Figure 2.7 at the position of the markers. The above values can now be substituted into the Darken equation:

$$\tilde{D} = N_B D_A + N_A D_B \tag{2.22}$$

$$v = (D_A - D_B)\frac{\partial N_A}{\partial x} \tag{2.23}$$

$$\text{So} \quad \begin{matrix} 5.5 \times 10^{-12} = 0.35 D_A + 0.65 D_B \\ 2.78 \times 10^{-10} = (D_A - D_B) \cdot 244 \end{matrix} \tag{2.24}$$

The solution of this pair of simultaneous equations 2.24 has a result;

$$D_A = 6.24 \times 10^{-12}$$
$$D_B = 5.10 \times 10^{-12}$$

These values inform that the flux of *A* atoms through the marker interface from right to left is approximately 1.2 times that of the flux of *B* atoms moving from left to right.

Therefore it is possible to calculate the intrinsic diffusivities of a binary diffusion system D_A and D_B.

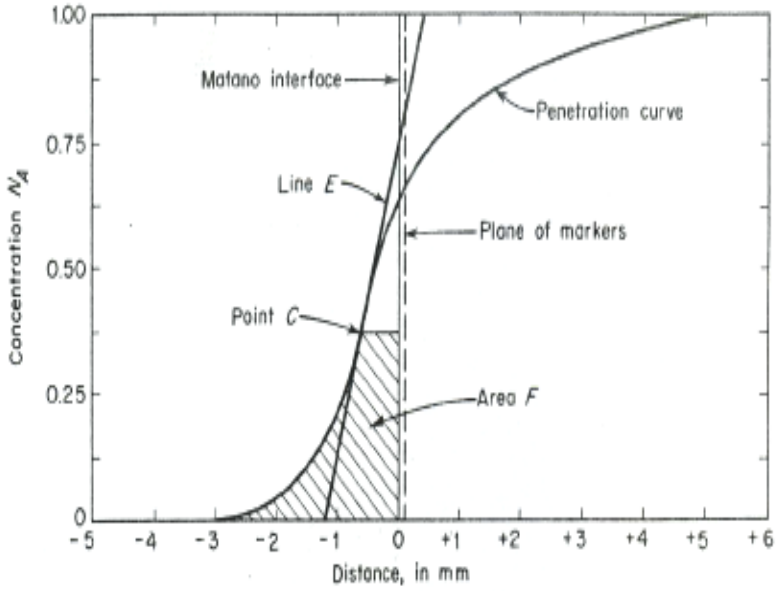

Figure 2.7 Plot of hypothetical diffusion data (Matano method)

Composition Atomic Percent Metal A	Diffusion from the Matano Interface, mm
100	5.08
93.75	3.14
87.5	1.93
81.25	1.03
75	0.51
68.75	0.18
62.5	-0.07
56.25	-0.27
50	-0.39
43.75	-0.52
37.5	-0.62
31.25	-0.72
25	-0.87
18.75	-1.07
12.5	-1.35
6.25	-1.82
0	-2.92

Table 2.1 Assumed diffusion data to illustrate the Matano method

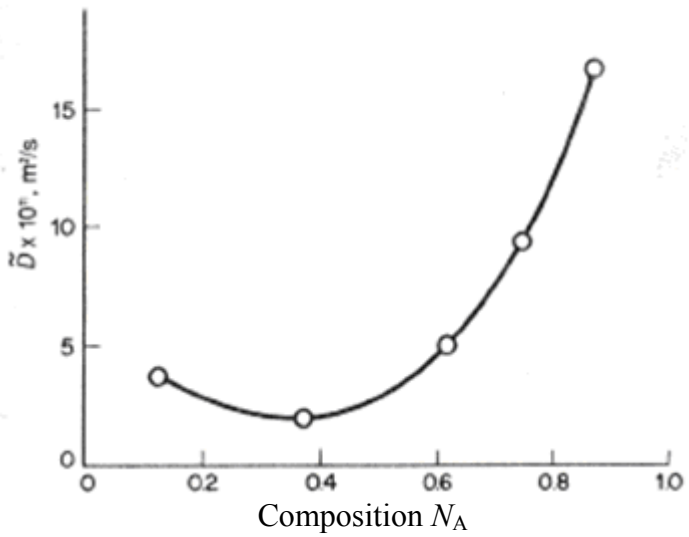

Figure 2.8 Variation of the interdiffusion coefficient $\tilde{D}$ with composition from the data of Table 2.1

2.7. Self-Diffusion and Tracer Diffusion

2.7.1. The Determination of Tracer Diffusion Coefficients

When atoms in pure crystal diffuse without a concentration gradient or other driving force, the process is called self-diffusion. In such cases, the atomic movements are random, with motion in one direction just as likely as another. The appropriate diffusion coefficient is called the self-diffusion coefficient and is given the symbol *D*.

To measure *D* of an atom, it is not achievable to keep track of the movements of one atom in a crystal composed of many identical atoms. However it is possible to measure something which is a very good approximation to the self-diffusion coefficient, if some of the atoms can be uniquely labelled and their movement tracked. In this case the diffusion coefficient that has been calculated is called the tracer diffusion coefficient, written D^*.

2.8. Darken's Equations

The first theoretical description of interdiffusion and the Kirkendall effect was attempted by Darken in 1948 [8]. In a binary alloy the interdiffusion coefficient is usually a composition –dependent quantity. On the other hand, interdiffusion is due to the diffusive motion of A and B atoms, which in general have different intrinsic diffusion coefficients. The Kirkendall velocity v_K can be expressed in terms of the intrinsic fluxes, j_A, j_B and partial molar volumes, $\tilde{V}_A, \tilde{V}_B$ as:

$$v_K = -\left(\tilde{V}_A \, j_A + \tilde{V}_B \, j_B \right) \tag{2.25}$$

and

$$\tilde{V}_A \, dC_A = -\tilde{V}_B \, dC_B$$

$$dC_A = -\left(\tilde{V}_B / \tilde{V}_A \right) dC_B \tag{2.26}$$

So we are able to write for the Kirkendall velocity,

$$v_K = \tilde{V}_B \left(D_B^I - D_A^I \right) \frac{\partial C_B}{\partial x} \tag{2.27}$$

where $\partial C_B / \partial x$ indicates the concentration gradient at the Kirkendall plane. With Darken's approach, the laboratory-fixed interdiffusion flux J (at the Kirkendall plane) can be written as the sum of an intrinsic diffusion flux of one of the components i plus (or minus) a Kirkendall drift term $v_K C_i$:

$$J = -D_i^I \frac{\partial C_i}{\partial x} \pm v_K C_i \quad i = A, B \tag{2.28}$$

Substituting equation 2.26 in equation 2.27 so the general expression for the interdiffusion coefficient is:

$$\tilde{D} = C_B \tilde{V}_B \, D_A^I + C_A \tilde{V}_A \, D_B^I \tag{2.29}$$

Equations 2.27 and 2.29 give a description of isothermal diffusion in a binary substitutional alloy. They also provide an option to conclude the intrinsic diffusivities from measurements of the interdiffusion coefficient and the Kirkendall velocity.

From a fundamental point of view, the postulation that the concentration gradients are the driving forces of diffusion as given by Fick's laws is not correct. Instead, the gradient of the chemical potential μ_i of component i is the real driving force. The flux of component i $(i = A, B)$ in a binary alloy can be written as [9, 10]:

$$j_i = -B_i C_i \frac{\partial \mu_i}{\partial x} \tag{2.30}$$

where B_i denotes the mobility of component i. The chemical potential can be expressed in terms of the thermodynamic activity, a_i using:

$$\mu_i = \mu_i^o + RT \ln a_i \tag{2.31}$$

where μ_i^o is the standard chemical potential and R is the ideal gas constant $(R = 8.3143 J\ mol^{-1}K^{-1})$. The atomic mobility B_i is connected to the tracer diffusion coefficient D_i^* of component i using the Nernst-Einstein relation (Appendix A):

$$D_i^* = B_i RT \tag{2.32}$$

Substituting equations 2.32 and 2.30 in the following equation as:

$$\begin{aligned} j_A &= -D_A^I \frac{\partial C_A}{\partial x} \\ j_B &= -D_B^I \frac{\partial C_B}{\partial x} \end{aligned} \tag{2.33}$$

And knowing that

$$C_A = N_A / V_m$$

and

$$dN_A = \left(V_m^2 / \tilde{V}_A \right) dC_A$$

So the relation between the intrinsic and tracer diffusion coefficients is as follows:

$$\begin{aligned} D_A^I &= D_A^* \frac{V_m}{\tilde{V}_B} \frac{\partial \ln a_A}{\partial \ln N_A} \\ D_B^I &= D_B^* \frac{V_m}{\tilde{V}_A} \frac{\partial \ln a_B}{\partial \ln N_B} \end{aligned} \tag{2.34}$$

The quantity $\phi \equiv \partial \ln a_i / \partial \ln N_i$ is indicated as the thermodynamic factor. The thermodynamics of binary systems informs us that the thermodynamic factor can also be expressed as follows [11]:

$$\phi = \frac{N_A N_B}{RT} \frac{d^2 G}{dN_i^2} = \frac{\partial \ln a_i}{\partial \ln N_i} = 1 + \frac{\partial \ln \gamma_i}{\partial \ln N_i} \tag{2.35}$$

Here G denotes the Gibbs free energy and $\gamma_i = a_i / N_i$ the coefficient of thermodynamic activity of species $i = A, or\ B$. In addition, as a result of the Gibbs-Duhem relation there is only one thermodynamic factor for a binary alloy:

$$\phi = \frac{\partial \ln a_A}{\partial \ln N_A} = \frac{\partial \ln a_B}{\partial \ln N_B} \tag{2.36}$$

Substituting equation 2.34 in equation 2.29 and signify by the relation,

$$C_i = N_i\left(C_A + C_B\right) = N_i / V_m \tag{2.37}$$

between concentrations and mole fractions, we obtain for the interdiffusion coefficient

$$\tilde{D}_{Darken} = \left(N_A D_B^* + N_B D_A^*\right)\phi \tag{2.38}$$

Equations 2.34 and 2.38 are called the Darken equations. Sometimes the name Darken-Dehlinger equation is used. These relations are widely used in practice for substitution binary alloys.

The Darken equations have been applied in many systems. Figures 2.9 and 2.10 contain experimental data for gold-nickel diffusion at 1173 K. At this temperature, gold and nickel dissolve totally in each other and form absolutely soluble alloys [7]. The importance of this experimental information is that it gives experimental confirmation of the Darken relationships.

In Figure 2.9, the tracer-diffusion coefficients are plotted as a function of composition. The tracer–diffusion rate of nickel atoms in pure gold is about 1000 times larger than nickel atoms in pure nickel. The interdiffusion coefficient as a function of composition is given in Figure 2.10. There is good agreement between the calculated interdiffusion coefficients from self diffusion coefficients Figure 2.9, and the observed one from direct chemical-diffusion measurements using Matano analysis.

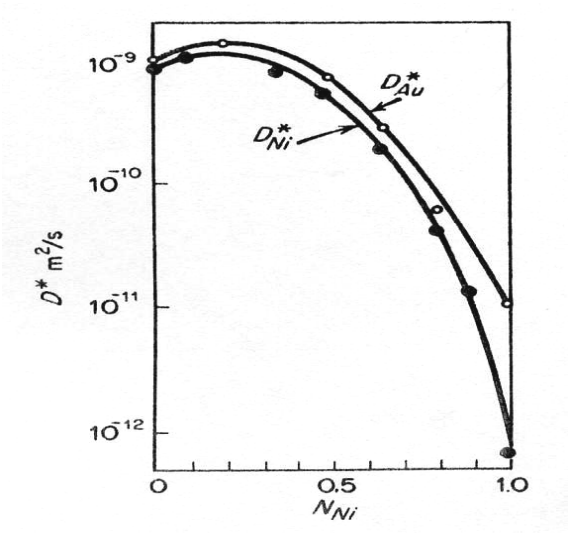

Figure 2.9 Self diffusion coefficients of Au and Ni in gold-nickel alloys at 1173 K [12]

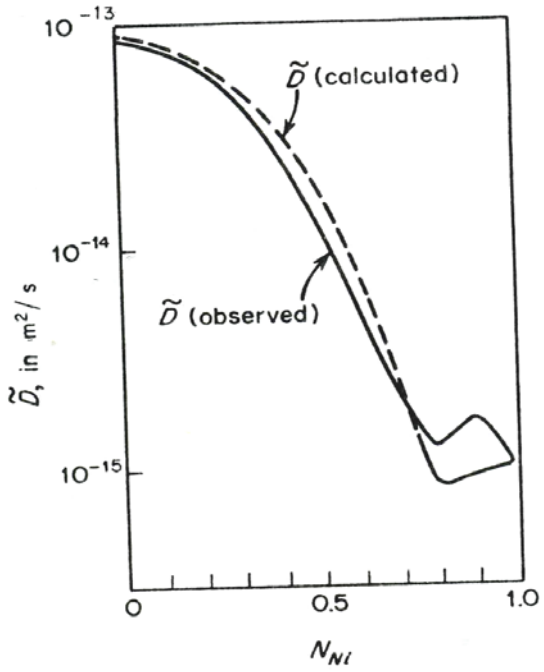

Figure 2.10 Calculated and observed interdiffusion coefficients in gold-nickel alloys at 1173 K [12]

Two curves are shown in Figure 2.10: the one marked *D* (calculated) has been derived from the self diffusion coefficients, Figure 2.9, and the thermodynamic factor (equation 2.36), the other marked *D* (observed) , has been obtained from direct chemical diffusion measurements using Matano analysis. Good agreement has been found between the calculated and observed curves. The small divergence between the two

curves at high nickel concentrations has been explained on the basis of experimental errors.

This section summarises some basic theories and experimental work to provide a framework for improved understanding of the processes of the diffusion.

2.9. Reported Diffusion Behaviour in Metallic Alloy

2.9.1. Diffusion Mechanisms and Kirkendall Effect

Ryusuke *et al.* [13] measured the intrinsic diffusivities of both components and the activation volume for interdiffusion in the B2 type *NiAl* phase at a high temperature region from 1473–1773 K.

Rods of $Ni_{60}Al_{40}$, $Ni_{54}Al_{46}$, $Ni_{51}Al_{49}$ and $Ni_{47}Al_{53}$ alloys were made by melting nickel pellets (99.97 %) and aluminum blocks (99.99 %) in an alumina crucible under argon gas atmosphere and then casting into a steel mould. These ingots were annealed under high purity hydrogen gas at 1723– 1773 K for 86.4 ks for homogenization and grain growth. The resultant grain sizes were 2–4 mm. The rods were cut to make specimens 8 × 5 × 4 mm^3 and 3 × 3 × 1.5 mm^3 in size under atmospheric pressure and under high pressure, respectively.

Titanium oxide particles were used as multiple markers; by spreading the particles on one face of the $Ni_{60}Al_{40}$ sample and sputtering a titanium sheet under active atmosphere. Two specimens, on one face of which the titanium oxide particles were dispersed, were diffusion-welded in a stainless steel holder by heating at 1173 K for 3.6 ks in a stream of high purity argon gas. From the diffusion- welded specimen, a plate 4 mm in thickness was machined so that the titanium oxide particles array, as the multiple markers made an angle of $\pi/4$ rad with the flat face. Titanium oxide particles as the

Kirkendall markers were also dispersed on one face of $Ni_{51}Al_{49}$. Then, a $Ni_{60}Al_{40}/Ni_{51}Al_{49}$ diffusion couple was made by putting the $Ni_{60}Al_{40}$ with the surrounded multiple markers and the $Ni_{51}Al_{49}$ with the Kirkendall marker into a stainless steel holder and by diffusion-welding at 1173 K for 3.6 ks. Subsequently, a $Ni_{54}Al_{46}/Ni_{47}Al_{53}$ diffusion couple with the Kirkendall marker was made by the same method as above. The diffusion couple was sealed in a quartz tube with high purity argon gas. The diffusion annealing was carried out at temperatures from 1473–1773 K for 21.6–604.8 ks. It was also done under the high pressures, 3 and 5 GPa, by a tungsten carbide cubic-anvil apparatus. The $Ni_{60}Al_{40}/Ni_{51}Al_{49}$ diffusion couple with 3 × 3 × 3 mm^3 size was placed in the cell for the high pressure experiment shown in Figure 2.11.

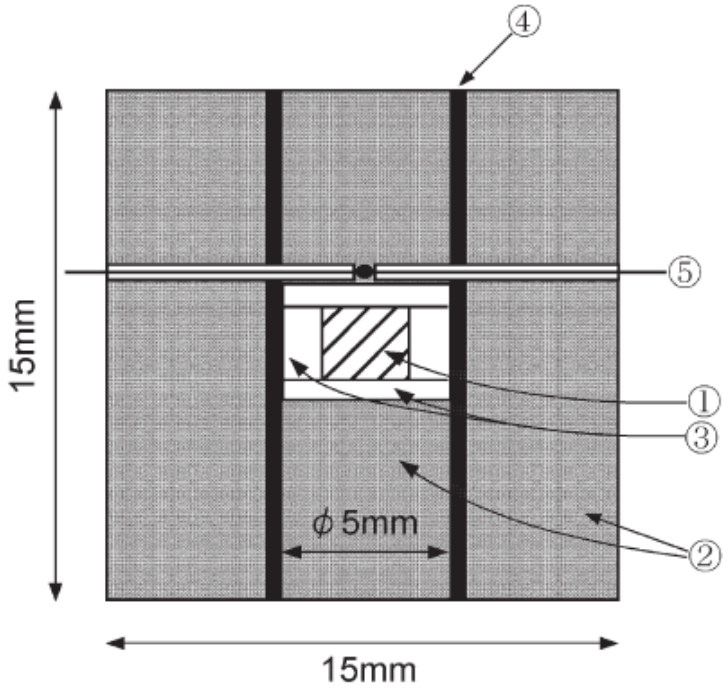

(1) Diffusion couple (2) Pyrophylite (3) BN

(4) Graphite heater (5) Thermocouple

Figure 2.11 The schematic diagram of high pressure cell [13]

Figure 2.12a shows the diffusion zone in the $Ni_{60}Al_{40}/Ni_{51}Al_{49}$ couple diffused at 1673 K for 86.4 ks. The titanium oxide particles array fixed in $Ni_{60}Al_{40}/Ni_{51}Al_{49}$ as the

Kirkendall marker and another array fixed in $Ni_{60}Al_{40}/Ni_{60}Al_{40}$, as the multiple markers, were observed to move from the original position (broken line) to the $Ni_{51}Al_{49}$ side. On the other hand, in Figure 2.12b the curved array of the Kirkendall marker was observed near the side-end of the $Ni_{60}Al_{40}/Ni_{51}Al_{49}$ couple. The Kirkendall marker near the side-end of the couple was fixed at the original welded plane during diffusion, and the side-end represented the reference plane for the shift of the marker. The Kirkendall marker in the area was 200 μm from the side-end of the couple shifted from the original plane to the $Ni_{51}Al_{49}$ side. The shift was 30–40 μm in the total interdiffusion zone of 2000–2400 μm. The determined Al concentration at the Kirkendall plane was 43.5 at%. The marker shifted to the Al-rich side which meant that the fluxes of Al atoms across the Kirkendall plane exceed the Ni atoms flux; the Al intrinsic diffusion coefficient, D_{Al}, is larger than the Ni intrinsic diffusion coefficient, D_{Ni}.

The concentration dependence of D_{A1} and D_{Ni} at 1573 K obtained by analyzing the shift of multiple markers was shown in Figure 2.13. It can be seen that D_{Al} are much larger than D_{Ni} in the concentration range from 42.5–43.5 at% Al and that D_{Ni} showed strong concentration dependence, while D_{Al} is almost constant.

Figure 2.14 shows the difference of Al concentration with the parameter $(x\text{-}x_m)/\sqrt{t}$ in the $Ni_{60}Al_{40}/Ni_{51}Al_{49}$ couple diffused at 1623 K under atmospheric pressure of 0.1 MPa and under high pressures of 3 and 5 GPa, where x_m represents the Matano plane. The total interdiffusion distance decreased with increasing pressure, indicating that the diffusion was developed by applying hydrostatic high pressure. Interdiffusion coefficients, $\tilde{D}$, at 1623 and 1773 K under 0.1 MPa–5 GPa were obtained by analyzing the concentration-penetration profiles as shown in Figure 2.15. The values of $\tilde{D}$ are plotted between 40 and 49 at% Al. The value of $\tilde{D}$ shows a minimum at about 47 at% Al and increases with decreasing Al concentration at each temperature and pressure.

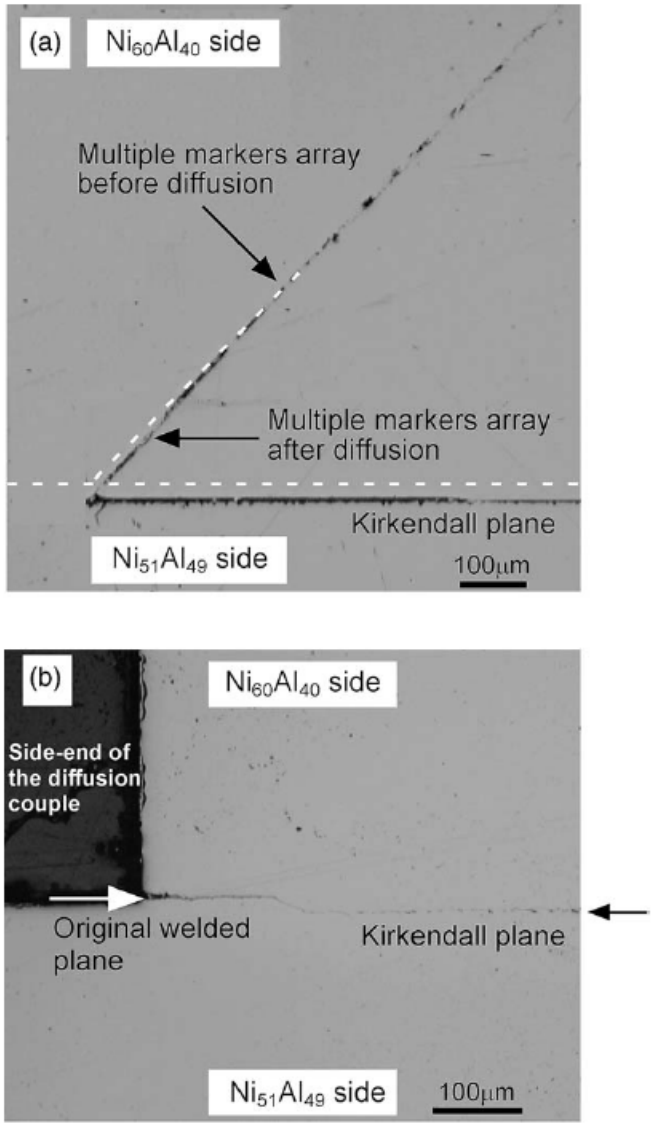

Figure 2.12 (a) Diffusion zone in the $Ni_{60}Al_{40}/Ni_{51}Al_{49}$ couple diffused at 1673 K for 86.4 ks. (b) Kirkendall markers near the side-end of the diffusion couple [13]

As shown in the above Figure 2.12, the dotted line in (a) represents the marker's distribution before diffusion.

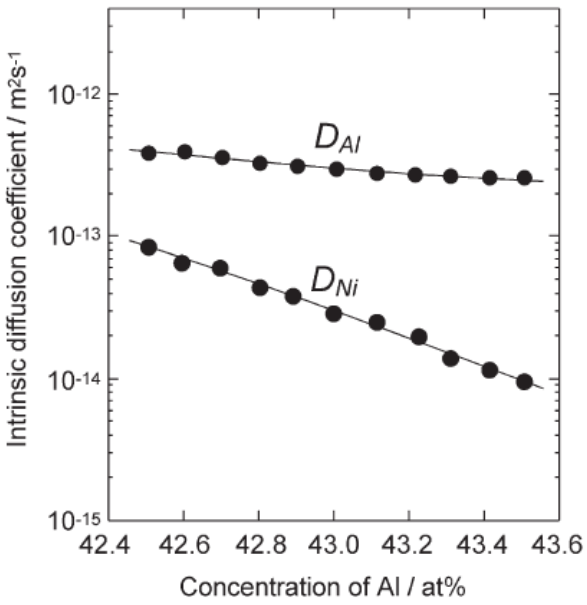

Figure 2.13 Concentration dependence of intrinsic diffusion coefficients of Al and Ni at 1573 K[13]

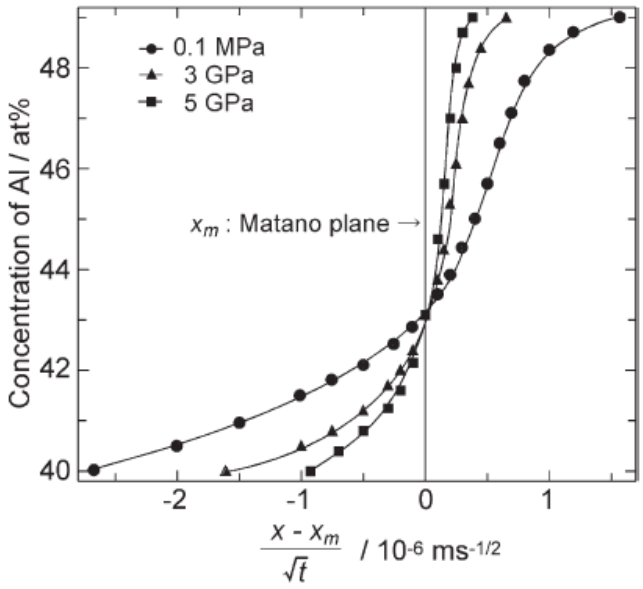

Figure 2.14 Concentration profiles obtained by $Ni_{60}Al_{40}/Ni_{51}Al_{49}$ couple diffused at 1623 K under 0.1 MPa, 3 and 5 GPa[13]

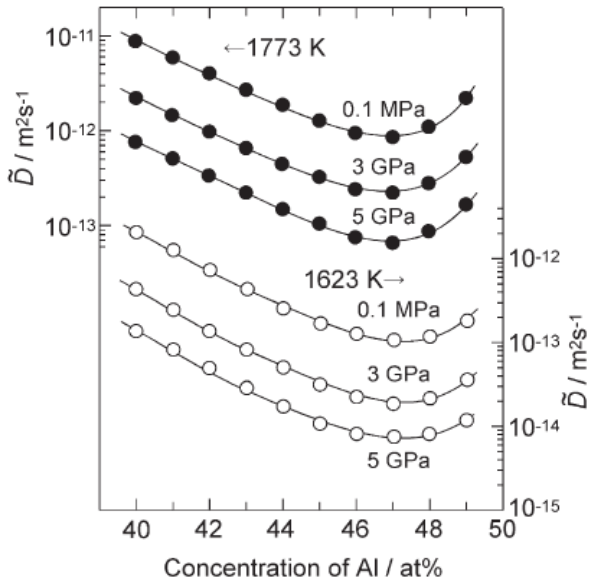

Figure 2.15 The concentration dependence of $\tilde{D}$ in NiAl

The activation volume for diffusion has been obtained from the pressure dependence of the diffusion coefficient, using the following relations:

$$D^* = gfa^2 v_o \exp(-\Delta G / RT) \tag{2.39}$$

D^* is the self-diffusion coefficient, g indicates the geometrical constant, f the correlation factor, a lattice parameter and v_o the attempt frequency. The Gibbs free energy, ΔG, could be decomposed as:

$$\Delta G = \Delta U + p\Delta V - T\Delta S \tag{2.40}$$

where p is the hydrostatic pressure, ΔU the activation enthalpy, ΔS the activation entropy and ΔV the activation volume. The activation volume ΔV is defined from the thermodynamic relationship, as follows:

$$\begin{aligned} \Delta V &= \left(\partial \Delta G / \partial p\right)_T \\ &= -RT\partial \ln D^* / \partial p + RT\partial \ln gfa^2 v_o / \partial p \\ &= -RT\partial \ln D^* / \partial p + RT\gamma_G K_T \end{aligned} \tag{2.41}$$

where γ_G and KT are Gruneisen's constant and the isothermal compressibility, respectively. The second term on the right hand side of equation 2.41 is a small correction term; not more than a few percent of the atomic volume [14].

The intrinsic diffusivities of both components and the activation volume for interdiffusion in the B2 type NiAl phase have been calculated in the high temperature region from 1473–1773 K. The activation volume for interdiffusion in 40–49 at% Al is found to be almost constant value of $1.0V_0$ (V_0: molar volume of alloys) at 1473–1773 K, and as shown in Figure 2.13, D_{Al} near the 43 at% Al is much larger than D_{Ni}.

2.9.2. Interdiffusion Analysis

Another study was carried out using solid-solid diffusion couples with discs of *Mo* and *Si* annealed over the temperature range (900 ^{o}C to 1350 ^{o}C), has been studied by P. C. Tortorici *et al.* [15] with the aim of determining the interdiffusion coefficients for the silicides of *Mo*. The integrated interdiffusion coefficients as well as energies of activation for interdiffusion were determined from the concentration profiles for the silicide layers.

Metallographically preferred 99.95 pct *Mo* and 99.9999 pct *Si* samples were used as diffusion couples which were subjected to diffusion experiments at selected temperatures between 900^{o}C and 1350^{o}C. Figure 2.16 presents an optical micrograph and the experimental concentration profiles for a *Mo vs Si* diffusion couple annealed at 1350 ^{o}C for 10 hours.

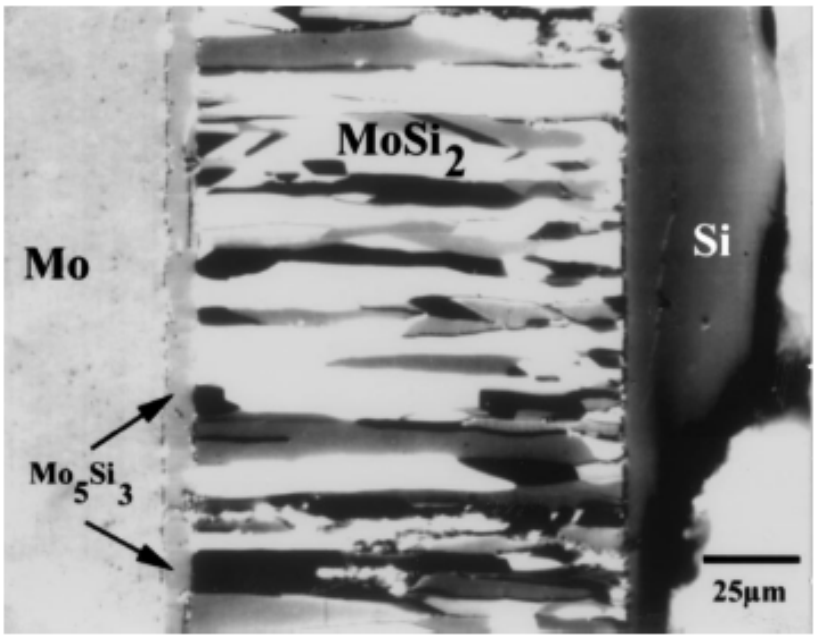

(*a*)

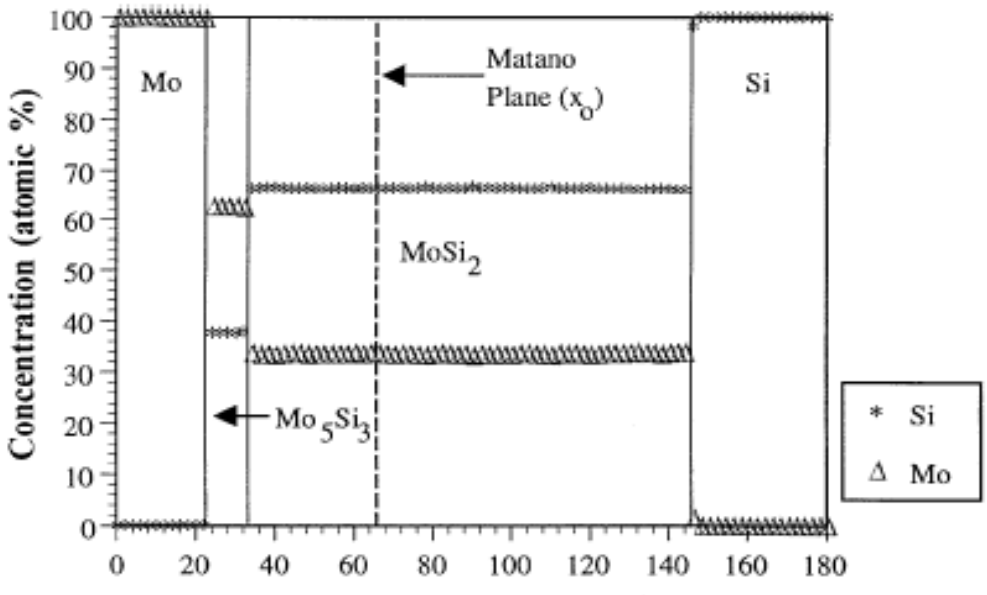

(*b*)

Figure 2.16 (*a*) Optical micrograph and (*b*) Experimental concentration profiles for the *Mo vs Si* diffusion couple annealed at 1350 7C for 10 hours[15]

The interdiffusion fluxes of all components in an isothermal, *n*-component solid-solid diffusion couple could be evaluated at any section of the concentration profiles without using Fick's law. The analysis is based on a direct integration of the continuity

equation over a concentration profile, and the interdiffusion flux at any section (x) at a given time (t) can be determined directly from the following equation [16, 17]:

$$\tilde{J}(x) = \frac{1}{2t} \int_{C_i^+ or C_i^-}^{C_i(x)} (x - x_o) dC_i \quad (i = 1, 2, \ldots, n) \tag{2.42}$$

Where $C_1$and C_2 denote the concentrations of component i in the terminal alloys, and x_0 is the place of the Matano plane. An integrated interdiffusion coefficient ($\tilde{D}_i^{\text{int}}$) can be calculated [18, 19] over a concentration range from $C_i(X_1)$ to $C_i(X_2)$ by:

$$\tilde{D}_i^{\text{int}} = \int_{x_1}^{x_2} \tilde{J}_i dx \qquad (i = 1, 2, \ldots, n) \tag{2.43}$$

where x_2 is greater than x_1 for positive fluxes, whereas x_2 is smaller than x_1 for negative fluxes. On the basis of Fick's law for binary diffusion, $\tilde{D}_i^{\text{int}}$ can be expressed by [20]:

$$\tilde{D}^{\text{int}} = \bar{\tilde{D}}\left[C_i(x_1) - C_i(x_2)\right] \tag{2.44}$$

where $\bar{\tilde{D}}$ is the average value of the interdiffusion coefficient $\tilde{D}$ over the selected composition range.

The integrated interdiffusion coefficients were calculated on the basis of equation 2.43 for the $MoSi_2$- and Mo_5Si_3-phase layers and are included in Table 2.2. The integrated interdiffusion coefficients for the Mo_5Si_3 phase are one to two orders of magnitude smaller than those for the $MoSi_2$ phase. The equations (2.42-2.44) are applicable to the analysis of isothermal multiphase diffusion couples that do not develop all the phase layers. The main condition for using these equations (2.42-2.44) is that

the growth of the observed layers must be parabolic and that the concentrations of the phases at the individual interfaces must be invariant with time under conditions of metastable or stable equilibrium. These conditions are satisfied by the Mo *vs* Si diffusion couples developing the $MoSi_2$- and Mo_5Si_3-phase layers, although a Mo_3Si layer is not observed in the diffusion zone.

The activation energies (Q) for interdiffusion of Mo and Si in the silicide layers were determined from plots of ln ($\tilde{D}^{int}$) *vs* $1/T$; Figure 2.17. The activation energies calculated from the slopes of the plots, were 130 ± 20 and 210 ± 10 kJ/mol for the $MoSi_2$ and Mo_5Si_3 phases, respectively. The energy of activation for interdiffusion in the Mo_5Si_3 phase is higher than that for interdiffusion in the $MoSi_2$ phase.

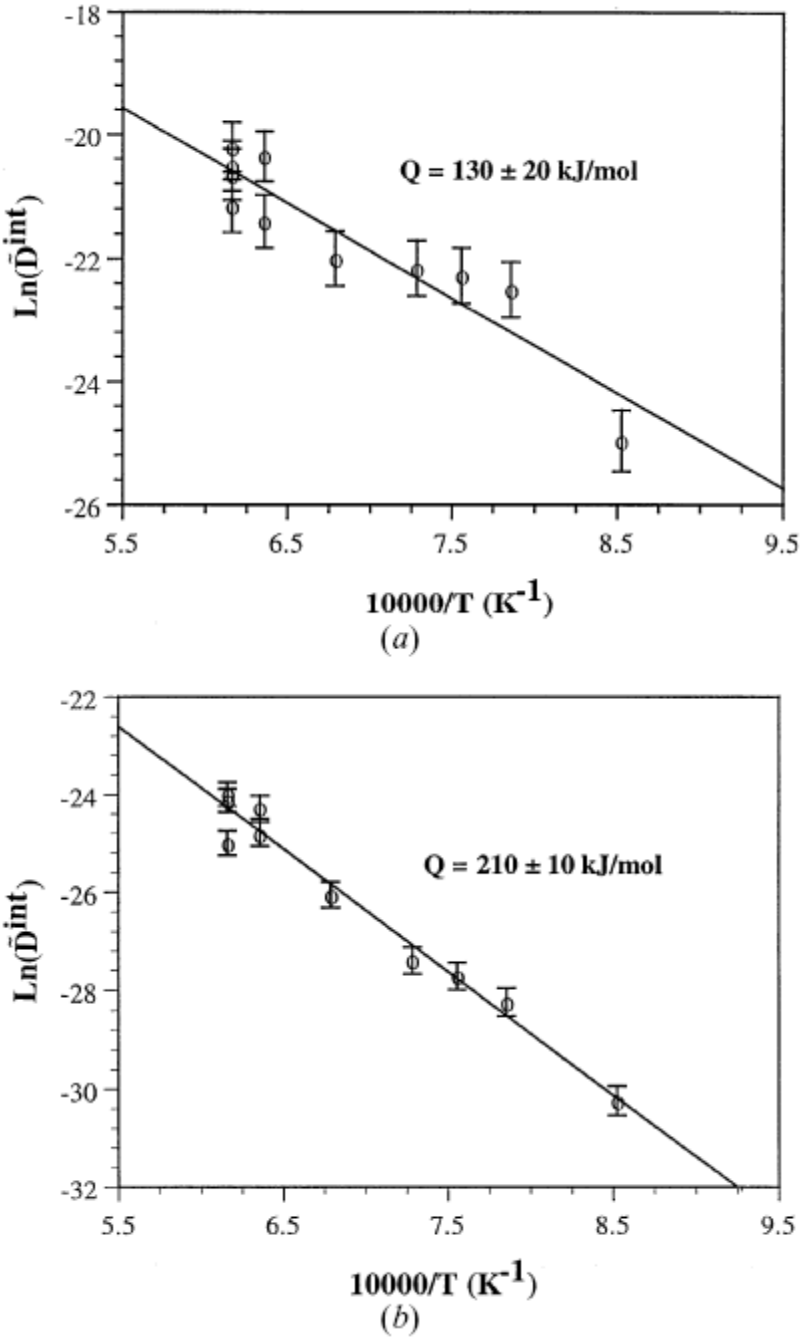

Figure 2.17 Ln ($\tilde{D}^{int}$) *vs* 1/*T* plots for (*a*) $MoSi_2$ and (*b*) Mo_5Si_3 phase layers developed in the Mo *vs* Si diffusion couples annealed at the temperature range (900^{o}C - 1350^{o}C)

From this study, the authors observed that the Layers of $MoSi_2$ and Mo_5Si_3 formed in the diffusion zone, and the $MoSi_2$ layer was around one to two orders of magnitude

larger in thickness than the Mo_5Si_3 layer as shown in Table 2.2, and the thickness of this layer ($MoSi_2$) varied parabolically with time [21].

Temperature C^o	Time h	$MoSi_2$ $\Delta x(\mu m)$	$\tilde{D}^{int}_{MoSi_2}$ [mol/(m.s)]	Mo_5Si_3 $\Delta x(\mu m)$	$\tilde{D}^{int}_{Mo_5Si_3}$ [mol/(m.s)] Mo_5Si_3 $\Delta x(\mu m)$
900	144	40	$1.4x10^{-11}$	1-2	$7.4x10^{-14}$
1000	120	125	$1.7x10^{-10}$	2	$5.5x10^{-13}$
1050	120	140	$2.1x10^{-10}$	3	$9.3x10^{-13}$
1100	72	115	$2.4x10^{-10}$	3	$1.3x10^{-12}$
1200	12	15	$2.8x10^{-10}$	4	$4.9x10^{-12}$
1300	11	110	$1.5x10^{-9}$	6	$1.7x10^{-11}$
1300	14	70	$5.0x10^{-10}$	16	$2.9x10^{-11}$
1350	7	74	$1.1x10^{-9}$	10	$3.4x10^{-11}$
1350	10	112	$1.7x10^{-9}$	10	$3.3x10^{-11}$
1350	16	120	$1.2x10^{-9}$	16	$3.8x10^{-11}$

Table 2.2 Layer thicknesses and integrated interdiffusion coefficients ($\tilde{D}^{int}$) for $MoSi_2$ and Mo_5Si_3 phases in the *Mo* vs *Si* diffusion couples

From the analysis of concentration profiles of the diffusion couples, integrated interdiffusion coefficients were determined for the $MoSi_2$ and Mo_5Si_3 phases. The $\tilde{D}^{int}$

values for the $MoSi_2$ phase are larger by one to two orders of magnitude than those for the Mo_5Si_3 phase over the temperature range from 900°C to 1350°C.

Ternary interdiffusion coefficients were measured in the *Ni* solid solution γ (fcc) phase of the *Ni-Cr-Al* system at 1100°C and 1200°C by Nesbitt *et al.* [22]. nickel was taken as the dependent concentration variable. Two analysis techniques were used to calculate the concentration dependence interdiffusion coefficients from the γ/γ ternary diffusion couple. The first technique, discussed by Kirkaldy [23], requires the positioning of a Matano plane. The second technique derived from the Boltzmann-Matano analysis without need for positioning of a Matano plane. Both techniques were used to determine the four interdiffusion coefficients at the intersection of two γ/γ diffusion couples. The starting equations for either technique are Fick's first law for ternary alloys [23] where the interdiffusion flux $\tilde{J}_i$ for Al and Cr is expressed as:

$$\tilde{J}_{Al} = -\tilde{D}^{Ni}_{AlAl}\frac{\partial C_{Al}}{\partial X} - \tilde{D}^{Ni}_{AlCr}\frac{\partial C_{Cr}}{\partial X} \tag{2.45a}$$

$$\tilde{J}_{Cr} = -\tilde{D}^{Ni}_{CrAl}\frac{\partial C_{Al}}{\partial X} - \tilde{D}^{Ni}_{CrCr}\frac{\partial C_{Cr}}{\partial X} \tag{2.45b}$$

The Matano plane is positioned such that:

$$\int_{C_i^{-\infty}}^{C_i^{+\infty}} X dC_i = 0 \quad \text{i=Al, Cr} \tag{2.46}$$

where $C_i^{-\infty}, C_i^{+\infty}$ are the concentration of aluminium and chromium at either end of the diffusion couple. The flux determined at any position *X (*measured from the Matano plane [16]) by the following equation:

$$\tilde{J}_i = \frac{1}{2t}\int_{C_i^{-\infty}}^{C_i^{+\infty}} X dC_i \qquad \text{i=Al, Cr} \tag{2.47}$$

So equations 2.45 and 2.47 were combined to obtain two equations:

$$\int_{C_{Al}^{-\infty}}^{C_{Al}^{*}} X dC_{AL} = -2t\left[\tilde{D}_{AlAl}^{Ni}\frac{\partial C_{Al}}{\partial X} - \tilde{D}_{AlCr}^{Ni}\frac{\partial C_{Cr}}{\partial X}\right]_{C_{Al}^{*}} \tag{2.48a}$$

$$\int_{C_{Cr}^{-\infty}}^{C_{Cr}^{*}} X dC_{Cr} = -2t\left[\tilde{D}_{CrAl}^{Ni}\frac{\partial C_{Al}}{\partial X} - \tilde{D}_{CrCr}^{Ni}\frac{\partial C_{Cr}}{\partial X}\right]_{C_{Cr}^{*}} \tag{2.48b}$$

where C_{Al}^{*} and C_{Cr}^{*} are exact concentration at a certain position X^{*}, measured from Matano plane. Equations 2.48a and 2.48b were estimated for two intersecting diffusion paths such that C_{Al}^{*} and C_{Cr}^{*} are the concentration at the common composition point of the intersecting paths. So the results were four equations with four diffusion equations instantaneously.

The four ternary interdiffusion coefficients were calculated without positioning a Matano plane, by inserting the parameter [24]:

$$Y_i = \frac{C_i - C_i^{-\infty}}{C_i^{+\infty} - C_i^{-\infty}} \quad \text{i=Al, Cr} \tag{2.49}$$

When we insert this into equation 2.48a we obtain:

$$\begin{aligned}&\tilde{D}_{AlAl}^{Ni} + \tilde{D}_{AlCr}^{Ni}\left[\frac{C_{Cr}^{+\infty} - C_{Cr}^{-\infty}}{C_{Al}^{+\infty} - C_{Al}^{-\infty}}\right]\frac{dY_{Cr}}{dY_{Al}} \\ &= \frac{1}{2t}\frac{dX}{dY_{Al}}\cdot\left[(1-Y_{Al}^{*})\int_{-\infty}^{X^{*}} Y_{AldX} + Y_{Al}^{*}\int_{X^{*}}^{+\infty}(1-Y_{Al})dX\right]\end{aligned} \tag{2.50}$$

Equation 2.48b was operated similar to the equation 2.48a. The four diffusion coefficients calculated by Whittle-Green technique [24] were identical to the values calculated by the Kirkaldy technique when the Matano planes are concurrent.

The results of the diffusivity measurements showed that $\tilde{D}_{AlAl}^{Ni}$ is approximately four times greater than $\tilde{D}_{AlCr}^{Ni}$, whereas $\tilde{D}_{CrAl}^{Ni}$ and $\tilde{D}_{CrCr}^{Ni}$ are the same magnitude Table

2.3. For all concentrations, $\tilde{D}^{Ni}_{AlAl}$ is two to three times greater than $\tilde{D}^{Ni}_{CrCr}$. $\tilde{D}^{Ni}_{AlAl}$ and $\tilde{D}^{Ni}_{AlCr}$ increased with increasing *Al* concentration and showed slight dependence on *Cr* concentration. $\tilde{D}^{Ni}_{CrAl}$ is strongly dependent on *Cr* concentration while $\tilde{D}^{Ni}_{CrCr}$ is more dependent on *Al* concentration. The four diffusion coefficients calculated by the Whittle-Green technique for the intersection of couples *Ni*-10*Al* / *W* and *Ni*-10-10/*Ni* annealed at 1100°C are shown in Table 2.3. The diffusion coefficients determined by the Whittle-Green technique were very close to the average of the values calculated by the Kirkaldy technique.

	$\tilde{D}^{Ni}_{AlCr}$	$\tilde{D}^{Ni}_{AlAl}$	$\tilde{D}^{Ni}_{CrAl}$	$\tilde{D}^{Ni}_{CrCr}$	$\times 10^{10}\, cm^2/s$
Kirkaldy technique	1.86	0.35	1.04	0.88	
(noncoincident	1.76	0.31	0.86	0.81	
Matano planes	1.71	0.39	1.27	0.82	
	1.62	0.35	1.1	0.74	
	1.35	0.35	1.03	0.88	
	1.44	0.39	1.24	0.97	
	1.53	0.31	0.7	0.96	
	1.62	0.35	0.91	1.05	
Average	1.61	0.35	1.02	0.89	
Standared deviation	0.16	0.03	0.18	0.09	
Whittle-Green technique	1.61	0.35	1.02	0.87	

Table 2.3 Calculated interdiffusion coefficients for intersecting couples *Ni*-6.7*Al/Ni*-12.0*Cr* (*Ni*-10*Al*/W) and *Ni*-15.2*Cr*-6.7*Al/Ni* (*Ni*-10-10/*Ni*) annealed at 1100°C for 100 hours

The interdiffusion in the γ phase of the Ni-Cr-Al system has been measured at 1100 and 1200°C.

Karunaratne *et al.* [25] determined the interdiffusion coefficients in the *Ni*-rich portion of the *Ni–Al–Ti* system, in the temperature range 900–1200°C, concentrated mainly on the face-centred cubic (γ) phase. The values were derived from concentration profiles measured by electron probe microanalysis, using a modified form of the Boltzmann–Matano method. The diffusion couples were of three types: γ/γ, γ/γ' and γ'/γ', where γ'denotes the $L1_2$ phase.

Fick's second law [26, 27] characterized a satisfactory description of the diffusion behaviour of the two solute atoms Al and Ti. Therefore, the concentrations of Al and Ti, denoted C_{Al} and C_{Ti}, respectively, are illustrated by:

$$\frac{\partial C_{Al}}{\partial t} = \frac{\partial}{\partial x}\left(\tilde{D}^{Ni}_{AlAl} \frac{\partial C_{Al}}{\partial x} \right) + \frac{\partial}{\partial x}\left(\tilde{D}^{Ni}_{AlTi} \frac{\partial C_{Ti}}{\partial x} \right) \tag{2.51}$$

$$\frac{\partial C_{Ti}}{\partial t} = \frac{\partial}{\partial x}\left(\tilde{D}^{Ni}_{TiAl} \frac{\partial C_{Al}}{\partial x} \right) + \frac{\partial}{\partial x}\left(\tilde{D}^{Ni}_{TiTi} \frac{\partial C_{Ti}}{\partial x} \right) \tag{2.52}$$

Here $\tilde{D}^{Ni}_{AlAl}$ and $\tilde{D}^{Ni}_{TiTi}$ are the director (major) interdiffusion coefficients which correspond to the influences of aluminum and titanium concentration gradients on their own fluxes, and $\tilde{D}^{Ni}_{AlTi}$ and $\tilde{D}^{Ni}_{TiAl}$ are the indirect (cross) diffusion coefficients which represent the influences of the concentration gradients of titanium and aluminum on the fluxes of aluminum and titanium, respectively. Time is denoted by the symbol *t*.

The solution to equation 2.46 for aluminum diffusion in Ni–Al–Ti is given by:

$$\int_{C^{-}_{Al}}^{C_{Al}} (x - x_o)\, dC_{Al} = -2t \left[\tilde{D}^{Ni}_{AlAl} \frac{\partial C_{Al}}{\partial x} + \tilde{D}^{Ni}_{AlTi} \frac{\partial C_{Ti}}{\partial x} \right] \tag{2.53}$$

where C^{-}_{Al} is the concentration of aluminum at one end of the diffusion couple. A similar expression was written for titanium. The position of the Matano interface at $x = x_o$ was determined using iterative procedures from equations of the form:

$$\int_{C_{Al}^{-}}^{C_{Al}^{+}} (x - x_o) dC_{Al} = 0 \tag{2.54}$$

C_{Al}^{-} and C_{Al}^{+} are the limiting compositions of the far ends of the couple.

The method was used by Karunaratne [25], does not require the Matano interface to be determined. So the diffusion coefficients are determined by solving the four simultaneous equations in ϕ_{Al} and ϕ_{Al} [28]:

$$\phi_{Al} = \frac{1}{2t}\left(\frac{dx}{dY_{Al}}\right)\left[(1 - Y_{Al})\int_{-\infty}^{x} Y_{Al} dx + Y_{Al}\int_{x}^{+\infty}(1 - Y_{Al}) dx\right] \tag{2.55}$$

$$\phi_{Ti} = \frac{1}{2t}\left(\frac{dx}{dY_{Ti}}\right)\left[(1 - Y_{Ti})\int_{-\infty}^{x} Y_{Ti} dx + Y_{Ti}\int_{x}^{+\infty}(1 - Y_{Ti}) dx\right] \tag{2.56}$$

$$\phi_{Al} = \tilde{D}_{AlAl}^{Ni} + \tilde{D}_{AlTi}^{Ni}\frac{dC_{Ti}}{dC_{Al}} \tag{2.57}$$

$$\phi_{Ti} = \tilde{D}_{TiTi}^{Ni} + \tilde{D}_{ATiAl}^{Ni}\frac{dC_{Al}}{dC_{Ti}} \tag{2.58}$$

The expression Y_i (i=Al, Ti) is the normalized concentration which is specified as:

$$Y_i = \frac{C_i - C_i^{-}}{C_i^{+} - C_i^{-}} \tag{2.59}$$

ϕ_{Al} and ϕ_{Ti} regarded as 'pseudo-binary' diffusion coefficients because they were calculated from [25] their own concentration profiles independently of the other components.

The two major interdiffusion coefficients $\tilde{D}_{AlAl}^{Ni,\gamma}$ and $\tilde{D}_{TiTi}^{Ni,\gamma}$ are almost equal, and vary slightly with composition. The minor diffusion coefficients $\tilde{D}_{AlTi}^{Ni,\gamma}$, $\tilde{D}_{TiAl}^{Ni,\gamma}$ are

much smaller than major interdiffusion coefficients. The general thermodynamic relationships between these coefficients are followed [26, 27, and 28]:

$$\tilde{D}^{Ni,\gamma}_{AlAl} + \tilde{D}^{Ni,\gamma}_{TiTi} \rangle 0 \tag{2.60a}$$

$$\tilde{D}^{Ni,\gamma}_{AlAl}\,\tilde{D}^{Ni,\gamma}_{TiTi} - \tilde{D}^{Ni,\gamma}_{AlTi}\,\tilde{D}^{Ni,\gamma}_{TiAl} \geq 0 \tag{2.60b}$$

$$\left(\tilde{D}^{Ni,\gamma}_{AlAl} + \tilde{D}^{Ni,\gamma}_{TiTi}\right)^2 \geq 4\left(\tilde{D}^{Ni,\gamma}_{AlAl}\,\tilde{D}^{Ni,\gamma}_{TiTi} - \tilde{D}^{Ni,\gamma}_{AlTi}\,\tilde{D}^{Ni,\gamma}_{TiAl}\right) \tag{2.60c}$$

Both the major coefficients $\tilde{D}^{Ni,\gamma}_{AlAl}$ $\tilde{D}^{Ni,\gamma}_{TiTi}$ and minor coefficients $\tilde{D}^{Ni,\gamma}_{AlTi}$ $\tilde{D}^{Ni,\gamma}_{TiAl}$ are positive. This indicates that the diffusion fluxes of *Al* and *Ti* are governed mostly by their own concentration gradients and the influence of the gradient of the other element is small and positive.

2.9.3. Interfdiffusion and Diffusion Structure

Tortorici *et al.* [29] determinated the interdiffusion coefficients and the activation energies for interdiffusion in various silicides developed in the couples. Several series of solid-solid diffusion couples, Me vs. $MoSi_2$, where Me= Mo, W, Re, Nb, or Ta were assembled with discs of Mo, W, Re, Nb, and Ta in contact with disks of a single crystal of $MoSi_2$, they were annealed at selected temperatures in the range 1300° - 1700°C. The couples were analyzed and characterized by Scanning Electron Microscope (SEM) and optical microscopy, microprobe analysis, X-ray diffraction and orientation imaging microscopy. Interdiffusion between Mo and Si was investigated [30,31] at temperatures over 900°– 1350°C for the determination of activation energies for the growth of silicide layers. The growth kinetics of Mo_5Si_3 and Mo_3Si between Mo and $MoSi_2$ was reported over 1200°–1900°C [32, 33]. Diffusion studies with Mo vs. Si diffusion

couples have been carried out over 900°–1350°C for the determination of interdiffusion coefficients for the $MoSi_2$ and Mo_5Si_3 phases; the energies of activation for interdiffusion in these phases have been reported to be 130 ± 20 and 210 ± 10 kJ mol^{-1}, respectively [34, 35].

So the authors' [29] aim was to investigate interdiffusion and the formation of silicide layers between $MoSi_2$ and selected refractory metals.

In studying the interdiffusion in various silicides, Me/ $MoSi_2$ couples were subjected to diffusion experiments at 1300 to 1700^{o}C (depending on the nature of Me).

After the diffusion experiments the diffusion couples were examined with a series of analytical instruments. Concentration profiles were determined by point-to-point counting techniques with a Cameca SX-50 microprobe equipped with four wavelength dispersive spectrometers at an accelerating voltage of 15 kV and a probe current of 20 nA.

In order to calculate the integrated and average effective interdiffusion coefficients, the authors' [29] used equations 2.42 and 2.43 for interdiffusion flux $\tilde{J}_i(x)$ and integrated interdiffusion coefficients. On the basis of Fick's law for multi-component diffusion:

$$\tilde{J}_i = -\sum_{j=1}^{n-1} \tilde{D}_{ij}^{\,n} \frac{\partial C_j}{\partial x} \qquad (i=1, 2\ldots n\text{-}1) \qquad (2.61)$$

where $\frac{\partial C_j}{\partial x}$ is the concentration gradient of component j and $\tilde{D}_{ij}^{\,n}$ were $(n\text{-}1)^2$ composition-dependent interdiffusion coefficients. On the basis of equation 2.43,

$$\tilde{D}_i^{\text{int}} = \int_{x_1}^{x_2} \tilde{J}_i dx \qquad (i = 1, 2, \ldots, n)$$

Equation 2.61 became [16];

$$\tilde{D}^{\,\mathrm{int}}_{i,\Delta x} = \sum_{j=1}^{n-1} \int_{C_{j(x_2)}}^{C_{j(x_1)}} \tilde{D}^{\,n}_{ij}\, dC_j = \sum_{j=1}^{n-1} \bar{\tilde{D}}^{\,n}_{ij} [C_j(x_1) - C_j(x_2)] \tag{2.62}$$

where $\bar{\tilde{D}}^{\,n}_{ij}$ corresponds to average values of the interdiffusion coefficients over the concentration range in the diffusion zone from x_1 to x_2. An average effective interdiffusion coefficient $\tilde{D}^{\,eff}_{i}$ for the component *i* over the interval is also defined by [16]:

$$\tilde{D}^{\,eff}_{i} = \frac{\tilde{D}^{\,\mathrm{int}}_{i,\Delta x}}{C_i(x_1) - C_i(x_2)} \tag{2.63}$$

In Table 2.4, the values of the integrated interdiffusion coefficients $\tilde{D}^{\,\mathrm{int}}_{i}$ calculated on the basis of equation 2.43 for Mo, W and Si in the W_5Si_3 and $(W, Mo)_5Si_3$ layers for the various couples were presented. The average effective interdiffusion coefficients calculated from equation 2.63 for W and Mo in the $(W, Mo)_5Si_3$ layer were presented in Table 2.5. In the binary W_5Si_3 layer, the $\tilde{D}^{\,\mathrm{int}}_{i}$ values are common to both W and Si. In the ternary $(W, Mo)_5Si_3$ layer, $\tilde{D}^{\,\mathrm{int}}_{Si}$ is larger than $\tilde{D}^{\,\mathrm{int}}_{W}$ and $\tilde{D}^{\,\mathrm{int}}_{Mo}$ in magnitude by a factor of (2–3). $\tilde{D}^{\,\mathrm{int}}_{Mo}$ is negative and specifies that the cumulative interdiffusion of Mo in the $(W, Mo)_5Si_3$ layer is against its own concentration gradient. The average effective interdiffusion coefficients of Mo and W in the $(W, Mo)_5Si_3$ layer are also of opposite signs, but of parallel magnitude. The negative values of $\tilde{D}^{\,eff}_{Mo}$ suggested that Mo interdiffuses uphill against its own concentration gradient.

Temperature (^{o}C)	Annealing time (h)	$\tilde{D}^{int}_{Mo}$ (mole m^{-1} s^{-1})	$\tilde{D}^{int}_{W}$ (mole m^{-1}s$^{-1)}$	$\tilde{D}^{int}_{Si}$ (mole m^{-1}s^{-1})
W_5Si_3 Layer				
1400	16	-	$8.1x10^{-13}$	$8.1\ x10^{-13}$
1500	6	-	$1.8\ x10^{-11}$	$1.8\ x10^{-11}$
1500	12	-	$8.1\ x10^{-12}$	$8.1\ x10^{-12}$
1500[b]	12	-	$8.3\ x10^{-12}$	$8.3\ x10^{-12}$
1600	8	-	$6.5\ x10^{-12}$	$6.5\ x10^{-12}$
1700	6	-	$9.6\ x10^{-11}$	$9.6\ x10^{-11}$
$(W, Mo)_5Si_3$				
1400	16	$-1.5x10^{-13}$	$2.6\ x10^{-13}$	$4.9\ x10^{-13}$
1500	6	$-8.0x10^{-13}$	$1.6\ x10^{-12}$	$2.4\ x10^{-12}$
1500	12	$-4.0x10^{-12}$	$6.2\ x10^{-12}$	$8.9\ x10^{-12}$
1500[b]	12	$-4.2x10^{-12}$	$6.7\ x10^{-12}$	$7.7\ x10^{-12}$
1600	8	$-8.8x10^{-12}$	$1.3\ x10^{-11}$	$2.2\ x10^{-11}$
1700	6	$-4.2x10^{-11}$	$3.1\ x10^{-11}$	$7.7\ x10^{-11}$

Table 2.4 Integrated interdiffusion coefficients in the W_5Si_3 and $(W, Mo)_5Si_3$ layers in the W vs. $MoSi_2$ diffusion couples annealed between 1400° and 1700°C

Temperature (C^o)	Annealing time (h)	$\tilde{D}^{eff}_{Mo}(m^2s^{-1})$	$\tilde{D}^{eff}_{W}(m^2s^{-1})$
1400	16	-2.4×10^{-17}	3.2×10^{-17}
1500	6	-1.0×10^{-15}	1.9×10^{-15}
1500	12	-2.6×10^{-16}	7.2×10^{-16}
1500[a]	12	-3.0×10^{-16}	6.5×10^{-15}
1600	8	-1.0×10^{15}	1.5×10^{-15}
1700	6	-4.9×10^{15}	3.6×10^{-15}

Table 2.5 Average effective interdiffusion coefficients for Mo and W in the $(W, Mo)_5Si_3$ phase layer in the W vs. $MoSi_2$ diffusion couples annealed between 1400° and 1700°C

Interdiffusion and diffusion structures were investigated in several Re and $MoSi_2$ diffusion couples at selected temperatures over 1425°–1700°C. A back-scattered electron micrograph and the experimental concentration profiles for a Re vs. $MoSi_2$ diffusion couple annealed at 1700°C for 6 hours are presented in Figure 2.18.

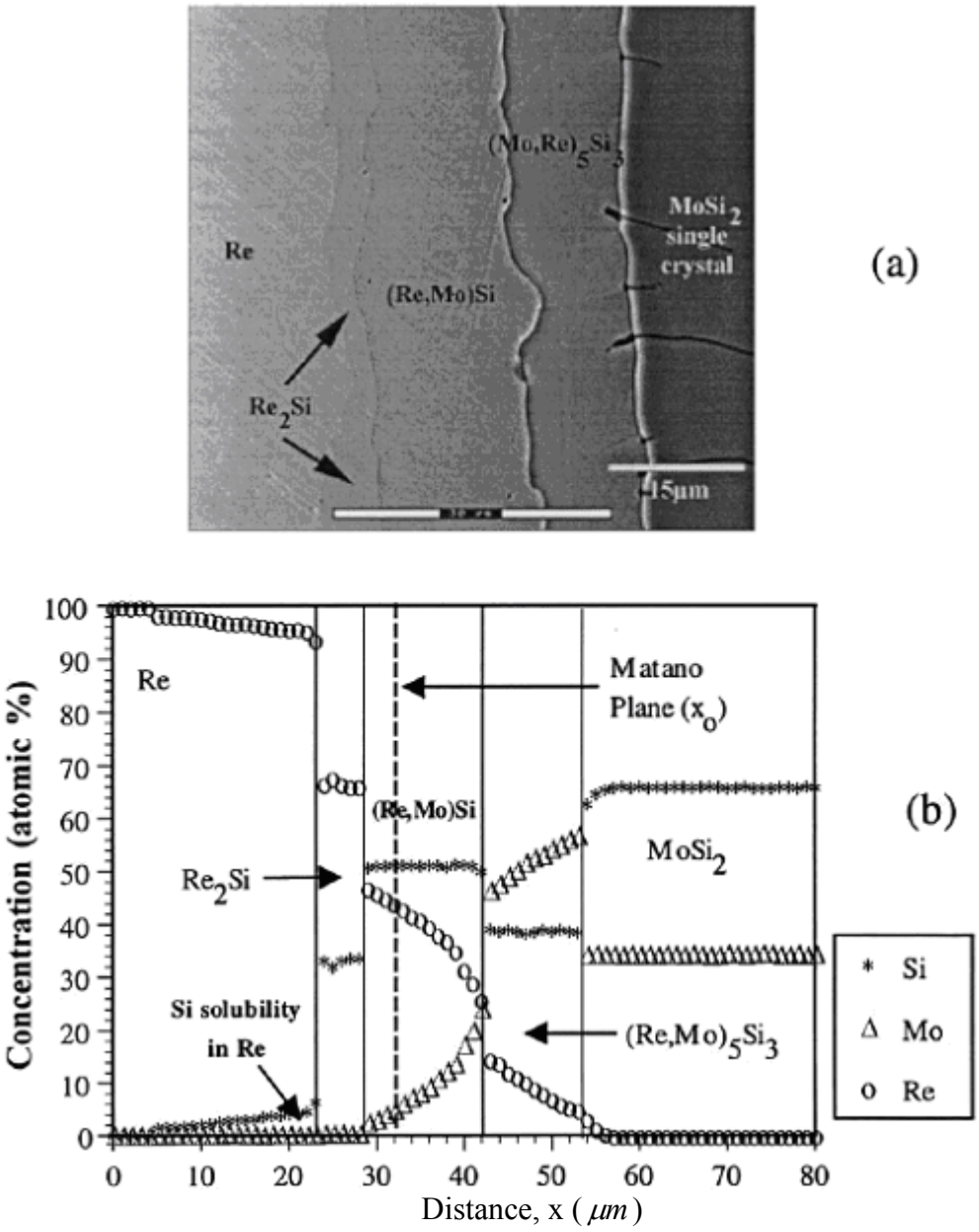

Figure 2.18 (a) Back-scattered electron micrograph and (b) experimental concentration profiles for the Re vs. $MoSi_2$ diffusion couple annealed at 1700°C for 6 hours [29]

The activation energies (Q) for the interdiffusion are presented in Table 2.6.

Layers	Q of Si &W
W_5Si_3	360 kJ mol^{-1}
$(W, Mo)_5Si_3$	450 kJ mol^{-1}

(a)

Phase	Q of Re & Si
Re_2Si	190 kJ mol^{-1}
(Re, Mo)Si	325 kJ mol^{-1}
$(Re, Mo)_5Si_3$	270 kJ mol^{-1}

(b)

Phase	Q of Si	Q of Nb
$(Nb, Mo)_5Si_3$	300 kJ mol^{-1}	240 kJ mol^{-1}

(c)

Table 2.6 (a) the activation energies of Si and W in the W_5Si_3 and $(W, Mo)_5Si_3$ layers; (b) the activation energies of Re and Si in the (Re, Mo)Si and $(Re, Mo)_5Si_3$ phases; (c) the activation energies of Si and Nb in $(Nb, Mo)_5Si_3$

Interdiffusion was investigated at selected temperatures in the range 1400° - 1700°C with several series of $MoSi_2$ vs. Me ternary couples, where Me=W, Re, Nb, or Ta. From an analysis of concentration profiles, integrated and average effective interdiffusion coefficients were determined for the components in the various silicide layers developed in the diffusion zone.

2.9.4. Generalized Darken Method GDM

Significant work on diffusion has been performed by *Datta et al.* [36] in the AMRI (Advanced Material Research Institute) in developing and applying of the Darken's Generalised Model (GDM) of Interdiffusion. The authors postulated that total mass flow is a sum of the diffusion and drift flows, and can be applied to the description of the diffusion transport in multi-component solid solutions. The equations of mass conservation (continuity equations) determine the appropriate expressions that describe the various fluxes based on the postulate of constant molar volume in the system. This allows a complete quantitative description of the diffusion transport processes both for the open and closed systems. Here the GDM is used for the calculation of the concentration profiles. Parameters used are as follows:

- $M_1,...,M_r$ - Molar masses of the elements (g*mol^{-1}), where r - is the number of components in the alloy;
- Λ - a position of the alloy/scale interface ;
- $\overset{0}{c}_1 = \overset{0}{c}_1(x),...,\overset{0}{c}_r = \overset{0}{c}_r(x)$ - The initial distributions of the components, such that:
  - $c_{alloy} = \overset{0}{c}_i = const.$

    where c_{alloy} is the molar concentration of the system
- $D_1^* = D_1^*(N),...,D_r^* = D_r^*(N)$ - Self diffusion coefficients of the components, which may depend on components' molar fractions, $N = (N_1,...N_r)$;
- $\mu_1 = \mu_1(N),...,\mu_r = \mu_r(N)$ - The chemical potentials of the components can be shown as a functions of components' concentration;

- $\hat{t}$ - The time of the process duration;

  $j_{i\Lambda}(t),\ i=1,...,r$ - Evolution of mass flow of the i-th component through the alloy /scale interface.

2.9.4.1. Physical Laws

Various physical laws are relevant to the models such as the law of the mass conservation of a i-th element. This law states that a local change of density of an i-th element is a result of its net in- or outflow only:

$$\frac{\partial c_i}{\partial t}+\frac{\partial J_i}{\partial x}=0 \quad i=1,...,r. \tag{2.64}$$

Following Darken's postulate [37, 38], it was postulated that the flux of the *i*-th element can be expressed in a form of the sum of the diffusional (Fick'ian) and drift flow;

$$J_i = c_i v_i = -\bar{D}_i \frac{\partial c_i}{\partial x} + c_i v \tag{2.65}$$

where:

$c_i = c_i(x,t)$ is the distribution of the i-th element after time t of the process.

The alloy was assumed to be constant molar volume. The consequence is that the molar concentration of the alloy, as a sum of the concentrations of all elements at any position for every time, is constant:

$$\frac{1}{M_1}c_1+.....+\frac{1}{M_r}c_r = c = const \quad \text{or} \quad c_1+...+c_r = c_{alloy} = const. \tag{2.66}$$

2.9.4.2. Initial Conditions

The initial density distributions of the components in the system:

$$\overset{0}{\tilde{n}}_i(x) = \tilde{n}_i(0,x) \qquad for\ x \in [-\Lambda, \Lambda],\ i = 1,...,r. \tag{2.67}$$

The following boundary conditions are postulated:

$$\begin{aligned} &J_i(t,-\Lambda) = j_{iL}(t), \qquad J_i(t,+\Lambda) = j_{iR}(t), \\ &for\ t \in [0,\hat{t}\ ],\ i = 1,...,r. \end{aligned} \tag{2.68}$$

In the open system the functions, $j_{iL}(t)$ and $j_{iR}(t)$, have to be known. They can be calculated for example, from the known rate of reactions at the boundary or from the experimental data. In the closed system the gradients of all components at both boundaries vanish, so that, the flux of an i-th component at the boundary equals zero:

$$J_i(t,\pm\Lambda) = 0 \qquad for\ t \in [0,\hat{t}\ ],\ i = 1,...,r. \tag{2.69}$$

2.9.4.3. Boundary Conditions

For the closed system (annealing in argon) boundary conditions - zero fluxes of the components though the boundary occur:

$$(c_i v_i)(t,\pm\Lambda) = 0 \text{ for i = 1,2,.....,r} \tag{2.70}$$

2.9.4.4. The Unknowns

Two variables in the system are unknown at the start of the experiment that is:

- Concentrations of the components in the alloy as functions of time and position,

$$c_i(t, x),\ i = 1, ..., r \tag{2.71}$$

- A drift velocity as a function of time and position, $\upsilon(t, x)$ [39, 40, 41]

Using these equations interdiffusion process can be modelled.

2.9.5. Modelling Interdiffusion in Cu-Fe-Ni Alloy Using GDM

The above equations were applied to demonstrate the possibility of interdiffusion modelling in the closed system (Cu-Fe-Ni) [42].

Interdiffusion modelling in the Cu-Fe-Ni closed system has been done using DifSim software [43] and compared with the experimental results [44]. For the calculations the following data were used:

- Initial concentration profiles – step functions defined by the terminal composition of the diffusion couple, Figure 2.19.

$$Cu = \begin{cases} 42\ wt.\% & x \in [-\Lambda, 0] \\ 0\ wt.\% & x \in]0, \Lambda] \end{cases}, \quad Fe = \begin{cases} 0\ wt.\% & x \in [-\Lambda, 0] \\ 24\ wt.\% & x \in]0, \Lambda] \end{cases}, \quad Ni = \begin{cases} 58\ wt.\% & x \in [-\Lambda, 0] \\ 76\ wt.\% & x \in]0, \Lambda] \end{cases}$$

- Average molar concentration of the Cu-Fe-Ni alloy, $c = 0.144 molcm^{-3}$.
- Thickness of the diffusion couple, $2\Lambda = 0.07 cm$.

- Calculated average self-diffusion coefficients of copper, iron and nickel in Cu-Fe-Ni diffusion couple [44] at 1273 K;

$$D_{Cu} = 2.89x10^{-11} cm^2 / s$$
$$D_{Fe} = 1.52x10^{-11} cm^2 / s$$
$$D_{Ni} = 2.09x10^{-11} cm^2 / s$$

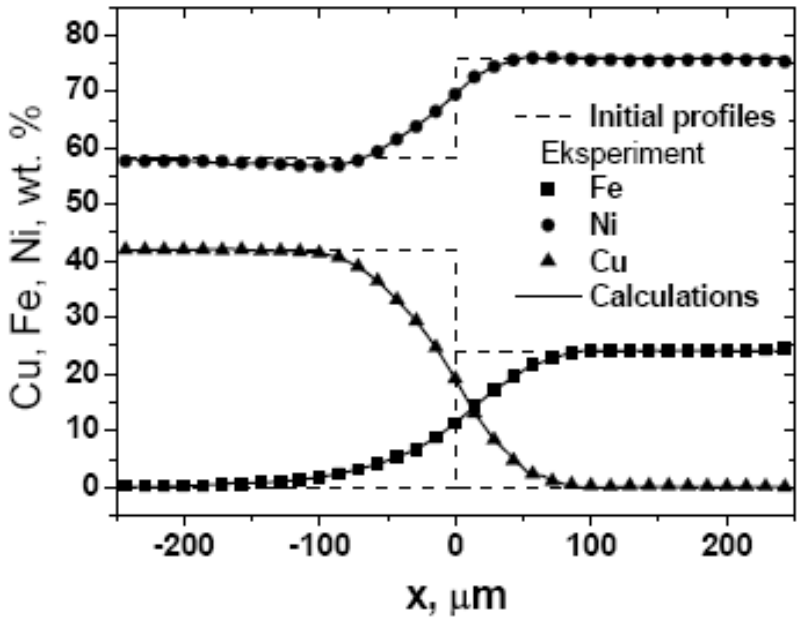

Figure 2.19 The calculated (solid lines) and experimental concentration profiles of the components in Cu-Fe-Ni alloy after 612 ks of diffusion annealing at 1273 K in argon [44]

Figure 2.19 shows the calculated concentration profiles of Cu, Fe, and Ni. Satisfactory agreement between the experimental results and the calculated concentration profiles was obtained.

A mathematical model of interdiffusion in a multi-component has been formulated. The model can be used both for a quantitative description of interdiffusion in the open and closed systems. Application of the model for modelling interdiffusion in the Cu-Fe-Ni diffusion couple (closed system) was demonstrated. The calculated concentration profiles were consistent with experimental results.

Filipek *et al*. [45] studied interdiffusion in Co-Fe-Ni alloys in a1373-1588 K temperature range. The Danielewski-Holly model was used for the description of the interdiffusion process in ternary Co-Fe-Ni diffusion couples both for the finite and infinite geometry. The average intrinsic diffusivities of components in the Co-Fe-Ni system were calculated by using the inverse method and compared with the results of the other authors. The inverse method allows calculation of the diffusion coefficients in the multi-component system.

The Danielewski-Holly model of interdiffusion is an initial boundary-value problem for partial differential equations, namely for the equations of mass conservation. The model describes diffusion in solid solutions. Equations (2.65-2.71) were applied to calculate the concentration profile for all the elements and the drift velocity. The author defined a new variable $w_i(t,x)$ that has a physical interpretation and denotes a deviation of *i*-th element mole fraction from its average in the alloy;

$$w_i(t,x) = N_i(t,x) - \bar{N}_i \tag{2.72}$$

Where $\bar{N}_i$ is an average mol fraction of *i*-th element in the alloy. Therefore the interdiffusion problem can be transformed as follows [46, 47]:

$$\begin{aligned} &\frac{\partial w_i}{\partial t}(t,x) = \frac{\partial}{\partial x}\left(D_i \frac{\partial w_i}{\partial x}(t,x) - \left(w_i(t,x) + \bar{N}_i \right) \sum_{j=1}^{r} D_j \frac{\partial w_j}{\partial x} \right) \\ &w_i(0,x) = \overset{0}{w}_i(x) \end{aligned} \tag{2.73}$$

Also another variable has been defined, $\hat{w}_i^t$-calculated molar deviation of *i*-th element for time $\hat{t}$ and diffusion coefficients $D_1,\ldots,D_r$. Calculations were performed using the Danielewski-Holly model (equation 2.73) for the following data:

- initial molar deviation distributions of elements $\overset{0}{w}_1(x),\ldots,\overset{0}{w}_r(x)$ in the alloy;
- time of process duration;

- $\overset{0}{w}_1,\ldots,\overset{0}{w}_r$ – (experimental) molar deviation distributions of the elements in the alloy after the time $\hat{t}$. So the error function, *err,* was defined:

$$err(D_1,\ldots,D_r)=\int_{-\Lambda}^{\Lambda}\sum_{i=1}^{r}\left(\hat{w}_i(x)-\hat{w}_i^t(x)\right)^2 \qquad (2.74)$$

The computation of the diffusion coefficients was to minimize the function *err* in *r*-dimensional space, equation 2.74, where *r* is the number of elements in the alloy. Software was used to calculate the diffusion coefficient of each element in the alloy Co-Fe-Ni system combined from sequential quadratic programming [48], multi-dimension downhill simplex method [49], and evolutionary operation algorithm [50].

Experimentally Cobalt, Iron and Nickel (99.98 pct purity) were used as initial materials. The binary alloys Co-Ni and Fe-Ni were induction melted to form 1 cm diameter rods. After 48 hours at 1573 K in argon atmosphere the rods were sectioned into discs of 1 mm thick with a diamond impregnated cut-off wheel to have parallel faces. The compositions of materials were determined by a chemical analysis and the level of homogeneity of materials used in subsequent diffusion experiments were determined by Energy Dispersive X-ray analysis (EDX). The actual compositions of samples used for diffusion experiments were Co–51.3±0.1 wt% Ni and Fe–51.9±0.1 wt% Ni. The couples were heat treated in argon atmosphere at temperatures and for the periods of time shown in the Table 2.7. The partial oxygen pressure was lower than 10^{-6} atm. The concentration profiles were analysed by point-to-point counting techniques.

Diffusion Couple	T [K]	Time [h]
P_1	1273	68
P_2	1323	50
P_3	1373	140
P_4	1423	85
P_5	1473	59
P_6	1523	24
P_7	1588	17
P_8	1588	131

Table 2.7 The examined diffusion couple

As a result the diffusion couples investigated in Table 2.7 and the experimental concentration profiles in the Co-Fe-Ni system for several diffusion couples were presented in the Figure 2.20. The average intrinsic diffusion coefficients of Co, Fe and Ni were calculated and presented in Table 2.8. The diffusion coefficients of cobalt, iron and nickel in the range 1373–1588 K followed Arrhenius equation Figure 2.21:

$$D = D_o \exp\left(-\frac{Q}{RT}\right) \tag{2.75}$$

The preexponential factor D_o , activation energy Q and its error were calculated and presented in Table 2.9. The calculated diffusivities of Co, Fe and Ni showed good agreement with the results of other authors for the ternary Co-Fe-Ni system [51] and for the binary Fe-Ni [52, 53, and 54], Co-Fe [53] and Co-Ni [55, 56, and 53] alloys, Figure 2.22.

T [K]	D_{Fe} (cm^2/s)	D_{Co}(cm^2/s)	D_{Ni}(cm^2/s)
1273	4.97×10^{-12}	1.53×10^{-12}	7.86×10^{-13}
1323	1.78×10^{-11}	3.83×10^{-12}	3.42×10^{-12}
1373	5.78×10^{-11}	1.53×10^{-11}	1.14×10^{-11}
1423	1.21×10^{-10}	3.44×10^{-11}	2.67×10^{-11}
1473	3.22×10^{-10}	1.06×10^{-10}	5.14×10^{-11}
1523	4.86×10^{-10}	1.43×10^{-10}	1.23×10^{-10}
1588	1.2×10^{-9}	4.28×10^{-10}	2.35×10^{-10}

Table 2.8 Calculated average intrinsic diffusion coefficients

Element	Q $kJmol^{-1}$	D_o cm^2/s
Fe	289 ± 13	4.62
Co	304 ± 13	4.45
Ni	301 ± 13	2.38

Table 2.9 Activation energy and preexponential factor for Co-Fe-Ni alloy in the range 1273-1588 K

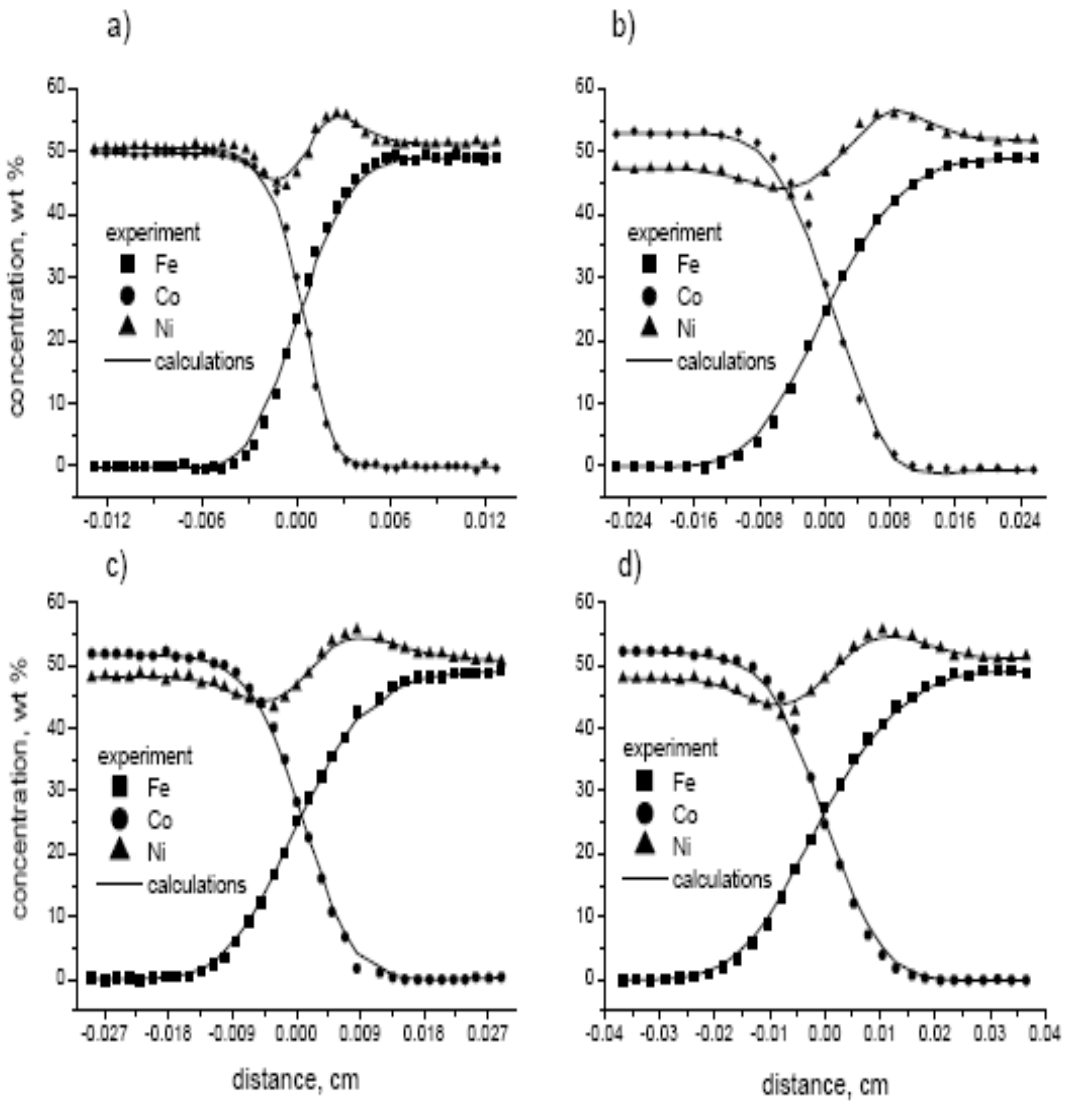

Figure 2.20 Interdiffusion in the Co-Fe-Ni diffusion couples: (a) P2 1323 K after 50 hours; (b) P3 1373 k after 10 hours; (c) P4 1423 K after 85 hours; (d) P5 1473 K after 59 hours [51]

Figure 2.20 demonstrate the experimental and calculated concentration profiles of Co, Fe and Ni using the Danielewski-Holly model and intrinsic diffusivities from the Table 2.7 are compared.

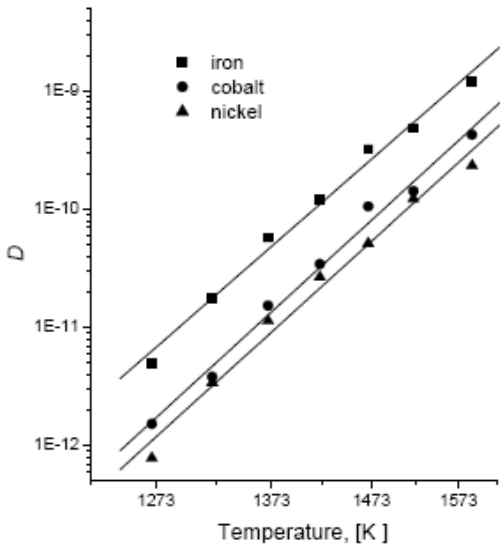

Figure 2.21 Temperature dependence of Co, Fe, and Ni intrinsic diffusivities in the Arrhenius plot [51]

Figure 2.21 shows the diffusion coefficients of cobalt, iron and nickel in the range 1373–1588 K followed Arrhenius equation (equation 2.75).

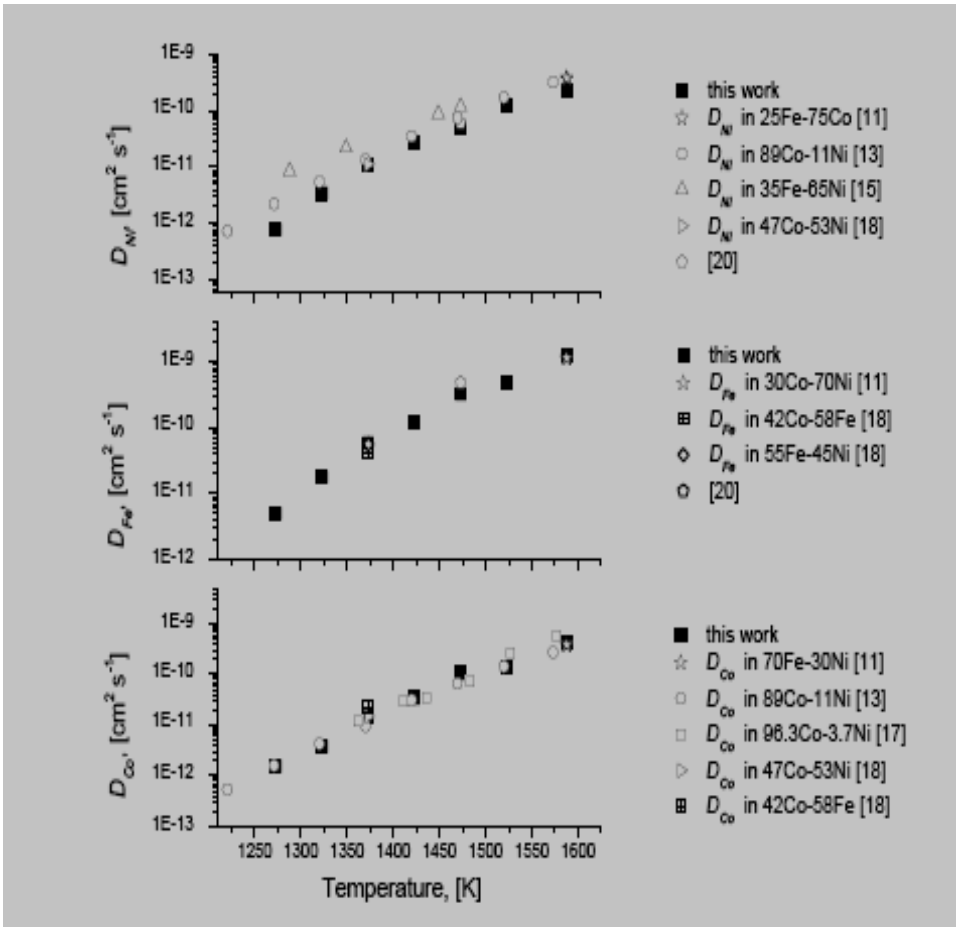

Figure 2.22 the intrinsic diffusion coefficients by different authors in Co-Fe-Ni alloys for different temperatures [51]

Figure 2.22 showed good agreement between the calculated intrinsic diffusivities of Co, Fe and Ni with the results of other authors for the ternary Co-Fe-Ni system [51] and for the binary Fe-Ni [52, 53, and 54], Co-Fe [53] and Co-Ni [55, 56, and 53] alloys.

The GDM of interdiffusion allows a quantitative description of complex diffusion transport process for an unlimited number of elements. It allows calculate the diffusivities and concentration profiles both for the infinite and finite system. Using the Danielewski-Holly model, the interdiffusion in the Co-Fe-Ni system was analysed and satisfied agreement of the calculated concentration profiles and the experimental. The calculated Iron intrinsic diffusivity is higher than Ni and Co, and was in good agreement

with data for the binary systems [52- 53]. The values of activation enthalpy of Co, Fe and Ni are similar and the errors were estimated to be less than 5%.

Filipek [42] presented the ternary system Cr-Fe-Ni as a practical application of Generalized Darken model (GDM) of interdiffusion. The evolution of the Cr-Ni was steeled because of its oxidation, i.e., the interdiffusion in open system due to reaction at the boundary. The computer simulation of interdiffusion process in binary Au-Ni alloy system in which diffusivities markedly vary with composition was shown.

2.9.6. Intrinsic Diffusivities in Cr-Fe-Ni Alloys

Filipek [42] performed computer simulations of interdiffusion process for open and closed systems in order to determine the intrinsic diffusivities. For calculations the following data were used:

- atomic masses of Cr, Fe and Ni;
- global concentration in the alloy: c= 0.146 mol cm^{-3};
- the initial density profiles were shown in Figure 2.23(dotted lines);
- experimental density profiles [59] were shown in Figure 2.23(points);
- the diffusional couple was formed by two alloy pellets of thickness Λ=400 μm each;
- annealing time ~ = 168 hours.

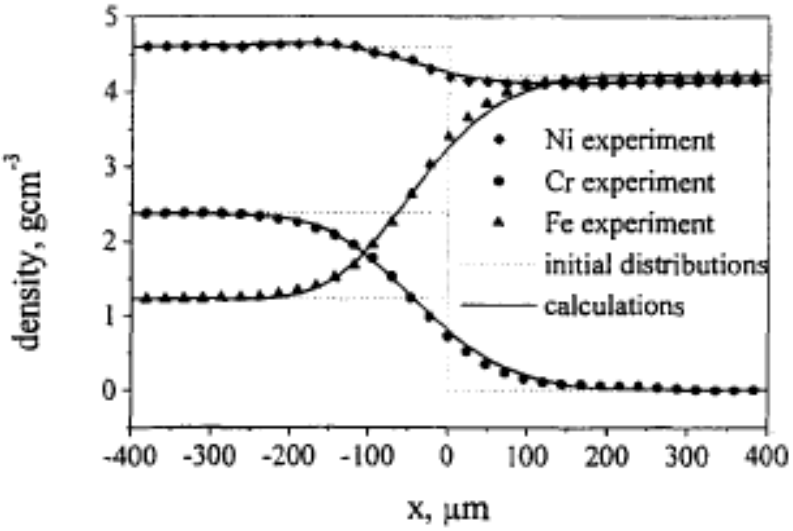

Figure 2.23 Comparison of the experimental [59] (points) and calculated (solid lines) density profiles of Cr, Fe and Ni in 32Cr- 16Fe-Ni/152Fe-Ni diffusional couple at 1373 K after 168 hours of diffusion annealing. Dotted lines represent initial distributions of the components

In Figure 2.23 the measured and calculated density profiles of Cr, Fe and Ni in the 32Cr-16Fe-Ni/52Fe-Ni diffusion couple are shown. Reasonable agreements of the results were obtained from the generalized model of interdiffusion with experimental data.

The intrinsic diffusivities of Cr, Fe and Ni were calculated using original software [43] and are shown in Table 2.10.

Diffusional couple	Intrinsic Diffusivities		Cm^2s^{-1}
32Cr-16Fe-Ni/52Fe-Ni	D_{Cr}	D_{Fe}	D_{Ni}
168 h [9]	$8.8x10^{-11}$	$2.9x10^{-11}$	$2.3x10^{-10}$

Table 2.10 Calculated intrinsic diffusivities in Cr-Fe-Ni system at 1373 K

2.9.7. Interdiffusion in the Binary Au-Ni Alloy (Variable Diffusion Coefficients)

The Au-Ni alloys were investigated by Reynolds *et al.* [60]. They determined the intrinsic diffusivities of gold and nickel in a wide range of nickel composition Figure 2.24. The author approximated Reynolds' data by the following function:

$$D_i = A_i \exp\left(B_i y + C_i y^2\right) \tag{2.76}$$

where A_i, B_i, C_i are the coefficients of approximation, i={Ni, Au} and y denotes nickel's mole fraction. In Table 2.11 the estimated values of coefficients A, B and C for nickel and gold are shown:

	Coefficients in Equation (82)		
Component	A,cm^2s^{-1}	B	C
Ni	9.39×10^{-10}	3.48	-8.13
Au	7.22×10^{-10}	5.16	-11.27

Table 2.11 Estimated values of coefficients A, B, C in equation 2.76 for nickel and gold

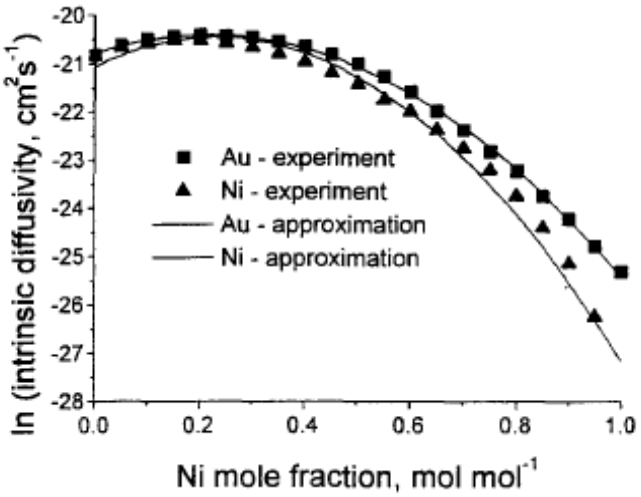

Figure 2.24 Intrinsic diffusivities of gold and nickel as a function of nickel mole fraction [60] at 1173 K

In Figure 2.24 the comparison of experimentally determined intrinsic diffusivities [60] and approximated by equation 2.76 was shown. For a simulation of interdiffusion in Au-Ni diffusional couple the following data were used:

1. total concentration in alloy c=0.12 mol cm^{-3};
2. variable intrinsic diffusivities of Au and Ni (equation (2.76) and Table 2.11;
3. Times of observation (process duration), 1, 5, 24 and 85 hours.

As a result the generalized model of interdiffusion in multicomponent open systems was presented. The method of calculation of the intrinsic diffusivities in the multicomponent system was also shown.

2.10. Conclusions

It is clear from the literature review that interdiffusion is a serious problem in many situations associated with the use of coatings at elevated temperatures. Substrate / coating interdiffusion can allow the migration of coating elements, critical for the

formation of protective scales, to the substrate and thus affecting adversely the efficiency of the coating. Equally the substrate coating interdiffusion can allow the incorporation of the damaging elements (from the substrate) within the coating raising the stress, initiating precipitation and delaying the processes of scale development. Hence an understanding of the processes of interdiffusion and the prediction of the effects of interdiffusion is essential for the design, development of coatings and assessing their performance. Thus interdiffusion modelling is a key issue and forms a significant part of this project. This project involves studies and modelling of interdiffusion.

However, most high performance coatings are multi-components in nature. The literature review clearly shows that modelling in multi-component systems is not easy and indeed no significant work has been done in this area except the recent work at Northumbria [39].

Attempts have been made by Datta *et. al* [39] in our group at Northumbria to model interdiffusion in multi component systems using the Generalised Darken method (GDM) with mixed successes. The limitations of Darkens method elaborated in chapter 3 clearly indicates the necessity of finding an alternative method of modelling interdiffusion which allows the inclusion of the cross-terms in the diffusion matrix:

$$\begin{bmatrix} D_{11} & D_{12} & \cdots & D_{1n} \\ D_{21} & D_{22} & \cdots & D_{2n} \\ \vdots & \vdots & \vdots & \vdots \\ D_{m1} & \cdots & \cdots & D_{mn} \end{bmatrix}$$

and also allows the consideration of composition dependent diffusion coefficients.

CHAPTER THREE

Design, Development, Preparation and Microstructure Analysis of the Coating Systems Considered

CHAPTER THREE

3.1. System Studied

This chapter discusses the systems which have been studied in this project. A range of systems varied in complexity have been considered. The systems studied included;

(1) carburization of iron (at 950^{o}C)

(2) Cu-Ni alloys

(3) Three component $Pt-Ni$ - aluminide system

(4) Multicomponent $Pt-Ni$ -aluminide coatings on MAR M002 System

(5) Ir and IrPt-Low Activity Aluminide/ MAR M002 System

(6) Four component systems - $TiAlCrY/TiAl$ system (subjected to oxidation at 750^{o}C), $Al_2Au/TiAl$ (subjected to oxidation at 750^{o}C) and formation of aluminised coatings on low alloy steels at 650^{o}C.

The first two systems were selected because of their simplicity and so that these can be used as standards for the diffusion modelling work. The three components and multicomponent $Pt-NiAl$ systems are extremely impotent systems in aerospace applications and much is known about these materials and much work has been done [39] in Northumbria including in this project. No modelling using numerical method has been attempted previously on these systems.

$TiAlCrY/TiAl$ and $Al_2Au/TiAl$ are newly developed coatings. Interdiffusion modelling has urgently needed on these materials to assess their performance. A part from the modelling effort this work required involvement in oxidation studies.

The systems involving the formation of aluminise coatings on low alloy steels represents an interesting case where interdiffusion modelling has allowed the

optimisation of the coating processes. Coatings were produced using varying processes parameters, pack compositions, activators processing temperatures and diffusion modelling played a significant role in producing the coatings with optimised process variables. In this area both the experimental and modelling work needed to be undertaken to select and optimise the high temperature processes parameters to apply the pack process to produce the coatings.

Interdiffusion modelling has been performed in two ways: microstructural modelling (where appropriate) and numerical modelling. It is important to point out microstructural modelling was undertaken to gain improved understanding the diffusion processes involved in the processing and property enhancing treatments. Numerical modelling was undertaken to develop methodologies to solve diffusion problems in multicomponent coating systems and to predict quantitatively the concentration profiles of the components of the coatings following interdiffusion at high temperatures.

Studies of these systems and modelling of the processes of interdiffusion in them constitute the main themes of this thesis.

3.2. Nonsteady-State Diffusion of Iron Carburized at 950^{o} C, 7.1 Hours

3.2.1. Introduction / Background Information

Carburizing involves addition of carbon to the surface of low-carbon steels (0.2% C) at temperatures generally between 850 and 950°C (1560 and 1740°F) with the aim of increasing surface hardness of steels. Austenite, with its high solubility for carbon, is the stable crystal structure at this temperature. High hardness is achieved by changing $\gamma \rightarrow$ martensite at the surface causing case hardening of the surface. The Carbon content of the surface reaches to ~ (0.8 to 1%) C.

3.2.2. Carburizing Methods

There are various methods for carburization of steel surfaces;

- Solid carburizing
- gas carburizing
- liquid carburizing
- plasma carburizing

In this project the focus on gas carburizing process. In this process a hydrocarbon gas e.g. CH_4 is used to provide carbon source. The most important parameters defining the carburization processes are;

- the temperature
- duration of the process
- depth of carbon penetration

Clearly the process involves diffusion of carbon through the surface. Diffusion equations have been solved for this system using both the analytical and numerical techniques (chapter 6). This system has been modelled using Runge-Kutta of order two and four (Figure 6.5). It was not necessary to use Genetic Algorithms method in this case because of the diffusion coefficient of carbon was available from the analytical solution ($D_C=1.6x10^{-11}m^2/s$).

3.3. A Binary Solid - Solid Diffusion System (Cu-Ni System)

3.3.1. Introduction /Background Information

A binary solid – solid diffusion system (*Cu-Ni*) alloy has been selected for diffusion analysis. Diffusion studies have been carried out using diffusion couples (3.2.2). Following is the copper - nickel phase's diagram.

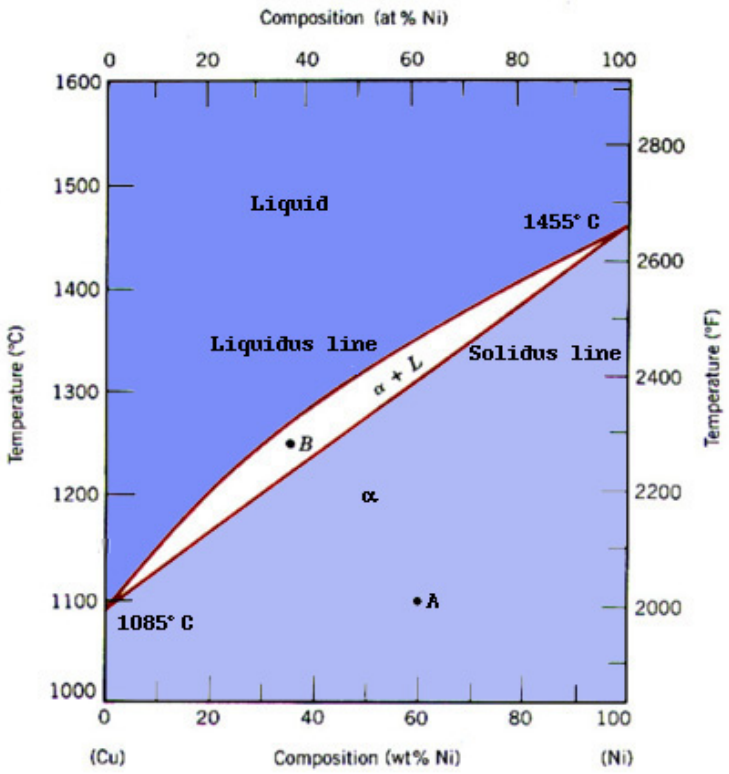

Figure 3.1 The copper-nickel phase's diagram

The system shows the formation of a single phase solid solution.

3.3.2. Formation of a Cu - Ni Diffusion Couple, Diffusion Treatment and Analysis

A Cu-Ni diffusion couple was made by welding together the two metals copper and nickel. In the plane of the weld shown in the centre of Figure 3.2, a number of fine Mo wires were incorporated in the diffusion couple. These wires served as inert markers by means of study the diffusion process. Copper and nickel had separated by the plane of weld. The specimen has been hardened at a temperature close to the melting point of the metals constituting the bar. Upon cooling the specimen to room temperature, it was placed in a lathe and thin layers parallel to the weld interface which removed from the bar. Each layer was then analysed chemically and the results plotted to give a curve showing schematically the composition of the bar as a function of distance along the bar as shown in Figure 3.3.

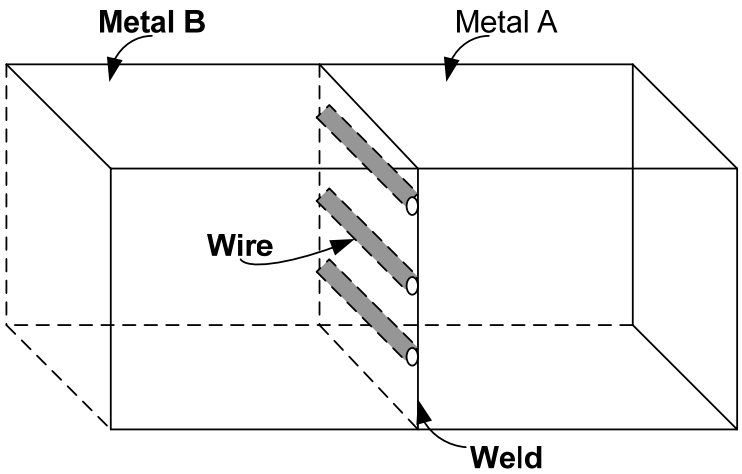

Figure 3.2 Kirkendall diffusion couple

The interesting result which obtained was that the wires moved during the diffusion process.

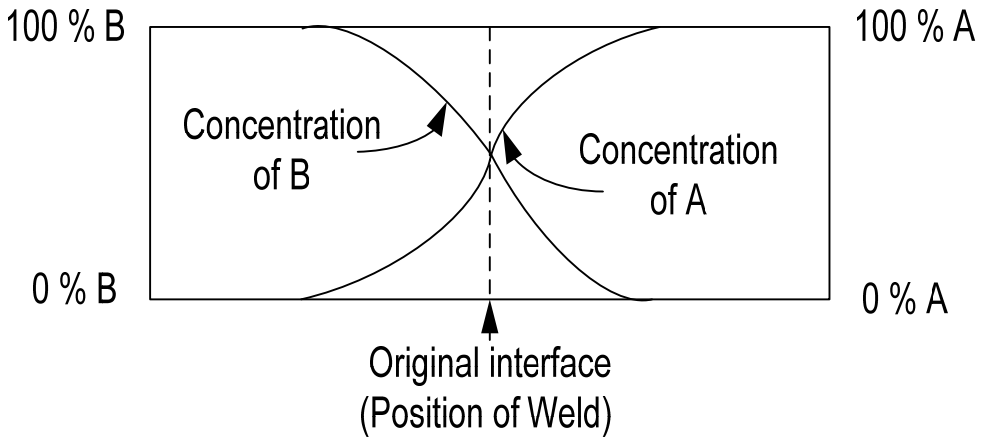

Figure 3.3 The curves showing concentration as a function of distance along a diffusion couple

Diffusion modelling for this system has been done previously [91] by analytical method. Using the analytically derived diffusion coefficient $D_{Cu}=8.35x10^{-10}cm^2/s$, the numerical modelling has been performed (chapter 6). Using the GAs technique, copper diffusion coefficient has been optimized. This optimized value has been used to determine the numerical concentration profile. The GAs method has been used to optimize D values assuming D is variable (concentration dependent), with a second order polynomial (equation 6.23).

3.4. Pt-Ni-Al Solid Alloy System Containing Three Elements

3.4.1. Introduction / Background Information

Interdiffusion studies have been carried out in a solid alloy system. In performing diffusion studies the samples were produced as follows: 2 mm thick slices were cut from an extruded $\beta - NiAl$ bar and polished up to 0.25 μm diamond pest [61]. An 8.0 ± 0.5 μm thick layer of Platinum was electroplated on the specimens. Such prepared diffusion couples, consisting of $\beta - NiAl$ and Pt coating, were heat treated at a constant temperature 1273 K in an argon atmosphere ($a_{O_2} \langle 10^{15} atm$) for 60 minutes.

The couples were sectioned for the purpose of analysing the concentration profiles which were measured using the EDS technique.

This system has been modelled and discussed in chapter 6 section 6.3. Trial and error technique has been used to calculate the diffusion coefficients for nickel and platinum (Figures 6.21 and 6.22). The GAs method has also been used to estimate constant diagonal D values for Ni, Figure 6.24, and Pt, Figure 6.25, constant cross and diagonal D values, Figure 6.27, and variable cross and diagonal D values, Figure 6.29. Additionally the fminbnd command in MATLAB has been used to optimise nickel diffusion coefficient (considering diagonal term) (Figures (6.31- 6.34). Finally Simplex search method as shown in Figures 6.35 and 6.36 has been used to optimize D value for nickel (D_{11Ni}) and using both diagonal and cross terms respectively.

3.5. Nickel Aluminise Coatings on MAR M002 Superalloys

3.5.1. Introduction / Background Information

Super alloys represent a class of materials which are considered as high temperature structural materials. In this class of alloys, Ni-base super alloys have received particular attention because of their suitability for use in aero engines as turbine blade components. These components in service encounter extreme external conditions –high tensile load, aggressive environments combined with the presence of high temperatures imposed by heating and cooling cycles of the engines.

Ni-base superalloys are the most highly designed structural alloys. Ni-base superalloys contain such elements as $Al, Ti, Cr, Co, Mo, W,$ Re, $Ta,$ and C. The main strengthening mechanism in cast superalloys is by precipitation hardening by coherent $\gamma' - Ni_3(Al, Ti)$ of volume fraction of 0.5 to 0.7. The matrix is $\gamma - Ni$. Cr

which is mostly in solid solution in $\gamma - Ni$ confers solid solution hardening and resistance to high temperature oxidation; and hot corrosion resistance is due to the formation of a slow-growing Cr_2O_3 . It is well known that the addition of Al forms a thermo dynamically stable Al_2O_3 scale capable of increasing the resistance to high temperature corrosion. The addition of Al is problematic. Due to the high amount of Al necessary to form Al_2O_3 it is difficult to achieve optimum strength and toughness. Another complication is that Al reduces the solubility of Cr in the matrix which adversely affects the resistance to hot corrosion. Thus Al is added merely to increase the strength of the alloy.

To overcome these problems and provide Ni-base superalloys with adequate strength, and resistance to high temperature corrosion, the approach has been to produce a coating based on Ni- aluminide $\beta - Ni\,Al$ to the alloy surface to form MAR M002.

Nickel aluminide coatings are the most extensively used intermetallic coatings. Nickel aluminide is an ordered intermetallic and exists over a composition range of 45 – 60 at % Al [62]. Because of its high oxidation resistance coupled with low density, nickel aluminide is used as a structural coating to stop the high temperature environmental degradation generally encountered in aero gas turbines.

The composition of gas turbine superalloys, optimized to supply a high content of the precipitation strengtheners (γ') in order to get sufficient creep resistance will adversely affect the high temperature corrosion resistance of these materials. Nickel aluminide coatings have been designed to confer the required corrosion resistance to the superalloys substrates.

3.5.2. Production of Nickel Aluminide Coatings on MAR M002 Superalloys

These coatings are produced by two types of pack processes [63, 64]. In one version the component is located in contact with a pack consisting of aluminium, a halide activator $(NH_4Cl, NaCl\ or\ CrF_2)$ and inert filler and subjected to a diffusion treatment (for 2 to 24h) within a temperature range of 750 to 1000°C. The Al halide formed, assisted by the decay of the halide activator, undergoes dissociation on the surface allowing Al diffusion into the substrate and leaving halide ions free to react with more Al and cause the cycle to continue. A modification of this technique, worded "out-of-pack", is alike to the chemical vapour deposition process (CVD) in that the components to be coated are not in contact with the powder of the pack, the aluminum halide gas generated being transported over the component/substrate surface by a carrier gas [63].

The protectivity of aluminide $NiAl$ coatings stems from their ability to form $\alpha-$alumina $(\alpha - Al_2O_3)$ scale. $\alpha-$alumina has an hcp construction of oxygen anions with two thirds of the octahedral sites filled by trivalent cations.

The high temperature protection afforded by the $\alpha - Al_2O_3$ grades is due to the oxides having low concentrations and mobilities of both ionic and electronic defects [66]. The slow growth rate of the oxide is connected to its low nonstoichiometry and large band gap width, which makes electronic conduction hard. In the main, $\alpha - Al_2O_3$ acts as an ionic conductor in which both oxygen and aluminium are mobile [67, 68].

The efficiency of aluminide coatings in stopping high temperature corrosion is undermined by the incorporation within the scale of the outwardly diffusing, damaging substrate elements. The high activity aluminide coatings are inwardly grown make it

easy for this incorporation. The incorporation of the damaging elements is more difficult in the outwardly grown, low activity coatings [63]. The efficiency of aluminides is further compromised by the increased attack by impurities in combustion gases caused by engines operating on lower grade fuel and in harsher situations. The limitations in the use of conventional nickel aluminide coatings deposited on Ni-base superalloys, e.g., MAR M002, to provide oxidation and hot- corrosion resistance, are well known [69], and are as follows:

- It's massively low ductility at ambient temperatures
- The very great difficulty of manufacturing anything useful from them

3.5.3. Pt Modified NiA1 Coatings on MAR M002 Superalloys

There are some advantages of adding platinum to overcome these limitations. A main move forward was made by adding Pt to nickel aluminide coatings. Such coatings out-perform the unmodified conventional aluminide coatings [66]. Two major kinds of $Pt-Al$ coatings are used:

(1) a single phase structure with a continuous $PtAl_2$ surface layer; and

(2) a two phase $PtAl + (Ni, Pt)Al$ structure with changing quantities and morphologies of Pt rich phases and with changing quantities of extent of substrate intervention in the (Ni, Pt) layer.

The Pt aluminide coatings have been found to show better oxidation resistance and a greater resistance to type-I [63] hot corrosion and a marginal development in type-II hot corrosion resistance. There is an improved adherence of a slow growing $\alpha - Al_2O_3$ scale, avoiding spallation and cracking, this is a major factor. This improvement in general, is considered to be due to:

- encouragement of the selective oxidation of Al;
- a capability for the oxide to regenerate following spallation, linked with enchanced Al diffusion in the coating;
- the creation of an Al reservoir during the attraction of Al for Pt;
- the inhibition of the coating/substrate interdiffusion;
- the barring or limiting the concentration of the substrate refractory elements in the outer zone of the coatings-such as elements undermine the integrity of the coatings;
- a decrease in the oxide growth stresses.

3.5.4. Production of Pt Modified NiA1 Coatings on MAR M002 Superalloys

The nominal composition of the superalloy MAR M002 is presented in Table 3.1. The platinum-modified coatings were prepared by Chromalloy (UK) Limited. Rod shaped specimens, $25\,mm$ in length and $6\,mm$ diameter, were coated with a platinum aluminide which normally contains $35-55\,\%\,Pt$. Initially, a layer of platinum was electroplated on the alloy surface. After a diffusion treatment, the surface was aluminized in a high activity pack. Following cooling, all the specimens were then diffusion heat treated for 1 hour at 1371 K in argon. Ultimately, all the specimens were thermally aged for 16 hours at 1143 K to precipitate the support gamma prime phase. Following heat treatment the specimens were washed in purified water and then ultrasonically cleaned in acetone, followed by hot air drying prior to testing.

Cr	Al	Ti	Co	W	Ta	Mo	Hf	Fe	Zr	B	C	Ni
9	5.5	1.5	10	10	2.5	0.5	1.25	<0.5	0.1	0	0	Bal

Table 3.1 Nominal chemical composition of MAR M002 substrate material ($wt\%$)

Some of the prepared specimens were diffusion annealed at selected temperatures in the 1073-1373 K temperature range in argon atmosphere. For the reason that the studied alloys have precipitations at the gamma phase the average concentration profiles of the components have been determined using the EDS (Energy Dispersive Spectrometer) technique.

3.5.5. Failure Mechanisms of *Pt*- Modified Coatings

Although the life of superalloys coated with $Pt-$modified coatings have been significantly improved, these coatings will eventually suffer failure. These coated superalloys are predominantly used as components in aircraft turbine engines which are normally operated at temperature $(>980^{o}C)$ during cruising with temperatures transiently increasing to $(>1200^{o}C)$ with the possibility of engine overheating. Thermal barrier coatings are used as protection against high temperature degradation mechanisms. However the exposure of the components to such high temperatures and for long periods will adversely affect the structural suitability of the materials and of the ceramic topcoat.

The dominant failure mechanics identified include:

- oxidation and hot corrosion
- coating substrate interdiffusion

High temperature degradation of coated $Ni-$base superalloys have been studied extensively [62]. The oxidation and hot corrosion failure mechanics of coated $Ni-$superalloys have been established and are well known [70]. In contrast, the coating / substrate interdiffusion processes responsible for some major failures have not been studied extensively. The main problem lies in the difficulty in quantifying the interdiffusion processes in multi-component systems such as coated $Ni-$base superalloys. This study has been undertaken to remedy this situation.

Thus the most critical issue is still the migration incorporation of the substrate elements and their incorporation in the coating and in the scale. The design of high performance $Pt-$modified $Ni-$ aluminide coatings requires information on coating / substrate elements interdiffusion.

These coatings constituted an important system for the present study. Interdiffusion processes in such systems have been modelled numerically using constant diagonal terms, constant diagonal and cross terms and variable diagonal and cross terms in the diffusion matrix. Optimization of the diffusion coefficients used was done using GAs technique given in chapter 6. The detailed analyses of GAs method have been presented in chapter 5.

3.6. Studies of *Ir* and *Ir*/*Pt* Low- Activity Aluminid / MAR M002 System: Assessment of the Oxidation Resistance and Microstructural Aspects / Modelling of Diffusion Process involved at (1100^{o}C)

3.6.1. Introduction / Background Information

The superior performance of the *Pt*-modified *Ni* aluminide coatings have been discussed in the previous section. It is to be noted that a stable oxide of *Pt* is not formed

and *Al* is relatively mobile in *Pt*-rich phases [71]. Thus *Pt* helps to create a reservoir of *Al* in the outer portion of the coating promoting an easy formation of the protective layer of Al_2O_3 [72]. The major disadvantage of *Pt* is that it is very expensive. Because of the high cost implication of *Pt*, attention has been focussed on replacing *Pt* by other noble metals for example Pd, Rh, and Ir. While the performance *Pd* , and *Rh* modified $Ni-$aluminide coatings have been reported [73], the performance of Ir modified coatings have not been extensively discussed. Fisher and Datta [74, 75] have manufactured and produced Ir-modified $Ni-$aliminide coatings on MAR M002 substrate and studied their oxidation performance after exposure to air at 1100^{o}C.

3.6.2. Production of Ir and IrPt Modified Coatings on MAR M002 System at 1100^{o}C

A number of MAR M002 directionally superalloy buttons (diameter 20 mm, width 5 mm) were sputter-coated with approximately 7 μm of Ir and then heat-treated for 1 hour at 1100°C. Half of the button samples were then electroplated with 7 μm of Pt and then heat-treated for 1 hour at 1100°C. The samples were then aluminized, Figure 3.4, using a high temperature, low-activity, out-of-pack process.

The oxidation performance of the coatings was evaluated using isothermal soaks at 1100°C for 25, 100 and 250 hours. The soaks were conducted using carbolite tube furnaces in still laboratory air. Both the as-processed and aged coatings were assessed using optical microscopy, SEM and XRD techniques.

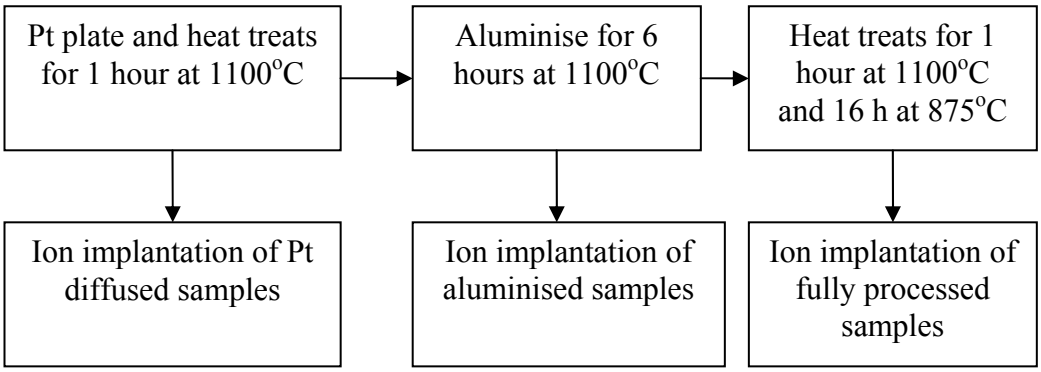

Figure 3.4 Schematic diagram of the production process for the samples

Interdiffusion processes in these systems have been modelled numerically using constant diagonal diffusion coefficient for the all the components (Al, Cr, Ir, Ni) and (Al, Cr, Ir, Ni, Pt). Variable diffusion matrix (diagonal and cross terms) have been also optimised using GAs technique. The detailed analyses of GAs method has been presented in chapter 5.

3.7. Aluminise Coating on low Alloy Steels at 650°C

3.7.1. Introduction / Rational for Development of Aluminise Diffusion Coatings

It is widely recognized that the higher efficiency of the steam power plants can be achieved by increasing the operation temperature above 650°C. The commonly used 9*Cr*-1*Mo* steels or the improved low alloy steels will suffer oxidation degradation in air or in steam at 650°C. To prevent such degradation coatings are needed.

It has been demonstrated by Xiang and Datta [76] and by others [77] that formation of surface coatings by pack process is one of the most elegant methods of creating

protective coatings. The approach was to enrich the surface with *Al* by pack cementation to form *Fe*- aluminide on low alloy steel [78, 79].

Most of the pack processes so far have been carried out at higher temperatures (900^{o}C). Only recently pack coatings have been used by Xiang and Datta [80, 81] on 2.25*Cr*-1*Mo* steel at 600 to 750^{o}C where effects of some process variables such as type of activator, pack composition and temperature have been investigated. $AlCl_3$ was found to be an effective activator.

3.7.2. Formation of Coatings

With this objective aluminide coatings were deposited on steel substrates *(Fe*-9*Cr*-1.0*Mo*-0.1*C*) using a pack deposition process. Steel samples measuring 20x10x2 mm cut, ground, degreased and weighed were pack aluminized. The powder mixtures for aluminizing contained suitable amounts of powders of *Al*, Al_2O_3 and $AlCl_3$.

The process was carried out in the following stages:

Firstly the sample fixed in pack powder was heated at 850^{o}C, secondly it was then heated at 150^{o}C for 1 hour, thirdly further heating at 650^{o}C for a predetermined time, and fourthly, the processed sample taken out of the furnace and weight change determined.

3.8. Studies of Interdiffusion Modelling in Al_2Au and TiAlCrY Coated Ti45Al8Nb Subjected to Air Oxidation at 750^{o}C for 1000 Hours for Al_2Au Coatings and 500 Hours for TiAlCrY Coatings

3.8.1. Introduction / Background Information

γ-*TiAl* and TiAl based alloys are a class of novel, promising materials for automotive, energy and aerospace applications. The specific stiffness and strength, of

these materials as compared to their low weight, potentially lead to large weight savings (50%) compared to the *Ni* base alloys. However, the major obstacles for wider uses of TiAl based materials are their susceptibility to severe environmental attack in oxidising, sulphidising, and hot corrosion environments at elevated temperatures of more than 650 °C.

The need to raise the service temperature and combat the oxidation, wear and corrosion problems of γ-TiAl materials has promoted extensive development of high temperature protective thin films for this class of materials. With this in mind a large EU project (InnovaTiAl) was initiated with University of Northumbria at Newcastle as one of the main partners. This project has several themes. The main themes are:

- Development of high performance coatings;
- Studies of the high temperature (700-900^{o}C) corrosion behaviour of the developed coating;
- Studies of their mechanical behaviour;
- Modelling of the processes of deposition and modelling of the response of these coatings to stress, temperature and environmental interactions including interdiffusion processes.

Under InnovaTiAl several high performance coatings have been developed: TiAlCrY; Al_2Au; CrAlYN/CrN+CrAlYON etched by Cr; CrAlYN/CrN+CrAlYON etched by CrAl; CrAlYN/CrN+CrAlYON etched by Y etc. The substrate material chosen in this project is Ti45Al8Nb.

New methods of producing coatings have been developed by the partners of InnovaTiAl project. These methods included Unbalanced Closed-Field Magnetron Sputtering System (UBM), and High Power Impulse Magnetron Sputtering System (HIPIMS).

However in our own study attention has been focussed on two coatings – Al_2Au and TiAlCrY deposited on Ti45Al8Nb. The study addresses the interdiffusion modelling issues surrounding oxidation of these coatings on Ti45Al8Nb at 750^oC for various times up to 1000 hours. Modelling of the interdiffusion processes involved was performed both by microstructural analysis and by numerical methods.

The rationale for selecting these coatings to prevent high temperature corrosion (700-900^oC) of materials in oxidising, sulphidising environments, is based on the fact that Al_2O_3 and Cr_2O_3 oxide scales are essential to provide the required degree of protection against environmental attacks. Thus an Al_2Au coating has been developed on the basis that in high temperature oxidising/sulphidising environments Al will oxidise to form a protective Al_2O_3 scale and gold is a novel material and its oxides will not affect the performance of Al_2Au coatings.

In the case of TiAlCrY coatings the expection was that Al and Cr will form protective Al_2O_3 and Cr_2O_3 scales; additionally Y was introduced to enhance the selective oxidation of aluminum.

3.8.2. Studies of Al_2Au Coatings – Production and Oxidation (750^oC up to 1000 Hours)

3.8.2.1. Production of Al_2Au Coatings

We investigated an *Al_2Au* phase demonstrating Zintl phase, (Zintl phases were named for the German chemist Eduard Zintl who investigated them in the 1930's [83]), with a cubic *CaF_2* structure. *Al_2Au* is hard and brittle at room temperature: it shows plastic deformation and possibility self-lubrication at high temperatures. The melting point for *Al_2Au,* which is the thermally most stable intermetalic phase within *Al-Au*

phase diagram, is 1060 ^{o}C, whereas the other phases $AlAu_2$, Al_2Au_5, and $AlAu_4$ show melting temperatures between 525 and 625 ^{o}C.

The Al_2Au coating used in this study was deposited using an unbalanced d. c magnetron sputtering system on Ti45Al8Nb material in argon atmosphere at 0.2 *Pa*. The substrate temperature, bias voltage and sputter power was 300 ^{o}C, 50*V* and 380W. Prior to deposition, all substrates (Ti45Al8Nb) used were metallographically ground, polished and ultrasonically cleaned with ethylene and acetone. After target (Al, Au) pre-cleaning and ion etching of the substrates within the deposition chamber, coatings in the thickness range between 0, 1, 7 μm were deposited [84]. The coated test specimens were approximately 15 *mm* in diameter and two mm thick with polished appearance and 0.5 mm hole near the rim to allow for platinum wire to be threaded for suspending the samples for subsequent tests.

3.8.2.2. Oxidation Studies of Al_2Au Coatings at 750^{o}C for 1000 Hours

The experiment in oxidising environment (pO_2=0.21 atm) was carried out discontinuously in the static air in an open tube at 750°C for 1000 hours. Heating rate was then 10^{o}C/min in order to reach 750^{o}C. The oxidation experiment was performed using a number of specimens. The ultrasonically cleaned and prepared samples were weighed to get the initial mass of the sample. To measure the mass gain, the following equation has to be applied;

$$M_2-M_1=M \qquad (3.1)$$

where M_2 is the mass after certain time (1000 hours), and M_1 is the initial mass, so M is the mass gain. The samples were withdrawn from the furnace periodically after a predetermined time, and weight changes measured, providing information on the kinetics of oxidation. After the experiment the furnace was cooled down to room temperature at the natural rate, by switching off the power supply. All exposed samples

were analysed by scanning electron microscope (SEM) and energy dispersive X-Ray spectroscopy (EDS).

3.8.3. Studies of TiAlCrY Coatings: Production and Oxidation at 750^{o}C up to 500 Hours

3.8.3.1. Production of TiAlCrY Coatings

The TiAlCr and TiAlCrY (Y as a dopant element was introduced in order to improve the selective oxidation of Al [85]) coatings with the composition of Ti43Al13Cr at % were produced by an unbalanced close field magnetron sputtering system. The TiAlCr coatings consist of γ-TiAl and TiAlCr Laves phase. The high content of Cr was introduced in order to produce Cr_2O_3 and enhance the selective oxidation of Al [86]. The sputtering parameters were as follows; argon pressure 0.2 Pa, power density ca. 4.2 W/cm^2, and substrate temperature 250^{o}C. Zhaolin *et*. *al*. note [87] that Ti-Al-Cr alloys containing a minimum of 8-10% Cr exhibite excellent oxidation resistance due to the formation of continuous Al_2O_3 scale.

3.8.3.2 Oxidation Studies of TiAlCrY Coatings at 750^{o}C for 500 Hours

Oxidation experiments were carried out in the static air (pO2=0.21atm) in an open tube at 750°C for 500 hours with a series of specimens. Heating rate was 10^{o}C/min in order to reach 750^{o}C. Each sample was weighed before the start of the experiment then periodically withdrawn and weighed. The weighed change was determined by equation 3.1. All exposed samples were examined using SEM surface, SEM cross – section and EDS analysis.

These coatings (Al_2Au and TiAlCrY coated Ti-45Al8Nb) composed an important system for the present study. Interdiffusion processes in these coatings have been modelled numerically using constant and variable diagonal and cross terms in the diffusion matrix. Optimization of the diffusion coefficients used was done using the GAs technique. The detailed analyses of the GAs method have been presented in chapter 5.

CHAPTER FOUR

Mathematics of Diffusion

CHAPTER FOUR

This chapter discusses some numerical techniques which are applicable to solve Fick's diffusion equations. Emphasis has been placed on these techniques which have been used in the present work.

4.1. Fick's Diffusion Laws

Diffusion is a time-dependent process. When we know how quickly diffusion takes place, we know the rate of mass transfer. This rate is usually expressed as a diffusion flux (J) [89, 90]

$$J = \frac{M}{At} \tag{4.1}$$

where (M) is the mass of a diffusing species through and perpendicular to a unit cross-sectional area (A) of solid per unit time (t). The units of (J) are kilograms or atoms per metre squared per second ($(kg/m^2.s)$ or (atoms/$m^2.s$). Equation 5.1 in differential form can be expressed as follows:

$$J = \frac{1}{A}\frac{dM}{dt} \tag{4.2}$$

If the diffusion flux does not change with time, a steady-state situation exists. One general case of steady-state diffusion is the diffusion of atoms of a gas through a plate

of metal for which the concentrations C of the diffusing types on both surfaces of the plate are supposed constant.

When the concentration (C) (which is usually expressed in weight percent $at\%$ or atomic percent $at\%$), is plotted against position or diffusion distance, within the solid x, the resultant curve is termed as the concentration profile. The slope at a particular point on this curve is the concentration gradient or penetration curve:

$$\text{Concentration gradient} = \frac{dC}{dx} \tag{4.3}$$

It is typically most suitable to express concentration (C) in terms of mass of diffusing types per unit volume of solid (kg/m^3 or g/cm^3).

The mathematics of steady-state diffusion in a single direction (x) is fairly straightforward, the flux is proportional to the concentration gradient as shown by the expression:

$$J = -D\frac{dC}{dx} \tag{4.4}$$

This equation is known as Fick's first law.

The constant of proportionality D is known as the diffusion coefficient, which is expressed in square metres per second. The negative sign in equation 4.4 designates that the direction of diffusion is down the concentration gradient, from a high to a law concentration. Equation 4.4 is Fick's first law, it fits the experiential fact that the flux goes to zero as the specimen becomes homogeneous or reaches equilibrium. The concentration can be given in a variety of units, but the flux must be expressed in consistent units.

Generally the practical diffusion circumstances are always in non-steady state. That is, the diffusion flux and the concentration gradient at some particular point in a solid differ with time. This is demonstrated in Figure 4.1, which shows concentration profiles at three different diffusion times.

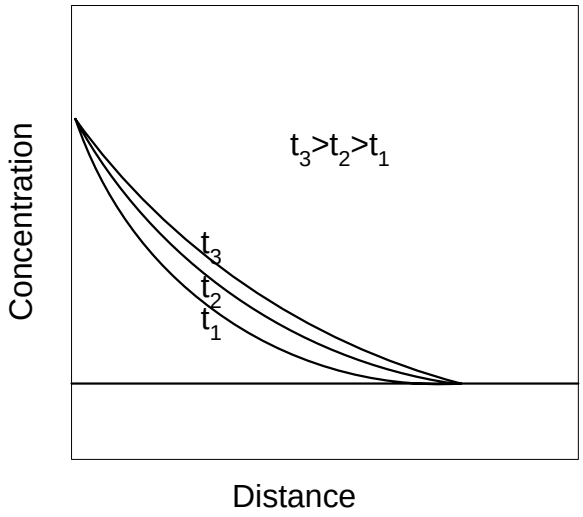

Figure 4.1 concentration profile for nonsteady-state diffusion taken at three different diffusion times t_1, t_2, and t_3

So under a nonsteady-state condition, using equation 4.4 is no longer suitable, it becomes necessary to consider the partial differential equation:

$$\frac{\partial C}{\partial t} = \frac{\partial}{\partial x}\left(D\frac{\partial C}{\partial x} \right) \tag{4.5}$$

This is known as Fick's second law. If the diffusion coefficient is independent of composition, then equation 4.5 simplifies to:

$$\frac{\partial C}{\partial t} = D\frac{\partial^2 C}{\partial x^2} \tag{4.6}$$

Equation 4.6 known as Fick's second law when the diffusion coefficient is constant [89, 90, 91, 92].

4.2. Solutions of Fick's Second Law

Fick's second law can be solved by analytical and numerical methods.

4.2.1. Analytical Solutions

One of the solutions of equation 4.6 (Fick's second law), for a semi-infinite solid, that is none of the diffusion atoms reaches the end of the bar when diffusion processes begin a function of position (diffusion distance), and time when the boundary conditions are specified. This is shown in Figure 4.2.

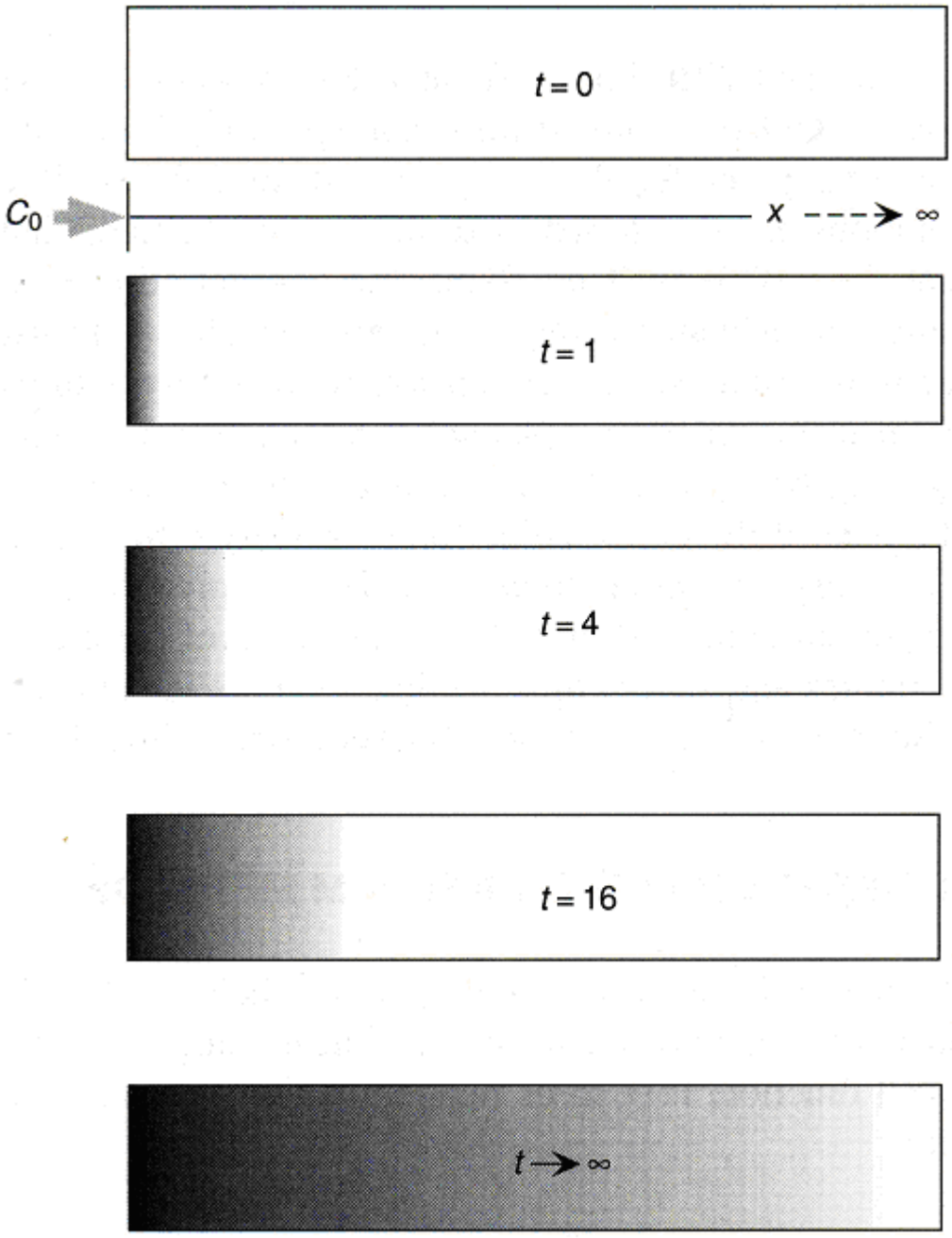

Figure 4.2 One dimensional diffusion into a semi-infinite medium. The concentration at $x = 0$ is maintained for all time at fixed value C_o while the diffusant spreads toward the right

The boundary conditions are:

For t=0, $C=C_o$ at $0 \leq x \leq \infty$ (4.7.a)

For t>0, $C=C_s$ at x=0 (4.7.b)

$C=C_o$ at $x=\infty$ when surface concentration is constant (5.7.c)

Applying these boundary conditions to Fick's second law (equation 4.6), then the solution becomes as follows:

$$\frac{C_x - C_o}{C_s - C_o} = 1 - erf\left(\frac{x}{2\sqrt{Dt}}\right) \tag{4.8}$$

where C_x is the concentration of the diffusion atoms at the location x below the surface and after time t, erf is the Gaaussian error function of the variable x [89]. The Gaaussian error function is defined by

$$erf\,(z) = \frac{2}{\sqrt{\pi}} \int_0^z e^{-y^2}\, dy \tag{4.9}$$

where $x/2\sqrt{Dt}$ has been replaced by the variable z. The values are given in a mathematical table for various $x/2\sqrt{Dt}$ values:

z	erf(z)	z	erf(z)	z	erf(z)
0	0	0.55	0.5633	1.3	0.934
0.025	0.0282	0.6	0.6039	1.4	0.9523
0.05	0.0564	0.65	0.642	1.5	0.9661
0.1	0.1125	0.7	0.6778	1.6	0.9763
0.15	0.168	0.75	0.7112	1.7	0.9838
0.2	0.2227	0.8	0.7421	1.8	0.9891
0.25	0.2763	0.85	0.7707	1.9	0.9928
0.3	0.3286	0.9	0.797	2	0.9953
0.35	0.3794	0.95	0.8209	2.2	0.9981
0.4	0.4284	1	0.8427	2.4	0.9993
0.45	0.4755	1.1	0.8802	2.6	0.9998
0.5	0.5205	1.2	0.9103	2.8	0.9999

Table 4.1 Tabulation of error function values

A second solution can be found in a plane source by differentiation as follows [90]:

$$C = \frac{A}{t^2}\exp(-x^2 / 4Dt) \tag{4.10}$$

where A is an arbitrary constant, for equation 4.6, Fick's second law, and when the diffusion takes place in one dimension and D is constant. Equation 4.10 is symmetrical with respect to:

$x = 0$

That is it tends to zero as x approaches infinity in the positive and negative side for $t > 0$, and for $t = 0$ it vanishes everywhere except $x = 0$, it becomes infinite. If the diffusion (or diffuser) is allowed to spread into two material bodies occupying the half-spaces $0 < x < \infty$ and $-\infty < x < 0$, which have an equal and constant diffusivity, this is shown in Figure 4.4, we obtain the following equation [90]:

$$M = \int_{-\infty}^{\infty} C dx \tag{4.11}$$

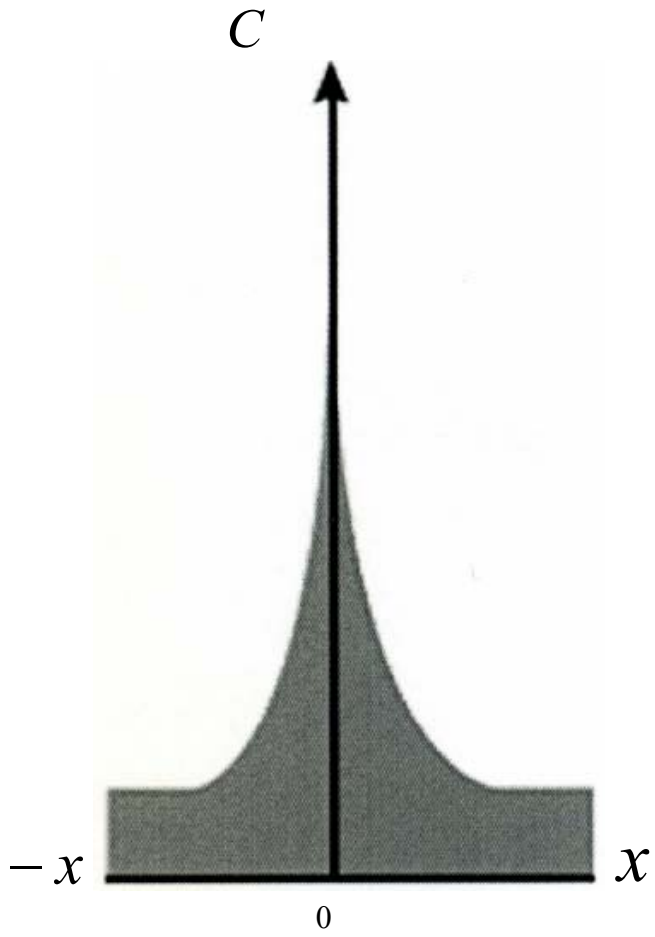

Figure 4.3 the substance (M) diffusing to the positive and negative side.

That is the whole substance M diffusing in an infinite length and unit cross section is known by. And if

$$x^2 / 4Dt = \xi^2 \tag{4.12}$$

$$\frac{2x\ dx}{4D\ t} = 2\xi\ d\xi \tag{4.13}$$

$$dx = 4Dt\xi\ d\xi / x \tag{4.14}$$

$$dx = \frac{4Dt\xi d\xi}{\sqrt{4Dt\xi^2}} = \frac{4Dt\xi d\xi}{2\xi(Dt)^{1/2}}$$

$$dx = 2(Dt)^{1/2} d\xi \tag{4.15}$$

So equation 4.11 becomes, using equation 4.10 and equation 4.15, as follows:

$$M = \int_{-\infty}^{\infty} \left(\frac{A}{t^{\frac{1}{2}}} \right) \exp\left(\frac{-x^2}{4Dt} \right) dx \tag{4.16}$$

$$M = 2AD^{\frac{1}{2}} \int_{-\infty}^{\infty} \exp(-\xi^2)\, d\xi = 2A(\pi D)^{\frac{1}{2}} \tag{4.17}$$

$$A = \frac{M}{2(\pi D)^{\frac{1}{2}}} \tag{4.18}$$

Equation 4.17 explains that the substance diffusing remains constant and equal to the amount of substance deposited in the plane $x = 0$.

Therefore, substituting A from equation 4.18 in equation 4.10, we get

$$C = \frac{M}{2(\pi Dt)^{\frac{1}{2}}} \exp(-x^2 / 4Dt) \tag{4.19}$$

Equation 4.19 is therefore the solution of Fick's second law which explains the spreading by diffusion of an amount of substance M deposited at time $t = 0$ in the plane $x = 0$. Figure 4.5 shows typical distributions at three successive times.

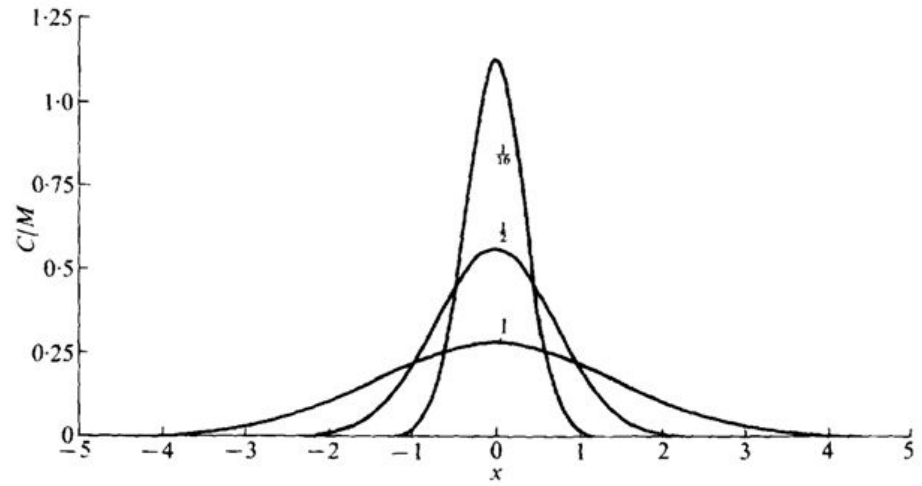

Figure 4.4 Concentration-distance curves for an instantaneous plane source. Numbers on curves are values of Dt

However, the analytical methods or solutions are not always possible, especially when the equations are not linear and contain variable coefficients. Further difficulty arises when the degree of the equation is higher than the first degree. Under this situation numerical methods need to be adopted to deal with the problems where there is no analytical solution available. Numerical methods have no such limitation. The solution is as a tabulation of the values of the function at a variety of values of the independent variable. In this project the numerical methods such as Euler's method, Modified Euler's method, and Runge-Kutta method of order four, which have been used are described in next chapters.

The next sections provide elaborations of Euler, Modified Euler, and fourth order Runge-Kutta numerical methods.

4.3. Taylor-Series Method, Euler Method, Modified Euler's Method and Runge-Kutta Method of Order Four

4.3.1. Taylor-Series Method

Taylor-series is not strictly a numerical method but from time to time it is used in combination with the numerical methods. Hence it is appropriate to start considering the Taylor-series. Consider this example [93]:

$$\frac{dy}{dx} = x + y \tag{4.20}$$

Considering the initial condition $y(x_o) = y_o$

$$x_o = 0$$
$$y_o = 1$$

The analytical solution is

$$y = 2e^x - x - 1 \tag{4.21}$$

This will be compared with the numerical result as follows:

The relation between y and x can be produced by finding the coefficients of the Taylor-series,

$$y(x)=y(x_o)+y'(x_o)(x-x_o)+\frac{y''(x_o)}{2!}(x-x_o)^2+\frac{y'''(x_o)}{3!}(x-x_o)^3+\cdots \tag{4.22}$$

If

$$x - x_o = h$$

Therefore the above series (equation 4.22) becomes as:

$$y(x) = y(x_o) + y'(x_o)h + \frac{y''(x_o)}{2!}h^2 + \frac{y'''(x_o)}{3!}h^3 + \cdots \qquad (4.23)$$

If Taylor- series uses the derivatives at zero, the series will be called a Maclaurin series.

When the initial condition is $y(x_o)$, (the first term is known from initial condition $y(0) = 1$. The coefficient of the second term can be calculated by substituting $x = 0, \quad y = 1$ into the equation 4.20 for the first derivative:

$$y'(x_o) = y'(0) = 0 + 1$$

The second and higher –order derivatives can be found by differentiating the equation 4.20. Each of these derivatives can be calculated corresponding to $x = 0$ to obtain the various coefficients:

$$\begin{aligned}
&y''(x) = 1 + y', && y''(0) = 1 + 1 = 2 \\
&y'''(x) = y'', && y'''(0) = 2 \\
&y^{iv}(x) = y''', && y^{iv}(0) = 2 \\
&\qquad\vdots && \qquad\vdots \\
&\vdots && y^{(n)}(0) = 2
\end{aligned}$$

Then the series solution for Y by substituting $x = h$ is as follows:

$$y(h) = 1 + h + h^2 + \frac{1}{3}h^3 + \frac{1}{12}h^4 + error \qquad (4.24)$$

The solution of equation 4.20 is given in Table 4.2:

X	y	y, analytical
0	1	1
0.1	1.1103	1.1103
0.2	1.2428	1.2428
0.3	1.3997	1.3997
0.4	1.5835	1.5836
0.5	1.7969	1.7974

Table 4.2 Tabulation of y values in the Taylor series and the analytical solution

In the above Table 4.2, the last two values in the column 2 and 3 the accuracy is not perfect, so it means we need more terms than we have considered obtaining four-decimal-place accuracy.

The error term of the Taylor-series after the term of h^4 is:

$$error = \frac{y^{(v)}\xi}{5!}h^5 \quad 0 < \xi < h \tag{4.25}$$

The error cannot be calculated here because the derivatives are known just at $x = 0$ and not at $x = h$. The Taylor-series is truncated when the contribution of the last term is negligible to the number of decimal places.

4.3.2. Euler and Modified Euler Methods

The Taylor-series method is difficult to apply if the various derivatives are complicated, and is also difficult to determine the error. So the application of Taylor's

method to a specific problem is complicated by the requirement to determine and calculate the high-order derivatives with respect to t.

It has been established that the error in Taylor's series will be small if the step size h (the interval beyond x_o where we evaluate the series), is small. If the step size h is small enough, only a small number of terms are necessary for good accuracy. The Euler method may be considered as following this plan, (only a small number of terms are necessary for good accuracy), to first order differential equations. So when h is small enough, then:

$$y(x_o + h) = y(x_o) + hy'(x_o) + \frac{y''(\xi)}{2}h^2, \qquad x_o < \xi < x_o + h \tag{4.26}$$

This equation has been written in the usual form of the error term for the truncated Taylor series. The value of $y(x_o)$ is given by the initial condition and $y'(x_o)$ can be calculated from $f(x_o, y_o)$, known from the differential equation:

$$\frac{dy}{dx} = f(x, y)$$

and then for $x = x_o + 2h$ after $y(x_o + h)$ has been found, then to $x = x_o = 3h$, etc. Assuming the subscript notation for the successive $y-$ values and demonstrating the error by the order relation, the Euler method algorithm could be written as:

$$y(x_o + h) = y(x_o) + hy'(x_o) + O(h^2)\ error \tag{4.27}$$

As an example, consider this simple equation (4.20):

$$\frac{dy}{dx} = x + y, \qquad y(0) = 1$$

It is suitable to organize the work as in Table 4.3. Let $h = 0.02$.

x_n	y_n	y'_n	hy'_n
0	1.0000	1.0000	0.0200
0.02	1.0200	1.0400	0.0208
0.04	1.0408	1.0808	0.0216
0.06	1.0624	1.1224	0.0224
0.08	1.0848	1.1648	0.0233
0.10	1.1081		

Table 4.3 Tabulation of y values from Euler method

Each of the y_n values is calculated using equation 4.27, adding hy'_n and y_n of the previous line in the above Table 4.3. Comparing the last result 1.1081 to the analytical answer $y(0.10) = 1.1103$, it can be seen that there is only two-decimal-place accuracy because the error is 0.0022. Therefore the difficulty with this mainly uncomplicated method is its lack of accuracy, requiring a very small step size h. In the simple Euler method, the slope at the beginning of the interval y'_n has been used to decide the increment to the function. So if the slope of the function were constant, the solution is a linear relation. Consequently the effort has been added to use an average slope over the interval to estimate the change in y with accuracy [93]. This is shown in Figure 5.6.

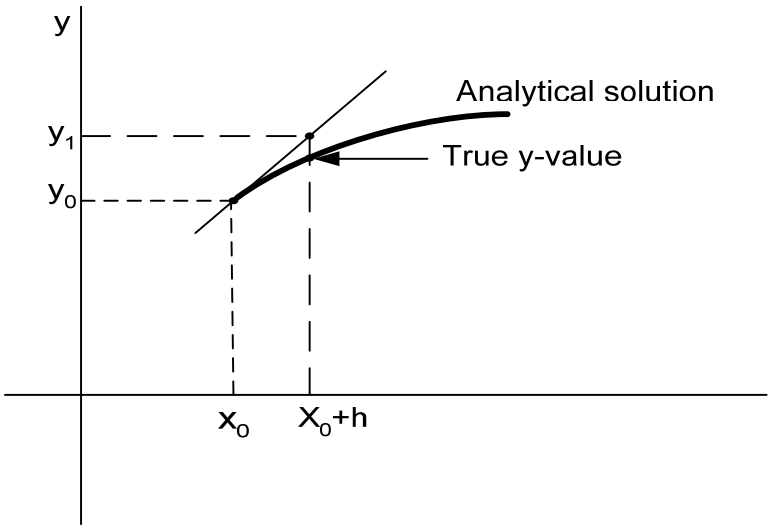

Figure 4.5 An improvement of Euler

Using the arithmetic average of the slopes at the beginning and end of the interval:

$$y_{n+1} = y_n + h\frac{y'_n + y'_{n+1}}{2} \qquad (4.28)$$

Consequently this gives an improved estimate for y at x_{n+1}. Equation 4.28 is the modified Euler method. Equation 4.28 cannot be used straight away, since the derivative y' is a function of x and y, so y'_{n+1} cannot be evaluated with y_{n+1} unknown. The Modified Euler-method overcomes the difficulty by approximating (or predicting) a value of y_{n+1} by the simple Euler-method shown in equation 4.27, and then use this value to calculate y'_{n+1}, giving an improved approximation (corrected value) for y_{n+1}. Hence the modified Euler-method is more efficient than Euler-method. This method also called Euler-predictor-corrector method, using the same example and earlier treatment. The solution using equation 4.27 is given in Table 4.4:

x_n	y_n	$y_n^{'}$	$hy_n^{'}$	y_{n+1}	$y_{n+1}^{'}$	$y_{av}^{'}$	$hy_{av}^{'}$
0	1.0000	1.0000	0.0200	1.0200	1.0400	1.0200	0.0204
				1.0204	1.0404	1.0202	0.0204
0.02	1.0204	1.0404	0.0208	1.0412	1.0812	1.0608	0.0212
				1.0416	1.0816	1.0610	0.0212
0.04	1.0416	1.0816	0.0216	1.0632	1.1232	1.1024	0.0220
				1.0636	1.1236	1.1026	0.0221
				1.0637	1.1237	1.1027	0.0221
0.06	1.0637	1.1237	0.0225	1.0862	1.1662	1.1449	0.0229
				1.0866	1.1666	1.1451	0.0229
0.08	1.0866	1.1666	0.0233	1.1099	1.2099	1.1883	0.0238
				1.1104	1.2104	1.1885	0.0238
0.10	1.1104						

Table 4.4 The solution using Modified Euler method

In this table, the corrected values of y_{n+1} have been tabulated in the same column as the predicted ones. $y_{av}^{'}$ is the mean of $y_n^{'}$ and the last value of $y_{n+1}^{'}$. The accuracy is 1 in the fourth decimal place. The error of the modified Euler method can be found by comparing with the Taylor series.

$$y_{n+1} = y_n + y_n^{'}h + \frac{1}{2}y_n^{''}h^2 + \frac{y^{'''}(\xi)}{6}h^3 , \qquad x_n < \xi < x_n + h \tag{4.29}$$

When we substitute the forward-difference approximation in the second derivative,

$$y^{''} = \frac{y_{n+1}^{'} - y_n^{'}}{h} \tag{4.30}$$

which has error of $O(h)$, and the error term as $O(h^3)$ is:

$$
\begin{aligned}
y_{n+1} &= y_n + h\left(y_n^{'} + \frac{1}{2}\left[\frac{y_{n+1}^{'} - y_n^{'}}{h} + O(h) \right] h \right) + O(h^3), \\
y_{n+1} &= y_n + h(y_n^{'} + \frac{1}{2} y_{n+1}^{'} - \frac{1}{2} y_n^{'}) + O(h^3), \\
y_{n+1} &= y_n + h\left(\frac{y_n^{'} + y_{n+1}^{'}}{2} \right) + O(h^2)
\end{aligned}
\qquad (4.31)
$$

The above equation (4.31) shows the error of one step of the modified Euler method is $O(h^3)$, and is called local error. The error will be accumulated from step to step; therefore the error over the whole range of application is called the global error and is $O(h^2)$. Since the number of steps into which the interval is subdivided is proportional to1/*h*; for this reason the order of the error is reduced to $O(h^2)$ on the continuing application.

4.3.3. Runge-Kutta Methods

An additional move forwards in efficiency and accuracy can be secured with a group of methods due to the German mathematicians Runge and Kutta. To express some thought of how Runge-Kutta methods are developed, the derivation of a second –order method is as follows:

$$
\begin{aligned}
y_{n+1} &= y_n + ak_1 + bk_2, \\
k_1 &= hf(x_n, y_n) \\
k_2 &= hf(x_n + \alpha h, y_n + \beta k_1)
\end{aligned}
\qquad (4.32)
$$

where

$$\frac{dy}{dx} = f(x, y)$$

The values k_1 and k_2 are the estimates of the change in y when x advances by h because they are the product of the change in x and a value for the slope of the curve, $\frac{dy}{dx}$ the Runge-Kutta method uses the first estimate of Δy the simple Euler method, the other estimates are taken with x and y moved up the fractions α and β of h and the earlier estimate of $\Delta y, k_1$. The difficulty is to create a method of choosing the four parameters a, b, α, β. Therefore equation 4.32 through Taylor-series expansion is as follows:

$$y_{n+1} = y_n + hf(x_n, y_n) + (h^2/2)f'(x_n, y_n) + \ldots$$

And since

$$df/dx = f_x + f_y\, dy/dx = f_x + f_y f$$

so

$$y_{n+1} = y_n + hf_n + h^2\left(\frac{1}{2}f_x + \frac{1}{2}f_y f\right)_n \qquad (4.33)$$

Equation 4.32, by substituting the definition of k_1 and k_2, becomes,

$$y_{n+1} = y_n + a\,h\, f(x_n, y_n) + bhf[x_n + \alpha h,\ y_n + \beta hf(x_n, y_n)] \qquad (4.34)$$

To construct the last term in equation 5.34 similar to equation 4.33, $f(x, y)$ in Taylor-series in term of x_n, y_n is

$$f[x_n + \alpha h, \beta\, h f(x_n, y_n)] = (f + f_x\, \alpha\, h + f_y \beta\, h\, f)_n \qquad (4.35)$$

In equations 5.33 and 5.35, f and its partial derivatives are all to be evaluated at (x_n, y_n).

When substituting from equation 5.35 into equation 5.34, we obtain the following:

$$\begin{aligned} y_{n+1} &= y_n + a\, h\, f_n + b\, h (f + f_x\, \alpha\, h + f_y \beta\, h\, f)_n \\ y_{n+1} &= y_n + (a+b)\, h\, f_n + h^2 (\alpha\, b\, f_x + \beta\, b\, f_y f)_n \end{aligned} \qquad (4.36)$$

Equation 4.36 is identical to equation 4.33 if

$$a + b = 1, \qquad \alpha\, b = \frac{1}{2}, \qquad \beta\, b = \frac{1}{2}$$

Therefore there are three equations and four unknowns, thus one value can be chosen arbitrarily, for example let $a = \frac{2}{3}$, then

$$b = \frac{1}{3}, \quad \alpha = \frac{3}{2}, \quad \beta = \frac{3}{2}$$

If $a = \frac{1}{2}$ then $b = \frac{1}{2}, \quad \alpha = 1, \quad \beta = 1$

and this last set of parameters presents a modified Euler algorithm: the modified Euler method is a special case of a second-order Runge-Kutta method.

A further move forwards in efficiency and accuracy can be achieved with Runge-Kutta method of order four as shown bellow:

$$
\begin{aligned}
y_{n+1} &= y_n + \frac{1}{6}(k_1 + 2k_2 + 2k_3 + k_4), \\
k_1 &= hf(x_n, y_n), \\
k_2 &= hf(x_n + \frac{1}{2}h, y_n + \frac{1}{2}k_1), \\
k_3 &= hf(x_n + \frac{1}{2}h, y_n + \frac{1}{2}k_2), \\
k_4 &= hf(x_n + h, y_n + k_3).
\end{aligned}
\tag{4.37}
$$

In the following section we are going to discuss briefly the application of Euler's method, modified Euler's method and Runge-Kutta method of order to Fick's second law.

As an example, when we solve $dy/dx = x + y, \quad y(0) = 1, \quad h = 0.1$

$$
\begin{aligned}
k_1 &= 0.1(0+1) = 0.10000, \\
k_2 &= 0.1(0.05+1.05) = 0.11000, \\
k_3 &= 0.1(0.05+1.055) = 0.11050, \\
k_4 &= 0.1(0.10+1.1105) = 0.12105, \\
y(0.1) &= 1.0000 + \frac{1}{6}(0.10000 + 0.2200 + 0.22100 + 0.12105) \\
&= 1.11034
\end{aligned}
$$

This agrees to five decimals with the analytical solution. The local error term for the fourth-order Runge-Kutta is $O(h^5)$: the global error would be about $O(h^4)$.

In the example problem $y' = x + y, \quad y(0) = 1$ the comparative results are shown in Table 4.5 for the y-value at $x = 0.1$.

Method	Step size	Result	Error	Number of function evaluations
Euler	0.02	1.1081	0.0022	5
Modified Euler	0.02	1.1104	0.0001	12
fourth-order Runge-Kutta	0.1	1.11034	0.00000	4

Table 4.5 Methods comparison result

4.3.4. Application of Euler Method, Modified Euler Method and Runge-Kutta Method of Order Four to Fick's Second Law

In this section applications of these numerical methods on Fick's second law (equation 4.6) when the diffusion coefficient D is constant are considered. Fick's second law is a partial differential equation. So initially the finite difference method has been used to convert equation 4.6 to an ordinary differential equation so that numerical methods can be applied:

$$\frac{\partial C}{\partial x} = \frac{C_{i+1} - C_i}{\Delta x} \tag{4.38}$$

$$\frac{\partial^2 C}{\partial x^2} = \frac{\dfrac{C_{i+1} - C_i}{\Delta x} - \dfrac{C_i - C_{i-1}}{\Delta x}}{\Delta x}$$

$$= \frac{C_{i+1} - 2C_i + C_{i-1}}{\Delta x^2} \tag{4.39}$$

So equation 4.6;

$$\frac{\partial C}{\partial t} = D\frac{\partial^2 C}{\partial x^2}$$

Converted when:

$$\Delta x = x_{i+1} - x_i$$

into:

$$\frac{\partial C}{\partial t} = \frac{D}{(\Delta x)^2}\left[C_{i+1} - 2C_i + C_{i-1}\right] \quad (i = 1,2,\cdots,n) \tag{4.40}$$

where D is the concentration independent diffusion coefficient when D is constant. So equation 4.40 can be explained if $i = 1,2,\cdots$ as follows:

$$\frac{\partial C}{\partial t} = \frac{D}{(\Delta x)^2}\left[C_2 - 2C_1 + C_o\right], \qquad i = 1$$
$$\frac{\partial C}{\partial t} = \frac{D}{(\Delta x)^2}\left[C_3 - 2C_2 + C_1\right], \qquad i = 2$$
$$\vdots$$

The equation 4.40 can be shown in matrix form as follows:

$$\begin{bmatrix} \frac{\partial C_1}{\partial t} \\ \frac{\partial C_2}{\partial t} \\ \vdots \\ \frac{\partial C_n}{\partial t} \end{bmatrix} = \frac{D}{\Delta x^2}\left\{\begin{bmatrix} -2 & 1 & \cdots & 0 & 0 \\ 1 & -2 & 1 & \cdots & 0 \\ 0 & 1 & -2 & 1 & \cdots \\ & \vdots & 1 & -2 & 1 \\ 0 & 0 & \cdots & 1 & -2 \end{bmatrix}\begin{bmatrix} C_1 \\ C_2 \\ \vdots \\ \vdots \\ C_n \end{bmatrix} + \begin{bmatrix} bd_o \\ 0 \\ \vdots \\ \vdots \\ bd_{n+1} \end{bmatrix}\right\} \tag{4.41}$$

where the $c_0 = bd_o$ and (bd_o, bd_{n+1}) are the boundary conditions. Therefore Fick's second law has been transformed to an ordinary differential equation. Then Euler's and modified Euler's methods are applicable now, which can be expressed respectively as follows:

$$C_{(x,t+h)} = C_{(x,t)} + h\left(\frac{\partial C}{\partial t}\right)_{(x,t)} \tag{4.42}$$

$$C_{(x,t+h)} = C_{(x,t)} + \frac{h}{2}\left\{\left(\frac{\partial C}{\partial t}\right)_{(x,t)} + \left(\frac{\partial C}{\partial t}\right)_{(x,t+h)}\right\} \tag{4.43}$$

It seems that by estimating a value of $C_{(x,t+h)}$ from Euler's method, and then using this value to determine $\left(\frac{\partial C}{\partial t}\right)_{(x,t+h)}$ we can then provide an improved or corrected value for $C_{(x,t+h)}$. By assuming (D) as a constant, the numerical solution of Fick's second law calculates the concentrations of diffusing species near the surface of the material as a function of time and distance.

Fourth-order Runge-Kutta method also can be applied on Fick's second law as follows:

$$C_{(x,t+h)} = C_{(x,t)} + \frac{1}{6}\left(K_1 + 2K_2 + 2K_3 + K_4\right) \text{[See Appendix B]} \tag{4.44}$$

Such that

$$K_1 = hf(t_n, C_n),$$
$$K_2 = hf\left(t_n + \frac{1}{2}h, C_n + \frac{1}{2}K_1\right),$$
$$K_3 = hf\left(t_n + \frac{1}{2}h, C_n + \frac{1}{2}K_2\right),$$
$$K_4 = hf\left(t_n + h, C_n + K_3\right)$$

where

$$f\left(t_n, C_n\right) = \left(\frac{\partial C}{\partial t}\right)_{(x,t)}$$

So K_1, K_2, K_3 and K_4 in terms of concentration are as follows:

$$K_1 = h\left(\frac{\partial C}{\partial t}\right)_{(x,t)}$$

$$K_2 = \frac{h}{2}\left\{\left(\frac{\partial C}{\partial t}\right)_{(x,t)} + \left(\frac{\partial C}{\partial t}\right)_{(x,t+h)}\right\}$$
$$K_3 = \frac{h}{2}\left\{\left(\frac{\partial C}{\partial t}\right)_{(x,t)} + \left(\frac{\partial C}{\partial t}\right)_{(x,t+2h)}\right\}$$
$$K_4 = h\left\{\left(\frac{\partial C}{\partial t}\right)_{(x,t)} + \left(\frac{\partial C}{\partial t}\right)_{(x,t+3h)}\right\}$$

Where

$$\left(\frac{\partial C}{\partial t}\right)_{(x,t)} = \frac{D}{\Delta x^2}\left\{\begin{bmatrix} -2 & 1 & \cdots & 0 & 0 \\ 1 & -2 & 1 & \cdots & 0 \\ 0 & 1 & -2 & 1 & \cdots \\ & \vdots & 1 & -2 & 1 \\ 0 & 0 & \cdots & 1 & -2 \end{bmatrix}\begin{bmatrix} C_1 \\ C_2 \\ \vdots \\ \vdots \\ C_n \end{bmatrix} + \begin{bmatrix} bd_o \\ 0 \\ \vdots \\ \vdots \\ bd_{n+1} \end{bmatrix}\right\}$$

Comparison between the modified Euler's method and the Runge-Kutta method of order four has been made in chapter 6, section 6.2 [nonsteady state diffusion -iron carburized at 950^o C, 7.1 hours].

4.4. Fick's Second Law for Variable Diffusion Coefficient (D)

In real situations the diffusion coefficient can be variable. The diffusion coefficient for a known composition can differ with time; it can change with composition. Since there is a concentration gradient, this means that (D) changes with position along the sample. In this case $C = D(x)$, and Fick's second Law (equation 4.6) must be written

$$\frac{\partial C}{\partial t} = \frac{\partial}{\partial x}\left(D\frac{\partial C}{\partial x} \right) \tag{4.45}$$

when the diffusion coefficient depends only on the concentration of diffusing substance. That is if the diffusion coefficient differs with concentration, it is also clear that the value of D assumed from the measurement of the steady rate of flow is some sort of mean value of variety of different concentrations. Thus, if D is a function of C, so the solution of equation 5.45 in one dimension becomes:

$$\frac{\partial C}{\partial t} = \frac{\partial}{\partial x}\left(D(C)\frac{\partial C}{\partial x} \right) \tag{4.46}$$

such that

$$C = C(\lambda) \quad \text{where} \quad \lambda = x/2\sqrt{t} \tag{4.47}$$

When we replace, equation 4.47, this converts the partial differential equation (equation 4.46) to ordinary differential equation in C and λ:

$$\begin{aligned} \frac{\partial C}{\partial t} &= -\frac{x}{4t^{3/2}}\frac{dC}{d\lambda} \\ \frac{\partial C}{\partial x} &= -\frac{1}{2t^{1/2}}\frac{dC}{d\lambda} \end{aligned} \tag{4.48}$$

And hence

$$\frac{\partial}{\partial x}\left(D\frac{\partial C}{\partial x}\right)=\frac{\partial}{\partial x}\left(\frac{-D}{2t^{1/2}}\frac{dC}{d\lambda}\right)=\frac{1}{4t}\frac{d}{d\lambda}\left(D\frac{dC}{d\lambda}\right) \tag{4.49}$$

So that finally equation 4.46 becomes

$$-2\lambda\frac{dC}{d\lambda}=\frac{d}{d\lambda}D\frac{dC}{d\lambda} \tag{4.50}$$

an ordinary differential equation which is known as Boltzmann equation [94, 95]. Equation 4.50 can be solved, provided the concentration is initially constant, and the boundary conditions are as follows:

$$\begin{aligned} C&=C_1, \qquad \lambda=-\infty, \\ C&=C_2, \qquad \lambda=+\infty \end{aligned} \tag{4.51}$$

Then the solution of equation 4.50 will be a unique solution of equation 4.6 (Fick's second law) [96, 97]. By differentiation equation 4.50 becomes:

$$-2\lambda\frac{d\lambda}{D}=\frac{dD}{D}+\frac{d^2C}{d\lambda^2}/\frac{dC}{d\lambda} \tag{4.52}$$

and integrating with respect to λ;

$$-\int_0^{\lambda}\frac{2\lambda}{D}d\lambda=\ln D+\ln\frac{dC}{d\lambda}+\ln k_1 \tag{4.53}$$

Integrating again gives the following equation, ($k_1 = \ln k_1$):

$$C = k_1 + k_2 \int_{-\infty}^{\lambda} \frac{d\lambda}{D} \exp \int_{0}^{\lambda} \left[-\frac{\lambda}{2D} d\lambda \right] \tag{4.54}$$

It seems that this is an integral equation, and there is not strictly a solution, because C becomes visible inside and outside the integral sign. In order to find the solution an examination solution must be done, $D(C)$ has to be evaluated numerically, then integrated numerically to obtain a new (C) and repeat awaiting (C) convergences. Equation 4.47 can be used when the diffusion takes place in infinite or semi-infinite media. The application of initial and boundary conditions,

$$C(x > 0, 0) = C_2 \text{ and } C(x < 0, 0) = C_1 \tag{4.54}$$

and

$$C(\infty, t > 0) = C_2 \text{ and } C(-\infty, t > 0) = C_1 \tag{4.55}$$

for the infinite media, and

$$C(x>0,\ t=0)=C_2 \qquad C(x=0,\ t=0)=C_1 \tag{4.56}$$

$$C(\infty,\ t>0)=C_2 \quad \text{and} \quad C(x=0,\ t>0)=C_1$$

for the semi-infinite media. The initial boundary conditions for the infinite and semi-infinite diffusion couples are stated in Figure 4.7,

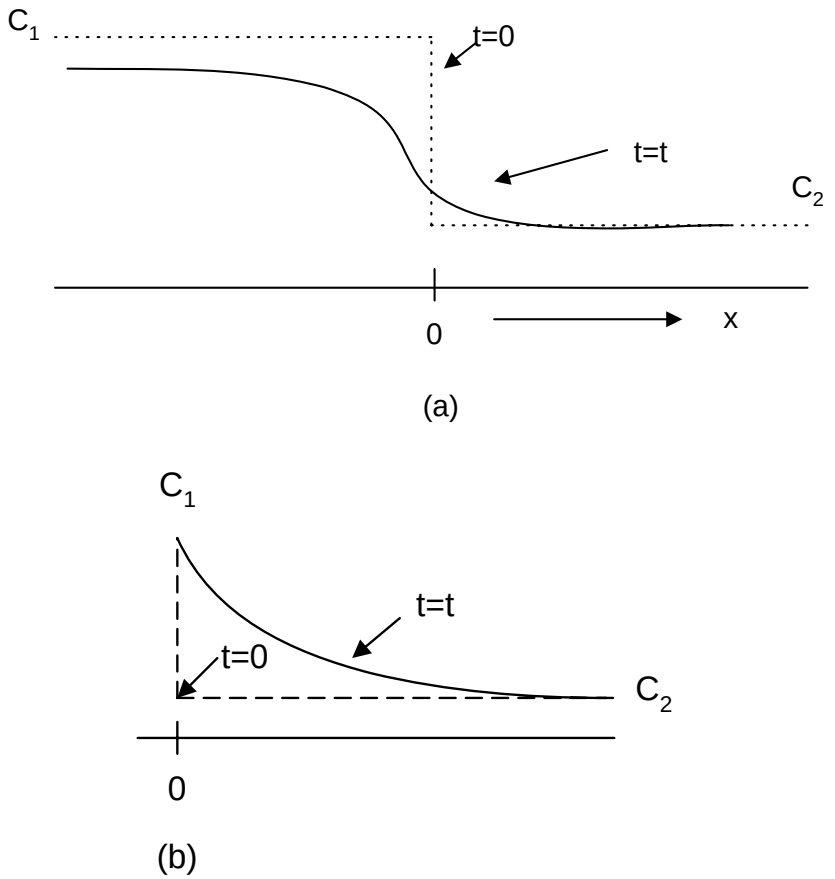

Figure 4.6 Boundary and initial conditions for: a) Infinite b) Semi-infinite diffusion couples

4.5. Comparison between the Experimental and Numerical Concentration

The method of least squares assumes that the best-fit curve of a given type is the curve that has the minimal sum of the deviations squared also known as least square error) from a given set of data.

Suppose that the data points are (x_1, y_1), (x_2, y_2), ..., (x_n, y_n) where x is the independent variable and y is the dependent variable. The fitting curve $f(x)$ has the

deviation (error) d from each data point, which means that $d_1 = y_1 - f(x_1), d_2 = y_2 - f(x_2), \ldots, d_n = y_n - f(x_n)$. According to the method of least squares, the best fitting curve has the property is shown by the following equation:

$$\prod = d_1^2 + d_2^2 + \ldots + d_n^2 = \sum_{i=1}^{n} d_i^2 = \sum_{i=1}^{n} \left[y_i - f(x_i) \right]^2 = a \min [98, 99, 100] \qquad (4.57)$$

Thus, a curve with a minimal deviation from all data points is desired. This best-fitting curve can be obtained by the method of least squares.

The Least squares method has been used to compare between the experimental and numerical concentration value for each component because, it can be practical without needing differential. Let Y_i corresponds to the experimental concentration for such a component, and y_i represents a numerical concentration value for the same component, consequently the error between the experimental and numerical concentration is as follows:

$$Error = \sum_{i=1}^{N} (Y_i - y_i)^2 \qquad (4.58)$$

Where N represents the number of points in the concentration profiles. Following that the error needs to be compared with the minimum error we set. If the error is close to the minimum error we set, then the diffusion coefficient value can be used to calculate the concentration profile. But if not, the error calculated in equation 4.58 is not close to the minimum error we set, then it indicates that the diffusion coefficient under consideration is not the optimum value that can be used to calculate the concentration profile for the component. Three optimization methods, Genetic algorithms method (GAs), bounded nonlinear function minimization (fminbnd), and Simplex method, can

be used to determine the optimum diffusion coefficient. These optimization methods have been investigated in chapter four in detail. The Genetic algorithms optimization method has been found be the best optimization method with the advantages that it can be used to find the optimal diffusion coefficient value, and the flow chart is in the Appendix C.

4.6. Conclusions

The use of three numerical methods - Euler method, Modified Euler method, and Runge-Kutta method of order four to solve Fick's second law to find the numerical concentration profile for each component in the system has been considered. Fick's second law is a partial differential equation: it has been shown how the finite difference method has been used to convert Fick's second law to an ordinary differential equation.

However to solve completely Fick's second law it would be necessary to optimize the diffusion coefficients. In the next chapter 6 we will discuss the optimization techniques that have been used in this thesis.

The Least squares method has been used to calculate the error between the experimental and numerical concentration for each component, and then we can compare this error with the error we set.

CHAPTER FIVE

Genetic Algorithms Method

CHAPTER FIVE

5.1. Introduction

The idea of evolutionary computing was introduced in 1960s by I. Rechenberg in his work "Evolution strategies", Evolutions strategies in original. His idea was further developed by other researchers. Genetic Algorithms (GAs) were invented by John Holland and developed by him and his students and colleagues [101]. This lead to Holland's book "Adaption in Natural and Artificial Systems" published in 1975. So Genetic Algorithms (GAs) was first introduced and analysed by John Holland (1975) and extended to functional optimisation by De Jong (1975) [102]. The GAs is a stochastic global search optimisation method.

Genetic Algorithms (GAs), (given by Goldberg 1989), [103] can be defined as search algorithms based on the mechanics of natural selection and natural Genetics. They combine “survival of the fittest” among string with a random structure. In every generation, a new set of artificial creatures (string) is created using bits and pieces of the fittest of the old: an occasional new part is tried for good measure. The GAs efficiently exploits historical information to speculate within new search points with expected improved performance. This method can handle a large number of parameters and also non-differentiable function. It is a stochastic iterative process, which is very robust in respect of the initial starting parameters estimates.

5.2. Outline of Genetic Algorithms

Genetic algorithms are stochastic search techniques based on the mechanism of natural selection and natural genetics. Genetic Algorithms differs from conventional search techniques, it starts with an initial set of randomly generated solutions called a

population. Each individual in the population is encoded as string, called a chromosome, representing a solution to the current problem. A chromosome is usually a string of symbols, such as binary bit string, ternary, integer, real valued etc. The chromosomes evolve through successive iterations, called generations. Each individual in the set generated, is assigned a fitness value by evaluating the fitness function for each individual, in order to create the next generation, new chromosomes, called offsprings. Offsprings are generated either by: a) merging two chromosomes from the current generation using a crossover operator or b) modifying a chromosome using a mutation operator. We select, according to the fitness values, some of the parents and offsprings and reject others in order to keep the number of chromosomes or population size constant. After a number of iterations the algorithms converge to the best chromosomes, which represent the optimum solution to the problem.

The outline of a traditional genetic algorithm is as follow:

- Initialise and encode a random population of chromosomes;
- Decode and evaluate each chromosome's fitness in the population;
- Reproduce a new generation by stochastically selecting current chromosomes as parents according to fitness to generate new children;
- Apply crossover and mutation operators to the new chromosomes;
- Repeat 2-4 until an adequate solution is found, (reproduction).

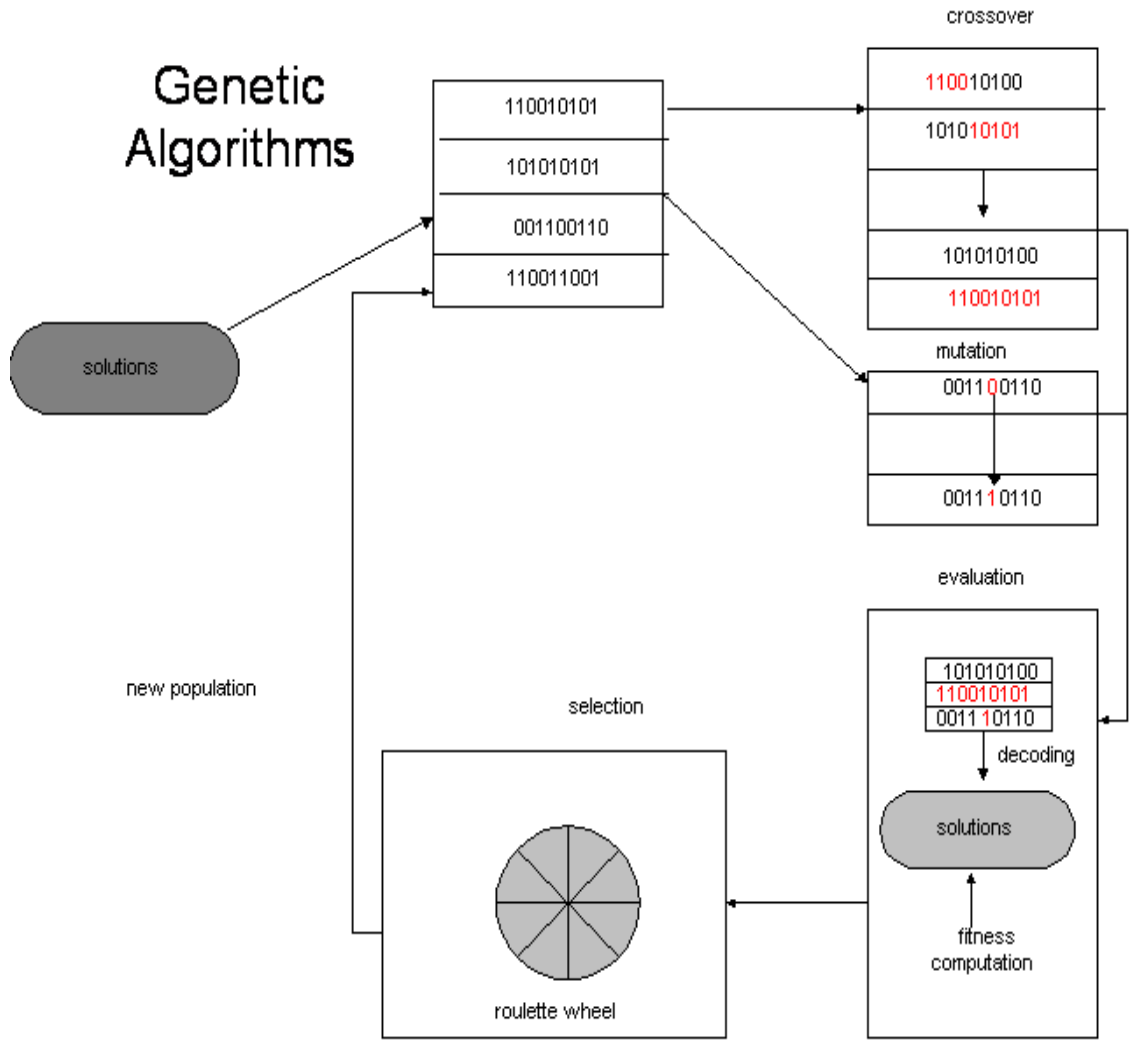

Figure 5.1 The general structure of Genetic Algorithms method

5.3. Genetic Algorithms versus Traditional Methods

The GAs method differs substantially from more traditional search and optimisation methods. The four most significant differences are [103]:

- GAs searchs a population of points in parallel, not a single point;
- GAs do not require derivative information or other auxiliary knowledge, only the objective function and corresponding fitness levels influence the directions of search;
- GAs use probabilistic transition rules, not deterministic ones;

- GAs works on an encoding of the parameter set rather than the parameter set itself except in where real-valued individuals are used.

It is notable that the GAs provides a number of potential solutions to a given problem and the choice of final solution is left to the user.

5.4. Major Elements of Genetic Algorithms

5.4.1. Population Representation and Initialisation

The GAs method operates on a number of encoding potential solutions, called a population, simultaneously. Thus, the encoding and decoding procedures are more relevant in the applications of the Genetic Algorithms. Typically, Genetic algorithms start their search with a population size, which is bounded between 30 and 100 individuals, however a variant called the micro GA uses very small populations, ≈ 10 individuals, with a restrictive reproduction and replacement strategy in an attempt to reach real-time execution [102].

Originally the most commonly used chromosome's representation in the GAs is the binary string. Here, each decision variable in the parameter set is encoded as a binary string of ones and zeros and these are ordered to form a chromosome. In addition, usually the binary strings used are of fixed length.

Although the binary-coded GAs is most commonly used, there is an increasing interest in alternative encoding strategies, such as integer and real-valued representations. For some problem domains it is argued that the binary representation is in fact deceptive in that it obscures the nature of the search [103].

The first step in the Genetic Algorithms method is to create an initial set of population. This can be achieved by generating the required size population using a random number generator that uniformly distributes numbers in the specific range. For

example, a binary population of M population whose chromosomes are of N bits long, $M \times N$ random numbers uniformly distributed from the set $\{0,1\}$ will be generated. However, an initial population can be seeded with individuals that are known to be in the range of the global minimum (maximum) [104, 105, and 106]. This is applicable if the nature of the problem is already well understood or if the Genetic Algorithms are used in connection with knowledge based system.

5.4.1.1. Binary String

In most applications of genetic algorithms, binary string representations are implemented to encode control variables. A binary string is defined using a binary alphabet $\{0,1\}$.An N-bit string belongs to a space $\mathrm{B}^N = \{0,1\}^N$. Each variable is encoded into a binary string of a particular, normally equal, length N_i defined by the user. So, the complete string has a length N :

$$N = \sum_{i=1}^{n} N_i \qquad (5.1)$$

where n is the number of variables. A binary string of length N_i has a total of 2^{N_i} search points. The string length used to encode a particular variable depends on the desired precision in that variable: normally the precision is equal for all the variables.

A typical encoding binary representation of n variables $\mathbf{x} = (x_1, x_2, \ldots x_n)$ can be illustrated as follows:

$$\overbrace{\underbrace{11001\cdots0}_{N_1}}^{x_1}\ \overbrace{\underbrace{1010\cdots0}_{N_2}}^{x_2}\cdots\overbrace{\underbrace{0110\cdots1}_{N_n}}^{x_n}$$

The variable x_1 has a string length N_1 and so on, usually all the strings have the same length. The binary representation of the variables allows genetic algorithms to be

applied to a wide variety of problems, because genetic algorithms deal with the string and not with the variables directly.

5.4.2. The Objective and Fitness Functions

The objective function is used to provide a measure of how individuals have participated in the problem domain. In the case of maximisation of the problem, the fit individuals will have the highest numerical value related to the objective function. This measurement of fitness is usually used as an intermediate step in order to induce the relative performance of individuals in a Genetic Algorithms. Another function, the relative fitness function, is usually used as an alternative of the objective function measure [104]. Thus the relative fitness function transforms the objective function value into a measure of relative fitness, thus:

$$F(x) = g(f(x)) \tag{5.2}$$

where f is the objective function, g transforms the value of the objective function to a non-negative number and F is the resulting relative fitness. The fitness function value corresponds to the number of an individual that can be a candidate to participate in the creation of the following generation. The most commonly used transformation is that of proportional fitness assignment [104]. Each individual fitness is evaluated as the individual's raw performance, $f(x_i)$, relative to the entire population as follows:

$$F(x_i) = \frac{f(x_i)}{\sum_{i=1}^{n} f(x_i)} \tag{5.3}$$

where n is the size of population and x_i is the phenotypic value of individual *i*. According to its relative fitness each individual has a probability of reproducing the next generation, however, this fitness assignment fails to account for negative objective function value. A linear transformation to offset the objective function [103] is usually used such that,

$$F(x) = af(x) + b \tag{5.4}$$

where a is a scaling factor, which is positive for maximising optimisation and negative for minimising optimisation, and b is used as offset factor to guarantee that the resulting fitness values are non-negative.

However, there are several scaling mechanisms that have been proposed, which are practically accepted [101, 102] such as Dynamic linear scaling, sigma truncation, power law scaling, and, logarithmic scaling.

5.4.3. Selection

Selection is one of the main operators used in Genetic Algorithms. Selection is the process of introducing the number of times a particular individual is selected for reproduction. This operator does not create any new solution; instead it selects relatively better solutions from the current population and deletes the remaining. Thus the selection provides the driving force in a genetic algorithm. The selection guides a genetic algorithm search in the direction of promising regions in the search space. Recently many selection methods have been introduced, examined, and compared such as Roulette wheel selection method, Tournament selection, Rank-based selection, Boltzmann selection, and other selection methods.

5.4.3.1. Roulette Wheel Selection

The simplest and most popular selection method is the Roulette Wheel selection method, which is a stochastic selection strategy. Each solution in the population occupies an area on the roulette wheel proportional to its fitness. Then the roulette wheel is spun as many times as the population size, each time selecting a solution marked by the roulette wheel pointer. Because the solutions are marked proportionally to their fitness, an individual with a higher fitness is always receiving more copies than an individual with a low fitness (see Figure 6.2).

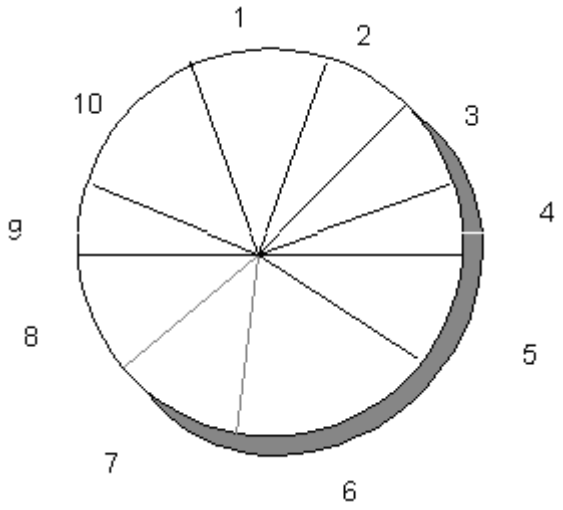

Figure 5.2 Roulette Wheel selection

5.4.3.2. Tournament Selection

A second popular method is the tournament selection. This procedure works by selecting randomly within a sub-population and allowing them to compete on the bases of their fitness. The individual in the sub-population with upper fitness wins the tournament, and then become the selected individual. All of the sub-population members are returned back into the general population, and the process is repeated [103, 107].

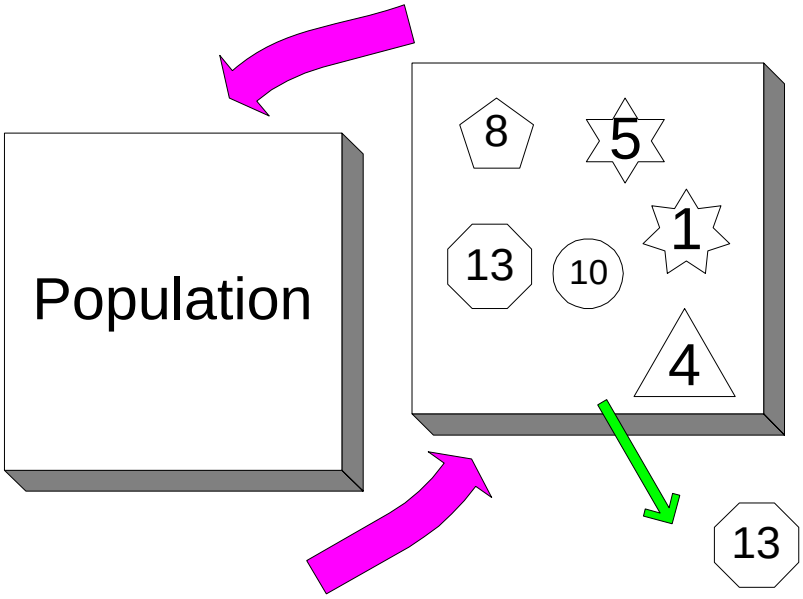

Figure 5.3 Tournament selection methods

5.4.4 The Crossover Operators

The crossover operator is a very important operator in genetic algorithms. Crossover is a process which introduces recombination of bit substrings through an exchange of segments between pairs of parents (chromosomes) in order to create two children (new chromosomes). Many kinds of crossovers have been developed: here the concepts of some crossover kinds will be introduced. A probability term, crossover rate, is set to determine the operation rate p_c . It has been shown that the best setting for the crossover rate depends on the other aspects of the entire genetic algorithm, such as population size, selection operator used and mutation rate. Inpractice [104], Pc $P_c \in [0.4,0.9]$ so that somewhere between 40% and 90% of a given population are chosen as parents for the next generation.

5.4.4.1 One-point Crossover

The one-point crossover process can be illustrated as follows:

- Given parent strings x, y;
- Crossover point selected randomly as an integer $k \in [1, N-1]$ where N is the length of the chromosomes;
- Every bit before k from the first chromosome is copied, and all the bits after this point from the second chromosome are copied as well to produce the first offspring;
- The second part of the first parent and the first part of the second parent are combined to produce the second offspring.

Crossover can be described like this:

Parent 1	11011
Parent 2	10101
Parent 1	11001
Parent 2	10111

5.4.4.2. Two-point Crossover

Two-point crossover is similar to one-point crossover except that two points will be selected and the bits between the two selected points will be exchanged. In this crossover the first and the last parts in each parent are preserved.

5.4.4.3. *N*-point Crossover

N-point crossover is similar to the two previous crossover types except that *N* crossover point are selected and only the bits successive crossover points are exchanged between the two parents to produce two new offsprings.

This operation can be shown as follows:

Parent1	10100111
Parent2	00010001

Child11	10010001
Child2	00110011

5.4.4.4. Uniform Crossover

The process of uniform crossover can be summarised as follows:

Randomly generate a number N of how many positions will be swapped.

Randomly generate N numbers say, $p_1, p_2, \cdots p_N$ which indicate the N position to be swapped.

For each p_i, exchange the $p_i th$ bit of one parent with $p_i th$ bit of the other parent, so generating two new children.

5.4.5. Mutation

Mutation generally refers from the creation of new chromosome from one and only one binary bit in the chromosome string. The mutation is used to ensure that all possible chromosomes are reachable. Since the crossover and selection operators may not be able to introduce all undiscovered bits then the mutation can simply overcome this by randomly selecting any bit position in a string and converting it.

Mutation consists of simply switching over one binary bit in the chromosome string of an eligible candidate which, again is chosen at random. The Genetic Algorithms mutation is randomly applied with low probability p_m typically $p_m \in [0.01,0.1]$, and modifies bits in the chromosomes.

The mutation operator is explained as follows:

Parent	10101010

Child	10100010

5.5. Step by Step Genetic Algorithms Example

In order to present a good understanding of the operation of the Genetic Algorithm approach, let us consider a function which will be used to demonstrate the application of GAs processes:

$$f(x,y) = -\left|\frac{\sin(\pi(x-3))}{\pi(x-3)}\right| \cdot \left|\frac{\sin(\pi(y-3))}{\pi(y-3)}\right|$$

This function is called objective function and is plotted in Figure (5.4) with the parameters x and y constrained between 0.0 and 8.0. This equation is a two-dimensional (2D) function, and involves a pair of the magnitude of the sine functions, which appear in many engineering designs. This function has a well-defined global minimum at (3.0, 3.0) and a number of local minimum and undifferentiable regions resulting from the magnitude operator.

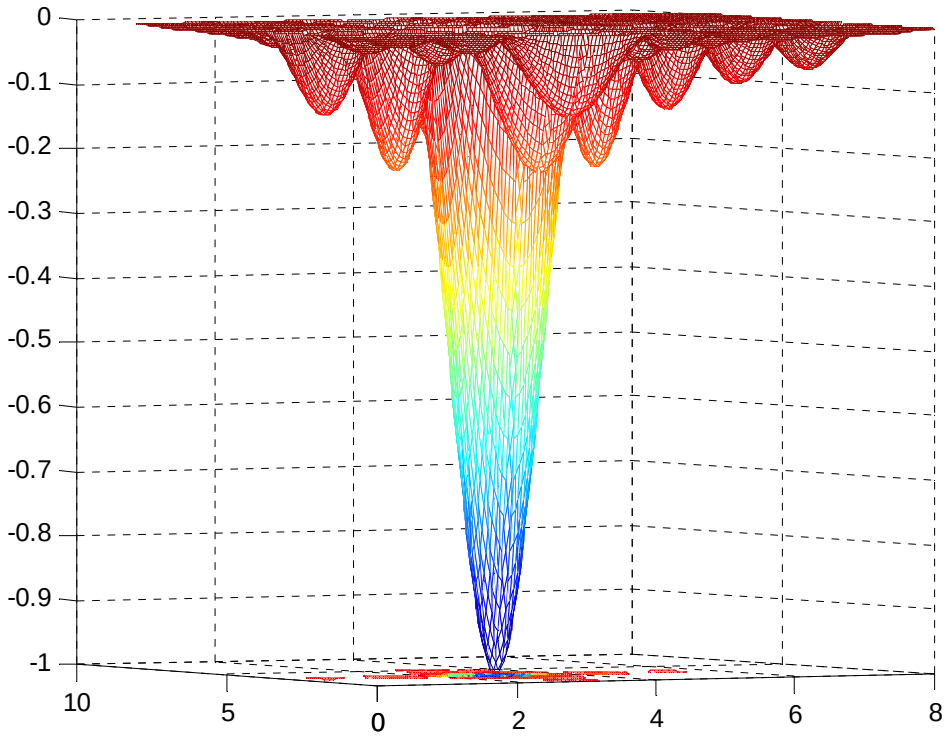

Figure 5.4 A plot of the solution surface for the 2D magnitude sine function

Initialisation

First we seed the algorithm with a set of initial random solutions of the function expressed as a binary representation system $\{1,0\}$.

Initial population

The initial population is randomly generated as follows:

$y_1 = [11010110100101011110]$
$y_2 = [00100100100111000010]$
$y_3 = [01011110001110010111]$
$y_4 = [01011110000110011111]$
$y_5 = [01111111001110011011]$
$y_6 = [01111100001100011110]$
$y_7 = [01101101001100011010]$
$y_8 = [01011101001100010111]$
$y_9 = [01101101000100010010]$
$y_{10} = [01011101001100010100]$

This initial population is converted to the corresponding real values as follows:

$$x_i = lob_i + v_i \times \frac{upb_i - lob_i}{2^{len-1} - 1}$$

where lob and upb are the lower bound and the upper bound of the variable x_i respectively, v_i is the decimal value of the substring y_i and m is the number of bits for each substring. The related real values of these binary populations are as follows:

$y_1 = [x, y] = [0.4962, 4.1916]$
$y_2 = [x, y] = [6.0450, 2.0176]$
$y_3 = [x, y] = [7.2727, 4.7937]$
$y_4 = [x, y] = [0.7038, 1.5861]$
$y_5 = [x, y] = [1.6774, 0.8426,]$
$y_6 = [x, y] = [1.3666, 1.6168]$
$y_7 = [x, y] = [0.4418, 7.1769]$
$y_8 = [x, y] = [1.6422, 1.8260]$
$y_9 = [x, y] = [1.1046, 6.2033]$
$y_{10} = [x, y] = [4.9423, 0.2581]$

Evaluation

The next step after converting the chromosome's genetype (binary representation) to its phenotype (decimal values) the objective function $f_i(y_i)$ is evaluated. Then convert the

value of the objective function into fitness. For minimisation problem, the fitness is equal to the value of the objective function as follows:

$$eval_i(y_i) = f_i(y_i)$$

The fitness function values of the above chromosomes are as follows:

$$eval(y_1) = f_1(x, y) = -0.0163$$
$$eval(y_2) = f_2(x, y) = -0.0141$$
$$eval(y_3) = f_{31}(x, y) = -0.0042$$
$$eval(y_4) = f_4(x, y) = -0.0249$$
$$eval(y_5) = f_5(x, y) = -0.0012$$
$$eval(y_6) = f_6(x, y) = -0.0054$$
$$eval(y_7) = f_7(x, y) = -0.0290$$
$$eval(y_8) = f_8(x, y) = -0.01784$$
$$eval(y_9) = f_9(x, y) = -0.0087$$
$$eval(y_{10}) = f_{10}(x, y) = -0.0003$$

From the above function evaluation we can conclude that the chromosome 7 is the strongest one and that the chromosome 10 is the weakest one.

Selection

A roulette wheel selection approach is the most practically adopted procedure. It is fitness-proportional selection, which select a new population according to the probability distribution based on fitness values. This procedure can be summarised as follows:

- Calculate the fitness value for each chromosome y_i;

  $$eval_i(y_i) = f_i(y_i)$$

- Calculate the total fitness for the population;

  $$F = \sum_{i=1}^{populaation-size} eval_i(y_i)$$

- Calculate the selection probability p_i for each chromosome y_i;

$$p_i = \frac{eval_i(y_i)}{F}$$

- Calculate cumulative probability q_i for each chromosome y_i;

$$q_i = \sum_{j=1}^{i} p_j$$

Now the selection starts by spinning the roulette wheel the population's size times: each time a single chromosome is selected for a new population as follows:

Generate a random number r from the range [0, 1];

- If $r \le q_1$ then select the first chromosome y_1; otherwise select the k[th] chromosome y_k, $2 \le k \le$ *population size* such that $q_{k-1} \le r \le q_k$.

The total fitness F of the population is

$$F = \sum_{i=1}^{10} eval_i(y_i) = 0.27564$$

The probability of a selection of each chromosome y_i $(i = 1,2,\cdots 10)$ is as follow:

$$p_1 = 0.1275, p_2 = 0.3457, p_3 = 0.0787, p_4 = 0.1119, p_5 = 0.1519,$$
$$p_6 = 0.0077, p_7 = 0.0367, p_8 = 0.0290, p_9 = 0.0815, p_{10} = 0.0293$$

The cumulative probabilities q_i for each chromosome y_i when i=1, 2, ..., 10 are as follows:

$$q_1 = 0.1275, q_2 = 0.4732, q_3 = 0.5519, q_4 = 06639, q_5 = 0.8157$$
$$q_6 = 0.8234, q_7 = 0.8601, q_8 = 0.8892, q_9 = 0.9707, q_{10} = 1$$

Now the roulette wheel is ready to be spinning 10 times each time we select a single chromosome for a new population. If the following 10 random numbers are generated:

$$r_1 = 0.6318, r_2 = 0.4083, r_3 = 0.7376, r_4 = 0.4033, r_5 = 0.5196$$
$$r_6 = 0.7281, r_7 = 0.4638, r_8 = 0.5694, r_9 = 0.1338, r_{10} = 0.5494$$

the first number $r_1 = 0.6318$ is greater than q_3 and smaller than q_4. This means that the chromosome 4 is selected for the new population. The second number $r_2 = 0.4083$ is greater than q_1 and smaller than q_2 meaning that the chromosome 2 is selected for the new population, and so on. Finally, the new population consists of the following chromosomes:

$$y_4 = [01011110000110011111] = y'_1$$
$$y_2 = [00100100100111000010] = y'_2$$
$$y_5 = [01111111001110011011] = y'_3$$
$$y_2 = [00100100100111000010] = y'_4$$
$$y_3 = [01011110001110010111] = y'_5$$
$$y_5 = [01111111001110011011] = y'_6$$
$$y_2 = [00100100100111000010] = y'_7$$
$$y_4 = [01011110000110011111] = y'_8$$
$$y_1 = [11010110100101011110] = y'_9$$
$$y_3 = [01011110001110010111] = y'_{10}$$

Crossover

Crossover used here is a one-point method, which randomly selects one cut-point and exchanges the right parts of two parents to generate offspring. The probability of the crossover is set to be as $p_c = 0.4$. This means that 4 chromosome's pairs will be selected for crossover operator. The other remaining chromosomes will migrate to the next generation. Four random numbers are generated as follows;

y_3', y_5', y_6' and y_9' were selected for crossover. We generate a random integer number pos from the range [1, 19] (because 20 is the total length of a chromosome) as a cutting point. We assume the generated crossover position is 9, the four selected chromosomes

are cut after bit number 9, and offspring are generated by exchanging the right parts between each two of them as follows:

$$y'_3 = [01111111001110011011]$$
$$y'_5 = [01011110001110010111]$$

$$y'_3 = [01111111001110010111]$$
$$y'_5 = [01011110001110011011]$$

$$y'_6 = [01111111001110011011]$$
$$y'_9 = [01001111001110010111]$$

$$y'_6 = [01111111001110010111]$$
$$y'_9 = [01001111001110011011]$$

Mutation

Mutation alters one or more genes with a probability equal to the mutation rate. The probability of the mutation rate is set as $p_m = 0.01$; this means that an average of 1% of the total bits of the population would undergo mutation. Since there are $10 \times 20 = 200$ bits in the entire population, 2 mutations per generation is excepted. All the bits have an equal chance to be mutated. Thus a sequence of random numbers $r_i (i = 1,2,\cdots 200)$ will be generated from the range [0, 1]. Suppose the following genes will go through mutation:

Bit position	Chromosome num.	Bit num.	Random num.
192	10	12	192
83	5	3	83

After mutation we get the final population as follows:

$$y'_1 = [01011110000110011111]$$
$$y'_2 = [01111100000110011110]$$
$$y'_3 = [01111111001110010111]$$
$$y'_4 = [01111100000110011110]$$
$$y'_5 = [01011110001110011011]$$
$$y'_6 = [01111111001110010111]$$
$$y'_7 = [01111100000110011110]$$
$$y'_8 = [01011110000110011111]$$
$$y'_9 = [01001111001110011011]$$
$$y'_{10} = [01111110001110010111]$$

The corresponding real values of variables $[x, y]$ and fitness are as follows:

$$f(05.7376,1.0255,) = -0.0126$$
$$f(1.0231,1.0238,) = -.00408$$
$$f(6.1658,.7884) = -0.02189$$
$$f(2.7767,4.9002 = -0.02344$$
$$f(1.1301,0.1543) = -0.01907$$
$$f(2.7621,1.9072) = -0.01835$$
$$f(2.7557,2.2571) = -0.42008$$
$$f(6.7244,3.39250) = -0.34680$$
$$f(0.8364,1.4930) = -0.017030$$
$$f(018344,7.1884) = -0.32152$$

Now we just completed one iteration of the genetic algorithm. This test run is terminated after the 200th generation. We have obtained that the best chromosome in the 42nd generation as follows:

$f(2.99997, 3.0005) = -1.000$

5.6. Conventional Methods of Optimization

It is considered appropriate at this stage to present a short description of some conventional methods of optimization so that comparison can be made between the Genetic Algorithms method and conventional methods.

5.6.1. FMINBND Bounded Nonlinear Function Minimization

The determination of maximum or minimum value of a real-valued function $f(x_1, ..., x_n)$ of n real variables in an n-dimensional space is a common problem in scientific computation. The words optimization refers to either the minimization or maximization of a function [108]. To find a minimum of a function of one variable on a fixed interval:

$$\min f(x) \quad \textit{such that} \quad x_1 < x < x_2$$

where x, x_1, and x_2 are scalars and $f(x)$ is a function.

There are several methods to optimize the above function such as Nelder-Mead method [109, 110], and Simplex algorithm [111, 112]

Fminbnd method is a combination of the Golden section search method [109], [113, 114] and a polynomial interpolation. The purpose of the next section is to show the

derivation of the golden section search method to find the minimum of a unimodal continuous function over an interval without using derivatives.

5.6.1.1. Derivation of the Golden Section Search

Let us consider a function f over the interval $[x_1, x_2]$. The function to be minimized has to be continuous over $[x_1, x_2]$; and that $f(x)$ is unimodal over $[x_1, x_2]$, that is: $f(x)$ has only one minimum in $[x_1, x_2]$. The function $f(x)$ is unimodal on $I = [x_1, x_2]$, if there exists a unique number $p \in [x_1, x_2]$ such that:

$f(x)$ is decreasing on $[x_1, p]$

and

$f(x)$ is increasing on $[p, x_2]$.

The purpose of this method is narrowing the interval that contains the minimum, so the root is supposed to have been bracketed in an interval $[x_1, x_2]$. A root of a function is known to be bracketed by a pair of points, a and b, when the function has an opposite sign at those two points. A minimum, by contrast, is known to be bracketed only when there is a triplet of points, $x_1 < x_2 < x_3$ or $(x_3 < x_2 < x_1)$, such that $f(x_2)$ is less than both $f(x_1)$ and; $f(x_3)$

$$f(x_2) < f(x_1)$$

and

$$f(x_2) < f(x_3)$$

In this case the function has a minimum in the interval $[x_1, x_3]$. Consider such a line segment,

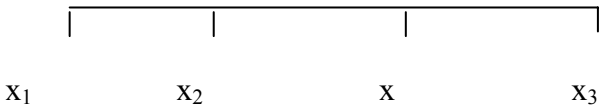

The way of bisection is to choose a new point x, either between x_1 and x_2 or between x_2 and x_3. Suppose, to be specific, the latter choice. Then evaluate $f(x)$. If $f(x_2) < f(x)$, then the new bracketing triplet of points is (x_1, x_2, x); in reverse if $f(x_2) > f(x)$, then the new bracketing triplet is (x_2, x, x_3). In all cases the middle point of the new triplet is the best minimum achieved, (see Figure 5.4). We can continue the process of bracketing until the distance between the two outer points of the triplet is tolerably small.

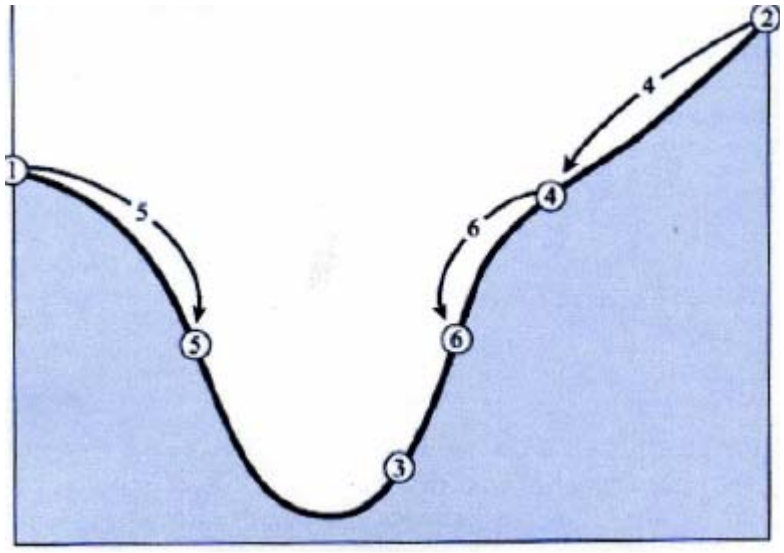

Figure 5.5 Diagram of a Golden section search method

Figure 5.5 shows successive bracketing of a minimum. The minimum is originally bracketed by points 1, 3, 2. The function is evaluated at 4, which replaces 1, and then at 6, which replaces 4. The rule at each stage is to keep a centre point that is lower than the two outside points. After the steps shown, the minimum is bracketed by points 5, 3, 6.

5.6.1.2. Restriction on Golden Search Method

- The function to be minimized must be continuous;
- fminbnd often exhibits slow convergence when the solution is on a boundary of the interval;
- fminbnd only handles real variables;
- fminbnd only give local solutions.

5.6.2. Simplex Search Optimization Method

To find the minimum of unconstrained multivariable function using a derivative-free method:

$$\min_x f(x)$$

where x is a vector and $f(x)$ is a function that returns a scalar.

5.6.2.1. Algorithms

The Simplex Search method is a direct search method that does not use numerical or analytic gradients [115]. If n is the length of x, a Simplex in n-dimensional space is characterized by the $(n+1)$ distinct vectors that are its vertices. In two-space, a Simplex is a triangle, in three-space, it is a tetrahedron. At each step of the search, a new point in or near the current simplex is generated. The function value at the new point is compared with the function's values at the vertices of the simplex and, usually, one of

the vertices is replaced by the new point, giving a new simplex. This step is repeated until the diameter of the simplex is less than the specified tolerance.

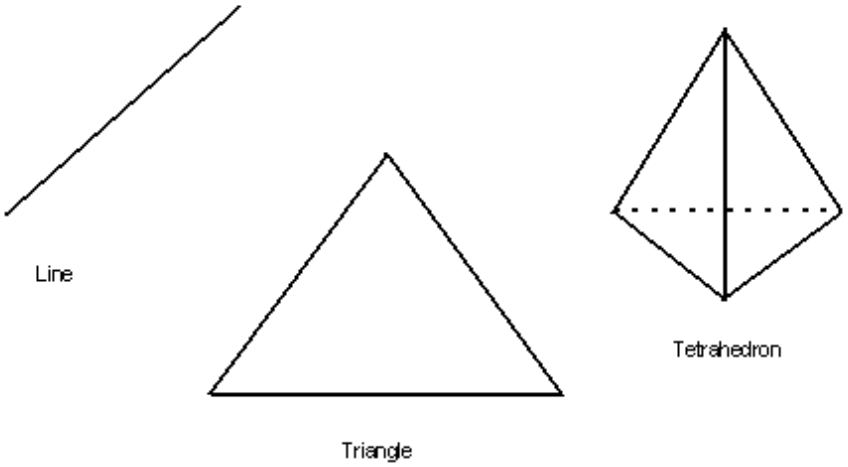

Figure 5.6 Geometric interpretation of lower dimensional simplices

The simplex methods are based on an initial design of $(k+1)$ trials, where k is the number of variables. A $(k+1)$ geometric figure in a k-dimensional space is called a simplex. The corners of this Figure are called vertices.

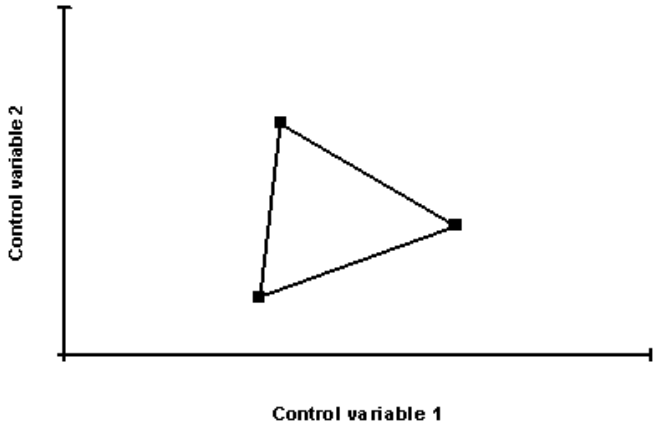

Figure 5.7 a Simplex defined by three different trial conditions for two control variables

With two variables the first simplex design is based on three trials, for three variables it is four trials, etc. This number of trials is also the minimum for defining a direction of improvement. Therefore, it is a timesaving and economical way to start an optimization project.

After the initial trials the simplex process is sequential, with the addition and evaluation of one new trial at a time. The simplex searches systematically for the best levels of the control variables. The optimization process ends when the optimization objective is reached or when the responses cannot be improved further.

5.6.2.2. The Restrictions on the Simplex Search Method

- Simplex search method solves nondifferentiable problems;
- It can often handle discontinuity, particularly if it does not occur near the solution;
- It might only give local solutions;
- It is only used to minimise the real numbers, that is, x must only consist of real numbers and $f(x)$ must only return real numbers. When x has complex variables, they must be split into real and imaginary parts.

The Simplex search method is not the preferred choice for solving problems that are sums of squares, that is, of the form:

$$\min_x \left\| f(x)_2^2 \right\| = \min_x (f_1(x)^2 + f_2(x)^2 + \cdots + f_n(x)^2)$$

5.6.3. Comparison between the Conventional Methods and Genetic Algorithms Method

The Genetic Algorithms method deviates significantly from other traditional search and optimisation methods. The most significant variations are:

- Genetic Algorithms possess the ability of implicit parallelism, to evaluate simultaneously many possible problem solutions;
- GAs does not require derivative information or other auxiliary knowledge; only the objective function and corresponding fitness levels influence the directions of search;
- Genetic Algorithms encode initial input data set information into strings, analogous to living being cellular chromosomes;
- GAs use probabilistic transition rules, not deterministic ones;
- GAs provides a number of potential solutions to a given problem and the choice of final solution is left to the user.

A typical Genetic Algorithms requires two things to be defined:

(1) a Genetic representation of the solution domain;

(2) a fitness function to evaluate the solution domain.

The main property that makes these Genetic representations convenient is that their parts are easily aligned due to their fixed size which facilitates simple crossover operation.

In a summary: often, GAs method can rapidly locate good solutions, even for difficult search spaces.

CHAPTER SIX

Results

CHAPTER SIX

6.1. Introduction

Chapter 6 is presented in two parts:

Part one presents for each of the case studies (chapter 3), *the results and discussion* of the information generated relating to the processes of coating production/surface treatments and oxidation tests of the coatings produced. The information presented here includes that collected from the literature, that produced in our laboratory and also that generated in the current project. Here emphasis has been placed on *microstructural* aspects of the diffusion processes involved both in the coating production and oxidation tests.

This presentation of the results along with their discussion will provide improved interpretation of the observed interactions between the microstructures and the involved diffusion processes.

The information available in the literature on the microstructural aspects of the diffusion processes involved in the coating production and in assessment of the oxidation resistance on the produced coatings has been found not to be consistent or systematic. In discussing the results this deficiency has been corrected. The information generated from numerical modelling has also been used, where appropriate, to elaborate on the information gathered from the literature and on the new information generated in this project.

Part two solely deals with the results obtained by numerical modelling.

6.2. Nonsteady State Diffusion of Iron Carburized at 950^{o} C, 7.1 Hours

Information from interdiffusion studies on iron carburized system at 950^{o} C, after 7.1 hours has been described in section 3.2.

6.2.1. Carburization – Microstructural Aspects/Microstructure Modelling of Diffusion Processes Involved – Results and Discussion

The understanding of the diffusion processes involved in carburizing processes can be facilitated by considering the following two cases:

(1) Carburization of pure iron at relatively low temperature below the eutectoid temperature for example at 700^{o}C;

(2) Carburization of steel above the eutectoid temperature of 950^{o}C.

Case-1- Carburization at Temperature below the Eutectoid Temperature

A rod of pure iron is subjected to a carbon rich source at one end as shown in Figure 6.1.

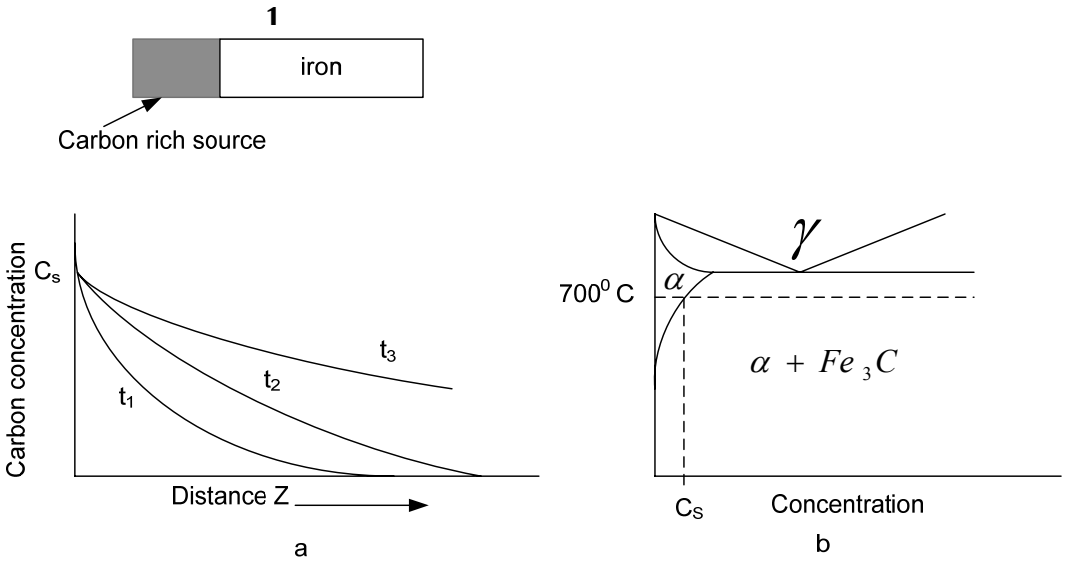

Figure 6.1 a) Composition profiles for carburizing iron. b) Relevant portion of iron – carbon phase diagram

After short exposure of the rod at 700°C a local equilibrium is expected to reach at interface 1 (Figure 6.1(a)). This means that the compositions of the two phases at interface 1 are given by the phase diagram (Figure 6.1(b)) which indicates that α-Fe is in equilibrium with Fe_3C. Because of the local equilibrium a carbide layer is formed on the surface giving carbon concentration (C_s). This means at the left of the interface the carbon concentration increases to C_s at time t=0 and stays there, establishing a large concentration gradient which drives the diffusion of carbon along the rod. The concentration profiles of carbon can be schematically represented as shown in Figure 6.1.

Case-2- Concentration at Temperature above the Eutectoid Temperature T_1

The iron rod of Figure 6.1 is heated to a temperature T_1, above the eutectoid temperature as shown in Figure 6.2(a).

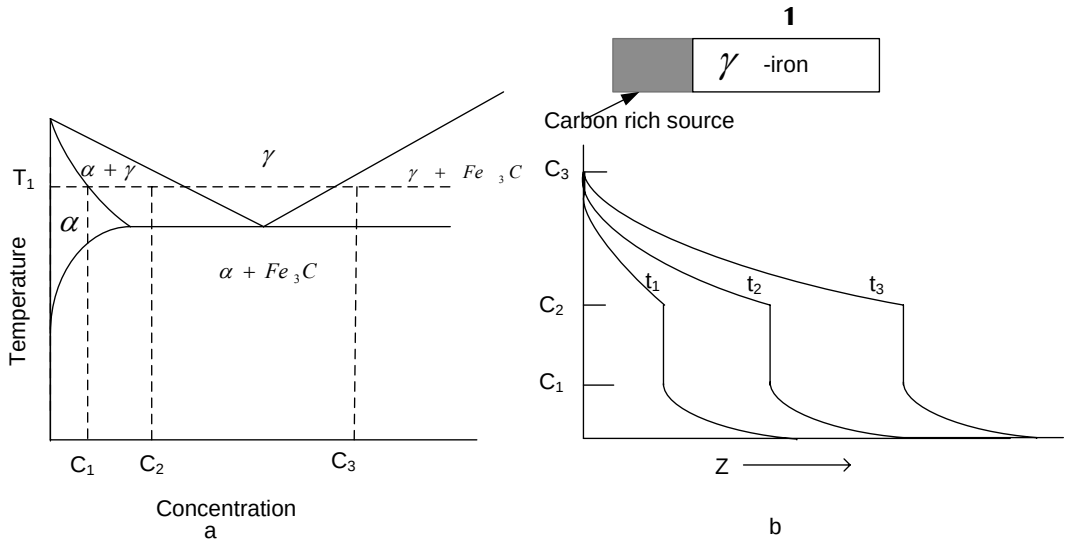

Figure 6.2 a) Relevant portion of iron – carbon phase diagram. b) Composition profiles for carburizing iron above the eutectoid temperature

This differs from case 1 in the following ways:

The local equilibrium at interface establishes the carbon composition at the left end of the bar at C_3. At C_3 we have γ iron at interface 1. At temperature T_1 iron with carbon content between C_3 and C_2, we have γ at interface 1.

At $C<C_1$ we have α iron;

C_1 =maximum amount of carbon in α;

C_2=minimum amount of carbon in γ;

Thus between C_1 and C_2 we have $\alpha + \gamma$.

It is important to note that the two phase regions never form a diffusion couple.

In the next section the results from numerical modelling for interdiffusion in iron carburizing has been presented.

6.2.2. Modelling the Diffusion Process using Analytical and Numerical Methods

Most realistic diffusion processes are of nonsteady-state nature. That is, the diffusion flux and the concentration gradient at some particular point in a solid differ with time. This is illustrated in Figure 6.3 which shows concentration profiles at three different diffusion times.

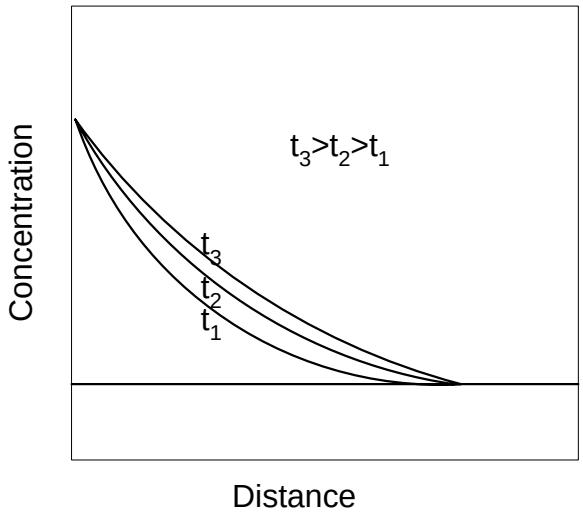

Figure 6.3 Concentration profile for nonsteady-state diffusion taken at three different diffusion times $t_1, t_2,$ and t_3 [89]

The surface carbon concentration of steel can be increased by carburising. Such an alloy originally had a consistent carbon concentration of (0.25 wt %). The process of carburising at 950^{o}C increased the surface carbon concentration to 1.20 wt %. Very often it becomes necessary to determine the carbon concentration at a particular distance (0.5 mm) below the surface after 7.1 hours. The diffusion coefficient of carbon in iron is known–this is $1.6\times10^{-11} m^2/s$ [89].

6.2.2.1. Analytical Solution of Iron Carburized at 950^{o} C, 7.1 Hours

This is a nonsteady-state diffusion problem in which the surface composition is supposed to be stable, so the following equation was used:

$$\frac{C_x - C_o}{C_s - C_o} = 1 - erf\left(\frac{x}{2\sqrt{Dt}}\right) \tag{6.1}$$

where C_x represents the concentration and can be determined at any time t and position x when the parameters (C_o, C_s and D) are known. C_o corresponds to the uniform carbon concentration before diffusion treatment, and C_s corresponds to the surface carbon concentration after diffusion treatment as shown in Figure 6.4.

Figure 6.4 Concentration profile for nonsteady-state diffusion concentration parameters relate to equation 7.1

when the following conditions are applied:

$C_o = 0.25\,wt\%\,C$

$C_s = 1.2\,wt\%\,C$

$x = 0.5\,mm = 5\times10^{-4}\,m$

$D = 1.6\times10^{-11}\,m^2/s$

$t = 25560\,s$

Thus equation 6.1 becomes:

$$C_x = (C_s - C_o)\left\{1 - erf\left(\frac{x}{2\sqrt{Dt}}\right)\right\} + C_o \qquad (6.2)$$

So at the position (0.5 mm) and after 7.1 hours (25560 s) the carbon concentration from equation 6.2, as follows:

$$erf\left(\frac{x}{2\sqrt{Dt}}\right) = erf\left(\frac{(0.5\times10^{-3})m}{2\sqrt{(1.6\times10^{-11})m^2/s\,(25560)s}}\right)$$

$$\Rightarrow erf(0.3909) = 0.4196$$

The expression $erf\left(\frac{x}{2\sqrt{Dt}}\right)$ is the Gaussian error function, values of which are given in mathematical tables for various values of $erf\left(\frac{x}{2\sqrt{Dt}}\right)$: a partial listing is given in Table 4.1 in chapter 4.

Therefore

$C_x = (1.2 - 0.25)\{1 - 0.4196\} + 0.25$

$C_x = 0.8\,wt\%\,C$

6.2.2.2 Numerical Solution of Iron Carburized at 950^{o} C, 7.1 Hours

The numerical solution or carbon numerical concentration for the above problem can be achieved by using modified Euler's method (Runge-Kutta method of order two):

$$y_{n+1} = y_n + h\frac{y_n^{'} + y_{n+1}^{'}}{2}$$

We can also use fourth order Runge-Kutta method:

$$C_{n+1} = \frac{1}{6}(k_1 + 2k_2 + 2k_3 + k_4),$$
$$k_1 = hf(x_n, y_n),$$
$$k_2 = hf(x_n + \frac{1}{2}h, y_n + \frac{1}{2}k_1),$$
$$k_3 = hf(x_n + \frac{1}{2}h, y_n + \frac{1}{2}k_2),$$
$$k_4 = hf(x_n + h, y_n + k_3).$$

This is applied on Fick's second law as follows:

$$\frac{\partial C}{\partial t} = D\frac{\partial^2 C}{\partial x^2} \qquad (6.3)$$

In Figure 6.5 the carbon diffusion coefficient is $1.6\text{x}10^{-11}\text{m}^2/\text{s}$ [89]. Using this diffusion coefficient the carbon numerical concentration was then calculated using the modified Euler's method (equation 4.32) and Rung-Kutta method of order four (equation 4.37) applied on Fick's second law (equation 4.3). The carbon concentration profile can be shown as follows:

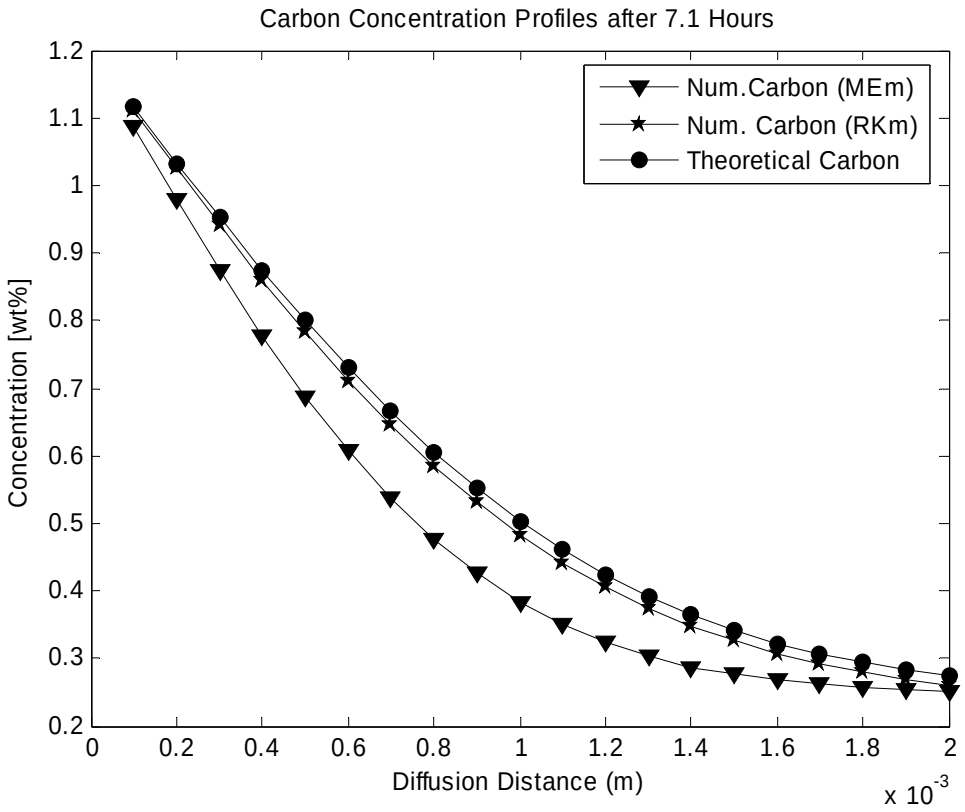

Figure 6.5 Carbon numerical and analytical concentration profiles after 7.1 hours diffusion treatment at 950^{o}C

As shown in Figure 6.5 the black circle (●) concentration profile curve is the carbon analytical concentration after 7.1 hours, the black star (★) concentration profile curve corresponds to the carbon numerical concentration after 7.1 hours using Runge-Kutta method of order four, and the black triangle concentration profile curve corresponds to the numerical concentration profile of carbon calculated from the Rung-Kutta method of order 2 (modified Euler's method). We can see that there is good agreement between the carbon analytical concentration profile obtained from equation 6.2 and carbon numerical concentration profile values obtained from Rung-Kutta method of order four for the whole range of diffusion distance. However there is a divergence between the carbon analytical concentration profile and the carbon numerical concentration profile obtained from modified Euler's method, indicating the importance of Runge-Kutta method of order four.

6.2.2.3. Conclusions of Iron Carburized at 950^{o} C, 7.1 Hours

Both Runge-Kutta method of order four and modified Euler's method (Runge-Kutta method of order two) have been used to calculate the carbon numerical concentration profile. The Least squares method has been used to calculate the absolute error between the carbon analytical and the numerical concentration profiles. The analytical method showed a carbon concentration of 0.80 w% at a position 0.5 mm below the surface of the sample after 7.1 hours. The carbon numerical concentration computed from Runge-Kutta method of order four was 0.82 w%, and the carbon numerical concentration computed from Runge-Kutta method of order two (modified Euler's method) was 0.88 w% at the same distance from the surface. Consequently the carbon numerical concentration obtained from fourth order Runge-Kutta method is more reliable compared with the modified Euler's method. The diffusion coefficient for carbon in iron at the temperature 950^{o}C was $1.6 \times 10^{-11} m^2 / s$.

This case confirms the validation of the numerical method which has been applied in the present project.

6.3. Copper-Nickel Diffusion Couple after 300 Hours

Background information from interdiffusion studies on copper-nickel system after 300 hours at 1054^{o}C has been described in section 3.3.

6.3.1. Copper-Nickel Diffusion Couple at 1054^{o}C after 300 Hours - Microstructural Aspects / Microstructural Modelling of the Diffusion Processes Involved - Results and Discussion

For understanding of the diffusive processes involved in the copper-nickel system, it is important to note the following facts:

- Cu, (copper atomic radius= 0.128 nm=128pm), and Ni, (nickel atomic radius=0.135 nm=135 pm), atoms have almost the same size.
- Copper and nickel mobility have nearly the same order of magnitude (similar size).

Considering the bar in Figure 6.6 (a) the copper atoms diffuse to the left faster than the nickel atoms (melting point of Cu= 1083^{o}C and melting point of Ni= 1453°C). With reference to the markers studies described in chapter 3, section 3.2 it is clear that the diffusion happened at elevated temperature and the net atoms transport from the right of the markers to their left since the Cu atoms are diffusing faster than the nickel atoms. The additional atoms which enter the left hand side of the marker will cause the lattice to expand to the left, while the loss of atoms from the right hand side will cause the lattice to shrink. Therefore the entire centre of the bar will shift to the left as shown in Figure 6.6 (b). This shift was reported in metals by Kirkendall and it is called Kerkendall shift.

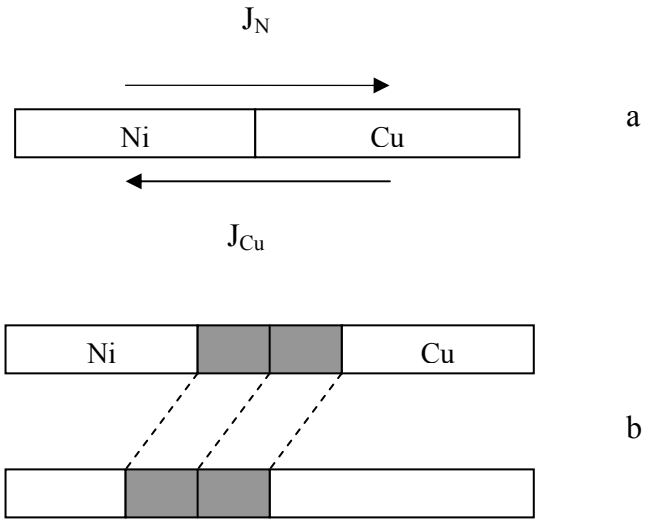

Figure 6.6 The Kirkendall shift

Consider that the copper –nickel diffusion couple shown in Figure 6.7 to be studied was subjected to an interdiffusion treatment at 1054^{o}C for 300 hours.

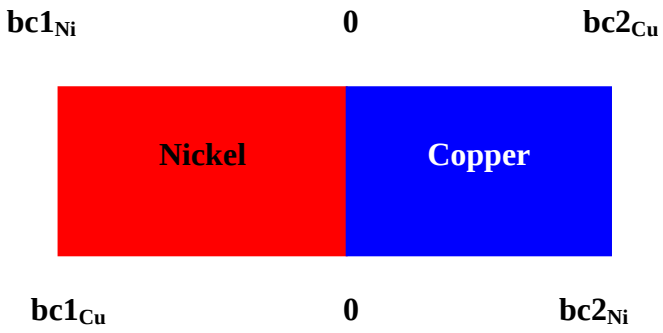

Figure 6.7 Copper –nickel diffusion couple

bc_{1Ni}, bc_{2Ni} are the boundary conditions of the nickel component, and bc_{1Cu} , bc_{2Cu} are the boundary conditions of the copper component.

The copper-nickel diffusion couple has the step function composition at t=0, and after such time at certain temperature, copper atoms will diffuse into nickel side and nickel atoms will diffuse into the copper side as explained in the following Figures; the Figures (A, B, C, and D) in Figure 6.8 represent the composition evolutions of Cu and Ni as a function of time. These composition profiles have been calculated by numerical

methods (given subsequently). It is instructive to see how the composition profiles change with time.

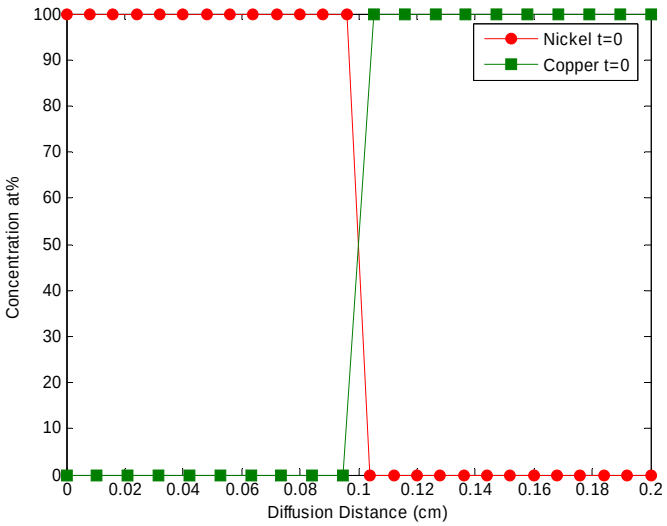

A

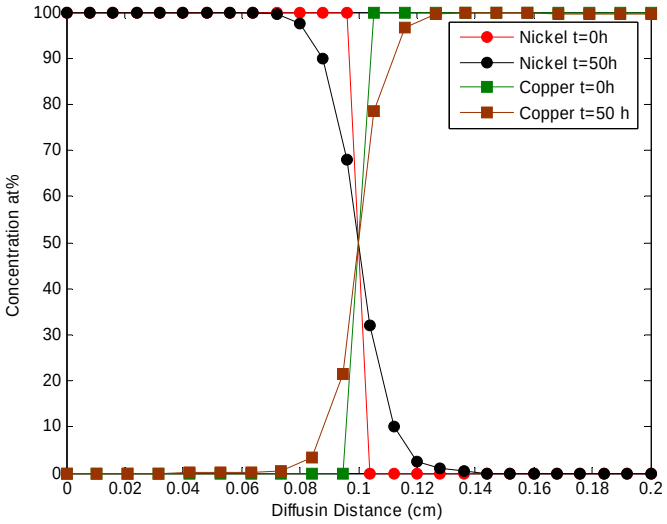

B

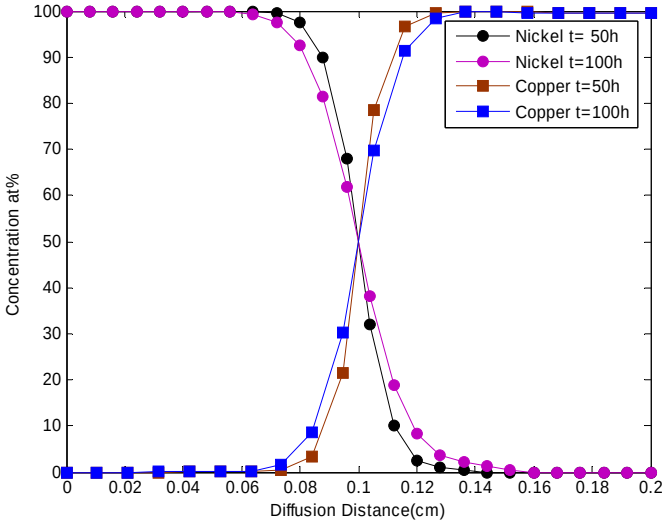

C

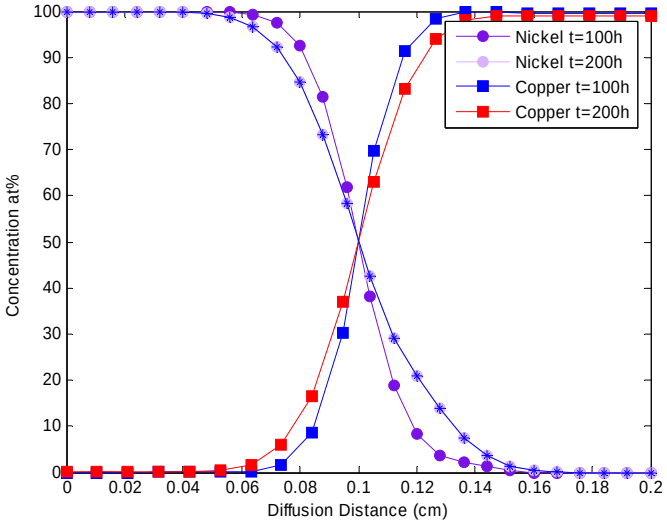

D

Figure 6.8 Copper numerical concentration profiles at A (t=0), after B (t=50h), C (t=100h), and D (t=200h) diffusion treatments at 1054^{o}C

The concentration profiles in the above Figure 6.8 (A-D) show the gradual distributions of copper and nickel atoms from t=0 until t=200 hours.

Experimental measurements have shown that the component with the lower melting point diffuses in at a faster rate than does the higher melting component [89] indicating that for a binary system the diffusion rates of the two components are not equal.

Let us now consider the composition profiles of Cu and Ni after 300 hours of diffusion. The experimental data of concentration profiles of *Cu* and *Ni* as a function of diffusion distance (taken from the literature [91]) is shown in Figure 6.9. The diffusion distances considered are shown below:

dx = [0 .005 0.01 0.015 0.02 0.025 0.03 0.035 0.04 0.045 0.05 0.055 0.06 0.065 0.07 0.075 0.08 0.085 0.09 0.1 0.109 0.118 0.128 0.143 0.175 0.185] cm .

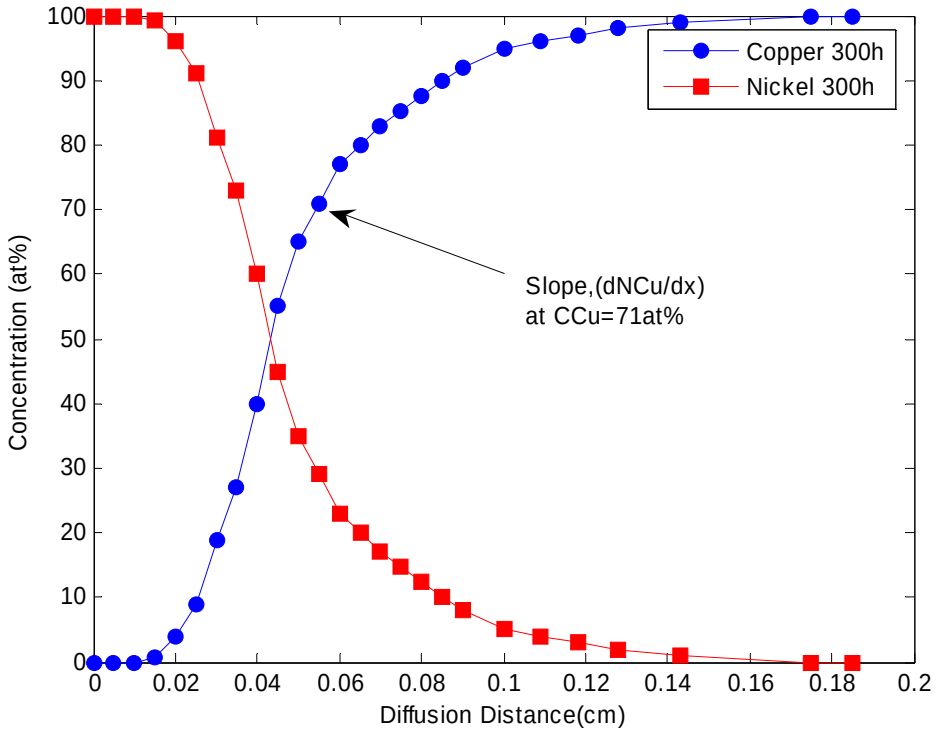

Figure 6.9 $Cu-Ni$ diffusion data at 1054°C after 300 hours diffusion treatment

Inert markers placed within the couple moved $0.02\,cm\,(200\mu m)$ during the period of the diffusion anneal.

To find out the concentration profile of the two metals (copper and nickel) numerically, the diffusion coefficient for each component should be determined, as described in the next section (6.3.2).

6.3.2. Analytical Solution for Cu-Ni System at 1054°C after 300 Hours

To determine the interdiffusion coefficient $\tilde{D}$ a Boltzmann-Matano analysis [90] has been used at the Matano interface ($C_{Cu} = 0.71\,at\%$). The $\tilde{D}$ value for Cu-Ni system at 1054°C after 300 h is equal to:

$$\tilde{D} = 3.16 \times 10^{-10}\,cm^2/s \quad \text{[Appendix D]} \qquad (7.4)$$

The Matano interface describes a plane X_M, within the diffusion couple, characterized by equivalent amounts of mass diffusion to the left and right. The location of the Matano interface may be determined through a mass-conservation condition. The mass conservation balances the loss of diffusant on the left side of the couple with the equivalent gain on the right side.

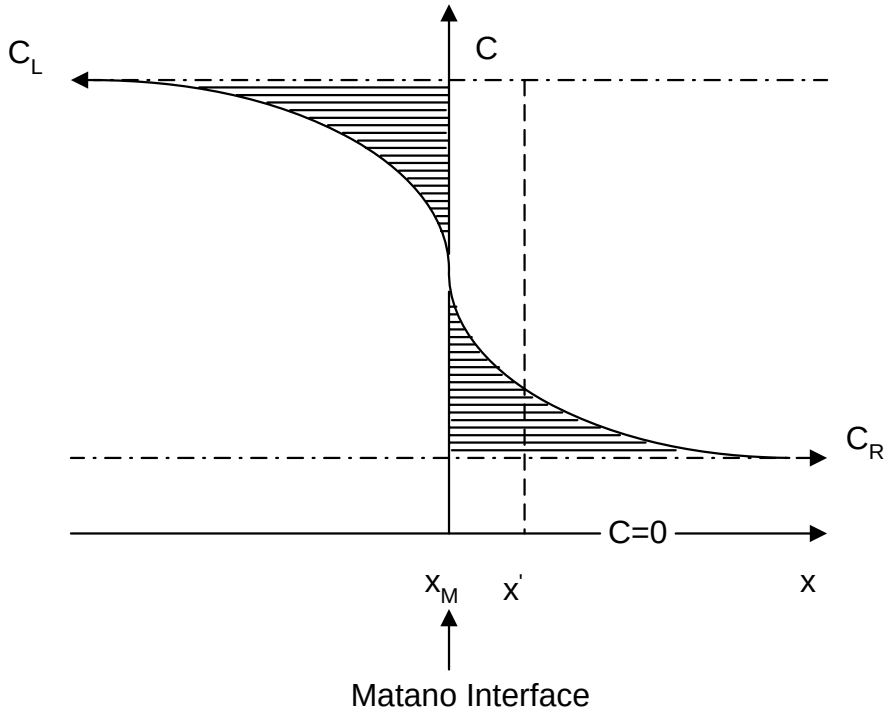

Figure 6.10 Matano interface for the diffusion couple

The grey areas in Figure 6.10 that represent the balanced gain and loss are separated by the Matano plane X_M and may possibly be expressed by two integrals as follows [91],

$$\underbrace{\int_{-\infty}^{X_M}[C_L - C(x)]dx}_{loss} = \underbrace{\int_{X_M}^{\infty}[C(x) - C_R]dx}_{gain} \tag{6.5}$$

In this case the initial conditions selected here for the above equation 6.5 are as follows:

$$C = \begin{Bmatrix} C_L & (x < 0, t = o) \\ C_R & (x > 0, t = 0) \end{Bmatrix} \tag{6.6}$$

The motion of the markers is the square of the dislocation, $X(t)$, and is proportional to the diffusion time *t*, as a result [91]

$$X^2(t) \propto t$$

$$X^2(t) = k \bullet t$$

$$\frac{X^2(t)}{t} = k \text{ (Constant)} \tag{6.7}$$

The matching marker velocity is:

$$u_M \equiv \frac{\partial X(t)}{\partial t} = \frac{k}{2X(t)} \tag{6.8}$$

But $k = \dfrac{X^2(t)}{t}$

Placing in the proportionality constant from equation 6.7 into equation 6.8 we obtain:

$$u_M = \frac{X(t)}{2t} \tag{6.9}$$

Substituting equation 6.9 u_M can be calculated after that as:

$$u_M = \frac{X(t)}{2t} = \frac{200[\mu m]}{2 \times (300) \times (3600)[s]}$$

$$u_M = 9.3 \times 10^{-5} \ [\mu m / s] \tag{6.10}$$

u_M is given by Darken's first equation [92]

$$u_M = (D_A - D_B)\frac{\partial C_A}{\partial x} \tag{6.11}$$

Thus in the present case:

$$u_M = (D_{Cu} - D_{Ni})\frac{\partial C_{Cu}}{\partial x} \tag{6.12}$$

Substituting equation 6.10 into equation 6.12 so

$$9.3 \times 10^{-9}[cm / s] = (D_{Cu} - D_{Ni}) \times 12.69 \text{ [mol. frac. /cm]} \tag{6.13}$$

Where $12.69 = \frac{\partial N_{Cu}}{\partial x}$ [i.e. the slope at $C_{Cu} = 71\ at\%$]

Using Darken's second equation [92]

$$\tilde{D} = N_B D_A + N_A D_B \tag{6.14}$$

And from equation 6.4

$$\tilde{D} = 0.71.\ D_{Ni} + 0.29.\ D_{Cu} = 3.16 \times 10^{-10} \tag{6.15}$$

where

D_{Ni} =Nickel diffusion coefficient

D_{Cu} =Copper diffusion coefficient

Consequently we can solve equations 6.15 and 6.13 simultaneously as follows:

$$9.3\times10^{-9} = 12.69\ D_{Ni} + 12.69\ D_{Cu}$$
$$D_{Ni} = (9.3\times10^{-9} + 12.69\ D_{Cu})/12.69 \qquad (6.16)$$

when we substitute equation 6.16 in equation 6.15 as follows we obtain:

$$3.16\times10^{-10} = 0.71\ ((9.3\times10^{-9} + 12.69\ D_{Cu})/12.69) + 0.29\ D_{Cu} \qquad (6.17)$$

Then $D_{Cu} = 8.35\times10^{-10}$

by substituting D_{Cu} in equation 6.16 the result becomes:

$D_{Ni} = 1.02\times10^{-10}$

Consequently the diffusivities are:

$$D_{Cu} = 8.35\times10^{-10}\,cm^2/s$$
$$D_{Ni} = 1.02\times10^{-10}\,cm^2/s \qquad (6.18)$$

The copper diffusion coefficient $D_{Cu} = 8.35\times10^{-10}\,cm^2/s$ has been used to find the numerical concentration profile of Cu as shown in Figure 6.11 using the numerical technique as explained in the next section 6.2.3.

6.3.3. Numerical Solution using GAs with the Numerical Methods

All copper nickel alloys consist of only one phase as the copper nickel binary system exhibits complete solid solubility, as shown by the phase diagram in Figure 3.1, and it is therefore amenable to modelling by both Darken's and numerical methods. The

trial and error, and Genetic Algorithms optimization method were used to calculate the diffusion coefficient of copper (Cu) in the $Cu-Ni$ binary system. Two cases were considered:

In case 1 the diffusion coefficient of copper was assumed constant and in case 2 diffusion coefficients was assumed to be concentration dependent (second orders polynomial). The obtained diffusion coefficient was used to calculate the numerical concentration of *Cu* in the system. The numerical concentration of the component was calculated by using the numerical method (Rung-Kutta of order four, equation 4.37) as follows:

$$C_{n+1} = \frac{1}{6}\left(k_1 + 2k_2 + 2k_3 + k_4\right),$$
$$k_1 = hf(x_n, y_n),$$
$$k_2 = hf(x_n + \frac{1}{2}h, y_n + \frac{1}{2}k_1),$$
$$k_3 = hf(x_n + \frac{1}{2}h, y_n + \frac{1}{2}k_2),$$
$$k_4 = hf(x_n + h, y_n + k_3).$$

By applying this technique to solve Ficks second law 4.6:

$$\frac{\partial C}{\partial t} = D\frac{\partial^2 C}{\partial x^2}$$

where D is the diffusion coefficient for each component (copper and nickel).

Case -1

Following the procedure given above (solving Fick's second law numerically and using the flow chart), the table below shows the numerical concentration profile of Cu (along with the experimental concentration).

Diffusion Distance dx	Experimental Concentration Cu	Numerical Concentration Cu
0	0	0.0005
0.005	0	0.0035
0.01	0	0.021
0.015	0.79	0.1097
0.02	4	0.5014
0.025	9	1.9678
0.03	19	6.4851
0.035	27	17.4832
0.04	40	37.4715
0.045	55	62.5285
0.05	65	82.5168
0.055	71	93.5149
0.06	77	98.0322
0.065	80	99.4986
0.07	83	99.8903
0.075	85.3	99.979
0.08	87.5	99.9964
0.085	90	99.9995
0.09	92	99.9999
0.1	95	100
0.109	96	100
0.118	97	100
0.128	98	100
0.143	99	100
0.175	100	100
0.185	100	100

Table 6.1 Tabulation of numerical-experimental concentrations of copper after 300 hours diffusion treatment

The copper penetration curves have been shown in Figure 6.11, where the boundary conditions are:

$$\begin{array}{ll} 0 & when \quad 0 \le x \le 0.1 \\ 1 & when \quad 0.1 \le x \le 0.2 \end{array} \qquad (6.19)$$

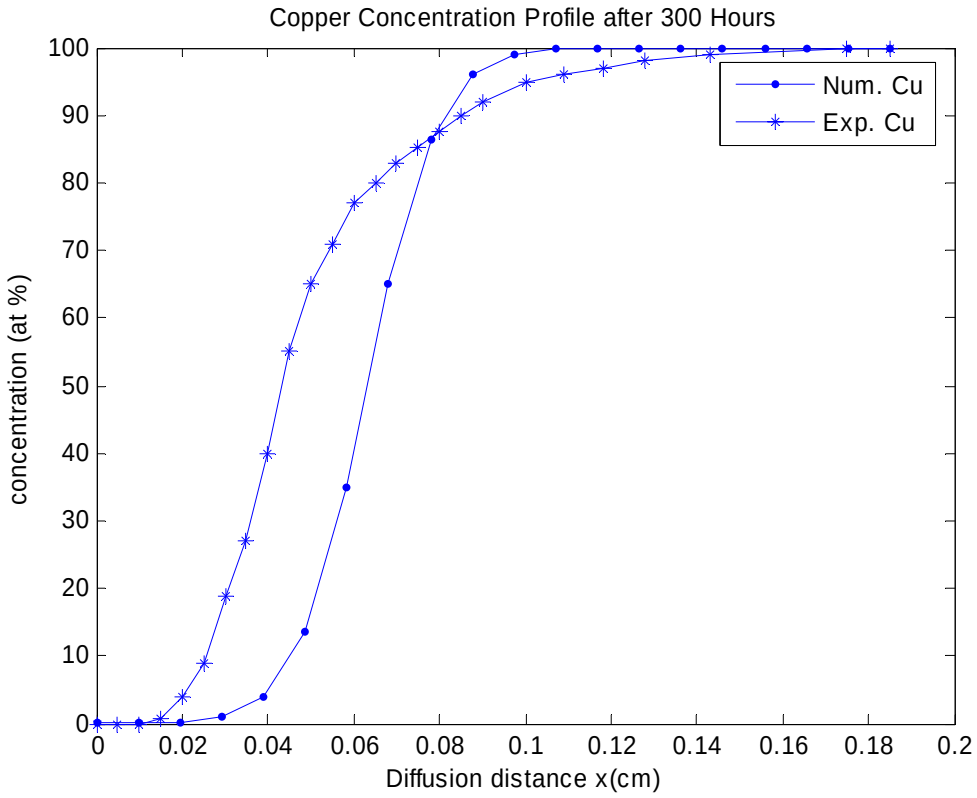

Figure 6.11 Copper numerical and experimental concentration profiles after 300 hours diffusion treatment

Figure 6.11 shows the numerical and experimental concentration for copper after 300 hours diffusion treatment. The copper diffusion coefficient used was $D_{Cu} = 8.3 \times 10^{-10} cm^2 / s$ (equation 6.18). The dotted (•) concentration profile represents the experimental concentration profile for copper after 300 hours and the star (*) concentration profile represents the copper numerical concentration profile after 300 hours, and at temperature 1054°C. There is good agreement between the copper numerical and experimental concentration profile from $(0 - 0.03) cm$, and

from $(0.09-0.2)\,cm$. There is however some divergence at $(0.04-0.08)\,cm$ diffusion distance, between the numerical and experimental concentration profile for copper after 300 hours diffusion treatment.

The numerical concentration for nickel can be calculated using the same procedure if the nickel diffusion coefficient is known and the boundary conditions are:

$$\begin{array}{ll} 1 & when \quad 0 \le x \le 0.1 \\ 0 & when \quad 0.1 \le x \le 0.2 \end{array} \qquad (6.20)$$

If, the nickel diffusion coefficient is unknown, then the following equation can be used:

$$C_{Ni} = 100 - C_{Cu} \qquad (6.21)$$

where

C_{Cu} is the concentration of copper in nickel.

C_{Ni} is the concentration of nickel in copper.

The numerical concentration of nickel in copper has been shown in Figure 6.12 using equation 6.21:

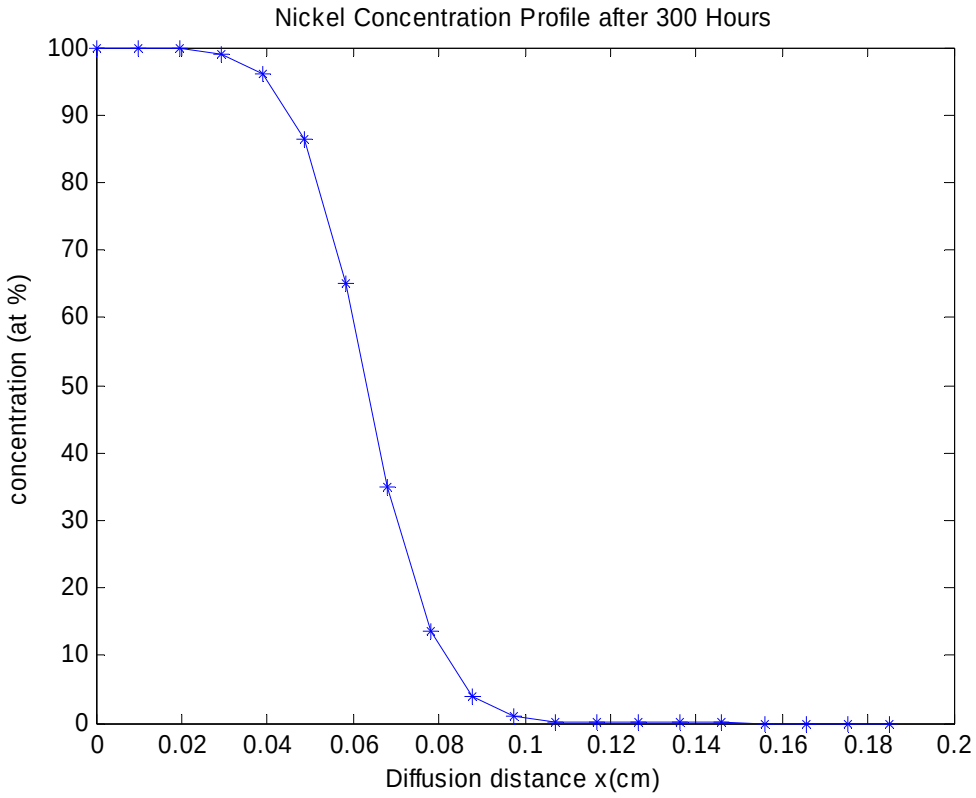

Figure 6.12 Nickel numerical concentration profile (equation 6.21) after 300 hours diffusion treatment

In the following Figure 6.13, the difference between the numerical and experimental concentration profiles for copper has been plotted against the diffusion distance.

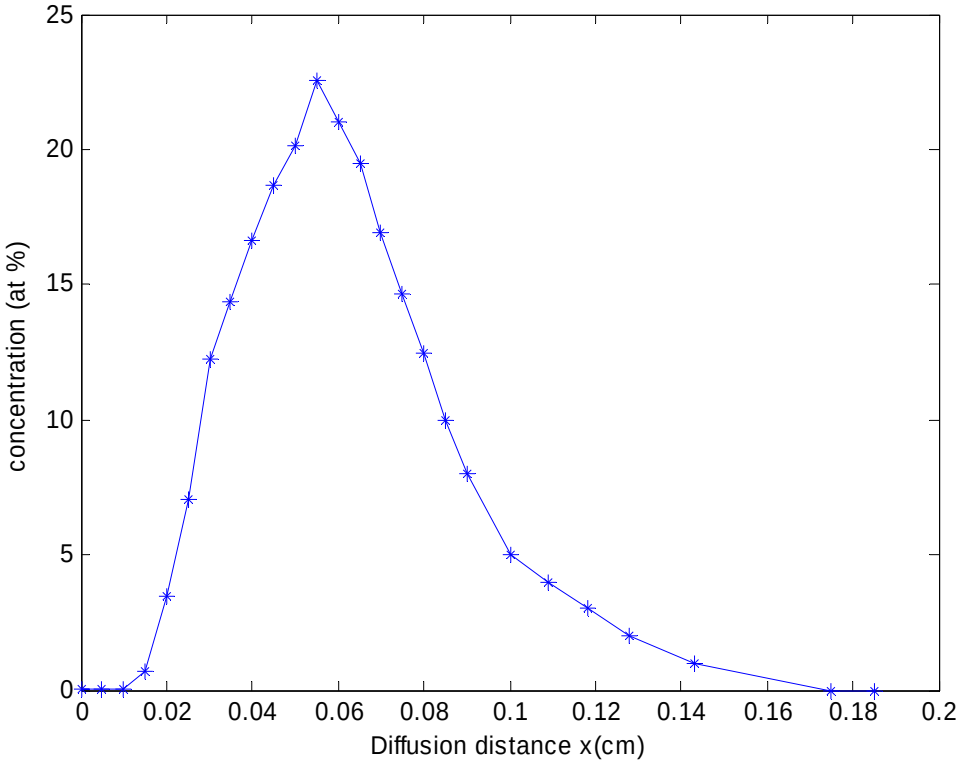

Figure 6.13 The absolute error between the copper numerical and experimental concentration profiles

Figure 6.13 shows the difference between copper experimental and numerical concentration profiles. Figure 6.13 shows that $(22.5149\,at\%)$ is the maximum difference between the copper numerical and experimental concentration profile.

6.3.3.1. Conclusions of Using the Analytical Diffusion Coefficient $D_{Cu}=8.3x10^{-10}cm^2/s$

A numerical concentration profile, from Fick's second law (equation 3.6) has been determined for a binary system with time step size (0.01 second). The concentration profile is a function of time and distance. The numerical concentration has been shown in Table 6.1. In Figure 6.11 the copper numerical and experimental concentration profiles have been presented after 300 hours. As shown from the Figure

6.11 there is a divergence between the copper numerical and experimental concentration for the $(0.04-0.08)\,cm$ diffusion distance, after 300 hours diffusion treatment. Figure 6.11 explains how the copper experimental concentration increases rapidly from $(0.02-0.09)\,cm$, while the numerical concentration increases gradually from $(0-0.05)\,cm$ and then rapidly $(0.09)\,cm$. In the diffusion couple formed from copper and nickel, Figure 7.11 demonstrates that copper moves faster than nickel, in agreement with the fact that copper melts at a lower temperature than Nickel. Figure 6.13 shows the maximum difference between the copper numerical and experimental concentration profiles is $(22.5149\,at\%)$. To reduce the divergence between the experimental and calculated concentration profile, the Genetic Algorithms method as described in chapter 5 has been applied and is described in the next section.

6.3.4. Numerical Solution using Genetic Algorithms Method to Determine Constant Diffusion Coefficient for Copper-Nickel System

The Genetic Algorithms optimization method was used to calculate the diffusion coefficient of copper (Cu) in the $Cu-Ni$ binary system. The diffusion coefficient of copper was assumed to be constant. This diffusion coefficient was used to calculate the numerical concentration of Cu in the system. The numerical concentration of the component was calculated by using the numerical method (Rung-Kutta of order four, equation 4.37). This technique has been applied to solve Ficks second law 4.6:

$$\frac{\partial C}{\partial t} = D\frac{\partial^2 C}{\partial x^2}$$

where D is the diffusion coefficient calculated from the Genetic Algorithms optimization technique.

Rung-Kutta method of order four (equation 4.37):

$$C_{n+1} = \frac{1}{6}(k_1 + 2k_2 + 2k_3 + k_4),$$
$$k_1 = hf(x_n, y_n),$$
$$k_2 = hf(x_n + \frac{1}{2}h, y_n + \frac{1}{2}k_1),$$
$$k_3 = hf(x_n + \frac{1}{2}h, y_n + \frac{1}{2}k_2),$$
$$k_4 = hf(x_n + h, y_n + k_3).$$

The error between the experimental and numerical concentration was calculated using the least squares approximations (equation 4.58):

$$Error = \sum_{i=1}^{N} (Y_i - y_i)^2$$

where Y_i corresponds to the experimental concentration for such a component, and y_i represents a numerical concentration value for the same component, and N represents the number of points in the concentration profile. In the following Figure 6.14 the experimental and the calculated numerical concentration of copper are presented.

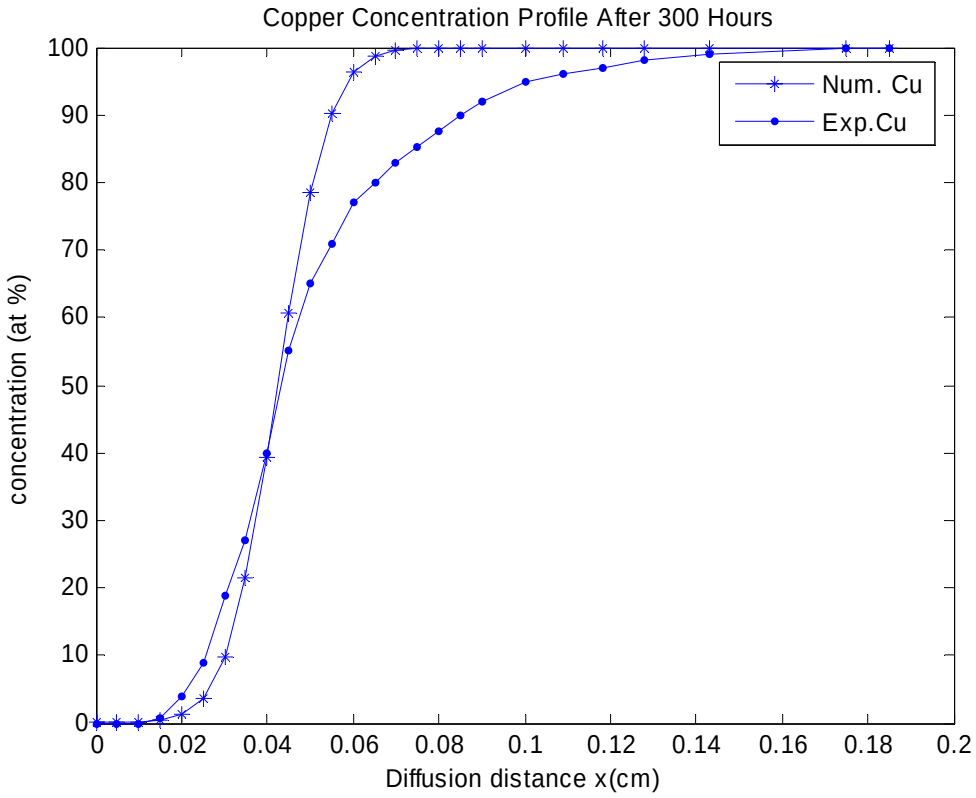

Figure 6.14 Copper numerical concentrations and experimental concentrations after 300 hours diffusion treatment with constant diffusion coefficient

Figure 6.14 shows copper experimental and numerical concentration after 300 hours diffusion treatment. The optimum value for the copper diffusion coefficient was $D_{Cu} = 1.54 \times 10^{-10} cm^2 / s$ calculated using the Genetic Algorithms method. There is good agreement between the experimental and numerical concentration profile of copper from $(0 - 0.05) cm$ diffusion distance, and between $(0.11 - 0.18) cm$ diffusion distances. Some divergence is seen between the experimental and numerical concentration profile for copper from the $(0.06 - 0.10) cm$ diffusion distance.

Figure 6.15 shows the difference between the numerical and experimental concentration profiles for copper against diffusion distance.

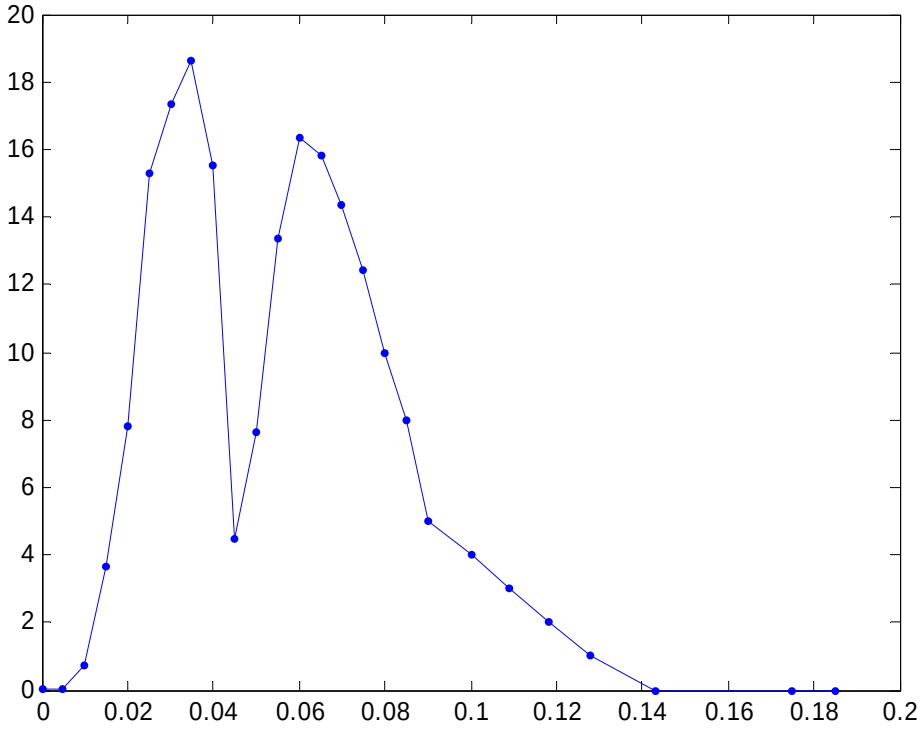

Figure 6.15 the difference between copper experimental and numerical concentration profiles

Figure 6.15 shows that 18.6139 is the maximum difference between the copper numerical and experimental concentration profile for the use of diffusion coefficient calculated from Genetic Algorithms method.

6.3.4.1. Conclusions for Copper-Nickel System Using Constant Diffusion Coefficient Determined From GAs Method

Fick's second law has been used to find the concentration profile for copper (Cu) using Rung-Kutta method of order four. Genetic Algorithms method allowed optimization of the value of the diffusion coefficient. The calculated concentration profiles have been compared with the experimental data using Least squares method. There is good agreement between the copper numerical concentration and experimental

concentration through the entire range of diffusion distance after 300 hours diffusion treatment. Using GAs method, the maximum difference between the copper experimental and numerical concentration profile curve was (18.6139) (Figure 6.15), while using the analytical diffusion coefficients, the maximum difference was (22.5149) as shown in Figure 6.13. Clearly there is an improvement in the numerical concentration profile when the Genetic Algorithms optimization method was used to calculate the copper diffusion coefficients (assumed constant).

6.3.5. Numerical Solution using Genetic Algorithms Method to Optimise Diffusion Coefficients with Assumption of their Dependence on Composition (i.e. Variable Diffusion Coefficients)

In this section Fick's second Law has been solved using a variable diffusion coefficient for the copper using Genetic Algorithms method. With variable diffusion coefficient Fick's second Law (equation 4.46), the diffusion matrix form becomes:

$$\begin{bmatrix} \frac{\partial C_{1i}}{\partial t} \\ \frac{\partial C_{2i}}{\partial t} \\ \vdots \\ \vdots \\ \frac{\partial C_{ni}}{\partial t} \end{bmatrix} = \frac{1}{\Delta x^2} \left\{ \begin{bmatrix} -2 & 1 & 0 & \cdots & \cdots & \cdots & 0 \\ 1 & -2 & 1 & 0 & & & \vdots \\ 0 & 1 & -2 & 1 & 0 & & \vdots \\ \vdots & 0 & 1 & -2 & 1 & 0 & \vdots \\ \vdots & & 0 & 1 & -2 & 1 & 0 \\ \vdots & & & 0 & 1 & -2 & 1 \\ 0 & 0 & 0 & \cdots & 0 & 1 & -2 \end{bmatrix} \begin{bmatrix} D \times C_{i1} \\ D \times C_{i2} \\ \vdots \\ \vdots \\ \\ \\ D \times C_{in} \end{bmatrix} + \begin{bmatrix} D \times bc_{1i} \\ 0 \\ \vdots \\ \vdots \\ \\ 0 \\ D \times bc_{2i} \end{bmatrix} \right\} \tag{6.22}$$

Case -2

In the earlier sections the diffusion coefficient for the copper component (Cu) was considered to be constant. In this section the diffusion coefficient has been considered to be concentration dependent. Second order polynomial has been used for concentration dependence diffusion coefficient such that:

$$D = m_o + m_1 \times C + m_2 \times C^2 \qquad (6.23)$$

where m_o, m_1, m_2 are the polynomial coefficients. In the following Figure 6.16 the experimental and the calculated numerical concentration have been presented.

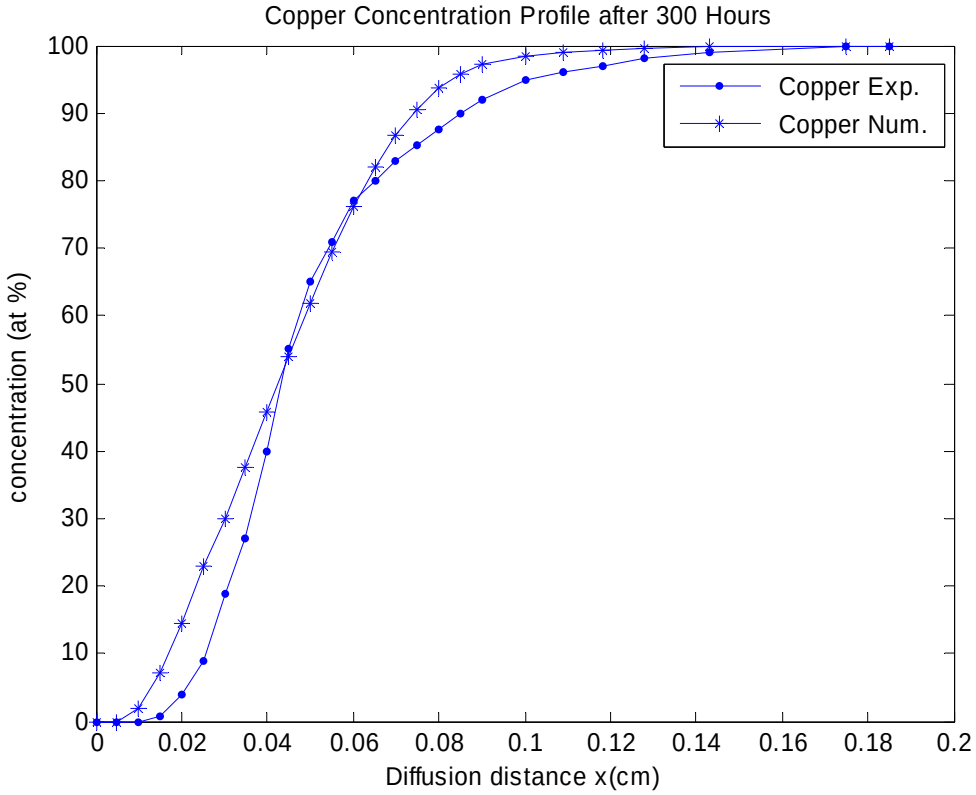

Figure 6.16 Copper numerical and experimental concentration profiles with variable diffusion coefficient

Figure 6.16 shows the numerical and experimental concentration values for copper after 300 hours of diffusion treatment assuming variable diffusion coefficient

(equation 6.23). There is very good agreement between the experimental concentration and numerical concentration for this component (Cu), through the entire range of diffusion distance. m_o, m_1, m_2 for equation 6.23 are as follows:

$$\begin{aligned} m_o &= 1.83\times10^{-10}\, cm^2/\sec \\ m_1 &= 1.2\times10^{-10}\, cm^2/\sec \\ m_2 &= 0.5\times10^{-10}\, cm^2/\sec \end{aligned} \qquad (6.24)$$

These coefficients have been optimized from Genetic Algorithms optimization method. C in the equation 6.23 is the initial copper concentration profile.

In the following Figure 6.17, the difference between the numerical and experimental concentration profiles for copper has been plotted against diffusion distance.

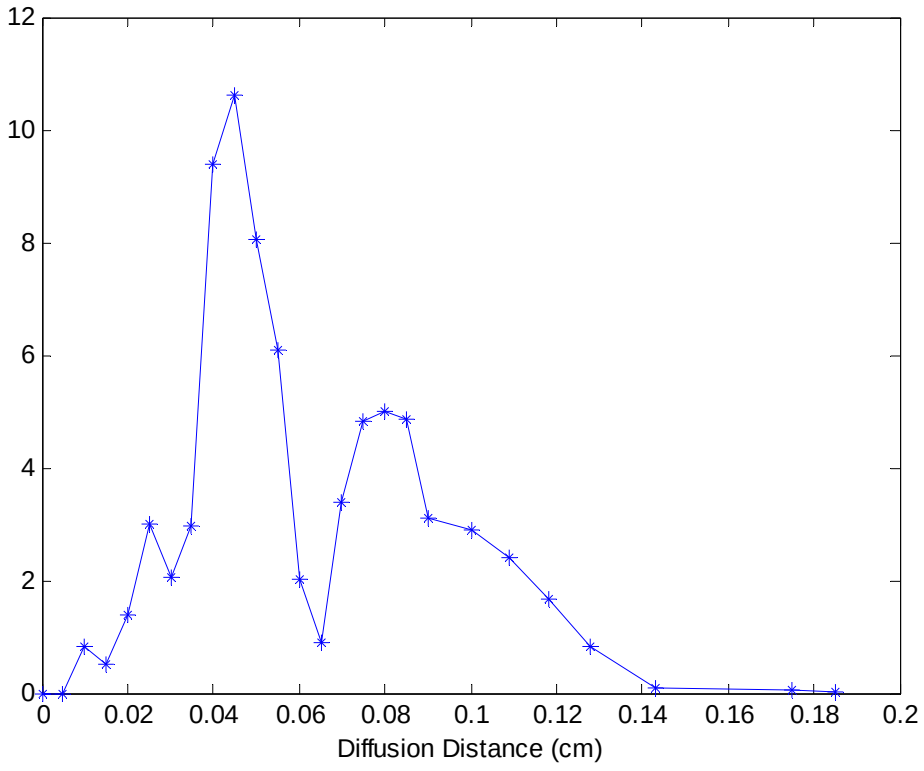

Figure 6.17 the difference between copper experimental and numerical concentration profiles

Figure 6.17 shows the difference between copper experimental and numerical concentration profiles. From the Figure, ($10.6100\,at\%$) was the maximum difference between the copper numerical and experimental concentration profile, when the diffusion coefficients assuming their concentration dependence (equation 6.23).

6.3.5.1. Conclusions for Copper-Nickel Diffusion Couple at 1054°C after 300 Hours Using Variable Diffusion Coefficient Determined from GAs Method

The Genetic Algorithms method has been used to determine the copper diffusion coefficient, assuming their concentration dependence. The Genetic Algorithms method has been used to optimize values of the polynomial's coefficients, m_o, m_1, m_2, for equation 6.23. Figure 6.16 shows a very good agreement between copper experimental and numerical concentration after 300 hours diffusion treatment through the entire range of diffusion distance. The maximum difference between copper experimental and numerical concentration profile has been reduced to ($10.6100\,at\%$) from Figure 6.17 when the diffusion coefficient was variable (second order polynomial). These results clearly show that in this case *D* values were strongly concentration dependent.

6.3.6. Inverse Method of Calculating Diffusion Coefficients from Experimental Concentration of *Cu*

In the earlier sections the aim was to calculate the diffusion coefficient of the components such as copper and nickel in the binary copper - nickel system, so as to calculate the concentration profiles of the components by solving Fick's second law.

However in some cases the concentrations of the components are known and the diffusion coefficients are unknown. In this section we are going to calculate the diffusion coefficient approximately from the concentration (reverse the procedure) profiles. Experimental concentration for the copper has been used to calculate the copper diffusion coefficient. The method of Finite difference was applied on Fick's second law as follows:

$$\frac{c_{i+1}-c_i}{\Delta t} = D \times \frac{c_{i+1}-2c_i+c_{i-1}}{(\Delta x)^2} \tag{6.25}$$

where $\Delta t = t_{i+1} - t_i$

$$\Rightarrow \Delta t = t_2 - t_1$$

$t_2 = 300\ hours = 108000\ \text{sec}ond$
$t_1 = 0$

$(\Delta x)^2 = (0.01)^2\ cm$

Consequently,

$$D = \frac{c_{i+1}-c_i}{\Delta t} \Big/ \frac{c_{i+1}-2c_i+c_{i-1}}{(\Delta x)^2} \tag{6.26}$$

The calculation's steps are as follows:

1. The last few points and beginning few points from the experimental concentration have been removed, that is the middle experimental concentration points from (19-90) at% have been chosen. Then equation 6.26 was applied to calculate *D*, followed by calculation of the arithmetic mean of the column of D.
2. From the experimental concentration, the average of every three points was computed as follows:

$$\frac{c_1 + c_2 + c_3}{3} = c_1'$$
$$\frac{c_4 + c_5 + c_6}{3} = c_2'$$
$$\vdots \qquad (6.27)$$
$$\frac{c_{n-2} + c_{n-1} + c_n}{3} = c_n'$$

Thus equation 6.26 was used to calculate D, followed by calculation of the arithmetic mean of the column of D.

3. Finally the average of step 1 and 2 was calculated as follows:

$$D = \frac{4.0791\times10^{-10} + 2.5250\times10^{-10}}{2} = 3.3021\times10^{-10}\, cm^2/s \quad .$$

In Table 6.2, the steps 1 and 2 are shown.

Middle Concentration Point at% Step 1	Diffusion Coefficient cm^2/s	Average concentration Points Step 2	Diffusion Coefficient cm^2/s
19			
27	2.41E-10		
40	6.94E-10	1.5967	
55	9.26E-10	18.3333	1.77E-10
65	2.78E-10	53.3333	3.94E-10
71	2.78E-10	76	1.87E-10
77	1.98E-10	85.2667	3.64E-10
80	1.74E-10	92.3333	2.70E-10
83	6.94E-10	97	1.23E-10
85.3	1.25E-10	99.6667	
87.5	1.07E-10		
90	7.72E-10		
	A1m= 4.0791e-010		A2m=2.5250e-010

Table 6.2 Copper experimental concentration and diffusion coefficients

Table 6.2 shows the steps 1 and 2 for diffusion coefficient calculation. A1m corresponds to the arithmetic mean of column (2) from the table step (1), and A2m corresponds to the arithmetic mean of column (4) from the table step (2). As a result the

approximated copper diffusion coefficient was $3.3021\times10^{-10} cm^2/s$ and the analytical diffusion coefficient for copper (equation 6.18) was $8.3\times10^{-10} cm^2/s$.

6.3.6.1. Conclusions

Copper experimental concentration has been used to calculate copper diffusion coefficient using equation 6.26. The procedure of inverse method has been explained in three steps, so instead of calculating the numerical concentration for copper after estimating its diffusion coefficient, the diffusion coefficient has been calculated approximately from the copper experimental concentration. The approximated copper diffusion coefficient was $3.3021\times10^{-10} cm^2/s$ while the analytical diffusion coefficient was $8.3\times10^{-10} cm^2/s$.

6.4. *Pt-Ni-Al* Solid Alloy System Containing Three Elements

The information from interdiffusion studies on Pt-Ni-Al solid system is as described in section 3.4.

6.4.1. Microstructural Aspects / Microstructural Modelling of the Diffusion Processes Involved - Results and Discussion

This system consists of three components – nickel, aluminium and platinum. It is a multicomponent system with limited number of elements. This is relatively simple but this simple multicomponent system has been used as a first step in modelling a complex multicomponent system.

Figure 6.18 shows the measured concentration profiles of the Pt, Ni and Al at 1073 K after 64.5 hours diffusion treatment. Figure 6.19 illustrates Pt, Ni and Al measured concentration profiles for the temperature 1173 K after 5 hours diffusion treatment, and Figure 6.20 demonstrates the measured concentration profiles for these components (Pt, Ni and Al) after 1273 K after 1 hour diffusion treatment. These profiles have been obtained from previous work in our laboratory [39].

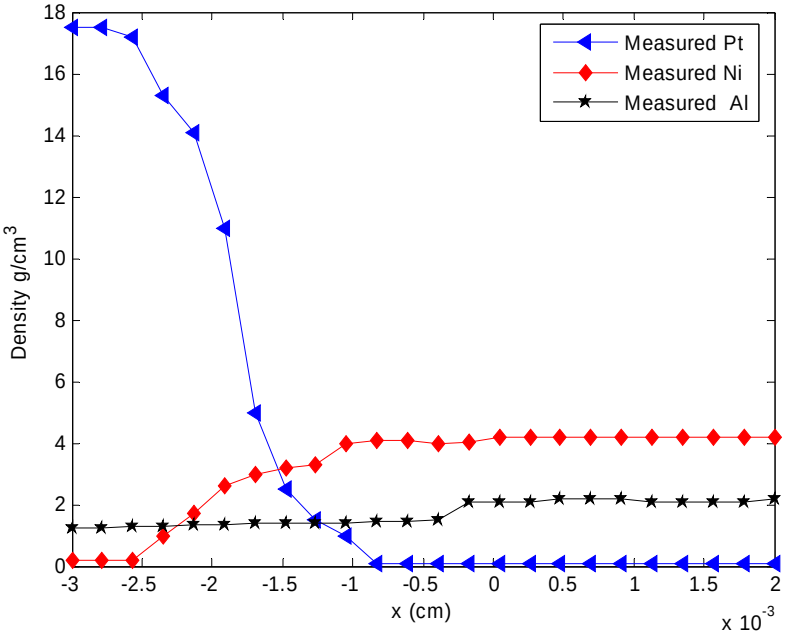

Figure 6.18 Measured concentration profiles in Pt/ β -NiAl system at 1073 after 64.5 hours diffusion treatment [39]

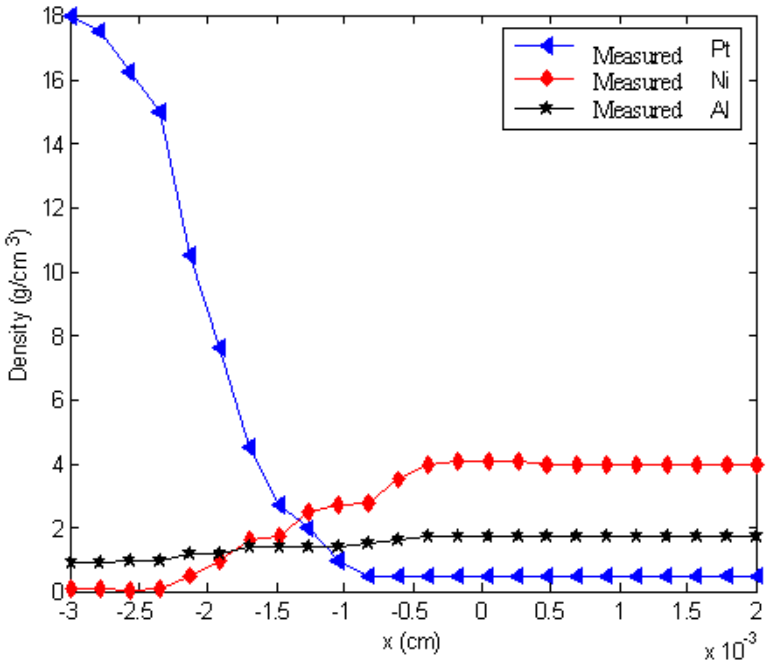

Figure 6.19 Measured concentration profiles in Pt/ β -NiAl system at 1173 after 5 hours diffusion treatment [39]

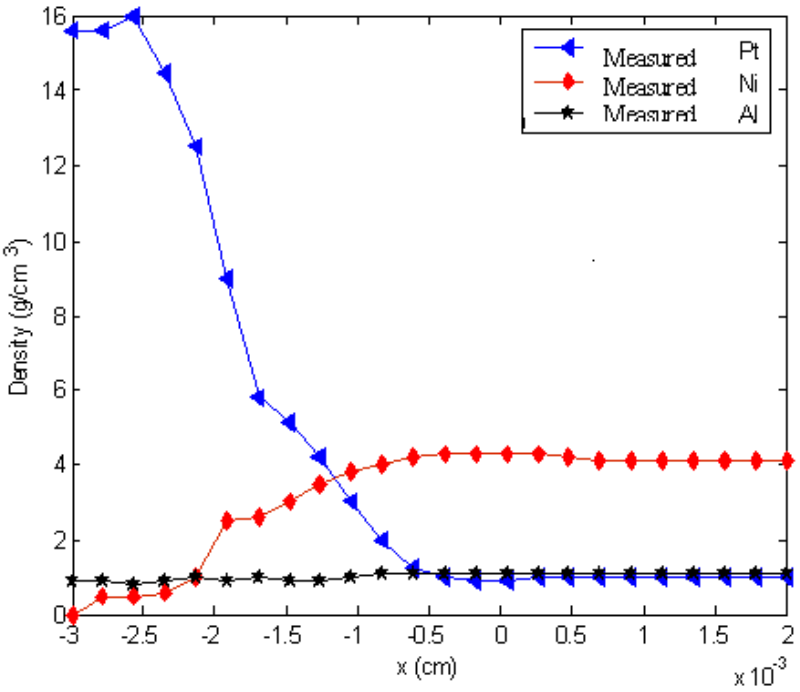

Figure 6.20 Measured concentration profiles in Pt/ β -NiAl system at 1273 after 1 hour diffusion treatment [39]

In the next section (6.4.2) the numerical modelling for interdiffusion for the three components (Ni, Pt, Al) system have been presented.

6.4.2. Modelling of Interdiffusion Using Runge-Kutta Method of Order Four

A trial and error technique was used to calculate the diffusion coefficient of nickel and platinum components (Ni, Pt) in $Pt/\beta - NiAl$. The hypothetical diffusion coefficients of each component have been employed to compute their numerical concentration. The numerical concentration of each component was calculated by using the numerical method (Runge-Kutta method of order four, equation 3.37),

$$C_{n+1} = \frac{1}{6}(k_1 + 2k_2 + 2k_3 + k_4),$$
$$k_1 = hf(x_n, y_n),$$
$$k_2 = hf(x_n + \frac{1}{2}h, y_n + \frac{1}{2}k_1),$$
$$k_3 = hf(x_n + \frac{1}{2}h, y_n + \frac{1}{2}k_2),$$
$$k_4 = hf(x_n + h, y_n + k_3).$$

was applied to Fick's second law 4.6

$$\frac{\partial C}{\partial t} = D\frac{\partial^2 C}{\partial x^2}$$

where D is the diffusion coefficient calculated from trial and error technique.

Fick's second law for the multi-component system can be written as:

$$\frac{\partial C_i}{\partial t} = \sum_{j=1}^{n-1} \tilde{D}_{ij}^{n} \frac{\partial^2 C_j}{\partial x^2} \tag{6.28}$$

$$\Rightarrow \begin{bmatrix} \frac{\partial C_1}{\partial t} \\ \frac{\partial C_2}{\partial t} \end{bmatrix} = \begin{bmatrix} \tilde{D}_{11}^{3} & \tilde{D}_{12}^{3} \\ \tilde{D}_{21}^{3} & \tilde{D}_{22}^{3} \end{bmatrix} \begin{bmatrix} \frac{\partial C_1}{\partial x^2} \\ \frac{\partial C_2}{\partial x^2} \end{bmatrix} \tag{6.29}$$

$$\begin{aligned} \frac{\partial C_1}{\partial t} &= \tilde{D}_{11}^{3} \frac{\partial^2 C_1}{\partial x^2} + \tilde{D}_{12}^{3} \frac{\partial^2 C_2}{\partial x^2} \\ \frac{\partial C_2}{\partial t} &= \tilde{D}_{21}^{3} \frac{\partial^2 C_1}{\partial x^2} + \tilde{D}_{22}^{3} \frac{\partial^2 C_2}{\partial x^2} \qquad (1 = Ni, \quad 2 = Pt, \quad 3 = Al) \end{aligned} \tag{6.30}$$

Thus the diffusion coefficients matrix can be written as:

$$\begin{bmatrix} D_{11} & D_{12} \\ D_{21} & D_{22} \end{bmatrix} \tag{6.31}$$

The Least squares approximations method (6.58)

$$Error = \sum_{i=1}^{n} (E_i - N_i)^2$$

was used to calculate the error between the numerical concentration and experimental concentration of each component in the sample. E_i is the experimental concentration for every component, and N_i is the numerical concentration.

In the first part of this investigation the diagonal diffusion coefficients, (in the diffusion matrix), were considered constant and the cross terms were considered to be zero.

In Figure 6.21 the nickel diffusion coefficient (D_{Ni}=4.7241x10^{-11}cm^2/s), calculated from trial and error technique, was used to calculate the nickel numerical concentration using Runge-Kutta method of order four.

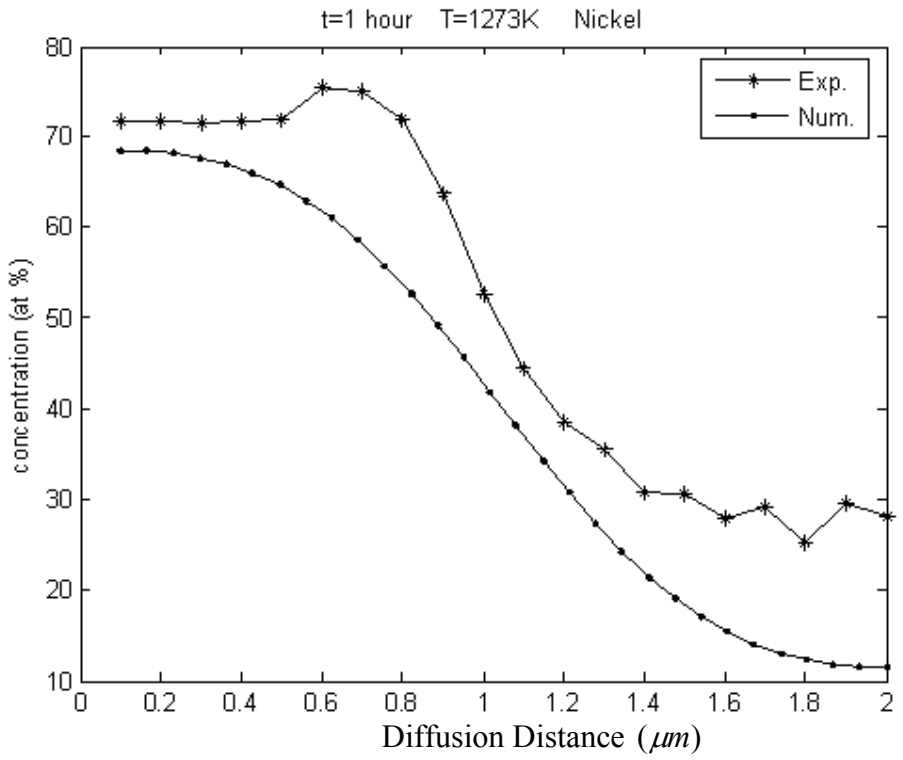

Figure 6.21 Nickel numerical and experimental concentration profiles after 1 hour diffusion treatment

As shown in the Figure 6.21 the star (*) concentration profile curve shows the nickel experimental concentration after 1 hour diffusion treatment, and the point (•) concentration profile curve represents the numerical concentration profile after1 hour. There is reasonable agreement between the numerical and experimental concentration profile for nickel component.

Figure 6.22 shows the experimental and numerical concentration profiles for platinum after 1 hour diffusion treatment. The diffusion coefficient is (D_{Pt}=6.973241x10^{-11}cm^2/s) and was calculated from trial and error technique.

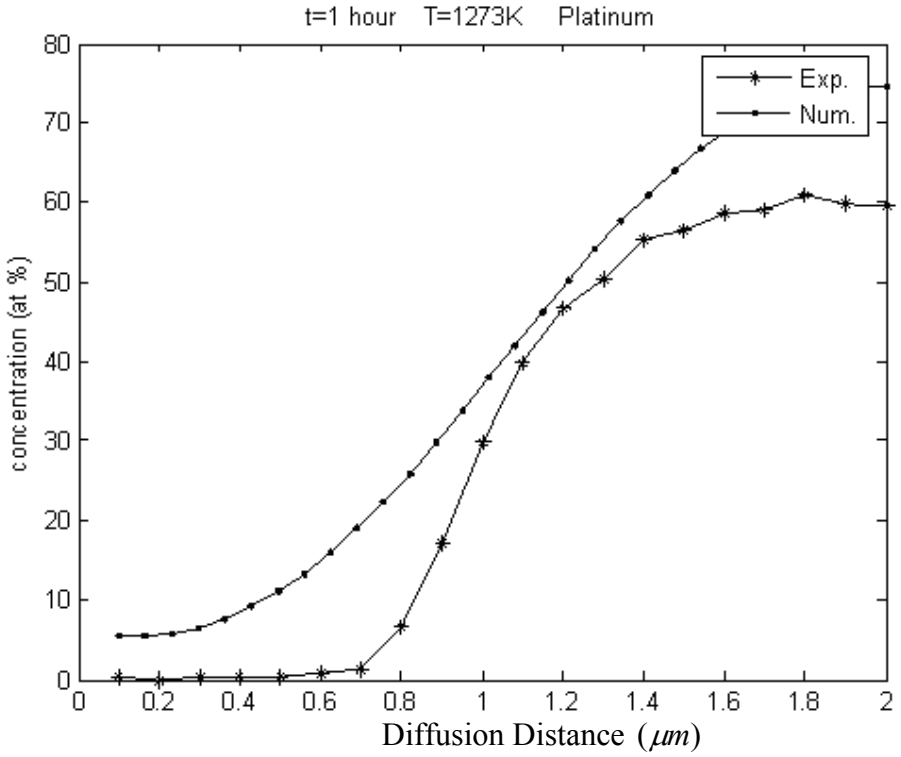

Figure 6.22 Platinum numerical and experimental concentration profiles for the diffusion coefficient (D_{Pt}=6.973241x10^{-11}cm^2/s)

As shown from the Figure 6.22 there is an agreement between the numerical concentration profile and experimental concentration profile of platinum for the

diffusion distances (0-0.4) x 10^{-3} μm, and (1-1.5) x 10^{-3} μm. There is some divergence between (0.5-0.9) x10^{-3} μm, and (1.6-2) x10^{-3} μm diffusion distance.

6.3.2.1. Conclusions of Using Trial and Error Technique

Fick's second law has been used to calculate the concentration profile for each component (*Ni, Pt*) using Rung-Kutta method of order four. A trial and error technique was used to calculate the diffusion coefficient of nickel and platinum components (*Ni, Pt*) of the sample. The Least squares method has been used to compute the absolute error between the numerical and experimental concentration profile for each component (*Ni, Pt*). There is reasonable agreement for nickel component between the experimental and numerical concentration profile, while there is some divergence between (0.5-0.9) x10^{-3} μm, and between the diffusion distances (1.6-2) x10^{-3} μm for platinum component. For the aluminum component, the numerical concentration can be calculated using the equation

$$C_1+C_2+C_3=100\% \qquad (6.32)$$

at any time of diffusion treatment (1=*Ni*, 2=*Pt*, and 3=*Al*), where C_1, C_2, C_3 are nickel, platinum, and aluminum concentration profile respectively So the aluminum numerical concentration is;

$$C_3=100\% - (C_1+C_2)$$

which has been presented in the following Figure 6.23. The absolute error between aluminum numerical concentration and experimental concentration is (291.0418).

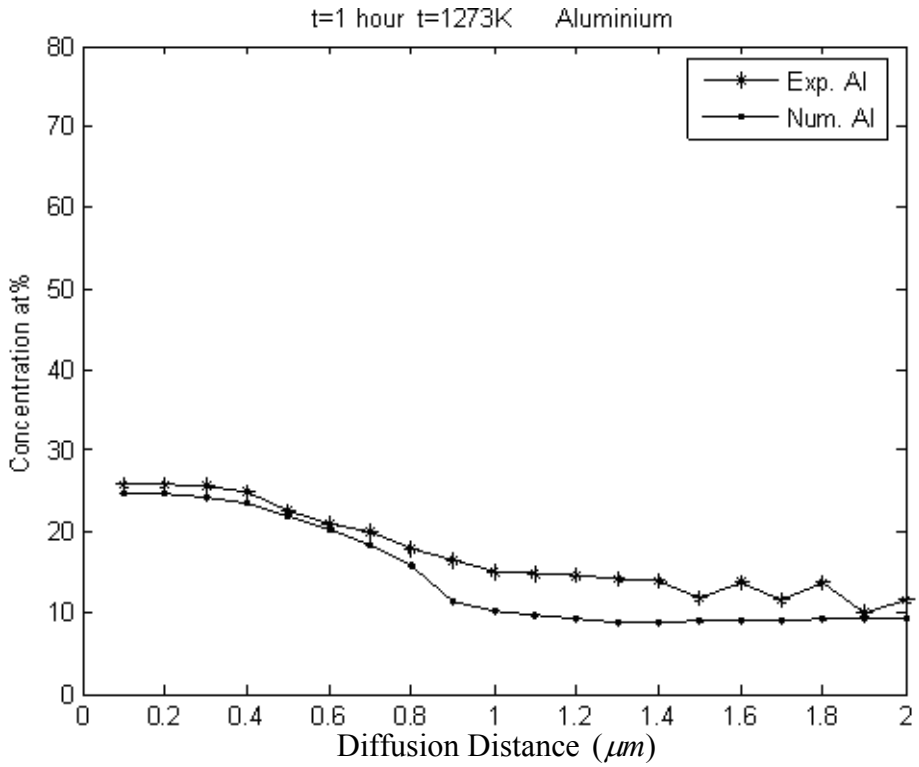

Figure 6.23 Aluminum numerical and experimental concentration profiles after 1 hour diffusion treatment

6.4.3. Calculation of the Diffusion Coefficients Using the Genetic Algorithms Method

The Genetic Algorithms method was used to calculate the diffusion coefficients for each component (Ni, Pt) of the sample (details in chapter 4). The diffusion coefficients of each component were then used to compute their numerical concentration using equation 4.37.

In this analysis only the diagonal diffusion coefficients were considered with the cross terms assumed zero.

In Figure 6.24 the numerical and experimental concentration profiles for nickel have been presented after 1 hour diffusion treatment. The nickel diffusion coefficient calculated from Genetic Algorithms method was $D_{Ni} = 6.7619 \times 10^{-11} cm^2 / s$. Similar

for platinum, the numerical and experimental concentrations have been presented in Figure 6.25;

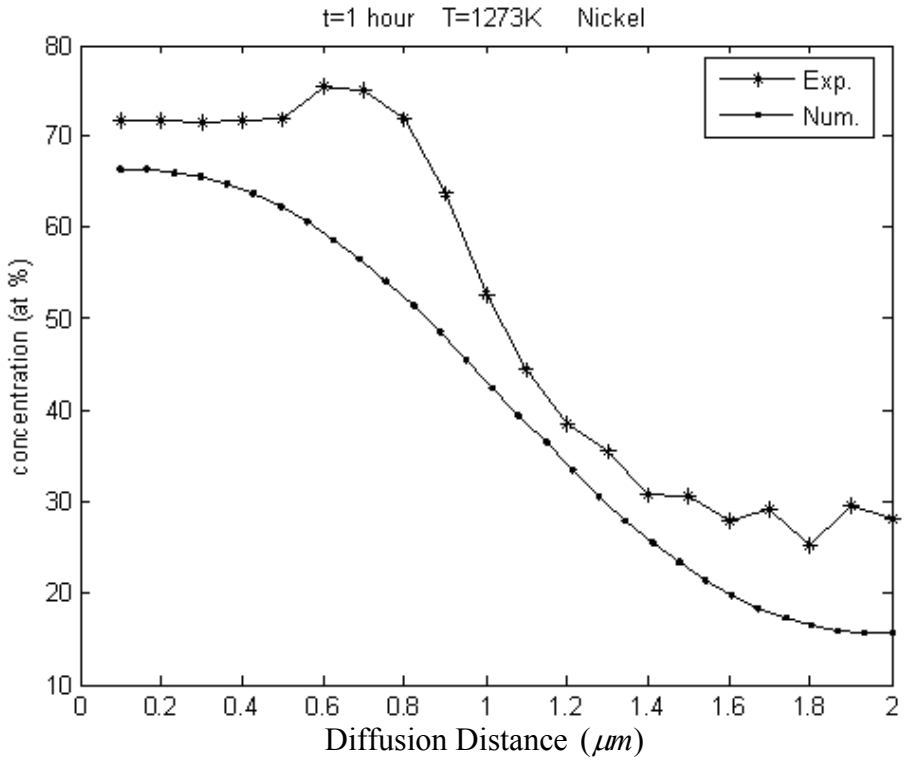

Figure 6.24 Numerical and experimental concentration profiles for nickel after 1 hour diffusion treatment

There is good agreement between the numerical and experimental concentration profiles of nickel for the diffusion distance (0.1-0.5) x10^{-3} μm, and some divergence can be seen for the diffusion distance (0.6-0.9) x10^{-3} μm.

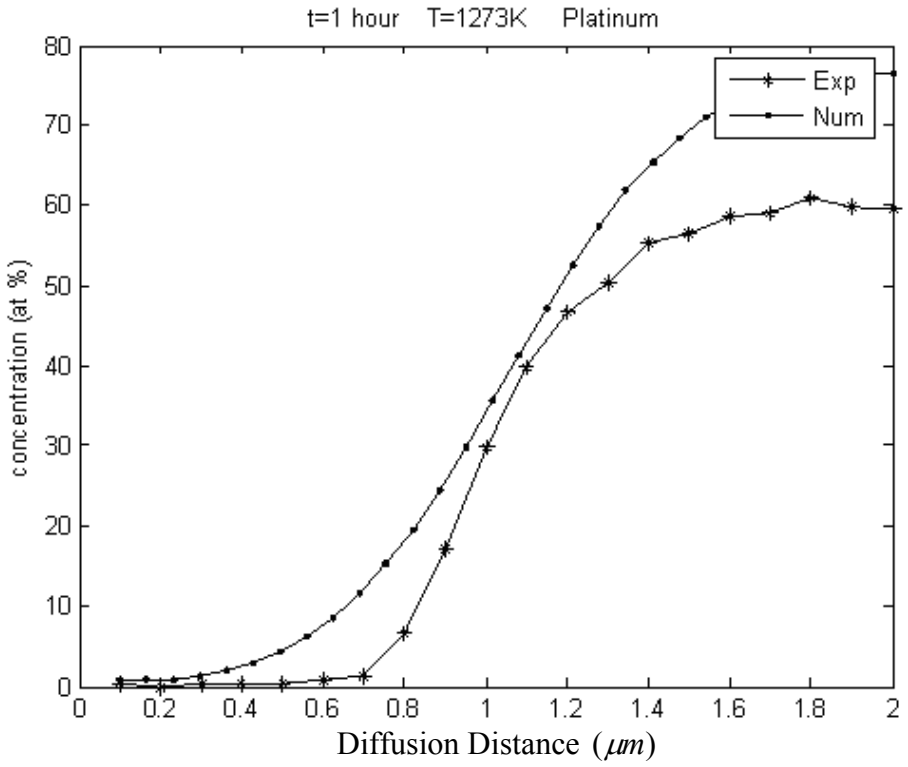

Figure 6.25 Platinum numerical and experimental concentration profiles after 1 hour diffusion treatment

Figure 6.25 illustrates the numerical and experimental concentration profiles for platinum after 1 hour diffusion treatment. The platinum diffusion coefficient (D_{Pt}=3.38712x10^{-11}cm^2/s) was calculated from Genetic Algorithms method. There is an agreement between the platinum experimental concentration and numerical concentration from (0-1.4) x10^{-3} μm diffusion distance, with some divergence from (1.5-2) x10^{-3} μm diffusion distance.

6.4.3.1. Conclusions for using GAs method (Constant Diagonal Terms)

Fick's second law has been solved using Runge-Kutta method of order four. The Genetic Algorithms method has been used to optimise the values of diffusion coefficients, in the diffusion matrix;

$$\begin{bmatrix} D_{11} & \\ & D_{22} \end{bmatrix}.$$

The intended concentration profiles have been compared with the experimental data using Least squares method. There is an agreement between the nickel numerical concentration and experimental concentration in almost the entire range of diffusion distance after 1 hour diffusion treatment. For platinum component there is good agreement between the numerical concentration and experimental concentration from (0-1.4) x10^{-3} μm diffusion distance, and a little divergence for the range (1.5-2) x10^{-3} μm diffusion distance after 1 hour diffusion treatment. According to equation 6.32 the numerical concentration for aluminum is presented in Figure 6.26. The absolute error between the aluminum experimental concentration and numerical concentration is (201.4900).

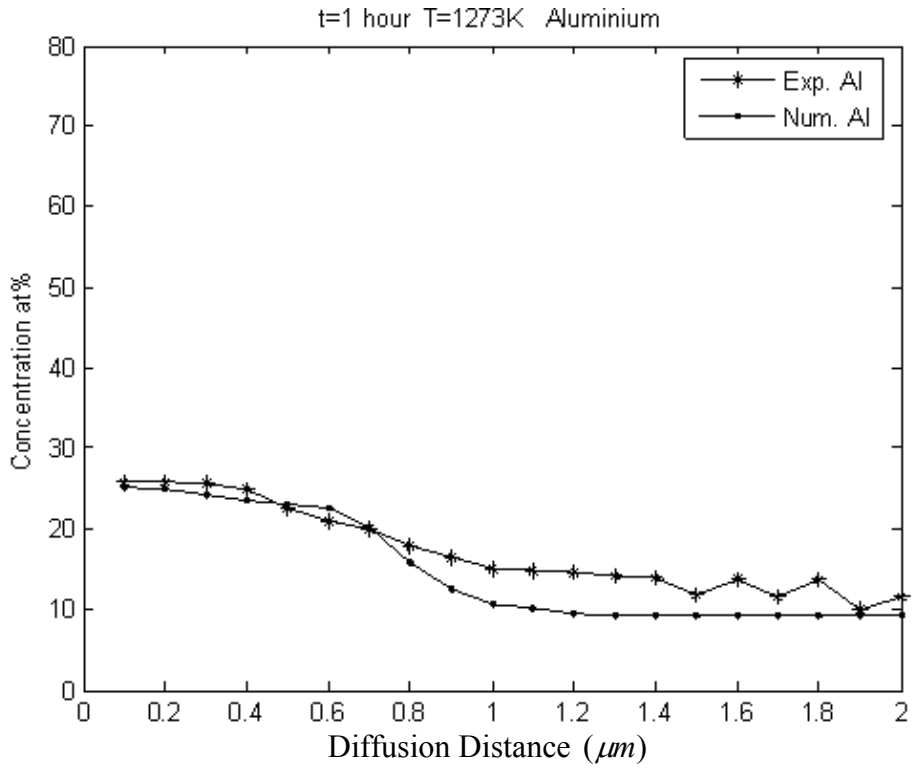

Figure 6.26 Aluminum numerical and experimental concentration profiles after 1 hour diffusion treatment from equation 6.32

6.4.4. Calculation Considering Constant Cross and Diagonal Terms Diffusion Coefficients

Fick's second law for muticomponent system can be written as follows:

$$\Rightarrow \begin{bmatrix} \dfrac{\partial C_1}{\partial t} \\ \dfrac{\partial C_2}{\partial t} \end{bmatrix} = \begin{bmatrix} \tilde{D}_{11}^{3} & \tilde{D}_{12}^{3} \\ \tilde{D}_{21}^{3} & \tilde{D}_{22}^{3} \end{bmatrix} \begin{bmatrix} \dfrac{\partial C_1}{\partial x^2} \\ \dfrac{\partial C_2}{\partial x^2} \end{bmatrix} \tag{6.33}$$

Equation 6.33 explains how the diagonal and cross terms diffusion coefficients are constants:

$$\Rightarrow \frac{\partial C_1}{\partial t} = \tilde{D}_{11}^{3} \frac{\partial^2 C_1}{\partial x^2} + \tilde{D}_{12}^{3} \frac{\partial^2 C_2}{\partial x^2}$$

$$\frac{\partial C_2}{\partial t} = \tilde{D}_{21}^{3} \frac{\partial^2 C_1}{\partial x^2} + \tilde{D}_{22}^{3} \frac{\partial^2 C_2}{\partial x^2} \tag{6.34}$$

$$\begin{bmatrix} D_{11} & D_{12} \\ D_{21} & D_{22} \end{bmatrix} \tag{6.35}$$

In this matrix the diagonal and cross terms have been assumed to be constant.

In Figure 6.27 the experimental and numerical concentration for the components (nickel and platinum), have been presented with the interdiffusion coefficients calculated from the Genetic Algorithms method and using equation 6.33, Fick's second law. Here the cross terms have been taken into account.

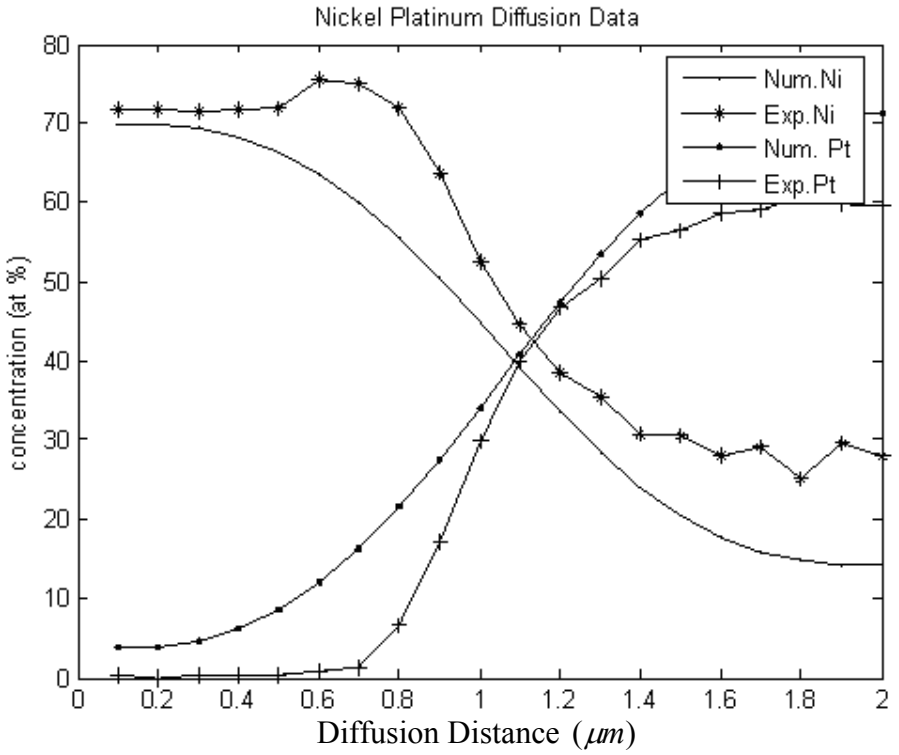

Figure 6.27 Nickel and platinum concentration profiles after 1 hour diffusion treatment (constant cross and diagonal terms)

Figure 6.27 demonstrates nickel platinum concentration (numerical and experimental) using constant diffusion coefficients $D_{11}, D_{12}, D_{21}, D_{22}$ determined from Genetic Algorithms optimization method:

$$\begin{aligned} D_{11} &= 4.594001\times10^{-11} cm^2/s \\ D_{12} &= 2.494231\times10^{-11} cm^2/s \\ D_{21} &= 0.700810\times10^{-11} cm^2/s \\ D_{22} &= 3.193216\times10^{-11} cm^2/s \end{aligned} \tag{6.36}$$

In the above Figure 6.27 the numerical concentration profile for the components (nickel and platinum) have been calculated considering constant cross terms and diagonal terms, in a diffusion matrix. There is reasonable agreement between the experimental and numerical concentration for both the components shown.

6.4.4.1. Conclusions for Using Constant Cross and Diagonal Terms Diffusion Coefficients

The same techniques (as in 6.4.2) have been used to calculate the concentration profiles using the Genetic Algorithms method for optimizing the values of diffusion coefficients, in the diffusion matrix (equation 6.35). There is good convergence between the experimental and numerical concentration for the components (*Ni, Pt*) when equation 6.34 was used to calculate the diffusion coefficients, taking into account the cross terms. The difference between the experimental and numerical concentration profiles for the components (*Ni, Pt*) has been reduced. It means the results or the numerical concentration profiles, for nickel and platinum show much improvement compared to the numerical concentration profiles when the cross terms were considered to be zero. An additional improvement the numerical concentration for aluminum shows more agreement with the experimental concentration when the cross terms are taken into account, that is the absolute error has been reduced. In Figure 6.28 the numerical concentration for aluminum has been presented and the absolute error was (140.051).

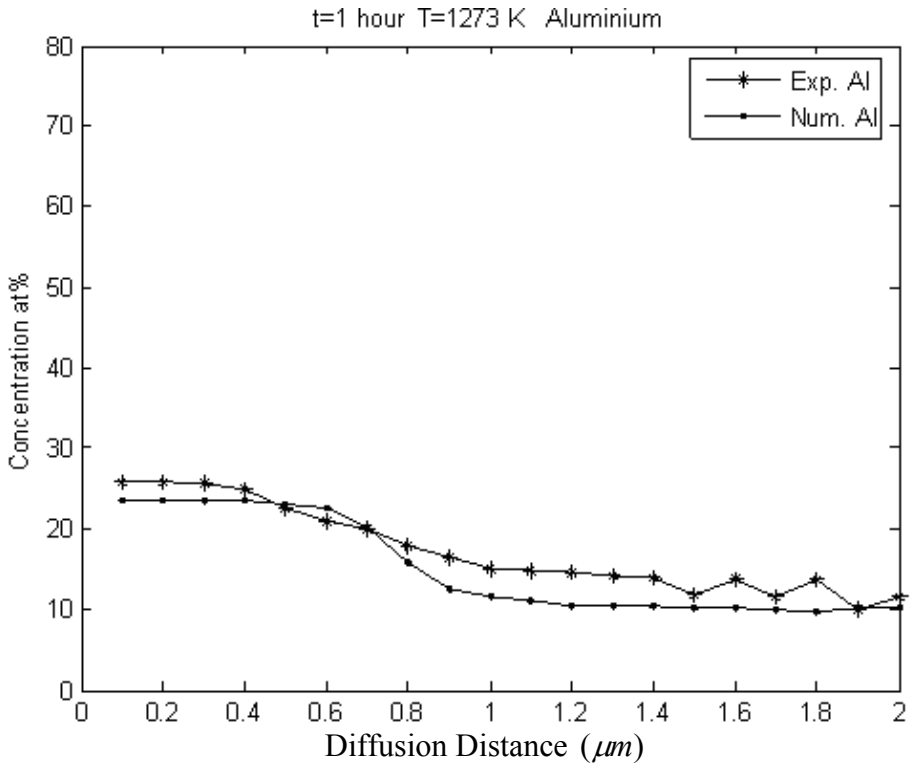

Figure 6.28 Aluminum concentration profiles after 1 hour diffusion treatment (constant cross and diagonal terms)

6.4.5. Calculation Considering Variable Cross and Diagonal Terms Diffusion Coefficients

In the previous part, (6.4.4), the diffusion coefficients (diagonal and cross terms) for the both components (*Ni, Pt*) were considered to be constant. In the present part the diffusion coefficients are considered to be concentration dependent (a function of concentration). A second order polynomial has been used for concentration dependence diffusion coefficients for nickel and platinum components, and the numerical concentration profile for nickel and platinum have been shown below:

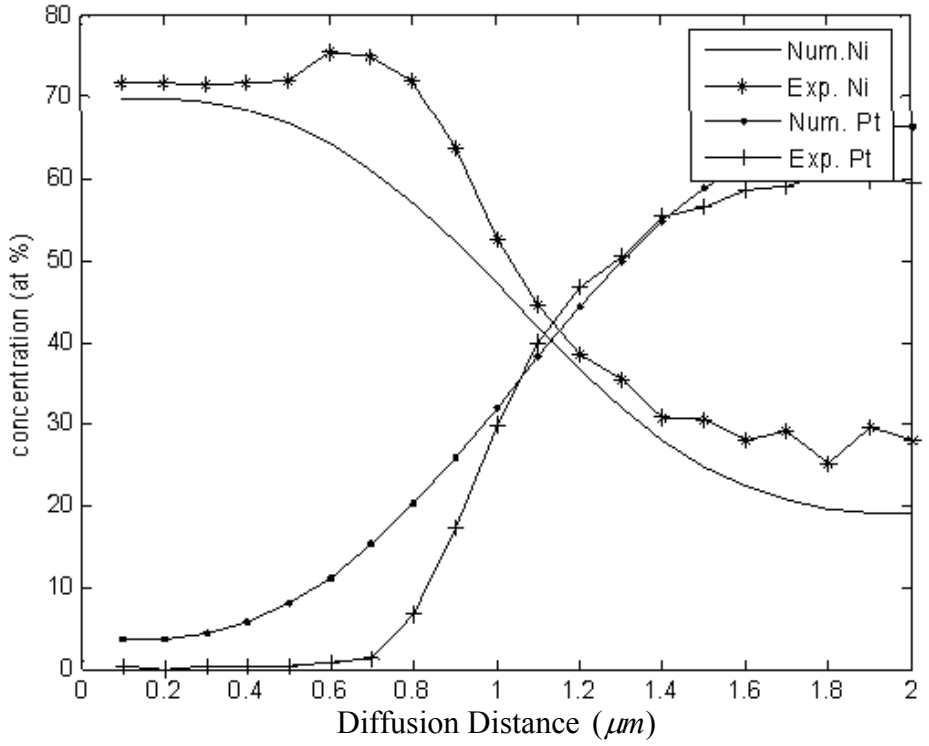

Figure 6.29 Nickel and platinum concentration profiles after 1 hour diffusion treatment (variable cross and diagonal terms)

Figure 6.29 illustrates the numerical and experimental concentrations for nickel and platinum with concentration dependent diffusion coefficients $D_{11}, D_{12}, D_{21}, D_{22}$ (second order polynomial) after 1 hour diffusion treatment. This can be shown mathematically as follows:

$$\begin{aligned} D_{11} &= x_1 + x_2 C_1 + x_3 C_1^{\,2} \\ D_{12} &= y_1 + y_2 C_1 C_2 \\ D_{21} &= z_1 C_2 + z_2 C_2^{\,2} \\ D_{22} &= v_1 + v_2 C_2 + v_3 C_2^{\,2} \end{aligned} \tag{6.37}$$

where C_1 and C_2 are the initial concentration for nickel and platinum respectively. $x_1, x_2, x_3, \cdots, v_1, v_2, v_3$ are the polynomial coefficients calculated using Genetic Algorithms optimization method. The diffusion coefficients values are as follows:

$$D_{11} = 1.3497 \times 10^{-11} cm^2 / s$$
$$D_{12} = 1.0013 \times 10^{-11} cm^2 / s$$
$$D_{21} = 0.1451 \times 10^{-11} cm^2 / s$$
$$D_{22} = 4.3519 \times 10^{-11} cm^2 / s$$

There was very good agreement in the numerical and experimental concentration values for nickel and platinum for the entire range of the diffusion distance.

6.4.5.1. Conclusions of Using Variable Cross and Diagonal Terms Diffusion Coefficients

Fick's second law has been used to determine the concentration profile for each component (*Ni, Pt*) using Rung-Kutta method of order four. The Genetic Algorithms method allows optimization of the values of the coefficients in the second order polynomial (equation 6.36) of diffusion coefficients, in diffusion matrix (equation 6.35). There is good convergence between the experimental and numerical concentration for the components (*Ni, Pt*) when equation 6.37 was used to calculate the diffusion coefficients, (taking into account the cross terms). The difference between the experimental and numerical concentration profiles for the components (*Ni, Pt*) has been reduced significantly. The minimum absolute error was (3.4256e+003) in Figure 6.24 while it was (2.0080e+003) in Figure 6.29. It means there is good convergence between the experimental and numerical concentration for the components (*Ni, Pt*) when equation 6.37 was used to calculate the diffusion coefficients (concentration dependent diffusion coefficients).

For the third component (aluminum) the numerical concentration has been presented in Figure 6.30 as regards to equation 7.32. The absolute error is (35.9284) between the numerical and experimental concentration for aluminum. As a result the absolute errors

for all the components (*Ni, Pt, and Al*) have been reduced when the diffusion coefficients is concentration dependent.

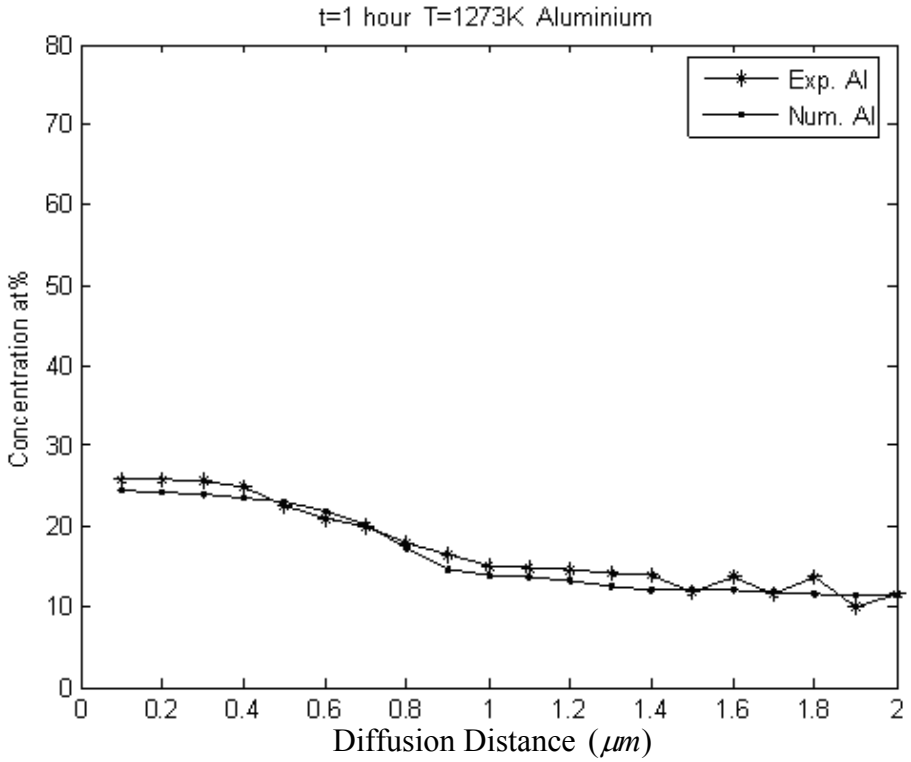

Figure 6.30 Aluminum concentration profiles after 1 hour diffusion treatment (variable cross and diagonal terms)

6.4.6. Calculation of the Constant Diagonal Diffusion Coefficients Using Bounded Nonlinear Function Minimization (fminbnd)

The bounded nonlinear function minimization method was used to calculate the diffusion coefficients for each component (Ni, Pt) of the sample (details in chapter three). The diffusion coefficients of each component were then used to compute their numerical concentration using Runge-Kutta method of order four.

In this analysis only the diagonal diffusion coefficients were considered. In Figure 6.31 the numerical and experimental concentration profiles for nickel have been

presented after 1 hour diffusion treatment. The nickel diffusion coefficient calculated from Bounded Nonlinear Function Minimization Method was $D_{Ni} = 1.5958 \times 10^{-10} cm^2 / s$.

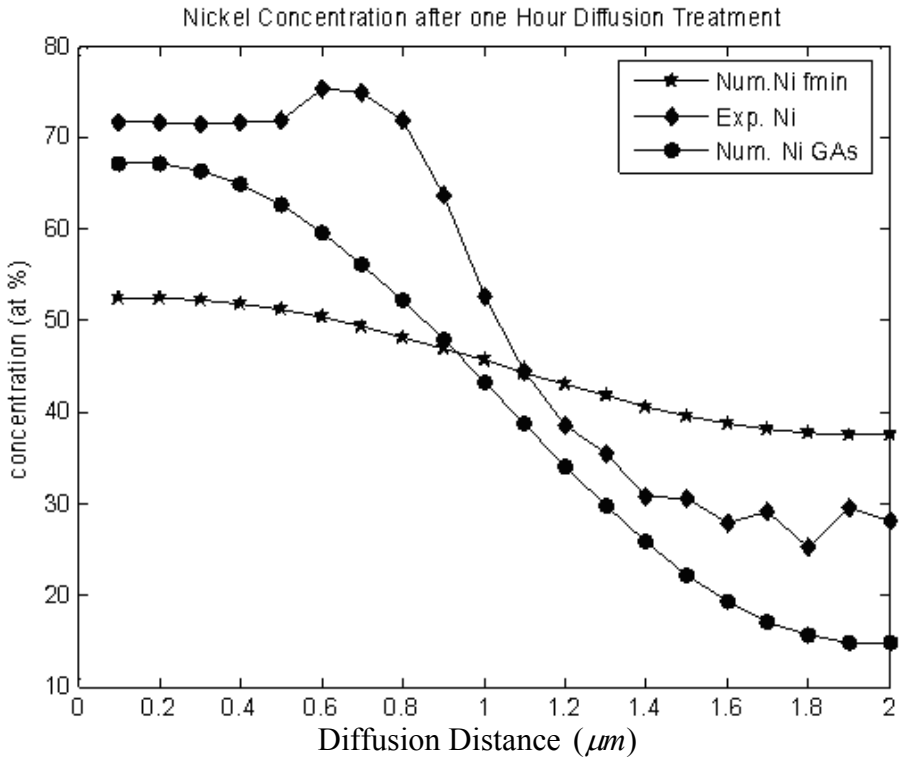

Figure 6.31 Nickel experimental and numerical concentrations after 1 hour diffusion treatment

As shown in the Figure 6.31 the star (*) concentration profile curve is the nickel numerical concentration after 1 hour diffusion treatment when the diffusion coefficient calculated from (fminbnd). The plus (●) concentration profile curve corresponds to the nickel numerical concentration after 1 hour diffusion treatment when the diffusion coefficient calculated from GAs method. The concentration profile (diamond) corresponds to the nickel experimental concentration after 1 hour. The initial guess (range) was (1.1×10^{-11}, 1.6×10^{-10}) to find the diffusion coefficient for both fminbnd method and GAs method. The diffusion coefficient calculated from GAs method as

shown in Figure 6.24 was $D_{Ni} = 6.7619 \times 10^{-11} cm^2 / s$. In the following Figure the numerical concentrations for nickel have been presented with different initial guess.

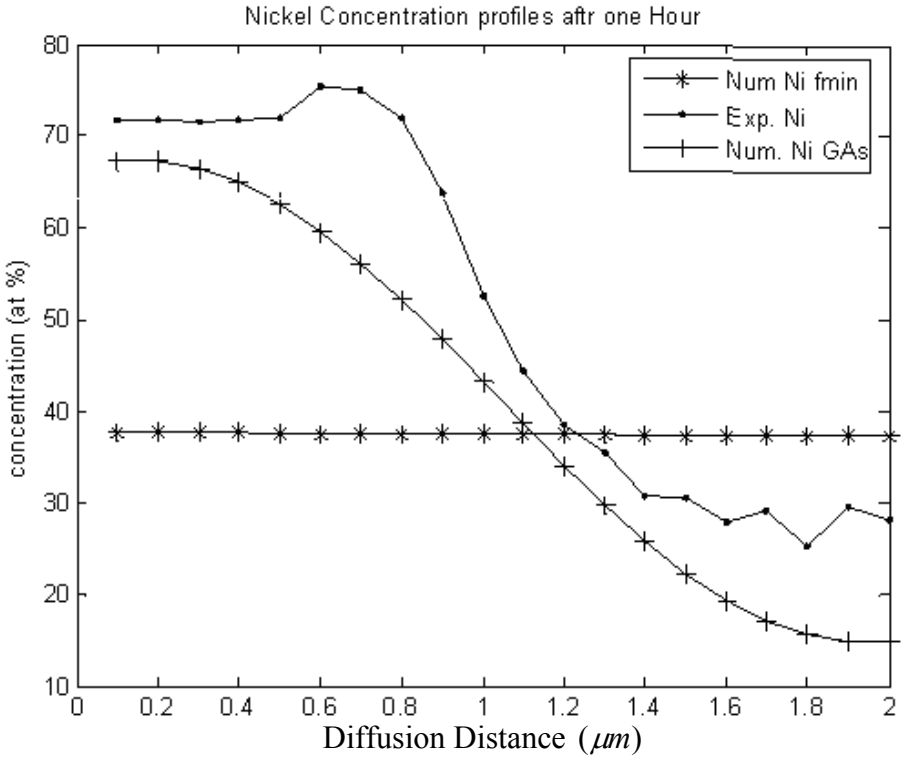

Figure 6.32 Nickel experimental and numerical concentration profiles after 1 hour diffusion treatment

In Figure 6.32 the star (*) concentration profile curve is the nickel numerical concentration after 1 hour diffusion treatment when the diffusion coefficient calculated from fminbnd. The plus (+) concentration profile curve corresponds to the nickel numerical concentration after 1 hour diffusion treatment when the diffusion coefficient calculated from GAs method. The point (.) concentration profile curve corresponds to nickel experimental concentration after 1 hour. The initial guess or range was $(0.71 \times 10^{-11}, 14 \times 10^{-10})$ to find the diffusion coefficient for both fminbnd method and GAs method. The diffusion coefficient calculated from GAs method as shown in Figure

6.24 was $D_{Ni} = 6.7619 \times 10^{-11} cm^2 / s$. The nickel diffusion coefficient calculated from Bounded nonlinear function minimization method was $D_{Ni} = 5.3909 \times 10^{-10} cm^2 / s$.

In Figure 6.33 the numerical and experimental concentration profiles for nickel have been presented after 1 hour diffusion treatment. The nickel diffusion coefficient calculated from Bounded nonlinear function minimization method was $D_{Ni} = 3.3501 \times 10^{-11} cm^2 / s$.

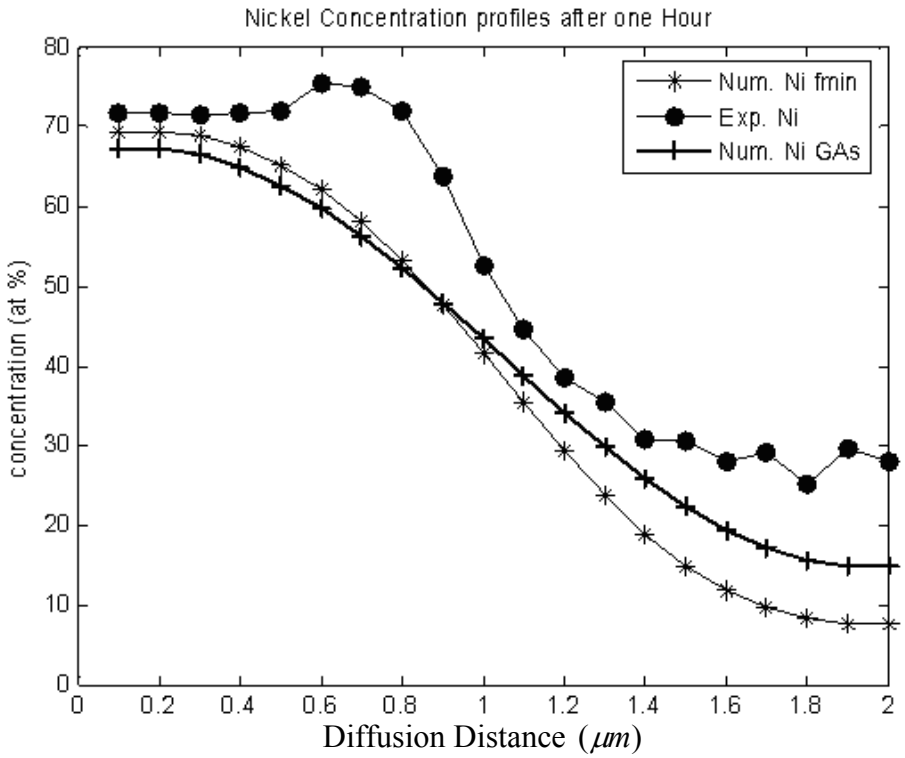

Figure 6.33 Nickel experimental and numerical concentrations profiles after 1 hour diffusion treatment

Figure 6.33 illustrates concentration profile (*****) for nickel numerical concentration after 1 hour diffusion treatment when the diffusion coefficient calculated from fminbnd. The concentration profile (+) for the nickel numerical concentration after 1 hour diffusion treatment when the diffusion coefficient was calculated from GAs method. The point (**.**) concentration profile curve corresponds to the nickel experimental

concentration after 1 hour diffusion treatment. The initial guess or range was $(1\times10^{-11}, 5\times10^{-11})$ to find the diffusion coefficient for both fminbnd method and GAs method. The diffusion coefficient calculated from GAs as shown in Figure 6.24 was $D_{Ni} = 6.7619\times10^{-11} cm^2/s$.

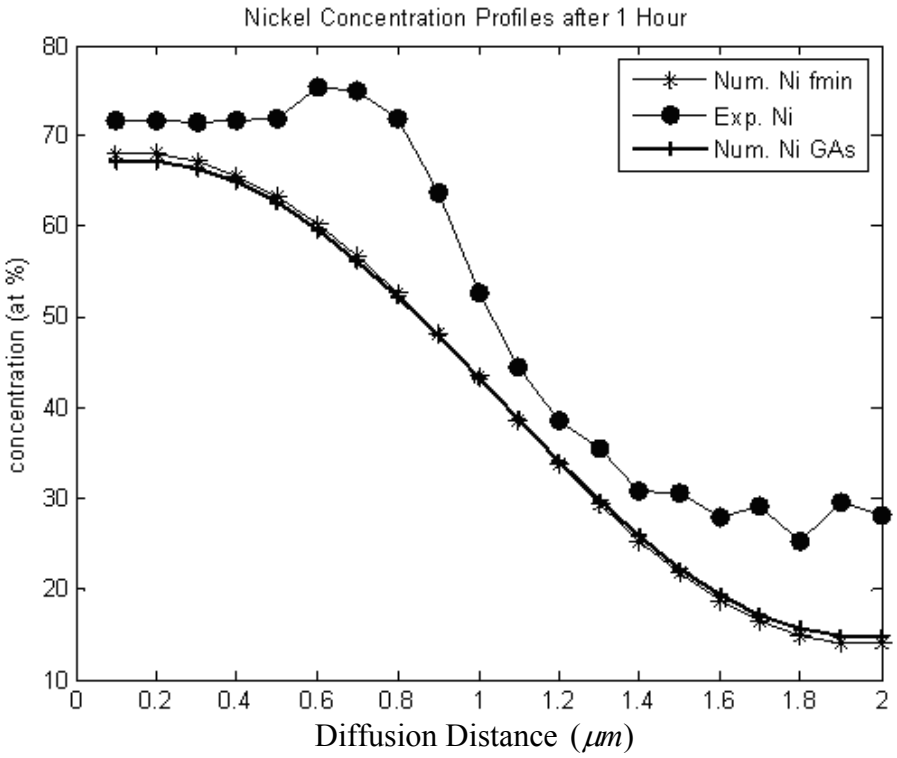

Figure 6.34 Nickel experimental and numerical concentrations after 1 hour diffusion treatment

As shown in the Figure 6.34 the star (*) concentration profile curve represents the nickel numerical concentration after 1 hour diffusion treatment when the diffusion coefficient calculated from (fminbnd). The plus (+) concentration profile curve corresponds to the nickel numerical concentration after 1 hour diffusion treatment when the diffusion coefficient calculated from the GAs method. The point (.) concentration profile curve corresponds to the nickel experimental concentration after 1 hour. The initial guess was $(2.71\times10^{-11}, 4\times10^{-11})$ to find the diffusion coefficient for both fminbnd method and GAs method. The diffusion coefficient calculated from the GAs

method as shown in Figure 6.24 was $D_{Ni} = 6.7619 \times 10^{-11} cm^2 / s$. The nickel diffusion coefficient calculated from bounded nonlinear function minimization method was $D_{Ni} = 4.52077 \times 10^{-11} cm^2 / s$. In this Figure there is a good agreement between the numerical concentration calculated from Genetic Algorithms method and the numerical concentration calculated from fminbnd. Therefore when the initial guess is close to the optimal solution (diffusion coefficient), fminbnd can be used to find the diffusion coefficient.

6.4.7. Calculation of the Constant Diagonal Diffusion Coefficients Using Simplex Search Method

The Simplex search method was used to calculate the diffusion coefficient for nickel (details in chapter 5). The diffusion coefficients of nickel component were then used to compute its numerical concentration. In this analysis the diagonal diffusion coefficients are taken into account and the cross terms were considered to be zero.

In the following Figure 6.35 Simplex search method was used to calculate the diffusion coefficient for nickel.

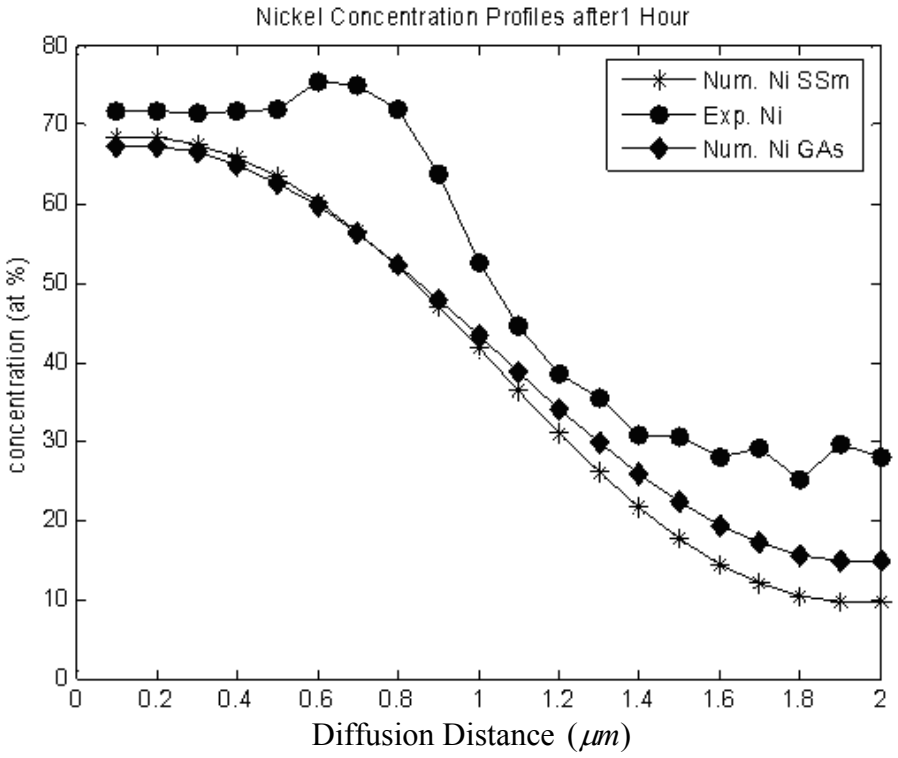

Figure 6.35 Nickel experimental and numerical concentrations after 1 hour diffusion treatment

Figure 6.35 shows the star (*) concentration profile curve which represents the nickel numerical concentration after 1 hour diffusion treatment when the diffusion coefficient was calculated from Simplex search method. The plus (+) concentration profile curve corresponds to the nickel numerical concentration after 1 hour diffusion treatment when the diffusion coefficient was calculated from GAs method. The point (.) concentration profile curve corresponds to the nickel experimental concentration after 1 hour. The initial guess (range) was (1×10^{-11}) to find the diffusion coefficient for both Simplex search method and GAs method. The diffusion coefficient calculated from GAs method as shown in Figure 6.24 was $D_{Ni} = 6.7619\times10^{-11} cm^2/s$. The nickel diffusion coefficient calculated from Simplex search method was $D_{Ni} = 3.3823\times10^{-11} cm^2/s$. In this figure there is a good agreement between the

numerical concentration calculated from Genetic Algorithms method and the numerical concentration calculated from Simplex search method.

6.4.8. Calculation of the Constant Diagonal and Cross Terms Diffusion Coefficients Using Simplex Search Method

In this section the diagonal and the cross terms from the diffusion matrix (equation 6.35)

$$\begin{bmatrix} D_{11} & D_{12} \\ D_{21} & D_{22} \end{bmatrix}$$

have been considered to be constant.

In Figure 6.36 the numerical and experimental concentration profiles for nickel and platinum have been presented after 1 hour diffusion treatment.

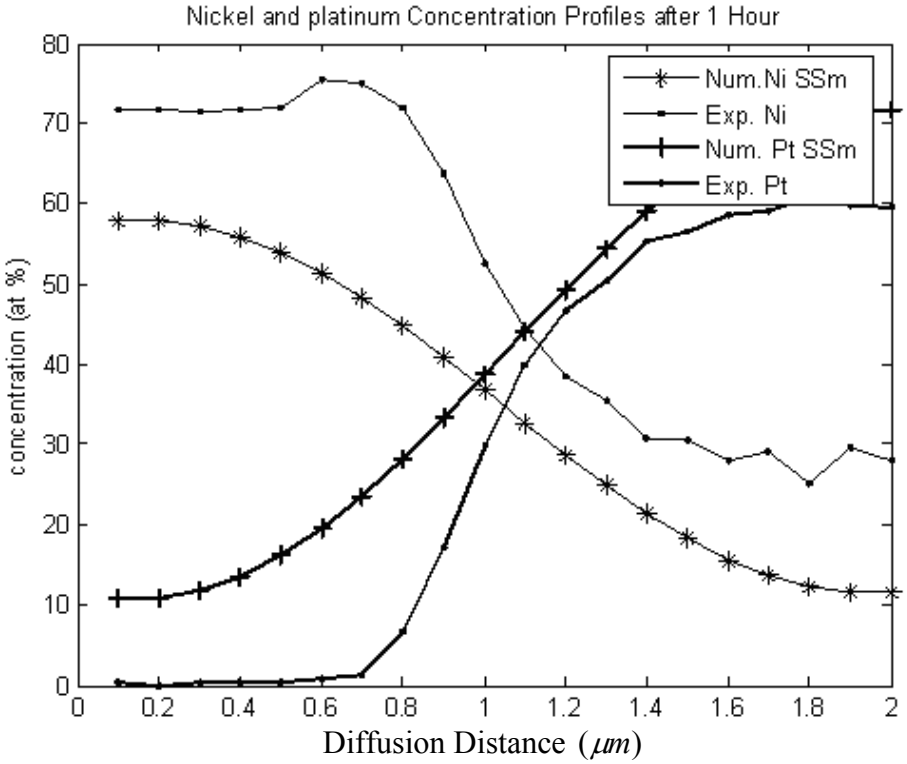

Figure 6.36 The experimental and numerical concentrations for nickel and platinum after 1 hour diffusion treatment

Figure 6.36 illustrates the numerical and experimental concentrations for nickel and platinum with concentration constant diffusion coefficients $D_{11}, D_{12}, D_{21}, D_{22}$ calculated from Simplex search method:

$$D_{11} = 0.1339 \times 10^{-8} cm^2 / s$$
$$D_{12} = 0.0977 \times 10^{-8} cm^2 / s$$
$$D_{21} = 0.1096 \times 10^{-8} cm^2 / s$$
$$D_{22} = 0.088 \times 10^{-8} cm^2 / s$$

when the initial guess for all of them were as follows:

$$D_{11} = 1 \times 10^{-9} cm^2 / s$$
$$D_{12} = 2 \times 10^{-9} cm^2 / s$$
$$D_{21} = 5.1 \times 10^{-9} cm^2 / s$$
$$D_{22} = 2.1 \times 10^{-9} cm^2 / s$$

6.4.9 Conclusions

The Genetic Algorithms optimization method (GAs), bounded nonlinear function minimization (fminbnd), and Simplex Search method (SSm) have been used to calculate the diffusion coefficient for nickel when just the diagonal terms from the diffusion matrix are taken into account. Simplex Search method also has been used to optimise the diffusion coefficients for nickel and platinum when the cross terms are included. There is an agreement between nickel and platinum numerical and experimental concentration profiles when GAs method has been used. There is good agreement between the numerical and experimental concentration for both components (*Ni, Pt*) if fminbnd and SSm have been used considering close initial guess (range) to the optimal

diffusion coefficients. This result shows the advantage of GAs method to optimise the diffusion coefficient without need for a very close initial guess (range) whereas the other two methods (fminbnd, SSm) need to have a close initial guess to the optimal solution.

6.5. Diffusion Processes Involved in Growth Mechanisms of Ni - aluminide and Pt-aluminide Coatings on MAR M002/Microstructure Formation / Microstructural Modelling - Results and Discussion

Background information on Ni-aluminide coatings and on Pt-modified nickel aluminide coatings including the rationales for the development of these coatings and their methods of production have been presented in section 3.4.

6.5.1. Microstructural Aspects of Diffusion Processes involved in the Formation of Nickel - aluminide Coating (without Pt) on MAR M002

It has been recognised that [40] aluminide coatings grow by two mechanisms depending on the employment of the low or high activity pack. The high aluminum activity process involves the inner diffusion of aluminum to form $\delta - Ni_2Al_3$ with a small amount of $NiAl$. The coating is heat treated to let Ni diffusion from the substrate to form $\beta - NiAl$, a much more ductile and oxidation resistant phase than the Ni_2Al_3 phase. A three-zone structure is formed consisting an outer zone containing α-Cr and

other substrate phases in a β-NiA1 matrix, a middle zone of a single phase $\beta - NiAl$ with Ti, Cr, Co, Mo in solution and a β-matrix inner zone holding carbides and σ phases as shown in Figure 7.37b [63,65].

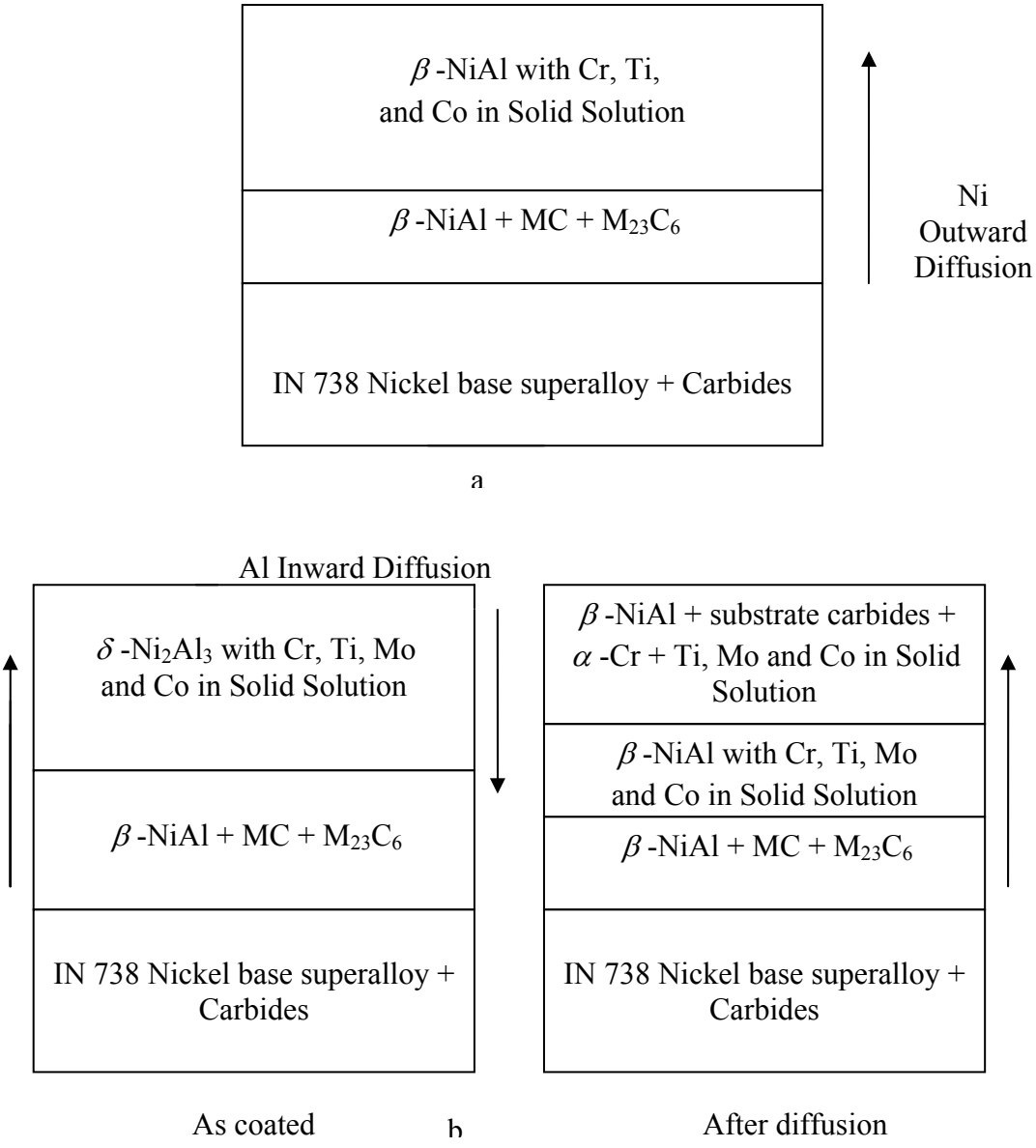

Figure 6.37 Microstructure of aluminide coatings formed on an IN738 nickel base superalloys: a) Low-activity process, b) High-activity process

The low aluminum activity process leads to the configuration of a two-zoned structure by the outward diffusion of Ni from the substrate reacting with Al. The outer zone consists of a single phase $\beta - NiAl$ with alloying elements diffusing out from the

substrate along with Ni. The inner zone contains carbides and/or phases shaped by the Ni removal from the $\beta - NiAl$ matrix as shown in Figure 6.37b [63].

6.5.2. Microstructural Aspects of Diffusion Processes involved in the Formation of Platinum Modified Nickel aluminide Coatings

The Pt diffusion treatment of the Pt electroplated coating (on Ni-base superalloy) leads to the enrichment of the superalloy surface with Pt which form a β-NiAl phase with Pt in substitution, that means the β-(Ni Pt) Al phase, during aluminising [J.Benoist 2005]. It has also been observed that during the aluminising process an intermetallic compound $PtAl_2$ is also formed in addition to the (Ni Pt) Al. $PtAl_2$ is an additional reservoir of Al.

The existence of a continuous $PtAl_2$ layer in the case of an Al rich donor can be described in Figure 6.38 following the frame work given in [J.Benoist 2005]:

- Initially at the interface I_1, Al atoms join with Pt atoms to form $PtAl_2$. At the same time, Ni atoms go through the Pt layer by diffusion through the interface I_2 to form a (Ni, Pt) solid solution;
- Aluminum diffusion continues to construct the in-depth $PtAl_2$ phase, producing a new interface I_2 which divides this phase from the (Ni, Pt) solid solution formed by outward Ni diffusion coming from the substrate. The limit between the (Ni, Pt) solid solution and the interdiffusion zone becomes the interface I_3 and the one between interdiffusion zone and the superalloy forms the boundary I_4, and during this step the complete $PtAl_2$ phase gets formed;
- All platinum atoms are joint with aluminum atoms to form $PtAl_2$, the remaining Al atoms diffuse through the later phase to form the (Ni, Pt) Al phase;

- The convergence of Al and Ni flux under the $PtAl_2$ layer, (Ni, Pt) Al phase continues to develop;
- The last step represents the final $PtAl_2 \rightarrow$(Ni, Pt) Al conversion by Ni atoms diffusion from the substrate.

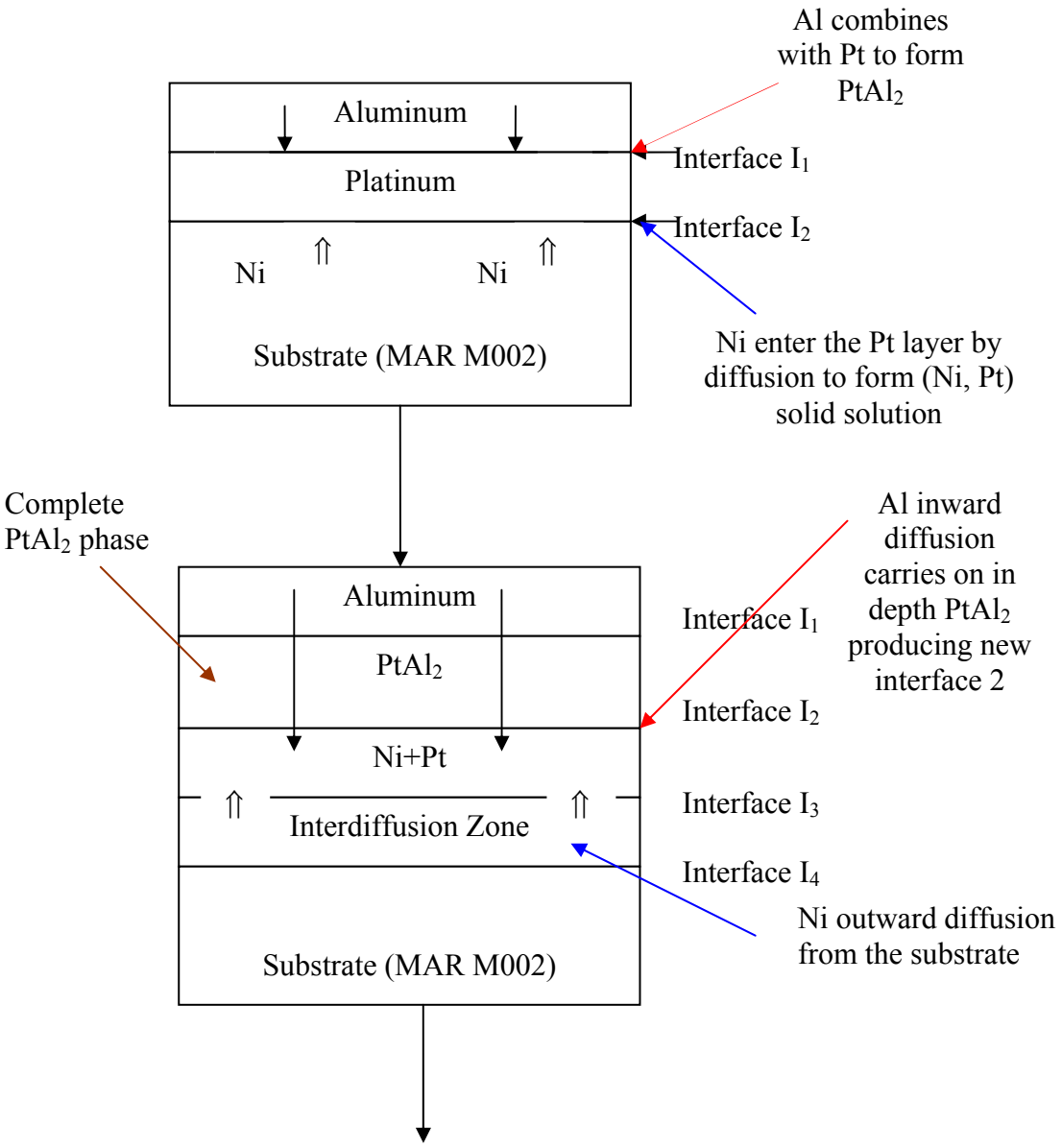

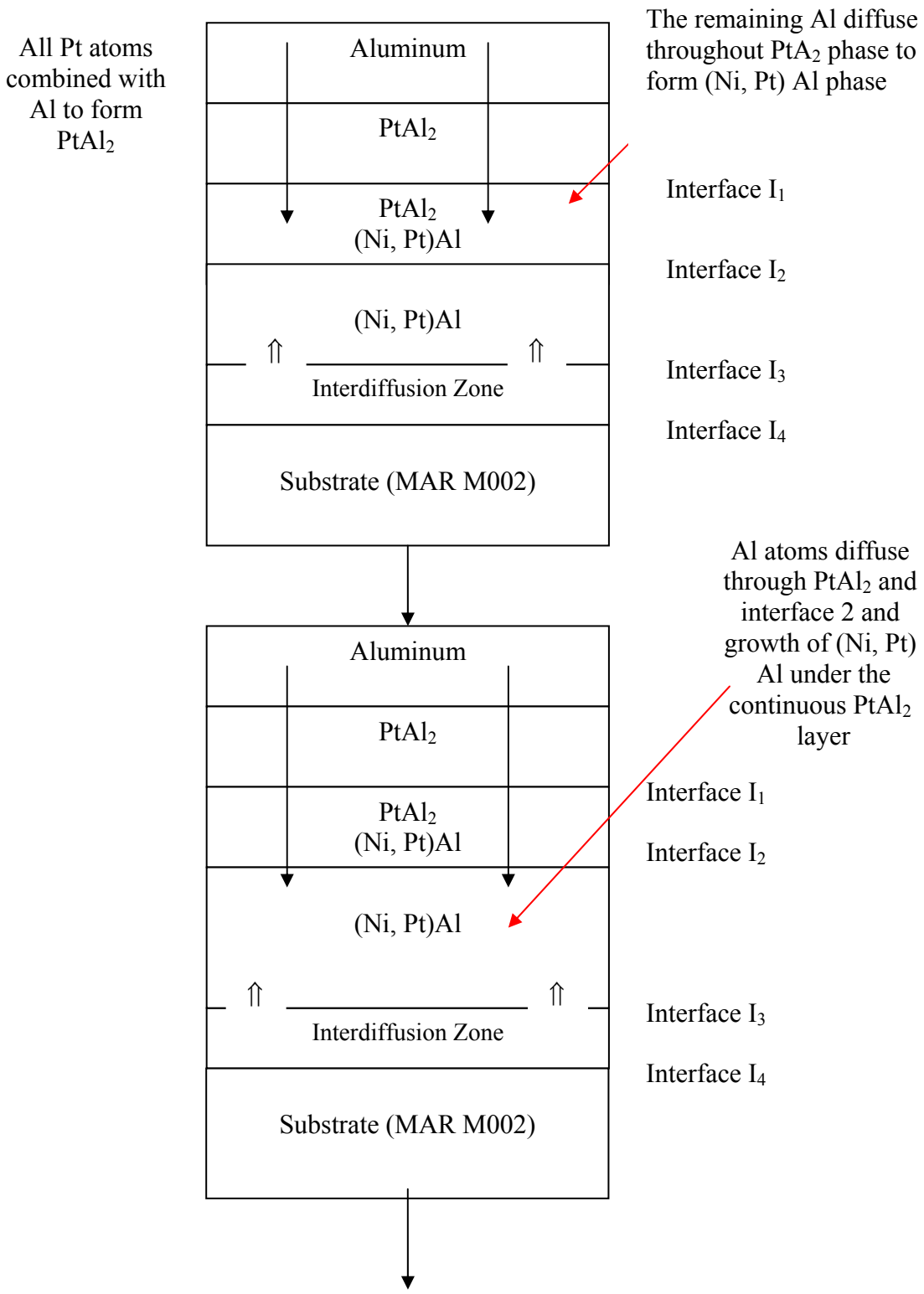
All Pt atoms combined with Al to form $PtAl_2$
Aluminum
$PtAl_2$
$PtAl_2$
(Ni, Pt)Al
(Ni, Pt)Al
Interdiffusion Zone
Substrate (MAR M002)
The remaining Al diffuse throughout PtA_2 phase to form (Ni, Pt) Al phase
Interface I_1
Interface I_2
Interface I_3
Interface I_4
Al atoms diffuse through $PtAl_2$ and interface 2 and growth of (Ni, Pt) Al under the continuous $PtAl_2$ layer
Aluminum
$PtAl_2$
$PtAl_2$
(Ni, Pt)Al
(Ni, Pt)Al
Interdiffusion Zone
Substrate (MAR M002)
Interface I_1
Interface I_2
Interface I_3
Interface I_4

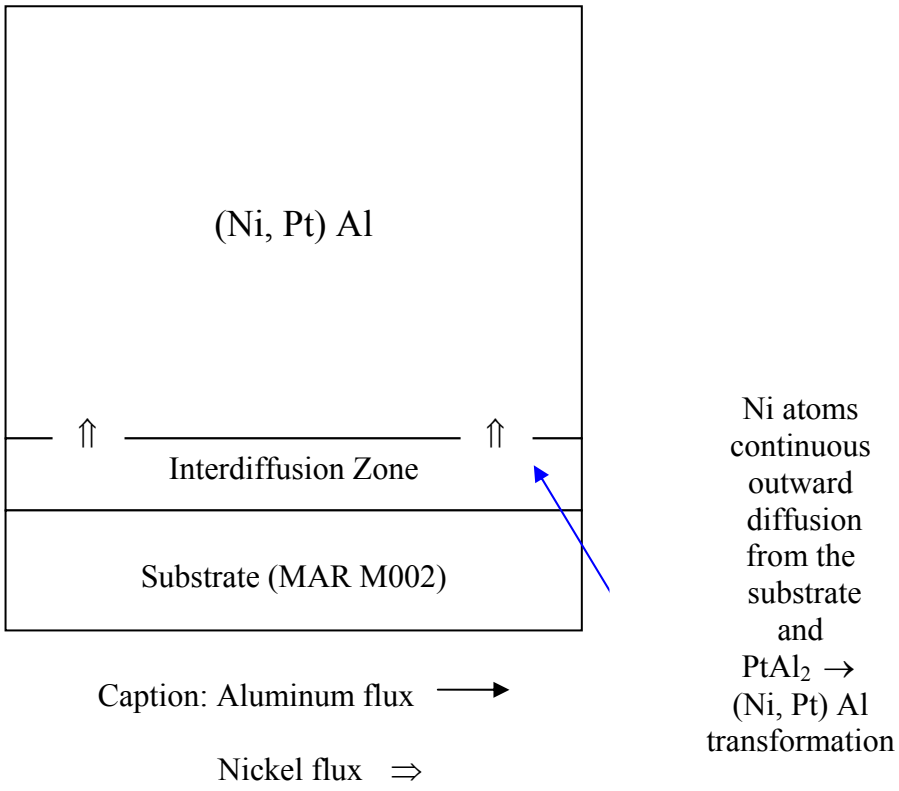

Figure 6.38 Schematic diagram of aluminizing process on MAR M002 substrate

In the next section 6.5.3 the numerical modelling for interdiffusion for the Pt-aluminide coatings on MAR M002 system have been presented.

6.5.3. Modelling Interdiffusion Using Genetic Algorithms Method (GAs) with the Numerical Method

The numerical method (Runge-Kutta method of order four) has been used to calculate the numerical concentration;

$$C_{n+1} = C_n + \frac{1}{6}(k_1 + 2k_2 + 2k_3 + k_4),$$
$$k_1 = hf(x_n, y_n),$$
$$k_2 = hf(x_n + \frac{1}{2}h, y_n + \frac{1}{2}k_1),$$
$$k_3 = hf(x_n + \frac{1}{2}h, y_n + \frac{1}{2}k_2),$$
$$k_4 = hf(x_n + h, y_n + k_3).$$

was applied to Fick's second law

$$\frac{\partial C}{\partial t} = D\frac{\partial^2 C}{\partial x^2}$$

where D is the diffusion coefficient.

In the first investigation only the diagonal diffusion coefficients in the diffusion matrix,

$$\begin{bmatrix} D_{11} & D_{12} & D_{13} & D_{14} \\ D_{21} & D_{22} & D_{23} & D_{24} \\ D_{31} & D_{32} & D_{33} & D_{34} \\ D_{41} & D_{42} & D_{43} & D_{44} \end{bmatrix} \tag{6.38}$$

$$i.e. \begin{bmatrix} D_{11} & & & \\ & D_{22} & & \\ & & D_{33} & \\ & & & D_{44} \end{bmatrix}$$

were considered, these were assumed constant and the cross terms were assumed to be zero. Using this assumption the composition profiles of Pt, Al, Cr, Ni, Co have been calculated.

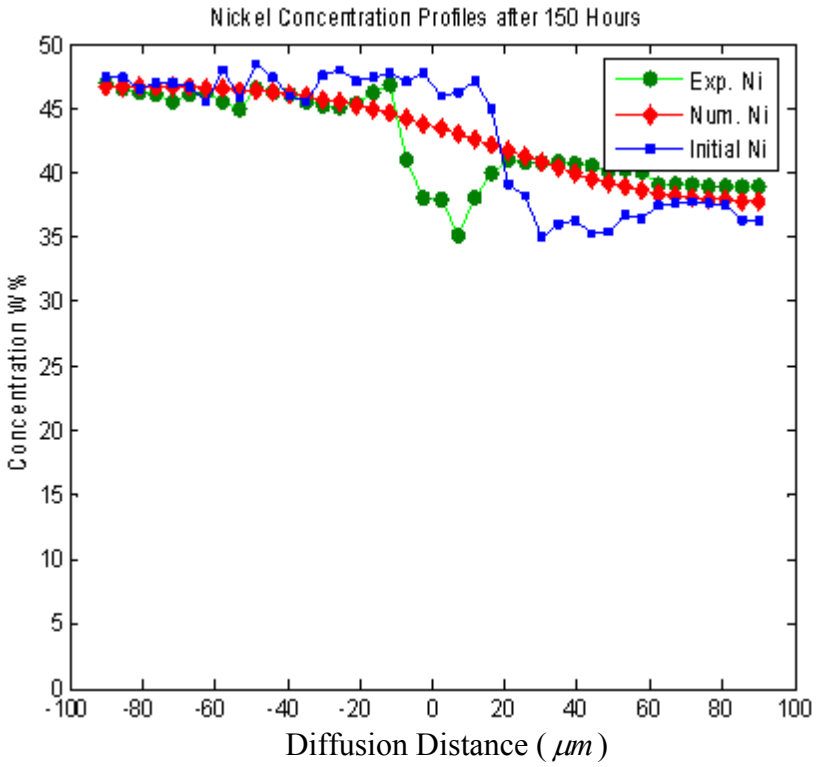

Figure 6.39 Nickel numerical and experimental concentrations after 150 hours of diffusion annealing

Figure 6.39 shows nickel concentration profiles (numerical and experimental) using the diffusion coefficient $(D_{Ni} = 12.368 \times 10^{-13} cm^2 / s)$ obtained from Genetic Algorithms method after 150 hours of diffusion annealing. The initial concentration profile of *Ni* used in the above Figure 6.39 has been taken from the experimental value of concentration at $t = 0$. There is a broad agreement between the numerical concentration and experimental concentration profiles between the diffusion distances (-100-(-10)) μm and between '(10-100) μm', and followed by divergence between the experimental and the numerical values from (-10-10) μm.

Similarly in Figure 6.40 the numerical and experimental concentrations of *Al* have been presented after 150 hours diffusion treatment using $(D_{Al} = 5.9181x10^{-13} cm^2 / s)$ calculated from Genetic Algorithms method.

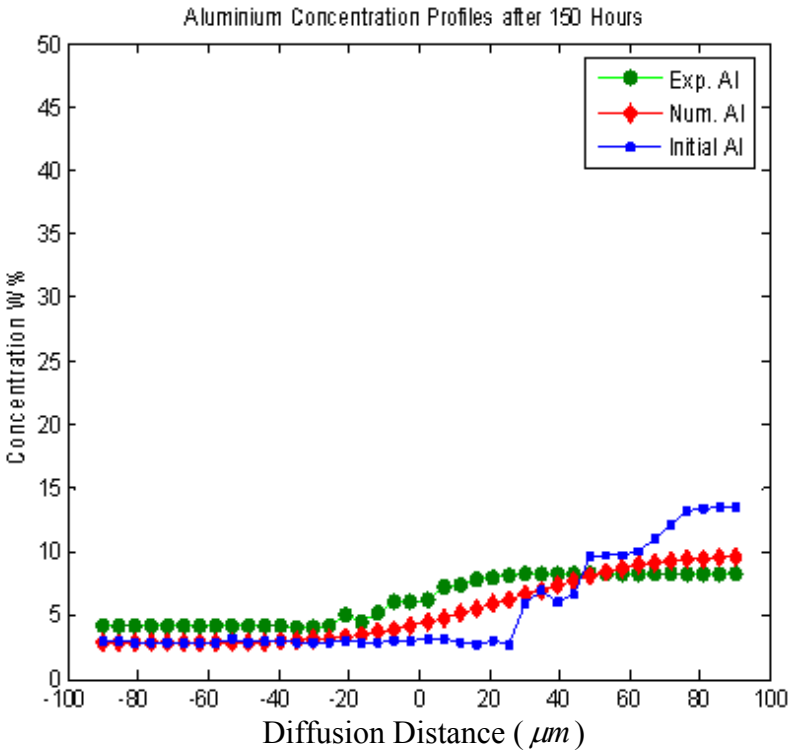

Figure 6.40 Aluminum numerical and experimental concentrations after 150 hours of diffusion annealing

The initial concentration profile of Al used in the above Figure has been taken from the experimental value of concentration at $t = 0$. Good agreement is shown between the numerical concentration and experimental concentration for Al in the whole range of diffusion distance.

In Figures 6.41 and 6.42 the experimental and numerical concentration profiles for the components cobalt and platinum have been presented with the interdiffusion coefficients calculated from Genetic Algorithms method.

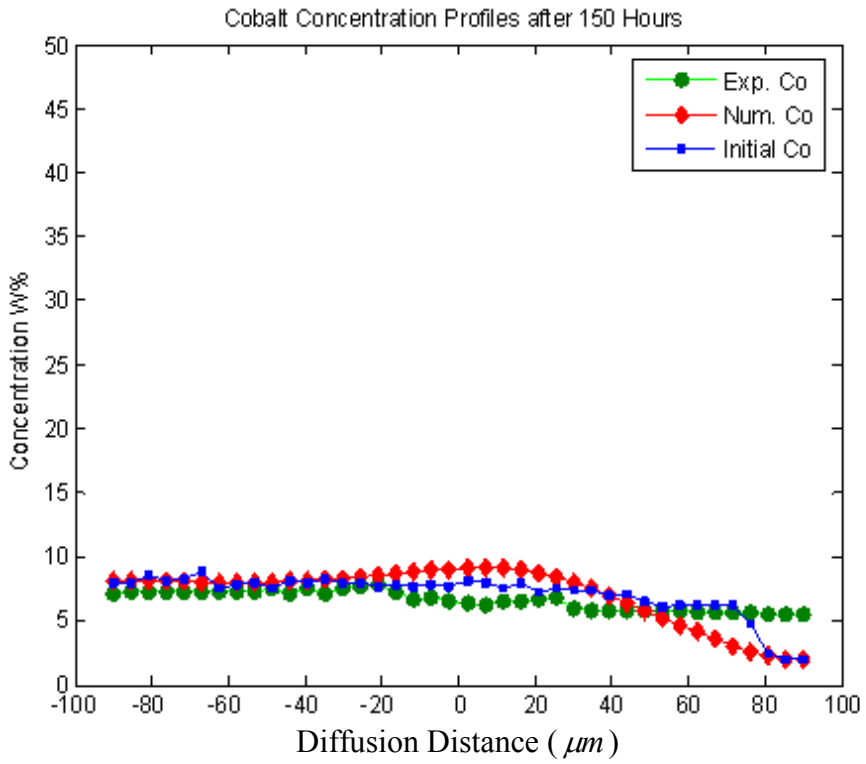

Figure 6.41 Cobalt numerical and experimental concentrations after 150 hours of diffusion annealing

Figure 6.41 shows cobalt concentration profiles (numerical and experimental) using the diffusion coefficient $(D_{Co} = 3.6412 \times 10^{-13} cm^2 / s)$ from Genetic Algorithms method after 150 hours diffusion treatment, and the initial concentration profile at $t = 0$. For the entire range of diffusion distance the experimental and numerical profiles show good agreement.

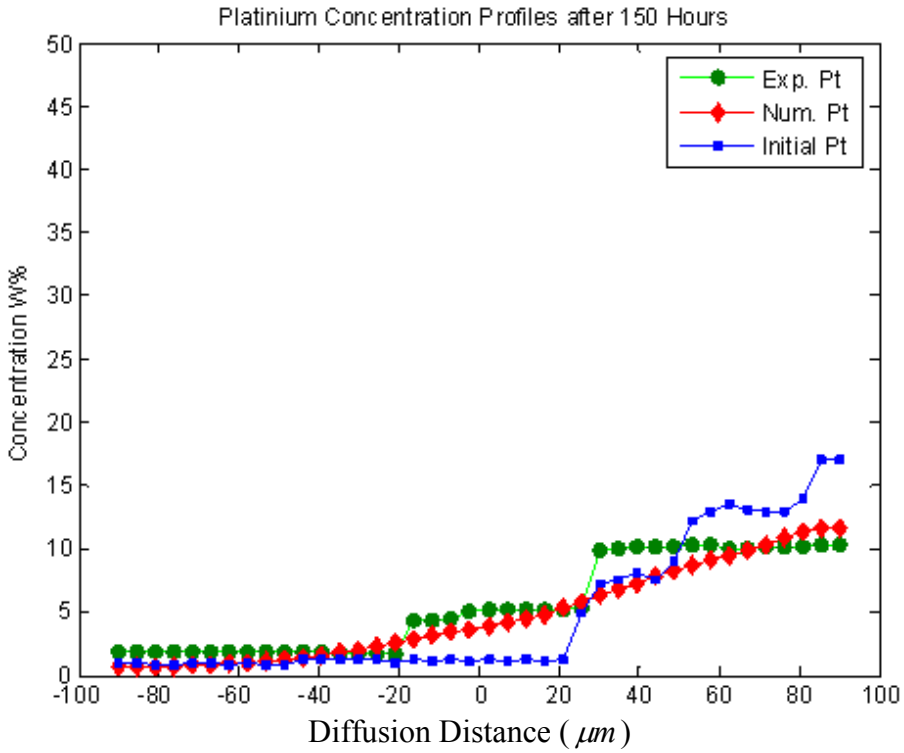

Figure 6.42 Platinum numerical and experimental concentrations after 150 hours of diffusion annealing

The platinum concentration profile (numerical and experimental) using the diffusion coefficient $(D_{Pt} = 8.0297 \times 10^{-13} cm^2 / s)$ from Genetic Algorithms method after 150 hours diffusion treatment is shown in Figure 6.42. The initial concentration profile of *Pt* used in the above Figure has been taken from the experimental value of concentration at $t = 0$. There is good agreement between the numerical concentration and experimental concentration for the whole range of diffusion distance.

6.5.3.1. Conclusions of Ni -aluminide and Pt-aluminide Coatings on MAR M002 Using Constant Diagonal Terms

Fick's second law has been used to find the concentration profile for each component (Ni, Al, Co, Pt) using Rung-Kutta method of order four. The Genetic

Algorithms method allows optimization of the values of diffusion coefficients, in diffusion matrix. The calculated concentration profiles have been compared with the experimental data using Least squares method. There is some divergence between the (Al, Co, Pt) numerical concentrations and experimental concentrations in some distances in the entire range of diffusion distance after 150 hours diffusion treatment. For the nickel component there is good agreement between the numerical concentration and experimental concentration profiles between the diffusion distances (-100-(-10)) μm, and between (10-100) μm, followed by divergence between the experimental and the numerical values from (-10-10) μm. Further improvement can be achieved considering the cross terms.

6.5.4. Calculation Considering Constant Cross and Diagonal Terms Diffusion Coefficients

Fick's second law for the muticomponent system can be written as follows:

$$\Rightarrow \begin{bmatrix} \frac{\partial C_1}{\partial t} \\ \frac{\partial C_2}{\partial t} \\ \frac{\partial C_3}{\partial t} \\ \frac{\partial C_4}{\partial t} \end{bmatrix} = \begin{bmatrix} D_{11}^5 & D_{12}^5 & D_{13}^5 & D_{14}^5 \\ D_{21}^5 & D_{22}^5 & D_{23}^5 & D_{24}^5 \\ D_{31}^5 & D_{32}^5 & D_{33}^5 & D_{34}^5 \\ D_{41}^5 & D_{42}^5 & D_{43}^5 & D_{44}^5 \end{bmatrix} \begin{bmatrix} \frac{\partial C_1}{\partial x^2} \\ \frac{\partial C_2}{\partial x^2} \\ \frac{\partial C_3}{\partial x^2} \\ \frac{\partial C_4}{\partial x^2} \end{bmatrix} \tag{6.39}$$

Equation 6.39 explains how the diagonal and cross terms diffusion coefficients are constants:

$$
\begin{aligned}
\Rightarrow \frac{\partial C_1}{\partial t} &= \tilde{D}^5_{11}\frac{\partial^2 C_1}{\partial x^2} + \tilde{D}^5_{12}\frac{\partial^2 C_2}{\partial x^2} + \tilde{D}^5_{13}\frac{\partial^2 C_3}{\partial x^2} + \tilde{D}^5_{14}\frac{\partial^2 C_4}{\partial x^2} \\
\frac{\partial C_2}{\partial t} &= \tilde{D}^5_{21}\frac{\partial^2 C_1}{\partial x^2} + \tilde{D}^5_{22}\frac{\partial^2 C_2}{\partial x^2} + \tilde{D}^5_{23}\frac{\partial^2 C_3}{\partial x^2} + \tilde{D}^5_{24}\frac{\partial^2 C_4}{\partial x^2} \\
\frac{\partial C_3}{\partial t} &= \tilde{D}^5_{31}\frac{\partial^2 C_1}{\partial x^2} + \tilde{D}^5_{32}\frac{\partial^2 C_2}{\partial x^2} + \tilde{D}^5_{33}\frac{\partial^2 C_3}{\partial x^2} + \tilde{D}^5_{34}\frac{\partial^2 C_4}{\partial x^2} \\
\frac{\partial C_4}{\partial t} &= \tilde{D}^5_{41}\frac{\partial^2 C_1}{\partial x^2} + \tilde{D}^5_{42}\frac{\partial^2 C_2}{\partial x^2} + \tilde{D}^5_{43}\frac{\partial^2 C_3}{\partial x^2} + \tilde{D}^5_{44}\frac{\partial^2 C_4}{\partial x^2}
\end{aligned}
\tag{6.40}
$$

Equation 6.40 clarifies in more depth

$$
\begin{bmatrix}
D_{11} & D_{12} & D_{13} & D_{14} \\
D_{21} & D_{22} & D_{23} & D_{24} \\
D_{31} & D_{32} & D_{33} & D_{34} \\
D_{41} & D_{42} & D_{43} & D_{44}
\end{bmatrix}
\tag{6.41}
$$

In this matrix (equation 6.41), the diagonal and cross terms have been considered to be constant.

In Figure 6.43 the experimental and numerical concentration for the components (nickel, aluminum, cobalt and platinum), have been presented with the interrdiffusion coefficients calculated from Genetic Algorithms method and using equation 6.40, Fick's second law. Here the cross terms have been taken into account.

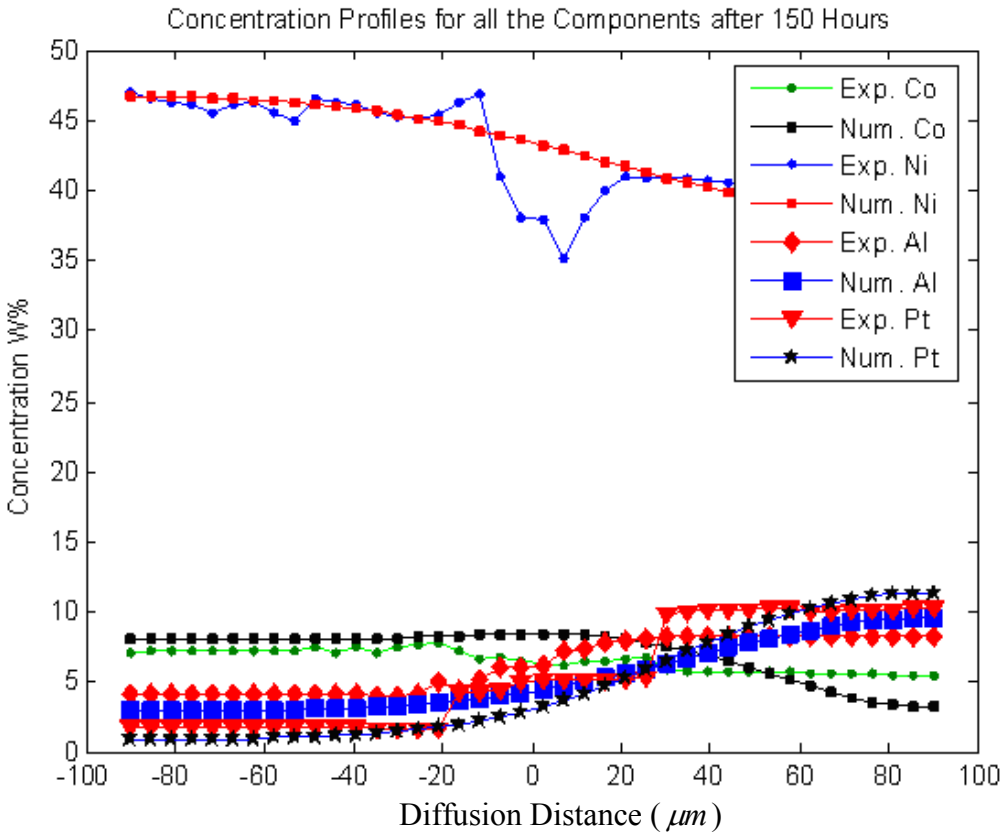

Figure 6.43 The numerical and experimental concentration profiles after 150 hours of diffusion annealing for all the components *Co, Ni, Al, and Pt*

The concentration profiles have been obtained using constant diffusion coefficients $D_{11}, D_{12}, D_{13}, D_{14}, D_{21}, D_{22}, D_{23}, D_{24}, D_{31}, D_{32}, D_{33}, D_{34}, D_{41}, D_{42}, D_{43}, D_{44}$ determined from Genetic Algorithms optimization method and the values are given below:

$$
\begin{aligned}
D_{11} &= 0.11209 \times 10^{-13}\, cm^2 / s \\
D_{12} &= 4.07423 \times 10^{-12}\, cm^2 / s \\
D_{13} &= 5.98021 \times 10^{-12}\, cm^2 / s \\
D_{14} &= 1.85621 \times 10^{-12}\, cm^2 / s \\
D_{21} &= 3.60980 \times 10^{-12}\, cm^2 / s \\
D_{22} &= 1.29180 \times 10^{-13}\, cm^2 / s \\
D_{23} &= 2.0543 \times 10^{-12}\, cm^2 / s \\
D_{24} &= 7.4541 \times 10^{-12}\, cm^2 / s \\
D_{31} &= 0.42101 \times 10^{-12}\, cm^2 / s \\
D_{32} &= 0.0169 \times 10^{-12}\, cm^2 / s \\
D_{33} &= 1.40131 \times 10^{-13}\, cm^2 / s \\
D_{34} &= 0.21040 \times 10^{-12}\, cm^2 / s \\
D_{41} &= 0.42101 \times 10^{-12}\, cm^2 / s \\
D_{42} &= 0.01061 \times 10^{-12}\, cm^2 / s \\
D_{43} &= 5.40011 \times 10^{-12}\, cm^2 / s \\
D_{44} &= 3.31098 \times 10^{-13}\, cm^2 / s
\end{aligned}
\qquad (6.42)
$$

In the above Figure 6.43 the numerical concentration profiles for the components (nickel, aluminum, cobalt and platinum) have been calculated considering constant cross terms and diagonal terms, in a diffusion matrix.

6.5.4.1. Conclusions (Constant Cross and Diagonal Terms Diffusion Coefficients)

Here the concentration profiles for each component nickel, aluminum, cobalt and platinum were calculated by solving Fick's second law using Rung-Kutta method of order four. Genetic Algorithms method has allowed optimization of the values of diffusion coefficients, in a diffusion matrix (equation 6.41). There is good convergence between the experimental and numerical concentration for the components

(Ni, Al, Co, Pt) when equation 6.40 was used to calculate the diffusion coefficients, taking into account the cross terms. The difference between the experimental and numerical concentration profiles for the components (Ni, Al, Co, Pt) has been reduced. It means the results (the numerical concentration profiles for (nickel, aluminum, cobalt and platinum) show much improvement compared to the numerical concentration profiles when the cross terms were considered to be zero.

6.5.5. Calculation Considering Variable Cross and Diagonal Terms Diffusion Coefficients

In the previous part 6.4.4 the diffusion coefficients (diagonal and cross terms) for the components (Ni, Al, Co, Pt) were considered to be constant. In the following analysis the diffusion coefficients are considered to be concentration dependent (a function of concentration). Second order polynomial has been used for concentration dependence diffusion coefficients for the (nickel, aluminum, cobalt and platinum). The following Figure presents the concentrations for the all components (Ni, Al, Co, Pt);

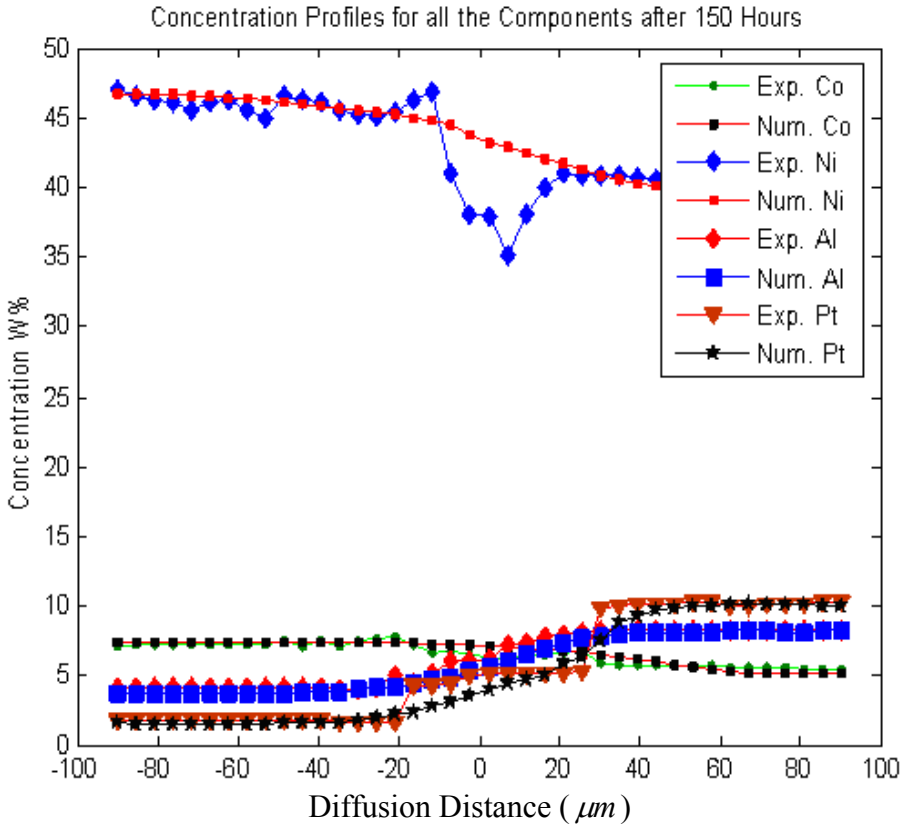

Figure 6.44 The numerical and experimental concentrations after 150 hours of diffusion annealing for all the components *Co, Ni, Al, and Pt* with variable diffusion coefficients

Figure 6.44 illustrates the numerical and experimental concentrations for the nickel, aluminum, cobalt and platinum with concentration dependent diffusion coefficients: $D_{11}, D_{12}, D_{13}, D_{14}, D_{21}, D_{22}, D_{23}, D_{24}, D_{31}, D_{32}, D_{33}, D_{34}, D_{41}, D_{42}, D_{43}, D_{44}$ (second order polynomial) after 150 hours diffusion treatment:

$$
\begin{aligned}
D_{11} &= w_1 + w_2 C_1 + w_3 C_1^{\,2} + w_4 C_3^2 + w_5 C_4^{\,2} \\
D_{12} &= x_1 + x_2 C_1 C_2 + x_3 C_2 \\
D_{13} &= y_1 C_2 + y_2 C_2^{\,2} \\
D_{14} &= z_1 C_3 + z_2 C_3^{\,2} \\
D_{21} &= s_1 C_1 + s_2 C_2 + s_3 C_2^{\,2} \\
D_{22} &= t_1 C_3 + t_2 C_2^2 + t_3 C_2 C_3 \\
D_{23} &= u_1 C_1^2 + u_2 C_3^2 \\
D_{24} &= v_1 C_2^2 + v_2 C_4^2 \\
D_{31} &= e_1 C_1 C_3 + e_2 C_3 \\
D_{32} &= f_1 C_3 + f_2 + f_3 C_3 + f_4 C_3 C_1 \\
D_{33} &= g_1 C_1 C_2 + g_2 C_3^2 \\
D_{34} &= h_1 C_1 C_4 + h_2 C_3^2 \\
D_{41} &= i_1 C_1 C_4 + i_2 C_1^2 \\
D_{42} &= j_1 C_3^2 + j_2 + j_3 C_3 C_4 + j_4 C_3 C_4 \\
D_{43} &= k_1 C_4^2 + k_2 C_1^2 \\
D_{44} &= l_1 C_1 C_4 + l_2 C_3
\end{aligned}
\qquad (6.43)
$$

where C_1, C_2, C_3 *and* C_4 are the initial concentration for nickel, aluminum, cobalt and platinum respectively. $w_1, w_2, w_3, \cdots, \cdots, l_1, l_2$ are the polynomial coefficients calculated using Genetic Algorithms optimization method. There were superior agreements in the numerical and experimental concentration values for nickel, aluminum, cobalt and platinum for the entire range of the diffusion distance.

6.5.5.1. Conclusions (Variable Cross and Diagonal Terms Diffusion Coefficients)

Fick's second law has been used to determine the concentration profile for each component (nickel, aluminum, cobalt and platinum) using Rung-Kutta method of order

four. Using Genetic Algorithms optimization method, the diffusion coefficients values in the diffusion matrix (equation 6.41) have been optimized. There is very good convergence (agreement) between the experimental and numerical concentration for the components (Ni, Al, Co, Pt) when equation 6.44 was used to calculate the diffusion coefficients, concentration dependent. The difference between the experimental and numerical concentration profiles for the components (Ni, Al, Co, Pt) has been reduced. It means the numerical concentration profiles for nickel, aluminum, cobalt and platinum show significant improvement compared to the numerical concentration profiles when the cross terms were considered to be zero and constant.

6.6. Studies of Ir and Ir/Pt Low-Activity Aluminide / MAR M002 System / Assessment of the Oxidation Resistance and Microstructural Aspects/Modelling of Diffusion Process Involved at (1100^{o}C) - Results and Discussion

Background information on this system including the production of Ir and IrPt modified coatings on MAR M002 system at 1100^{o}C have been given in section 3.6.

6.6.1. As Processed *Ir*-aluminide and *Pt*-*Ir*-aluminide

Figure 6.45 gives the EDS – X-ray mapping for as processed Ir- aluminide coating. Figure 6.46 gives the EDS – X-ray mapping for as processed IrPt- aluminide coating. Figures 6.45 and 6.46 show that the outer layer was Ni or Ni, Pt-rich, while the inner layer was Ir-rich, with Al distributed during the coatings [64]. Inside the Ir-aluminide

the substrate elements such as W and Ta were limited within the Ir-rich layer, but for the IrPt-aluminide, such elements were excluded from the coating.

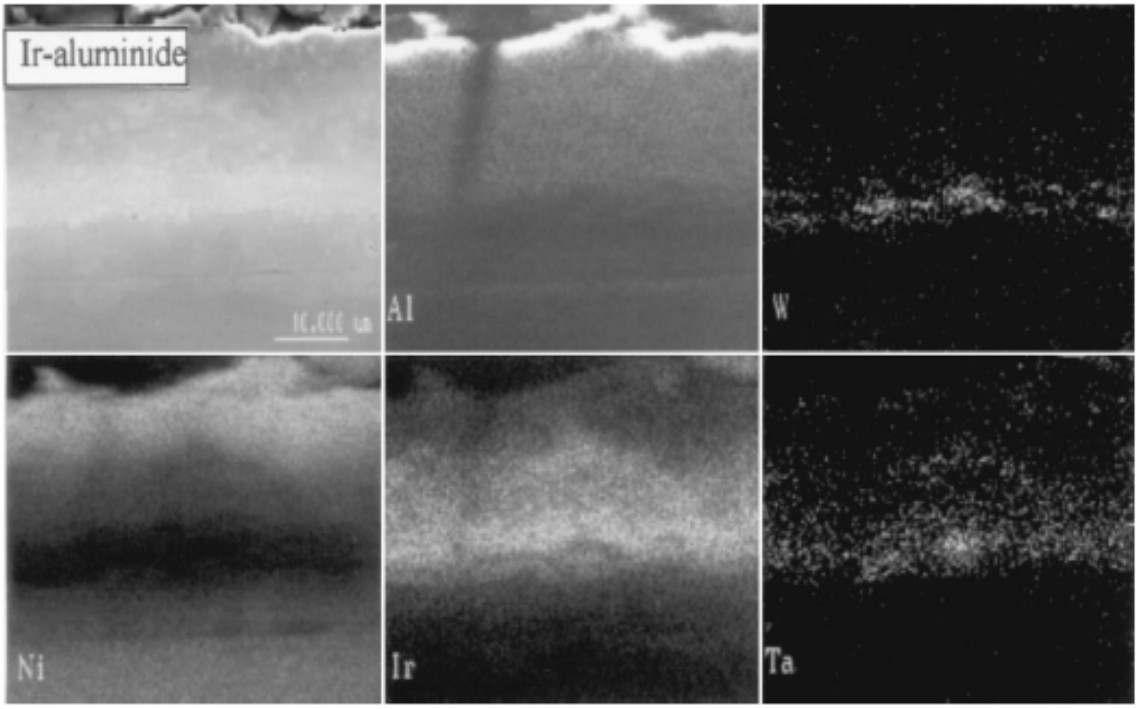

Figure 6.45 Digimap of the $Ir-$aluminide, as-processed, in section

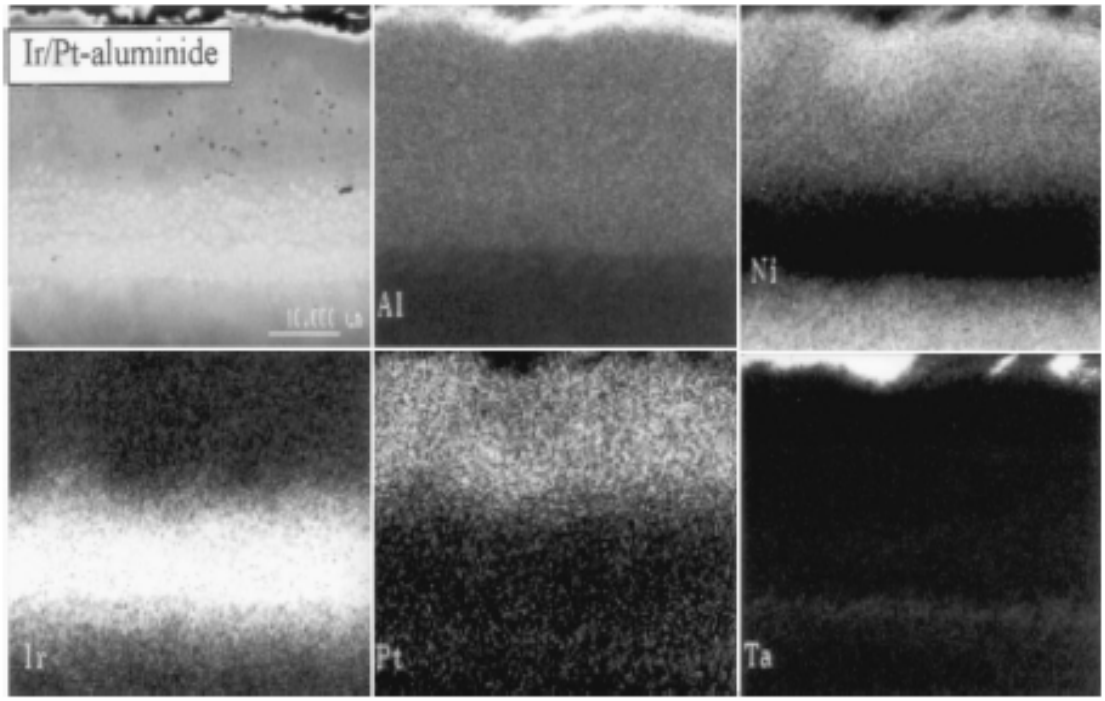

Figure 6.46 Digimap of the *Ir Pt*- aluminide, as-processed, in section

In the case of the *Ir*-aluminide coating, the *Ir*-rich layer contained the substrate elements-*W*, *Ta*. For the *Ir*-*Pt* aluminide coatings the substrate elements were excluded from the coating.

The cross-sectioned EDS analysis shown in Figure 6.47 and 6.48 confirmed the distribution of the elements. The XRD analysis (not presented) exposed that the outer layers of the systems had a structure similar to that of β-NiAl.

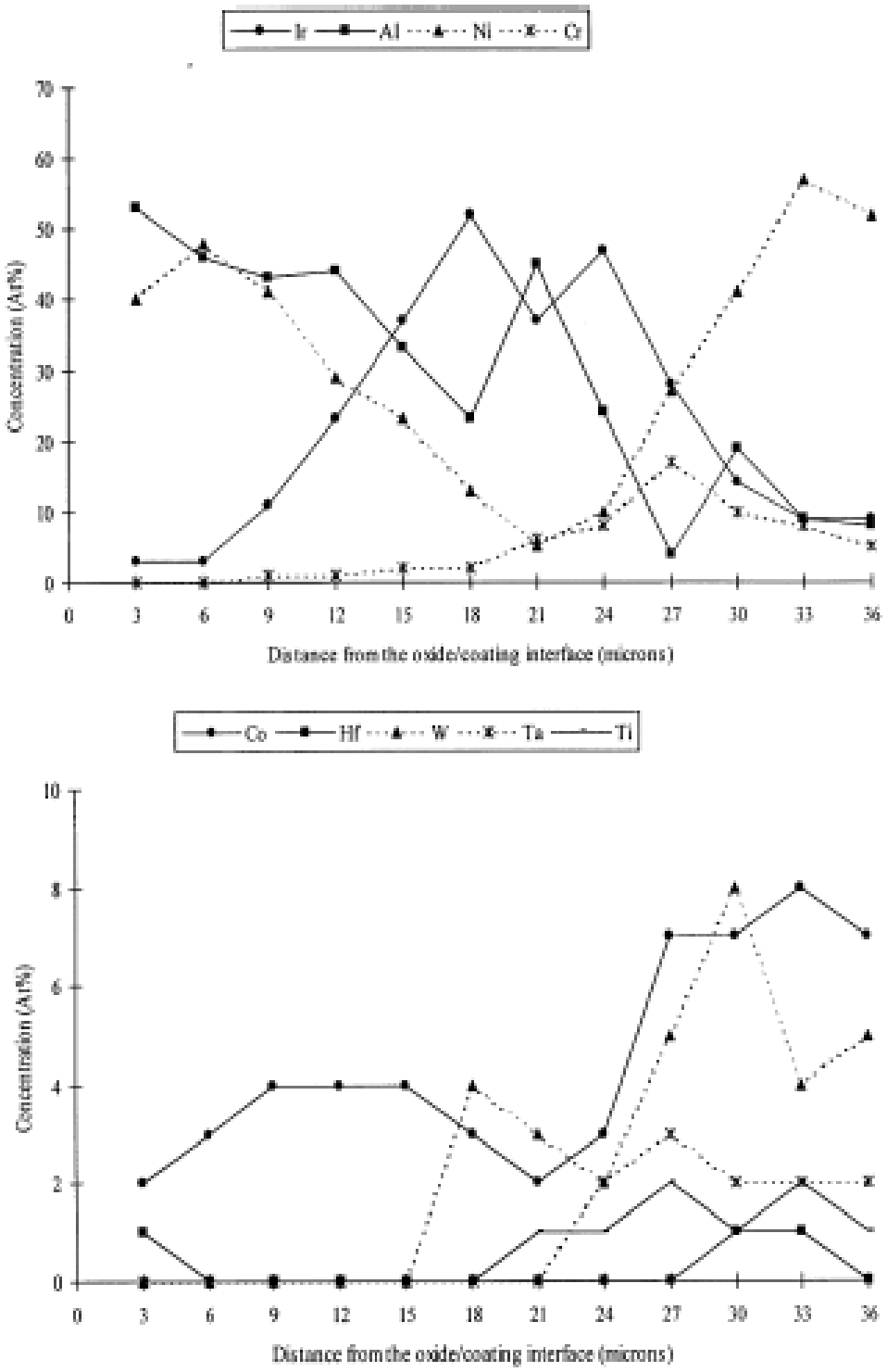

Figure 6.47 ZAF analysis of the $Ir-$aluminide, as-processed, in section

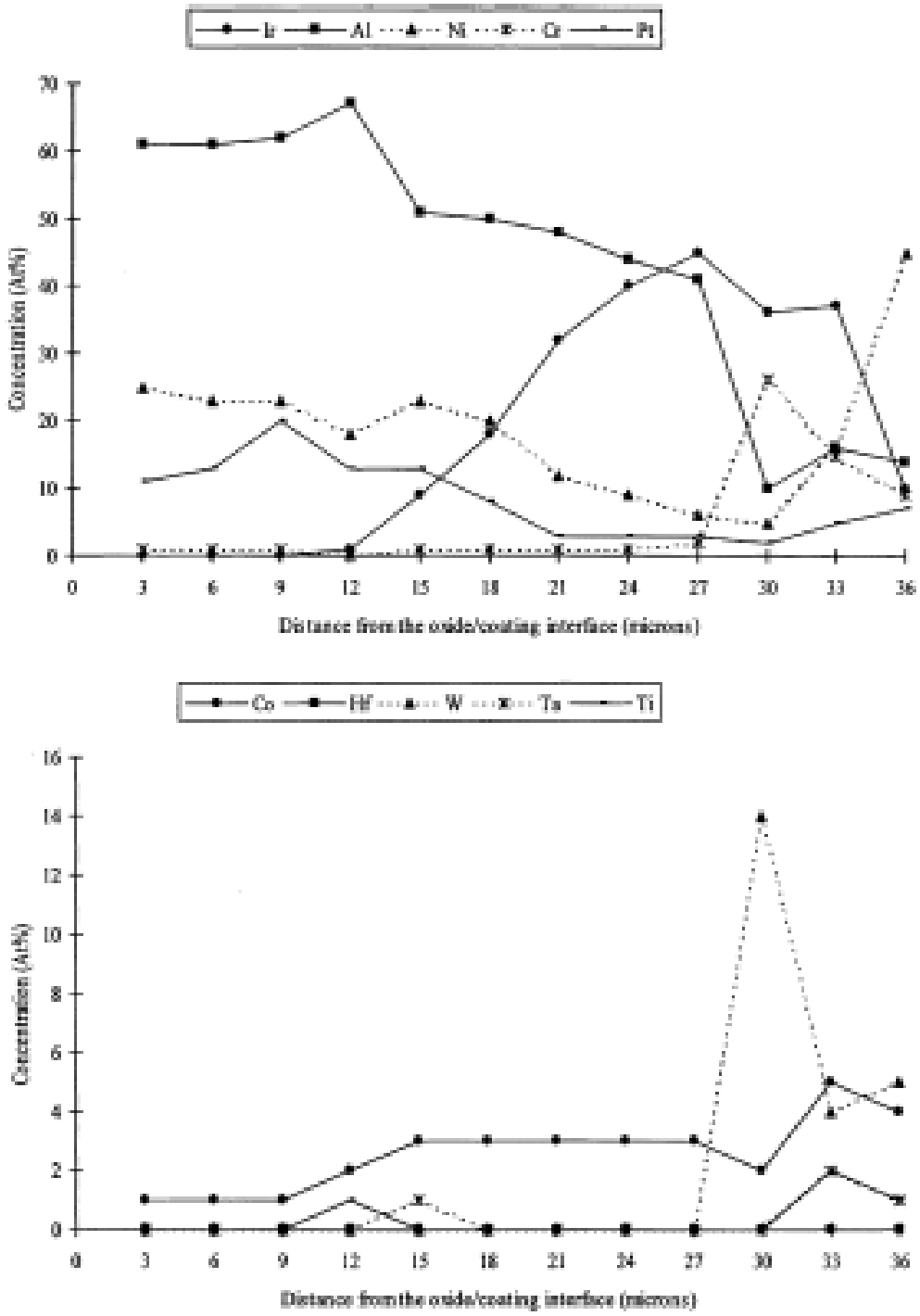

Figure 6.48 ZAF analysis of the $Ir-Pt-$ aluminide, as-processed, in section

6.6.1.1. Summary of the Diffusion Processes involved in the Formation of Ir-aluminide and IrPt-aluminide Coatings

During the manufacturing stage of the coatings a $\beta NiAl$ layer developed due to the selective diffusion of *Ni* which reacted with *Al*. This diffusion process created a large *Ir*-rich interdiffusion zone which also contained substrate elements *Cr, W, Ta, Ti* due to the outward diffusion of these elements.

In the case of *Pt*-*Ir*-*Ni*-aluminide there also developed a *Ir*-rich inner layer. There was no outward diffusion of the substrate elements. *Pt* was distributed in the top part of the coating.

6.6.2. Oxidation of *Ir*-aluminide and *Pt*-*Ir* aluminide Coatings at 1100^{o}C for 100 Hours

6.6.2.1. *Ir*-aluminide Coatings

After oxidation of Ir-aluminide coatings at 1100^{o}C for 100 hours the samples were subjected to EDS analysis for EDS-X ray maps (Figure 6.49).

The EDS-X ray maps (Figure 6.49) show:

- the formation of an Al_2O_3 scale (deduced);
- the virtually consumed $\beta NiAl$;
- the concentration of *Al* in the *Ir*-rich inner layer;
- the formation of an internal oxidation zone containing *Ti.*

6.6.2.2. *Pt-Ir*-aluminide Coatings

After oxidation of IrPt-aluminide coatings at 1100^{o}C for 100 hours the samples were subjected to EDS analysis for EDS-X ray maps (Figure 6.50).

The EDS-X ray maps shown in Figure 6.50 confirm:

- the formation of an outer scale Al_2O_3;
- the distribution of *Pt* and *Ir* throughout;
- the incorporation of Ti and *Hf* just below the scale;
- *W* residing in the substrate.

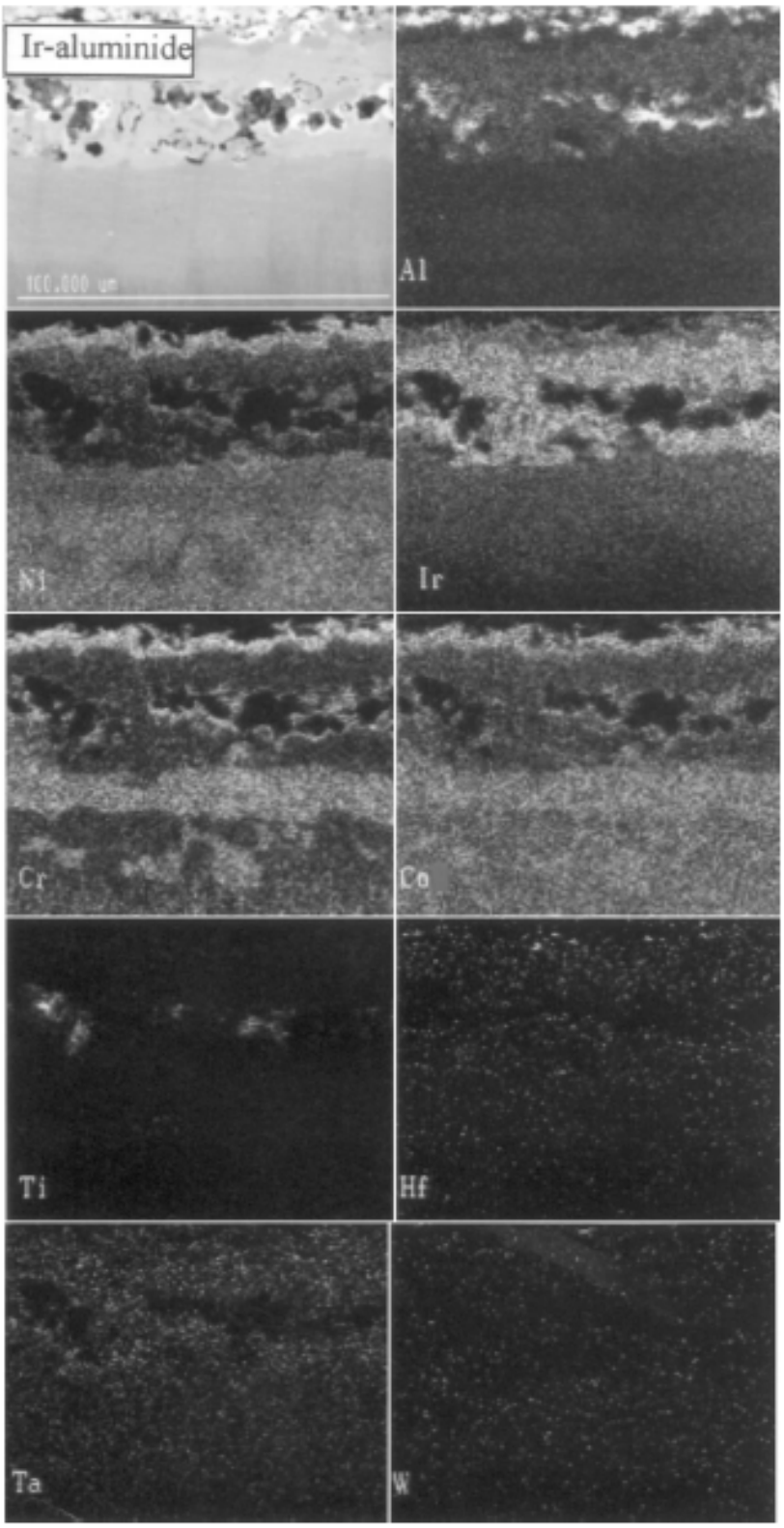

Figure 6.49 Digimap analysis of the *Ir*-aluminide, aged for 100 hours at 1100°C, in section

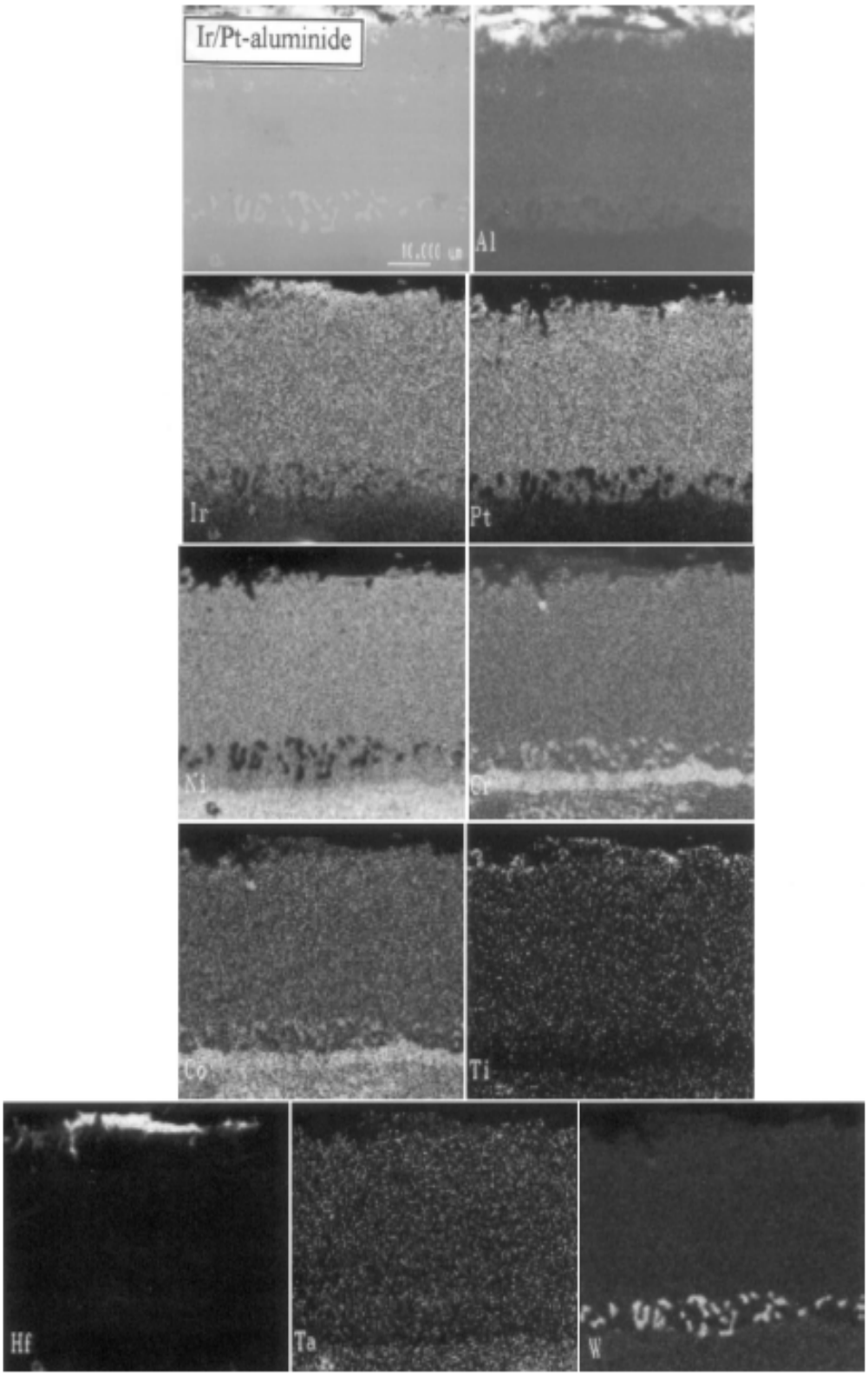

Figure 6.50 Digimap analysis of the *IrPt*-aluminide, aged for 100 hours at 1100°C, in section

6.6.3. *Ir*-aluminide Information on Structure

6.6.3.1. As Processed

EDS (ZAF analysis), (Figure 6.47), confirms the following structure:

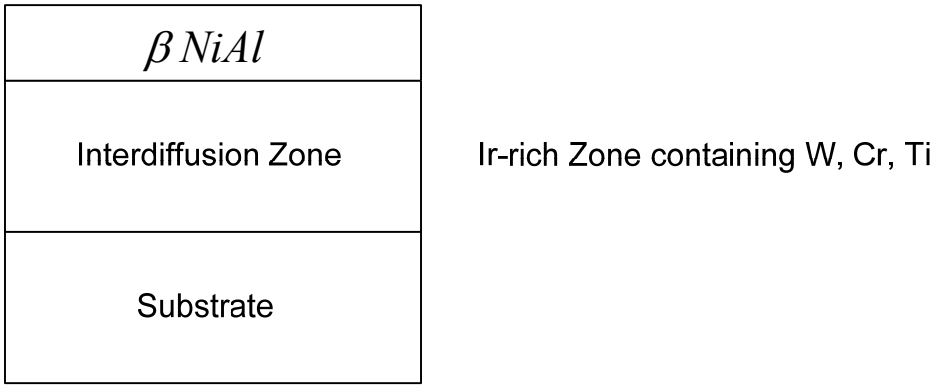

6.6.3.2. *Ir*-aluminide

Oxidation at 1100^{o}C 100 hours:

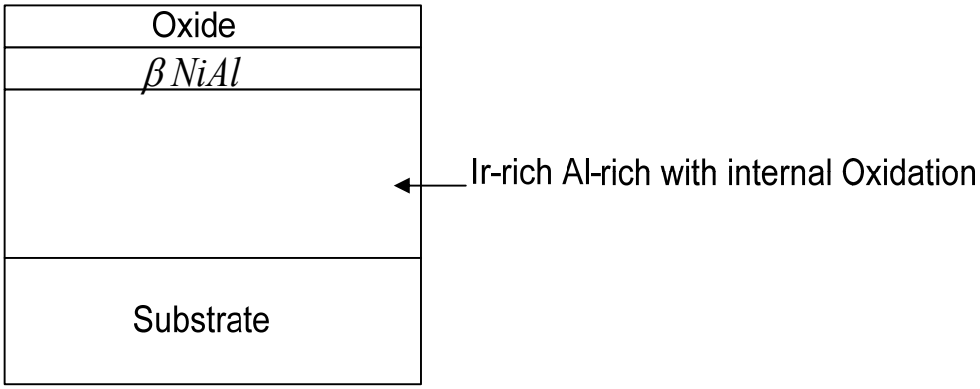

6.6.4. *Ir*-*Pt*-aluminide Information on Structure

6.6.4.1. As Processed

EDS data confirms using ZAF analysis, Figure 6.48, the following scheme:

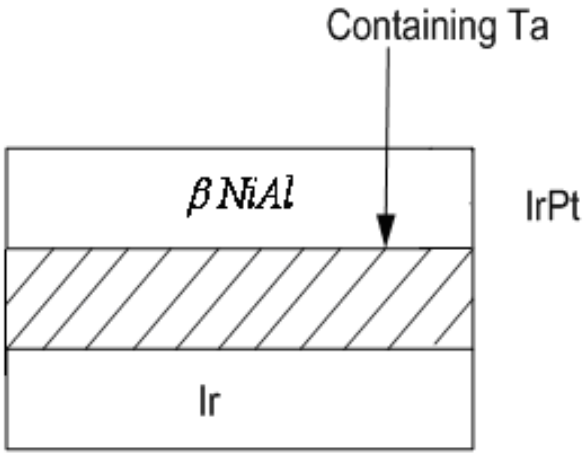

6.6.4.2. *Ir*-*Pt*-aluminide

When the metals are subjected to oxidation at 1100°C for 100 hours;

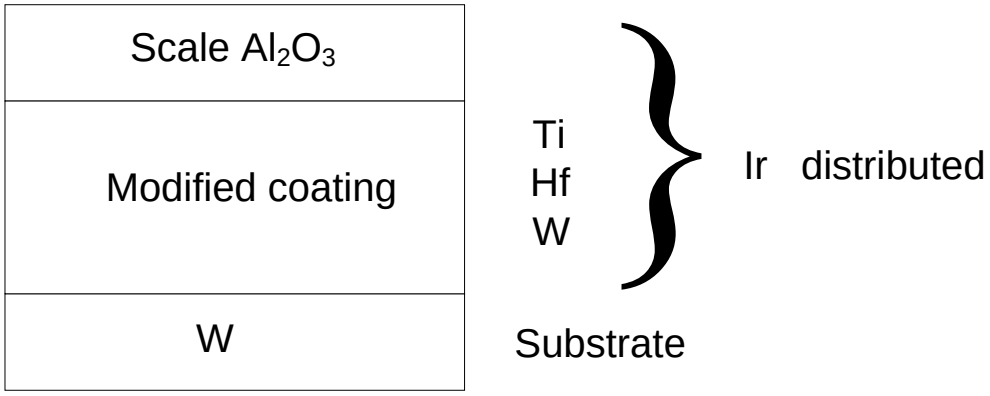

In the next section 6.6.5 the numerical modelling of interdiffusion for this system has been presented.

6.6.5. Modelling Interdiffusion Using Genetic Algorithms Method (GAs) with the Numerical Method

Genetic Algorithms method was used to calculate the diffusion coefficients for each component (Al, Cr, Ir, Ni) and (Al, Cr, Ir, Ni, Pt) of the samples (details in chapter

3). The diffusion coefficients of each component were then used to compute their numerical concentration using the equation, (Runge-Kutta method of order four):

$$C_{n+1} = \frac{1}{6}(k_1 + 2k_2 + 2k_3 + k_4),$$
$$k_1 = hf(x_n, y_n),$$
$$k_2 = hf(x_n + \frac{1}{2}h, y_n + \frac{1}{2}k_1),$$
$$k_3 = hf(x_n + \frac{1}{2}h, y_n + \frac{1}{2}k_2),$$
$$k_4 = hf(x_n + h, y_n + k_3).$$

was applied to Fick's second law

$$\frac{\partial C}{\partial t} = D\frac{\partial^2 C}{\partial x^2}$$

where D is the diffusion coefficient calculated from Genetic Algorithms method. With this method the results found are shown below where we have supposed constant diffusion coefficient in the diffusion matrix:

$$\begin{bmatrix} D_{11} & D_{12} & D_{13} & D_{14} \\ D_{21} & D_{22} & D_{23} & D_{24} \\ D_{31} & D_{32} & D_{33} & D_{34} \\ D_{41} & D_{42} & D_{43} & D_{44} \end{bmatrix} \tag{6.44}$$

$$\begin{bmatrix} D_{11} & D_{12} & D_{13} & D_{14} & D_{15} \\ D_{21} & D_{22} & D_{23} & D_{24} & D_{25} \\ D_{31} & D_{32} & D_{33} & D_{34} & D_{35} \\ D_{41} & D_{42} & D_{43} & D_{44} & D_{45} \\ D_{51} & D_{52} & D_{53} & D_{54} & D_{55} \end{bmatrix} \tag{6.45}$$

where the diagonal terms $(D_{11}, D_{22}, D_{33}, D_{44})$ and $(D_{11}, D_{22}, D_{33}, D_{44}, D_{55})$ are taking into account and the cross terms are considered to be zero from the diffusion matrixes (equations 6.44 and 6.45 respectively).

In the following Figure the aluminum concentration profiles have been presented at 1100°C after 100 hours diffusion treatment:

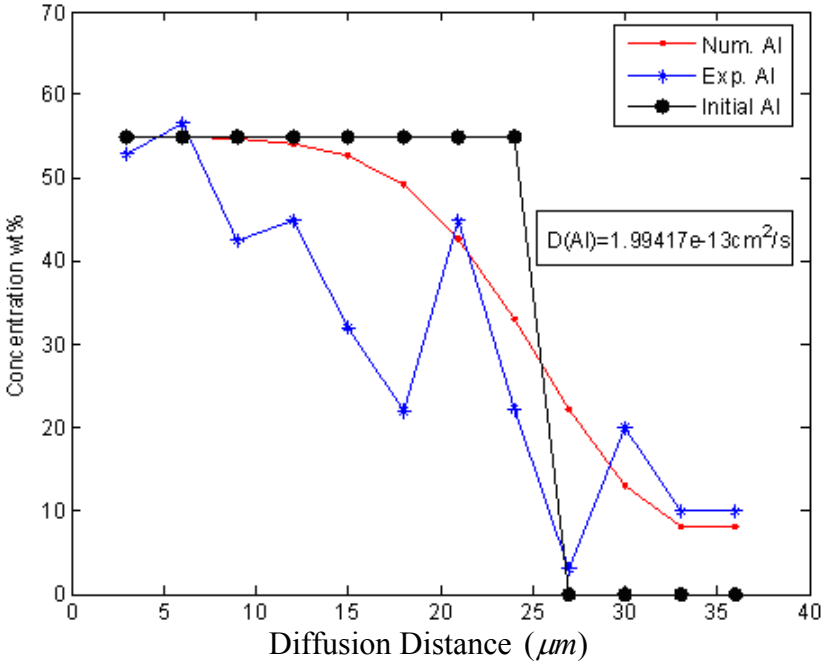

Figure 6.51 Aluminum concentration profiles in an iridium/low-activity aluminide/ MAR M002 system at 1100°C after 100 hours diffusion treatment

Figure 6.51 shows the numerical concentration calculated using only the composition independent diagonal terms of diffusion matrix, and experimental concentration after 100 hours diffusion treatment. The optimum value of aluminum diffusion coefficient is $1.99417 \times 10^{-13} cm^2 / s$ in $Ir-$aluminide system. This coefficient has been calculated by using Genetic Algorithms optimization method. The blue star curve (represents the aluminum experimental profile after 100 hours diffusion treatment), the red dot curve represents the numerical concentration profile for aluminum after 100 hours diffusion treatment, and the black solid circle curve

represents the initial aluminum concentration profile. There is an agreement between the aluminum numerical and experimental concentration profiles for the whole range of diffusion distance after 100 hours diffusion treatment.

Similarly, in Figure 6.52 aluminum concentration profiles are presented in $IrPt-$aluminide system:

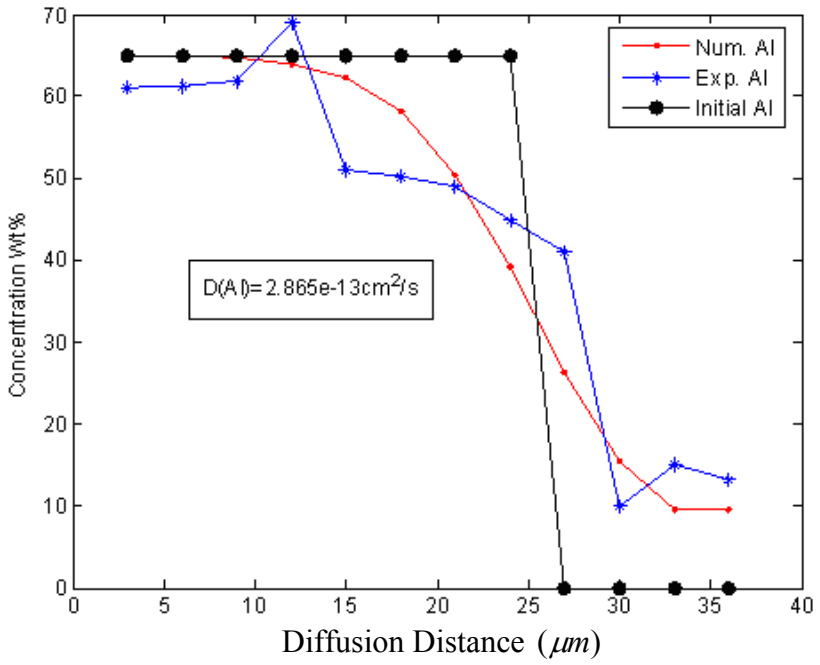

Figure 6.52 Aluminum concentration profiles in an iridium platinum/low-activity aluminide/ MAR M002 system at 1100°C after 100 hours diffusion treatment

As shown in Figure 6.52, there is an agreement between the numerical concentration and experimental concentration for aluminum. $2.865\times10^{-13}cm^2/s$ is the optimum aluminum diffusion coefficient value determined from GAs method.

In the following Figures (6.53, 6.54) the chromium concentrations profiles have been presented (in both systems $Ir-$aluminide and $Ir\,Pt-$ aluminide);

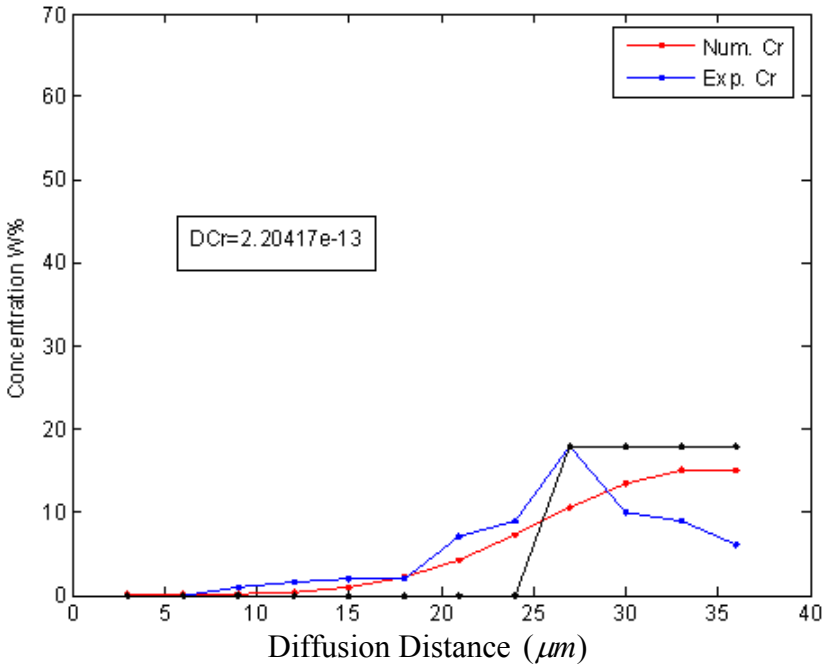

Figure 6.53 Chromium concentration profiles in an iridium/low-activity aluminide/ MAR M002 system at 1100°C after 100 hours diffusion treatment

Figure 6.53 shows the numerical and experimental concentration profiles after 100 hours diffusion treatment calculated using $D(Cr) = 2.20417 \times 10^{-13} cm^2 / s$ determined from GAs method.

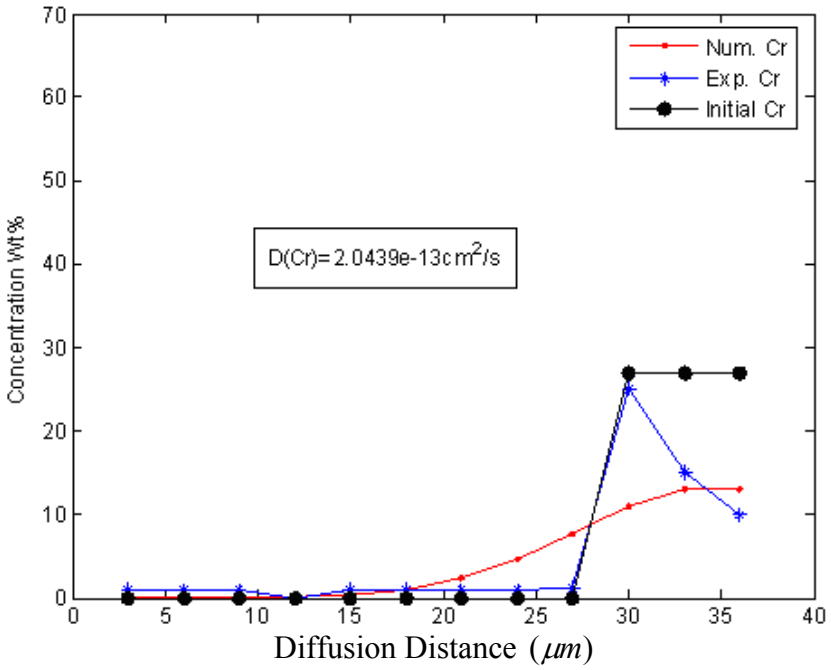

Figure 6.54 Chromium concentration profiles in an iridium platinum/low-activity aluminide/ MAR M002 system at 1100°C after 100 hours diffusion treatment

As presented in Figures 6.53 and 6.54 there is an agreement between the chromium numerical and experimental concentration profiles for the whole range of diffusion distance after 100 hours diffusion treatment.

In Figures (6.55 – 6.59) the iridium, nickel, and platinum concentrations profiles are presented using GAs method to determine the diffusion coefficients:

$D(Ir) = 7.94321 \times 10^{-14} cm^2 / s$ in $Ir -$ aluminide

$D(Ir) = 4.9265 \times 10^{-14} cm^2 / s$ in $IrPt -$ aluminide

$D(Ni) = 3.54204 \times 10^{-14} cm^2 / s$ in $Ir -$ aluminide

$D(Ni) = 3.1085 \times 10^{-14} cm^2 / s$ in $IrPt -$ aluminide

$D(Pt) = 4.6120 \times 10^{-14} cm^2 / s$ in $IrPt -$ aluminide

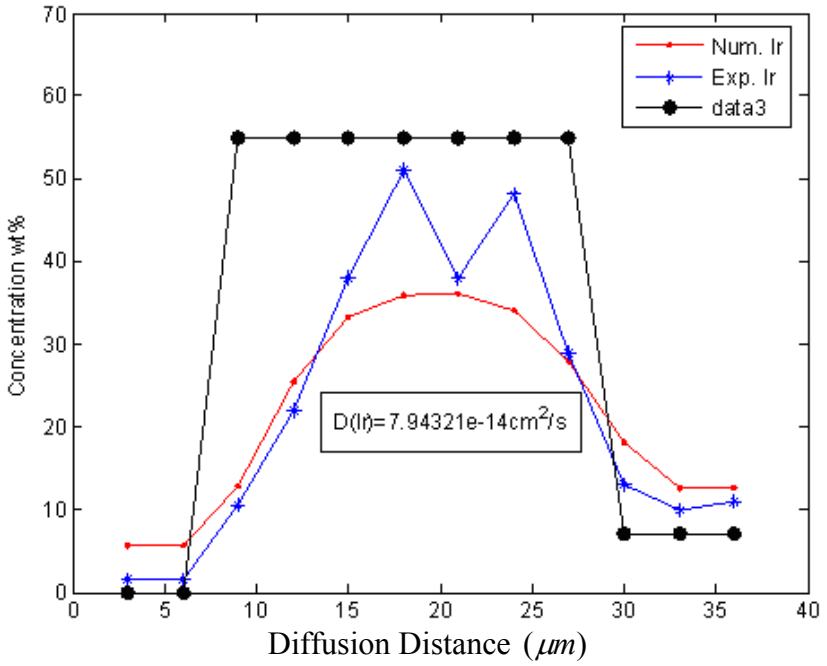

Figure 6.55 Iridium concentration profiles in an iridium/low-activity aluminide/ MAR M002 system at 1100°C beyond 100 hours diffusion treatment

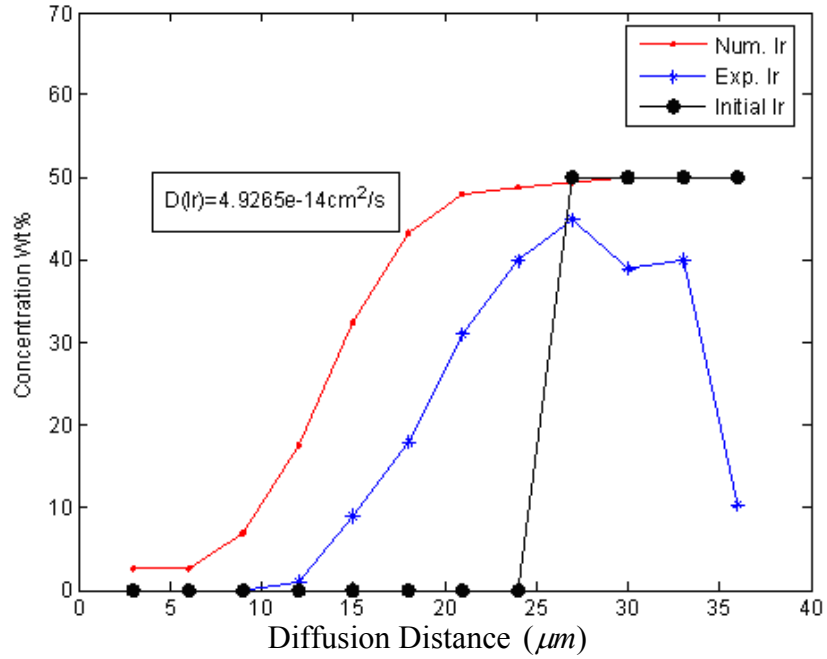

Figure 6.56 Iridium concentration profiles in an iridium platinum/low-activity aluminide/ MAR M002 system at 1100°C after 100 hours diffusion treatment

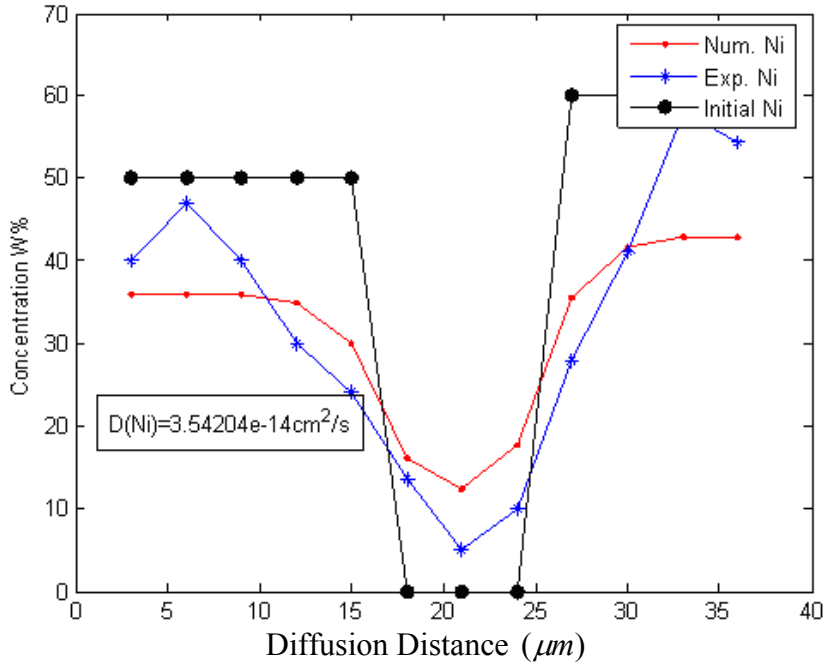

Figure 6.57 Nickel concentration profiles in an iridium/low-activity aluminide/ MAR M002 system at 1100°C behind 100 hours diffusion treatment

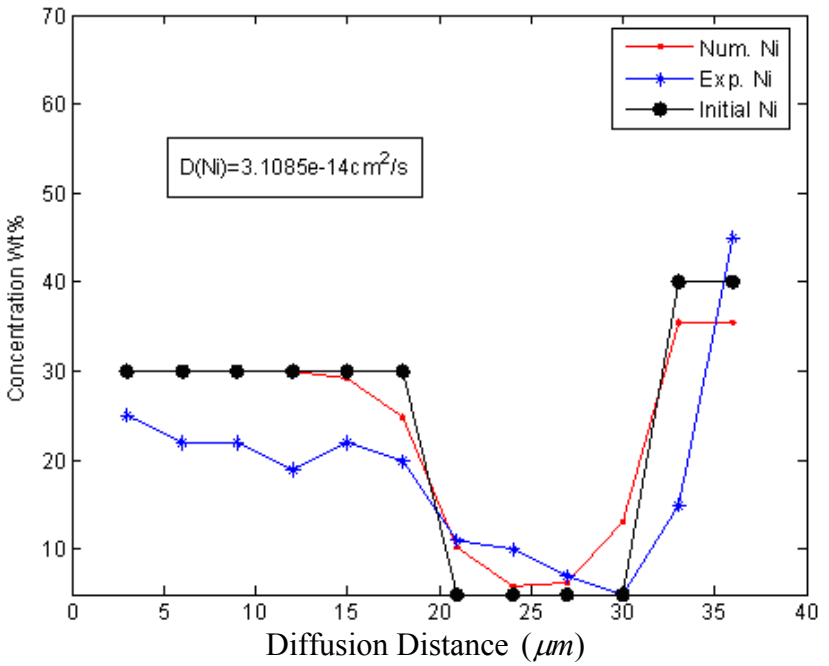

Figure 6.58 Nickel concentration profiles in iridium-platinum/low-activity aluminide/ MAR M002 system at 1100°C after 100 hours diffusion treatment

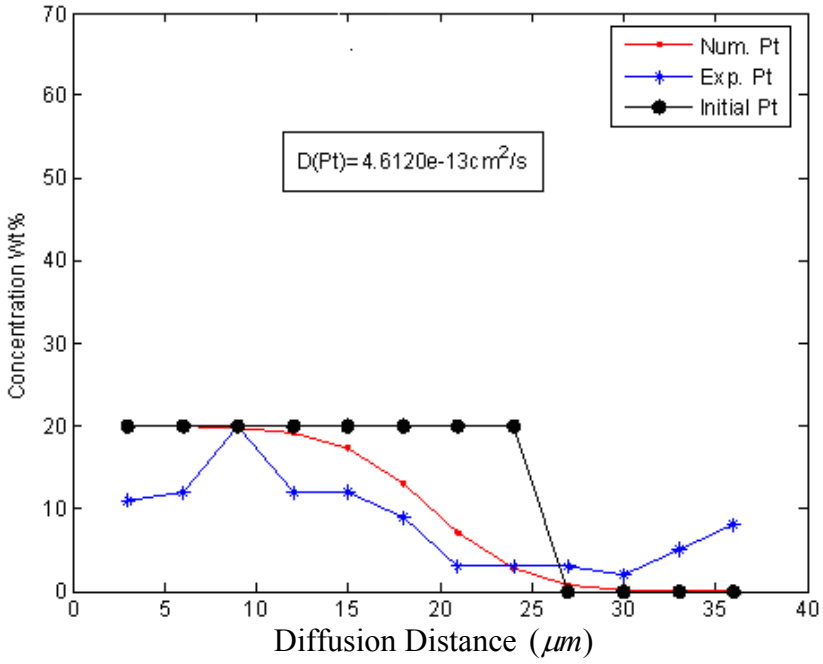

Figure 6.59 Platinum concentration profiles in an iridium platinum/low-activity aluminide/ MAR M002 system at 1100°C behind 100 hours diffusion treatment

All the Figures from (6.55 - 6.59) show a little divergence between the experimental and numerical concentration profiles for the diffusion distance (15-25) μm beyond 100 hours.

6.6.5.1. Conclusions of *Ir*-aluminide and *Pt-Ir* aluminide Coatings at 1100°C for 100 Hours (Constant Diagonal Terms)

Fick's second law has been used to find the concentration profile for each component, (Al, Cr, Ir, Ni, Pt) using Rung-Kutta method of order four. The Genetic Algorithms method allows optimization of the values of diffusion coefficients. The calculated concentration profiles have been compared with the experimental data using Least squares method. The results from Genetic Algorithms optimization method (GAs), the diffusion coefficients for each component, show reasonable agreement

between the numerical and experimental concentration profiles for these components (Al, Cr, Ir, Ni, Pt). Further improvement can be achieved by introducing composition dependent diffusion coefficients and taking into account the cross terms in diffusion matrix.

6.6.6. Calculation Considering Constant Cross and Diagonal Terms Diffusion Coefficients

Fick's second law for multicomponent systems (four independent component (Al, Cr, Ir, Ni) and five independent components (Al, Cr, Ir, Ni, Pt) systems) can be written as:

$$\frac{\partial C_i}{\partial t} = \sum_{j=1}^{n-1} \tilde{D}_{ij}^{n} \frac{\partial^2 C_j}{\partial x^2} \quad i = 1,2,3,4 \tag{6.46}$$

$$\Rightarrow \begin{bmatrix} \frac{\partial C_1}{\partial t} \\ \frac{\partial C_2}{\partial t} \\ \frac{\partial C_3}{\partial t} \\ \frac{\partial C_4}{\partial t} \end{bmatrix} = \begin{bmatrix} D_{11} & D_{12} & D_{13} & D_{14} \\ D_{21} & D_{22} & D_{23} & D_{24} \\ D_{31} & D_{32} & D_{33} & D_{31} \\ D_{41} & D_{42} & D_{43} & D_{44} \end{bmatrix} \begin{bmatrix} \frac{\partial C_1}{\partial x^2} \\ \frac{\partial C_2}{\partial x^2} \\ \frac{\partial C_3}{\partial x^2} \\ \frac{\partial C_4}{\partial x^2} \end{bmatrix} \tag{6.47}$$

where the number 1 means aluminum, 2 means chromium, 3 means iridium, and 4 means nickel.

And for five independent components (Al, Cr, Ir, Ni, Pt) system, Fick's second law can be written as follows:

$$\begin{bmatrix} \frac{\partial C_1}{\partial t} \\ \frac{\partial C_2}{\partial t} \\ \frac{\partial C_3}{\partial t} \\ \frac{\partial C_4}{\partial t} \\ \frac{\partial C_5}{\partial t} \end{bmatrix} = \begin{bmatrix} D_{11} & D_{12} & D_{13} & D_{14} & D_{15} \\ D_{21} & D_{22} & D_{23} & D_{24} & D_{25} \\ D_{31} & D_{32} & D_{33} & D_{34} & D_{35} \\ D_{41} & D_{42} & D_{43} & D_{44} & D_{45} \\ D_{51} & D_{52} & D_{53} & D_{54} & D_{55} \end{bmatrix} \begin{bmatrix} \frac{\partial C_1}{\partial x^2} \\ \frac{\partial C_2}{\partial x^2} \\ \frac{\partial C_3}{\partial x^2} \\ \frac{\partial C_4}{\partial x^2} \\ \frac{\partial C_5}{\partial x^2} \end{bmatrix} \tag{6.48}$$

Numbers 1, 2, 3, 4, and 5 belong to aluminum, chromium, iridium, nickel, and platinum respectively.

So the diffusion coefficients matrix is as follows:

$$\begin{bmatrix} D_{11} & D_{12} & D_{13} & D_{14} \\ D_{21} & D_{22} & D_{23} & D_{24} \\ D_{31} & D_{32} & D_{33} & D_{31} \\ D_{41} & D_{42} & D_{43} & D_{44} \end{bmatrix} \tag{6.49}$$

$$\begin{bmatrix} D_{11} & D_{12} & D_{13} & D_{14} & D_{15} \\ D_{21} & D_{22} & D_{23} & D_{24} & D_{25} \\ D_{31} & D_{32} & D_{33} & D_{34} & D_{35} \\ D_{41} & D_{42} & D_{43} & D_{44} & D_{45} \\ D_{51} & D_{52} & D_{53} & D_{54} & D_{55} \end{bmatrix} \tag{6.50}$$

In these matrixes the diagonal and cross terms have been considered to be constant.

In Figures 6.60 and 6.63 the experimental and numerical concentration for the components (aluminum, chromium, iridium, and nickel) and for the components (aluminum, chromium, iridium, nickel, and platinum) have been presented with the interrdiffusion coefficients calculated from Genetic Algorithms method and using

equations 6.47 and 6.48 respectively (applying Fick's second law). Here the cross terms have been taken into account.

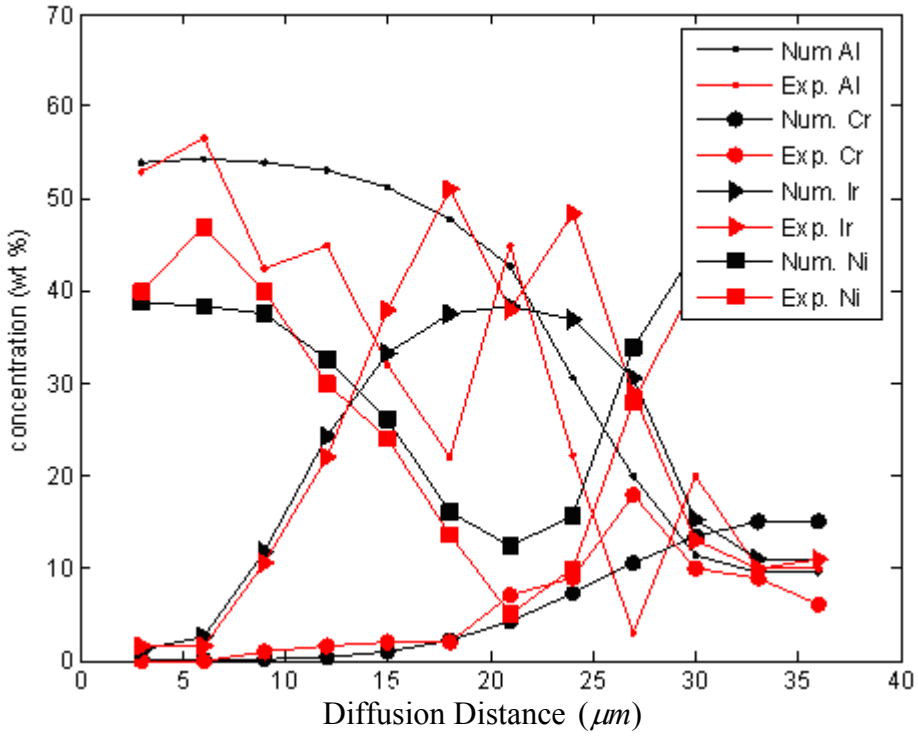

Figure 6.60 Numerical and experimental concentration profiles for all the components (aluminum, chromium, iridium, and nickel) in an iridium/low-activity aluminide/ MAR M002 system at 1100°C after 100 hours diffusion treatment considering constant cross and diagonal terms

Figure 6.60 demonstrates aluminum, chromium, iridium, and nickel concentrations (numerical and experimental) using constant diffusion coefficients $D_{11}, D_{12}, D_{13}, D_{14}, D_{21}, D_{22}, D_{23}, D_{24}, D_{31}, D_{32}, D_{33}, D_{34}, D_{41}, D_{42}, D_{43}, D_{44}$ determined from Genetic Algorithms optimization method described in chapter 5 as:

$$
\begin{aligned}
D_{11} &= 1.7831\times10^{-13}\,cm^2/s \\
D_{12} &= 2.494231\times10^{-12}\,cm^2/s \\
D_{13} &= 0.7215\times10^{-12}\,cm^2/s \\
D_{14} &= 1.3585\times10^{-12}\,cm^2/s \\
D_{21} &= 0.7008\times10^{-12}\,cm^2/s \\
D_{22} &= 1.9104\times10^{-13}\,cm^2/s \\
D_{23} &= 1.0332\times10^{-12}\,cm^2/s \\
D_{24} &= 1.9431\times10^{-12}\,cm^2/s \\
D_{31} &= 0.0261\times10^{-13}\,cm^2/s \\
D_{32} &= 0.0167\times10^{-13}\,cm^2/s \\
D_{33} &= 6.3217\times10^{-14}\,cm^2/s \\
D_{34} &= 2.9081\times10^{-13}\,cm^2/s \\
D_{41} &= 2.4261\times10^{-13}\,cm^2/s \\
D_{42} &= 2.0167\times10^{-13}\,cm^2/s \\
D_{43} &= 4.7217\times10^{-13}\,cm^2/s \\
D_{44} &= 4.0091\times10^{-14}\,cm^2/s
\end{aligned}
\qquad (6.51)
$$

In the above Figure 6.60 the numerical concentration profiles for the components aluminum, chromium, iridium, and nickel have been calculated considering constant cross terms and diagonal terms, in a diffusion matrix. There is improved agreement between the experimental and numerical concentration for all the components shown. This improvement can be explained in the following Figures (6.61 and 6.62):

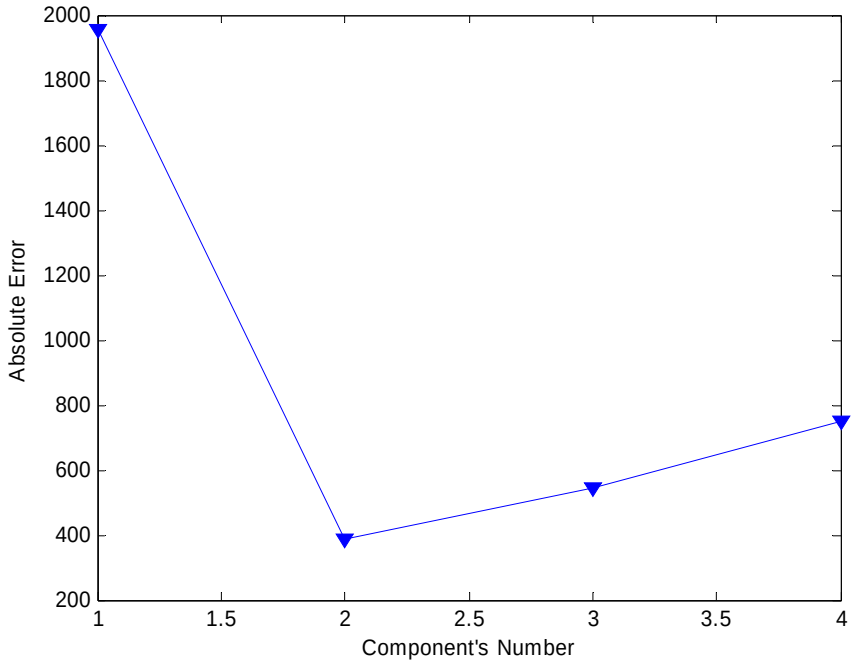

Figure 6.61 The absolute error for the components aluminum, chromium iridium and nickel with the constant diagonal diffusion coefficients Ir – aluminide system

As shown in Figure 6.61 the absolute error for aluminum is (1945.3), for chromium is (385.8003), for iridium is (544.6138), and for nickel is (752.134). Whereas if we look to the following Figure 6.62 the absolute error for aluminum is (1680.3), for chromium is (197.6218), for iridium is (355.8656), and for nickel is (327.3896). The numbers 1, 2, 3, and 4 represent Al, Cr, Ir, and Ni respectively.

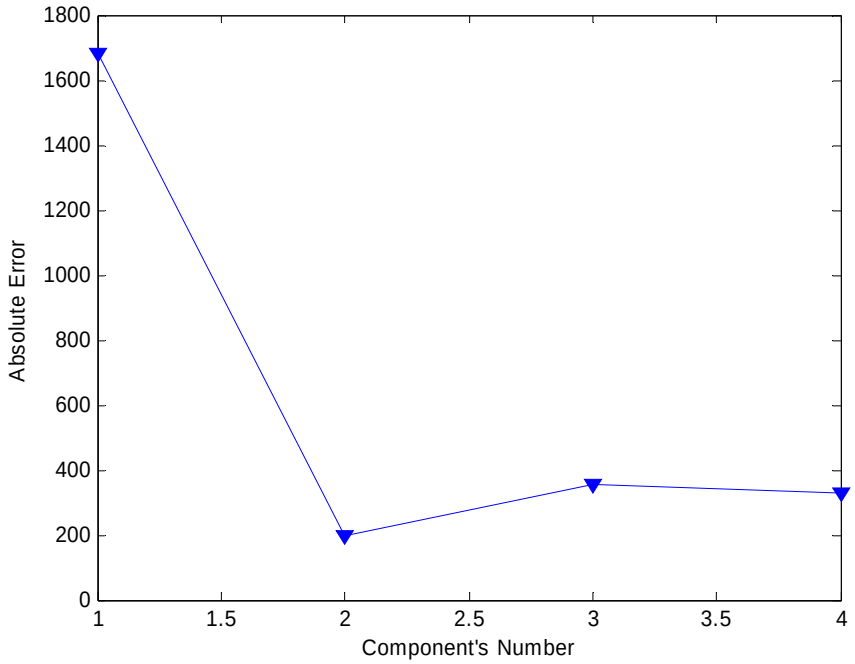

Figure 6.62 The absolute error for the components aluminum, chromium, iridium and nickel (whole constant diffusion coefficient matrix, equation 6.47) for Ir – aluminide system

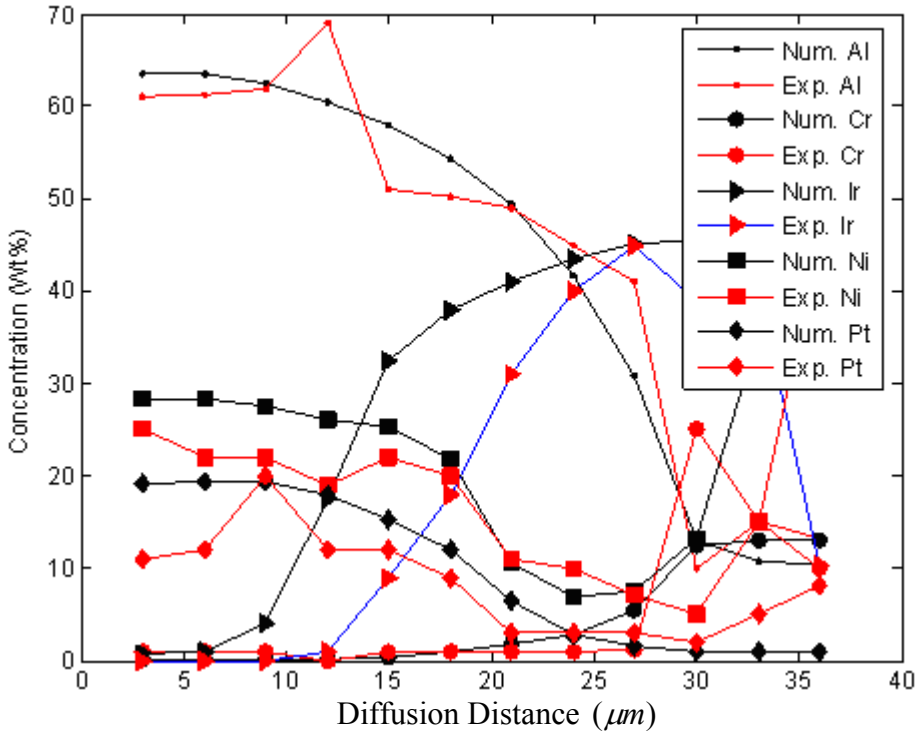

Figure 6.63 Numerical and experimental concentration profiles for all the components (aluminum, chromium, iridium, nickel and platinum) in an iridium platinum /low-activity aluminide/ MAR M002 system at 1100^{o}C after 100 Hours diffusion treatment considering constant cross and diagonal terms

Figure 6.63 shows aluminum, chromium, iridium, nickel, and platinum concentrations (numerical and experimental) using constant diffusion coefficients $D_{11}, D_{12}, D_{13}, D_{14}, D_{15}, D_{21}, D_{22}, D_{23}, D_{24}, D_{25} D_{31}, D_{32}, D_{33}, D_{34}, D_{35}, D_{41}, D_{42}, D_{43}, D_{44}, D_{45}, D_{51}, D_{52}, D_{53}, D_{54}, D_{55}$ determined from Genetic Algorithms optimization method (chapter 5) as:

$$
\begin{aligned}
D_{11} &= 1.0171\times10^{-13}\,cm^2/s \\
D_{12} &= 2.92651\times10^{-12}\,cm^2/s \\
D_{13} &= 0.9187\times10^{-12}\,cm^2/s \\
D_{14} &= 1.3209\times10^{-12}\,cm^2/s \\
D_{15} &= 2.0724\times10^{-12}\,cm^2/s \\
D_{21} &= 0.423\times10^{-12}\,cm^2/s \\
D_{22} &= 2.09874\times10^{-13}\,cm^2/s \\
D_{23} &= 5.0001\times10^{-12}\,cm^2/s \\
D_{24} &= 1.0254\times10^{-12}\,cm^2/s \\
D_{25} &= 2.1987\times10^{-12}\,cm^2/s \\
D_{31} &= 0.3273\times10^{-13}\,cm^2/s \\
D_{32} &= 0.00087\times10^{-13}\,cm^2/s \\
D_{33} &= 5.8637\times10^{-14}\,cm^2/s \\
D_{34} &= 2.2987\times10^{-13}\,cm^2/s \\
D_{35} &= 3.9143\times10^{-13}\,cm^2/s \\
D_{41} &= 2.8461\times10^{-13}\,cm^2/s \\
D_{42} &= 2.09897\times10^{-13}\,cm^2/s \\
D_{43} &= 6.0091\times10^{-13}\,cm^2/s \\
D_{44} &= 4.1651\times10^{-14}\,cm^2/s \\
D_{45} &= 7.009\times10^{-14}\,cm^2/s \\
D_{51} &= 0.4283\times10^{-13}\,cm^2/s \\
D_{52} &= 0.8707\times10^{-13}\,cm^2/s \\
D_{53} &= 5.1947\times10^{-14}\,cm^2/s \\
D_{54} &= 2.2700\times10^{-13}\,cm^2/s \\
D_{55} &= 3.0513\times10^{-13}\,cm^2/s
\end{aligned}
\qquad (6.52)
$$

A similar picture is presented in Figures 6.64 and 6.65 for the $IrPt-$ aluminide system.

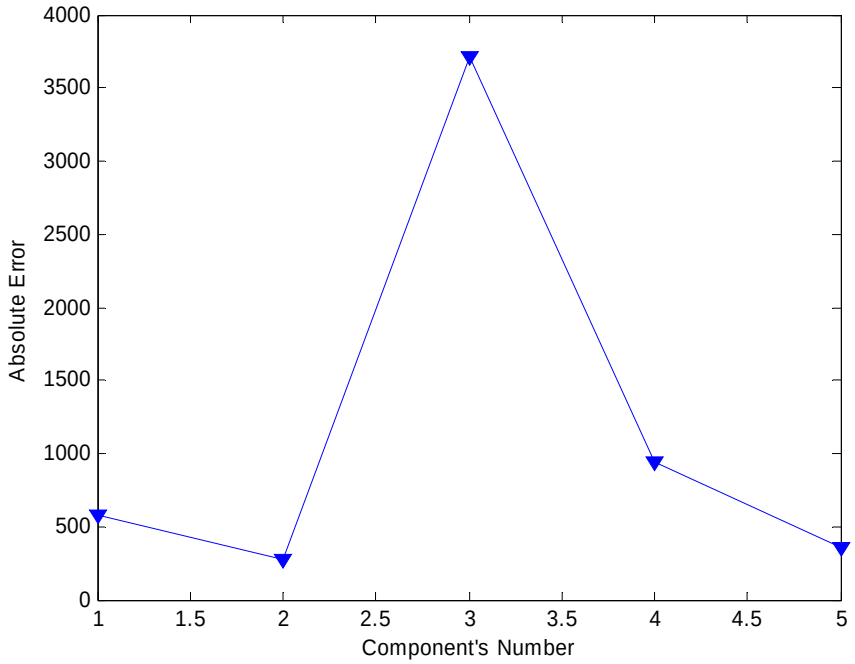

Figure 6.64 The absolute error for the components aluminum, chromium iridium, nickel and platinum with the constant diagonal diffusion coefficients *IrPt* – aluminide system

As shown in Figure 6.64 the absolute error for aluminum is (576.6679), for chromium is (270.9045), for iridium is (3.7174e3), for nickel is (943.9835) and for platinum is (351.1695).

However in Figure 6.64 the absolute error for aluminum is (298.1100), for chromium is (196.1750), for iridium is (2.6893e+003), for nickel is (730.8212), and for platinum is (256.7069).

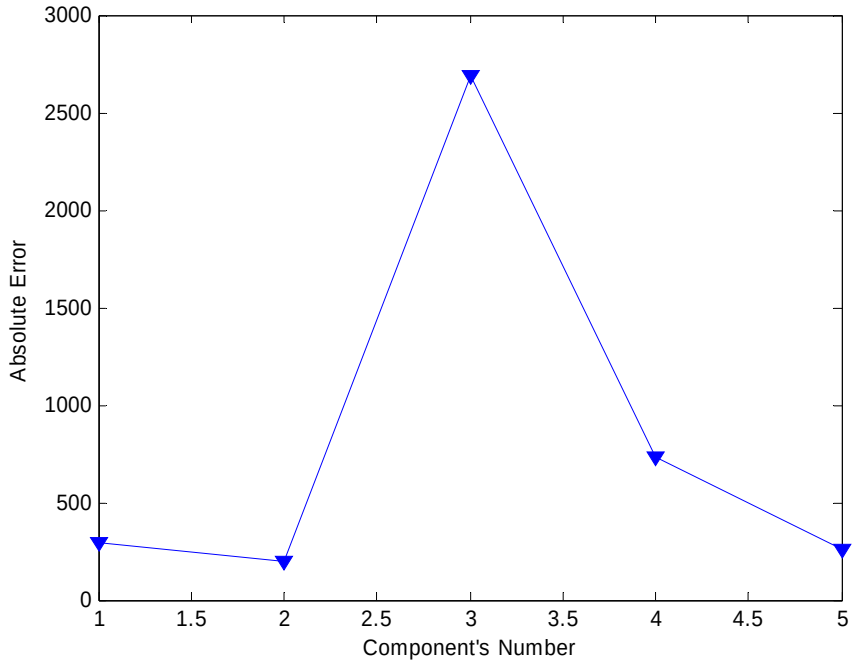

Figure 6.65 The absolute error for the components aluminum, chromium, iridium nickel and platinum (whole constant diffusion coefficient matrix, equation 6.51)

6.6.6.1. Conclusions Considering Constant Cross and Diagonal Terms Diffusion Coefficients

Numerical modelling has been done using the same technique as above. Data presented show good convergence between the experimental and numerical concentration for the components (Al, Cr, Ir, Ni) when equation 6.47 was used to calculate the diffusion coefficients, taking into account the cross terms. In a similar way for the system (Al, Cr, Ir, Ni, Pt), equation 6.48 has been done. The absolute error between the experimental and numerical concentration profiles for both systems has been reduced, Figures (6.61, 6.62, 6.64, and 6.65). It means the numerical concentration profiles for all the components show much improvement when the cross terms are taken into account.

6.6.7. Calculation Considering Variable Cross and Diagonal Terms Diffusion Coefficients

In the previous part, (6.6.6), the diffusion coefficients (diagonal and cross terms) for the all the components $(Al, Cr, Ir, Ni), (Al, Cr, Ir, Ni, Pt)$ were considered to be constant. In the present part the diffusion coefficients are considered to be concentration dependent (a function of concentration). Second order polynomials have been used for concentration dependence diffusion coefficients for aluminum, chromium, iridium and nickel, and platinum. The concentration profiles have been presented in the Figure 6.66:

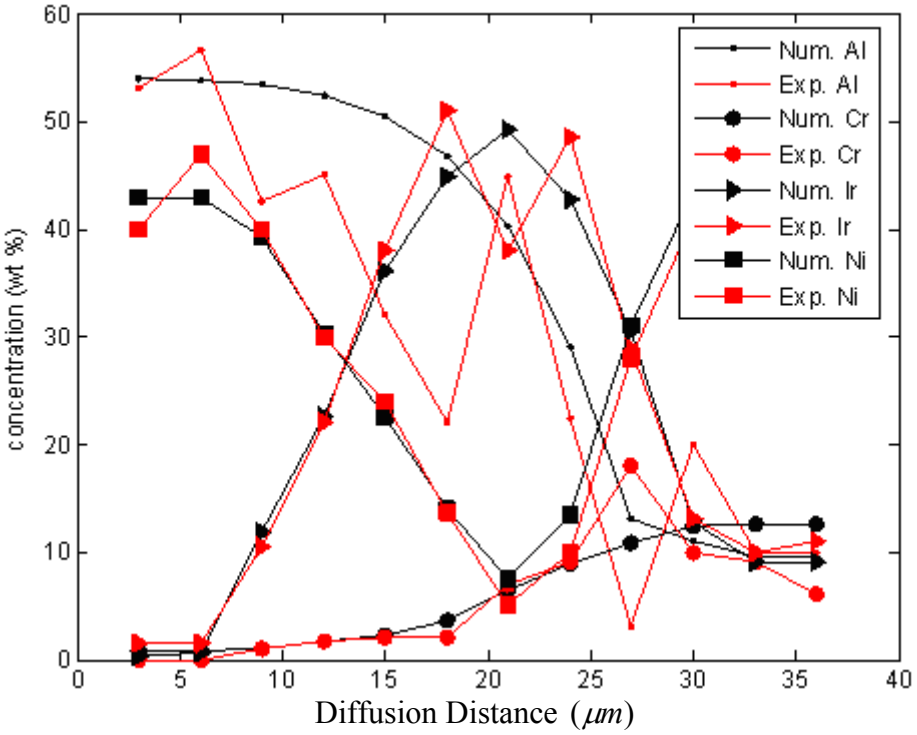

Figure 6.66 Numerical and experimental concentration profiles for all the components (aluminium, chromium, iridium, and nickel) in an iridium/low-activity aluminide/ MAR M002 system at 1100°C after 100 hours diffusion treatment considering variable cross and diagonal terms

Figure 6.66 illustrates the numerical and experimental concentrations for (aluminum, chromium, iridium, and nickel) with concentration dependent diffusion coefficients $\begin{matrix} D_{11}, D_{12}, D_{13}, D_{14}, D_{21}, D_{22}, D_{23}, D_{24}, \\ D_{31}, D_{32}, D_{33}, D_{34}, D_{41}, D_{42}, D_{43}, D_{44} \end{matrix}$ (second order polynomial) after 100 hours diffusion treatment:

$$
\begin{aligned}
D_{11} &= a_1 + a_2 C_1 + a_3 C_1^{\,2} + a_4 C_3^2 \\
D_{12} &= b_1 + b_2 C_1 C_2 + b_3 C_2 + b_4 C_4^2 \\
D_{13} &= c_1 C_2 + c_2 C_2^{\,2} \\
D_{14} &= d_1 C_3 + d_2 C_1 C_4 \\
D_{21} &= e_1 C_1 + e_2 C_2 + e_3 C_2^{\,2} \\
D_{22} &= f_1 C_3 + f_2 C_2^2 + f_3 C_2 C_3 \\
D_{23} &= g_1 C_1^2 + g_2 C_3^2 \\
D_{24} &= h_1 C_1 C_3 \\
D_{31} &= i_1 C_1 C_3 + i_2 C_3 \\
D_{32} &= j_1 C_3 + j_2 + j_3 C_3 + j_4 C_3 C_1 \\
D_{33} &= k_1 C_1 C_2 + k_2 C_3^2 \\
D_{34} &= l_1 C_3 C_4 + l_2 C_2^2 \\
D_{41} &= m_1 C_2^2 + m_2 C_4^2 \\
D_{42} &= n_1 + n_2 C_3 C_4 \\
D_{43} &= o_1 C_1^2 + o_2 C_3^2 \\
D_{44} &= p_1 + p_2 C_1^2
\end{aligned}
\qquad (6.53)
$$

The values of D's are as follows:

$$D_{11} = 2.0479 \times 10^{-13} cm^2 / s$$
$$D_{12} = 4.0084 \times 10^{-12} cm^2 / s$$
$$D_{13} = 0.9815 \times 10^{-12} cm^2 / s$$
$$D_{14} = 1.0587 \times 10^{-12} cm^2 / s$$
$$D_{21} = 1.0701 \times 10^{-12} cm^2 / s$$
$$D_{22} = 1.2314 \times 10^{-13} cm^2 / s$$
$$D_{23} = 2.9312 \times 10^{-12} cm^2 / s$$
$$D_{24} = 2.7730 \times 10^{-12} cm^2 / s$$
$$D_{31} = 1.0654 \times 10^{-13} cm^2 / s$$
$$D_{32} = 0.0121 \times 10^{-13} cm^2 / s$$
$$D_{33} = 6.5211 \times 10^{-14} cm^2 / s$$
$$D_{34} = 2.0042 \times 10^{-13} cm^2 / s$$
$$D_{41} = 2.0181 \times 10^{-13} cm^2 / s$$
$$D_{42} = 3.1115 \times 10^{-13} cm^2 / s$$
$$D_{43} = 4.9145 \times 10^{-13} cm^2 / s$$
$$D_{44} = 4.0054 \times 10^{-14} cm^2 / s$$

where C_1, C_2, C_3, C_4 are the initial concentrations for aluminum, chromium, iridium, and nickel respectively. $a_1, a_2, a_3, \cdots, \cdots, p_1, p_2$ are the polynomial's coefficients calculated using Genetic Algorithms optimization method. There were good agreements in the numerical and experimental concentration values for (aluminum, chromium, iridium, and nickel) of the entire range of the diffusion distance.

In the following Figure 6.67 the absolute error for the components (aluminum, chromium, iridium, and nickel) have been plotted against the number of the components as 1, 2, 3 and 4 belong to the aluminum, chromium, iridium, and nickel respectively. In this Figure the diffusion coefficients for the whole diffusion matrix, equation 6.49, have been considered concentration dependence (second order polynomial):

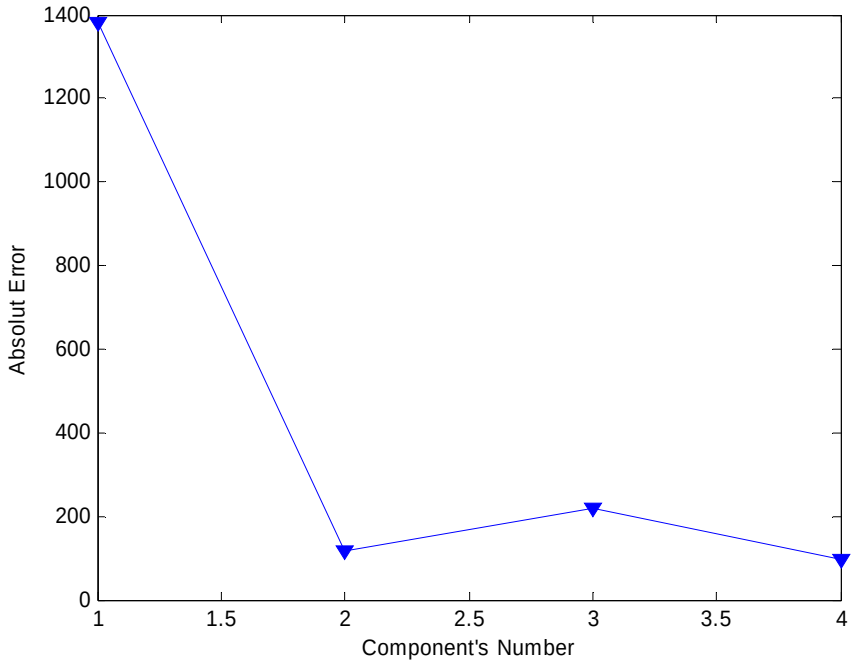

Figure 6.67 The absolute error for the components aluminum, chromium, iridium and nickel (whole variable diffusion coefficient matrix, equation 6.49)

The following Figure 6.68 illustrates the numerical and experimental concentration for the iridium platinum –aluminide system:

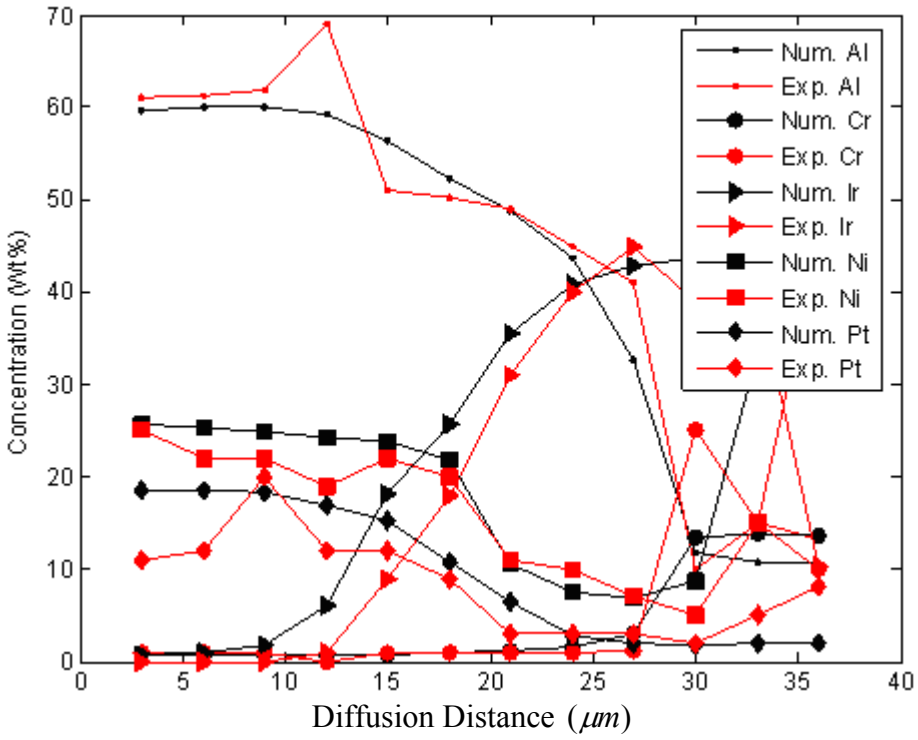

Figure 6.68 Numerical and experimental concentration profiles for all the components (aluminum, chromium, iridium, nickel, and platinum) in an iridium platinum/low-activity aluminide/ MAR M002 system at 1100°C after 100 hours considering variable cross and diagonal terms

Figure 6.68 demonstrates the numerical and experimental concentrations for aluminum, chromium, iridium, nickel and platinum with concentration dependent diffusion coefficients $D_{11}, D_{12}, D_{13}, D_{14}, D_{15}, D_{21}, D_{22}, D_{23}, D_{24}, D_{25}, D_{31}, D_{32}, D_{33}, D_{34}, D_{35}, D_{41}, D_{42}, D_{43}, D_{44}, D_{45}, D_{51}, D_{52}, D_{53}, D_{54}, D_{55}$, (second order polynomial) after 100 hours diffusion treatment:

$$
\begin{aligned}
D_{11} &= a_1 + a_2 C_1 + a_3 C_1^{\,2} + a_4 C_3^2 \\
D_{12} &= b_1 + b_2 C_1 C_2 + b_3 C_2 + b_4 C_4^2 \\
D_{13} &= c_1 C_2 + c_2 C_2^{\,2} \\
D_{14} &= d_1 C_3 + d_2 C_1 C_4 \\
D_{15} &= e_1 C_2 + e_2 C_1 C_5 \\
D_{21} &= f_1 C_1 + f_2 C_2 + f_3 C_2^{\,2} \\
D_{22} &= g_1 C_3 + g_2 C_2^2 + g_3 C_2 C_3 \\
D_{23} &= h_1 C_1^2 + h_2 C_3^2 \\
D_{24} &= i_1 C_1 C_3 \\
D_{25} &= j_1 C_3 C_5 + j_2 C_1 \\
D_{31} &= k_1 C_1 C_3 + k_2 C_3 \\
D_{32} &= l_1 C_3 + l_2 + l_3 C_3 + l_4 C_3 C_1 \\
D_{33} &= m_1 C_1 C_2 + m_2 C_3^2 \\
D_{34} &= n_1 C_3 C_4 + n_2 C_2^2 \\
D_{35} &= o_1 C_3 C_5 + o_2 C_3^2 \\
D_{41} &= p_1 C_2^2 + p_2 C_4^2 \\
D_{42} &= q_1 + q_2 C_3 C_4 \\
D_{43} &= r_1 C_1^2 + r_2 C_3^2 \\
D_{44} &= s_1 + s_2 C_1^2 \\
D_{45} &= t_1 C_3 + t_2 C_2^2 \\
D_{51} &= u_1 C_2^2 + u_2 C_4^2 \\
D_{52} &= v_1 C_2 + v_2 C_3 C_4 \\
D_{53} &= x_1 C_5^2 + x_2 C_2^2 \\
D_{54} &= y_1 C_1 + y_2 C_1^2 \\
D_{55} &= z_1 C_2 + z_2 C_3^2
\end{aligned}
\tag{6.54}
$$

The values of *D*'s are as follows:

$$D_{11} = 3.0779\times10^{-12}\,cm^2/s$$
$$D_{12} = 4.3304\times10^{-13}\,cm^2/s$$
$$D_{13} = 0.1813\times10^{-13}\,cm^2/s$$
$$D_{14} = 0.9511\times10^{-12}\,cm^2/s$$
$$D_{15} = 1.0627\times10^{-12}\,cm^2/s$$
$$D_{21} = 3.0101\times10^{-12}\,cm^2/s$$
$$D_{22} = 2.0014\times10^{-13}\,cm^2/s$$
$$D_{23} = 1.2112\times10^{-12}\,cm^2/s$$
$$D_{24} = 2.1640\times10^{-12}\,cm^2/s$$
$$D_{25} = 2.2710\times10^{-12}\,cm^2/s$$
$$D_{31} = 1.12654\times10^{-13}\,cm^2/s$$
$$D_{32} = 0.0981\times10^{-13}\,cm^2/s$$
$$D_{33} = 4.3001\times10^{-14}\,cm^2/s$$
$$D_{34} = 2.9002\times10^{-13}\,cm^2/s$$
$$D_{35} = 1.9242\times10^{-13}\,cm^2/s$$
$$D_{41} = 2.0921\times10^{-13}\,cm^2/s$$
$$D_{42} = 3.1665\times10^{-13}\,cm^2/s$$
$$D_{43} = 4.2145\times10^{-13}\,cm^2/s$$
$$D_{44} = 4.4454\times10^{-14}\,cm^2/s$$
$$D_{45} = 4.0764\times10^{-14}\,cm^2/s$$
$$D_{51} = 1.9810\times10^{-13}\,cm^2/s$$
$$D_{52} = 3.0185\times10^{-13}\,cm^2/s$$
$$D_{53} = 4.6745\times10^{-13}\,cm^2/s$$
$$D_{54} = 4.0394\times10^{-14}\,cm^2/s$$
$$D_{55} = 5.0954\times10^{-14}\,cm^2/s$$

Similar to Figure 6.68 the absolute error for the components (aluminum, chromium, iridium, nickel, and platinum) have been plotted (Figure 6.69) against the number of the components as 1, 2, 3, 4, and 5 belong to the aluminum, chromium, iridium, nickel, and platinum respectively, in this Figure the diffusion coefficients for the whole diffusion matrix, equation 6.50, have been considered a concentration dependence (second order polynomial):

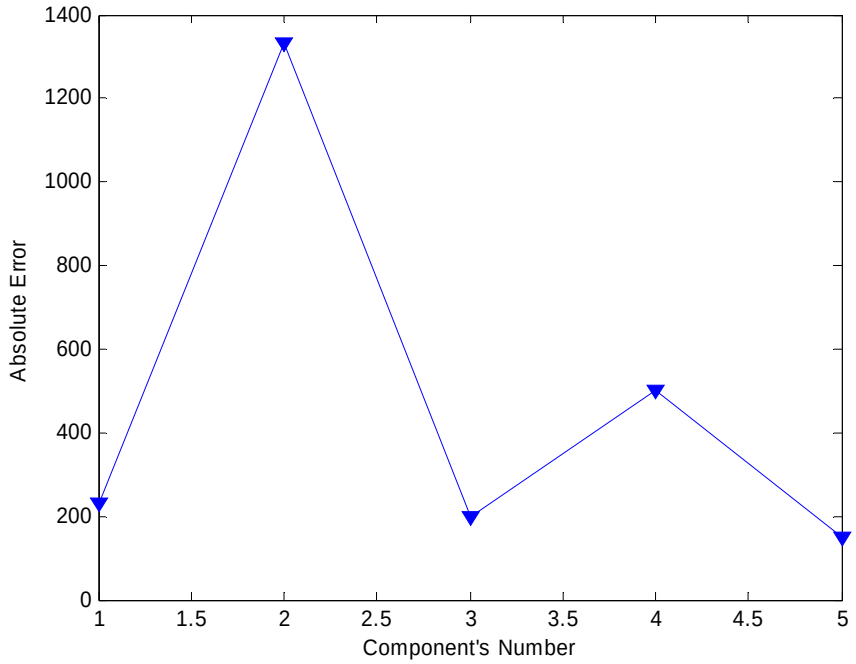

Figure 6.69 The absolute error for the components aluminum, chromium, iridium, nickel, and platinum (whole variable diffusion coefficient matrix, equation 6.50)

Figure 6.69 shows better agreement between the experimental and numerical concentration profiles for the components (Al, Cr, Ir, Ni, Pt).

6.6.7.1. Conclusions

There is very good convergence between the experimental and numerical concentration for the components $(Al, Cr, Ir, Ni), (Al, Cr, Ir, Ni, Pt)$ when equations 6.49 and 6.50 were used to calculate the diffusion coefficients, (taking into account the cross terms). The absolute error between the experimental and numerical concentration profiles for the components $(Al, Cr, Ir, Ni), (Al, Cr, Ir, Ni, Pt)$ have been reduced significantly, (Figures 6.61, 6.62, 6.67) for $Ir-$aluminide system and (Figures 6.64, 6.65, and 6.69) for $IrPt-$ aluminide system. In the following table the diffusion coefficients for the components in both systems are shown:

	Systems	
D's values (cm^2/s)	Ir-aluminide	IrPt-aluminide
D(Al)	1.99E-13	2.87E-13
D(Cr)	2.20E-13	2.04E-13
D(Ir)	7.94E-14	4.93E-14
D(Ni)	3.54E-14	3.11E-14

Table 6.3 Diffusion coefficients for the components (Al, Cr, Ir, Ni) in both systems $Ir-$aluminide and $IrPt-$ aluminide

6.7. Diffusion Processes Involved in the Formation and Oxidation Studies of Aluminise Coating on low Alloy Steels at 650°C /Microstructure Formation - Microstructural Modelling -Results and Discussion

Background information on aluminise coating on low alloy steels at 650°C together with the method of formation have been presented in section 3.6.

6.7.1. Studies of the Microstructures of the Coating and Diffusion Processes Involved

Figure 6.70 shows a cross-sectional SEM image and depth profiles of the main elements measured by EDS in a coating formed at 650° C for 8 hours in a pack containing $6\,wt\%\,Al, 2\,wt\%\,Al_2Cl_3$ and $94\,wt\%\,Al_2O_3$. It shows a uniform coating layer with a thickness of $\sim 39\,\mu m$. The fractures at the top of the coating were created during sample preparation for analysis. It is clear from the depth profile that the Al

concentration decreased slowly from about $87\,at\%$ at the surface to about $73\,at\%$ at a depth of about $8\,\mu m$ and remained constant with sudden fall to zero at the coating/substrate interface. The formation of an abrupt interface such as this suggests coating development by a reaction-diffusion controlled mechanism, leading to the formation of intermetallic compounds. The observed smooth surface of the as coated sample without any entrapped pack particles indicated that the coating was formed mainly through the inward diffusion of Al. XRD analysis shown in Figure 6.71 confirms that the major phase in the surface layer was $Fe_{14}Al_{86}$. Figure 6.72 shows the molar ratio of Al/Fe as a function of the coating depth, and reveals that, in the inner layer of the coating at depths below $(\sim 8\,\mu m)$, the molar ratio of Al/Fe is (~ 3), indicating that the major phase in the inner layer is $FeAl_3$. Figure 6.70a indicates precipitates containing a high concentration of Cr in the coating layers. Cr has a limited solubility in $Fe_{14}Al_{86}$ and $FeAl_3$.

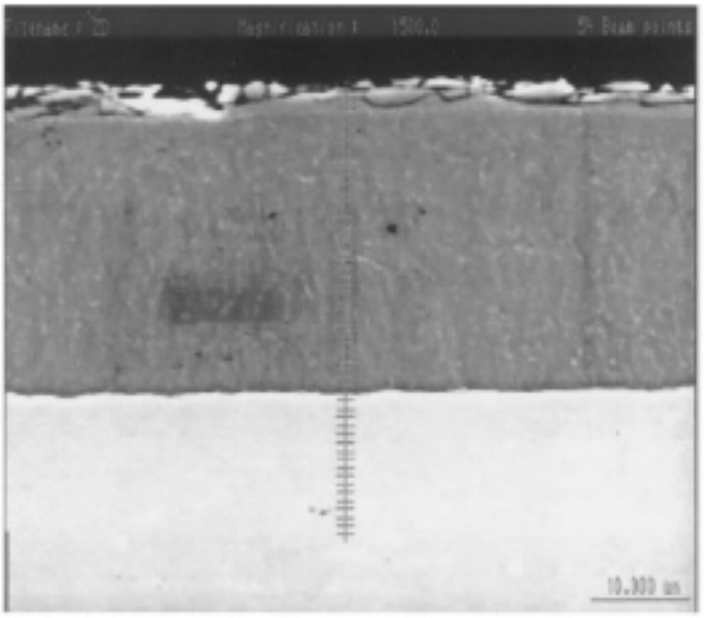

(a)

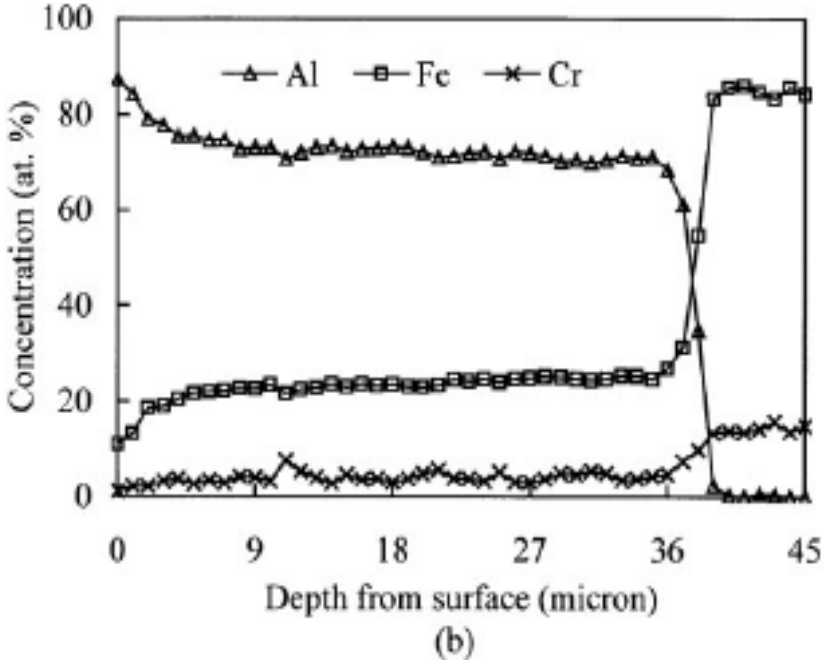

(b)

Figure 6.70 Cross-sectional SEM image and depth profiles of major elements in the coating layer formed at 650° C for 8 hours in a pack of $6\,wt\%\,Al, 2\,wt\%\,Al_2Cl_3$ and $94\,wt\%\,Al_2O_3$

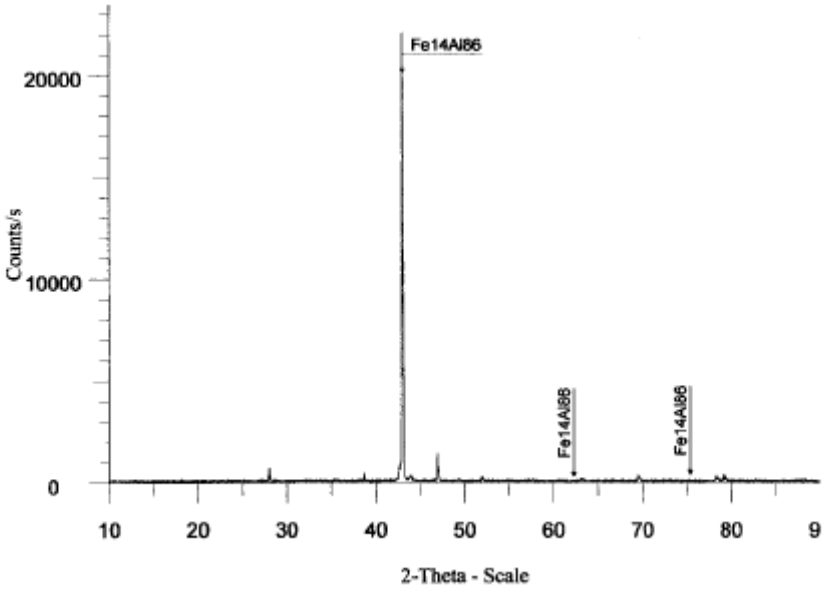

Figure 6.71 XRD pattern measured from the as-coated surface

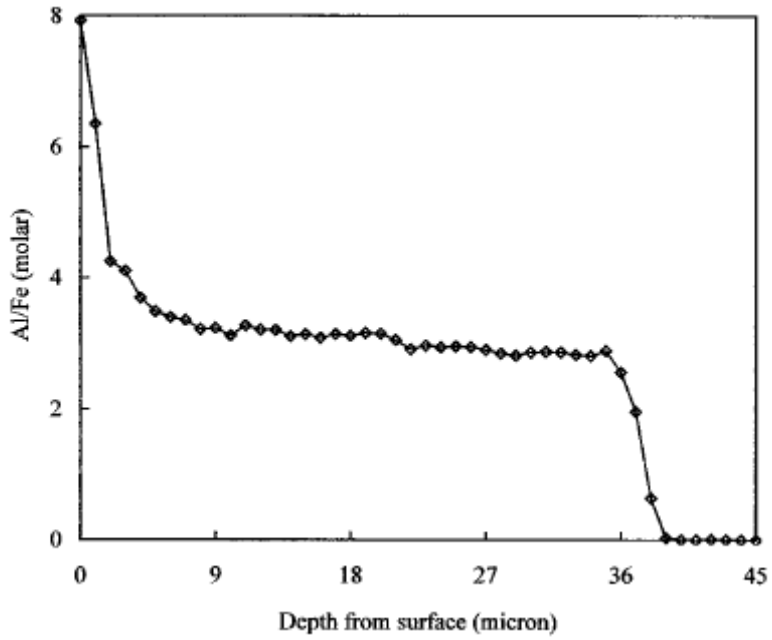

Figure 6.72 Molar ratio of Al/Fe in the coating layer

6.7.2. Effect of Pack *Al* Content

The effect of pack Al content on the coating growth was studied by changing Al content from $(1.4-6\,wt\%)$ while fixing the pack $AlCl_3$ content at $2\,wt\%$. The specimens were all coated at 650°C for 8 hours. The Al depth profiles of the coatings

given in Figure 6.73 show the coating thickness increasing with pack Al content. The Al concentrations at the coating surface and at equivalent depths within the coating layer stayed unaffected by the pack Al content. The main phase as determined by XRD in the surface layer of all the coatings was $Fe_{14}Al_{86}$. EDS data also confirms this. The Al concentration at depths greater than $8\,\mu m$ was constant and the molar ratio of Al/Fe at these depths was close to 3, indicating a $FeAl_3$ phase in the inner layer of all the coatings. The Al concentration fell rapidly to effectively zero at the coating/substrate interface, demonstrating that the coatings were all formed using the same reactive diffusion mechanism. Certainly, the microstructure of all the coatings showed essentially the same features as in Figure 6.70 (a). Figure 6.74 shows the growth kinetics. Figure 6.74 realistically demonstrates that the coating thickness increased progressively from approximately $(19\,\mu m)$ to about $(39\,\mu m)$ as the pack Al content was increased from $(1.4-6\,wt\%)$. It can consequently be concluded that the coating growth rate increased with the pack Al content in the range studied.

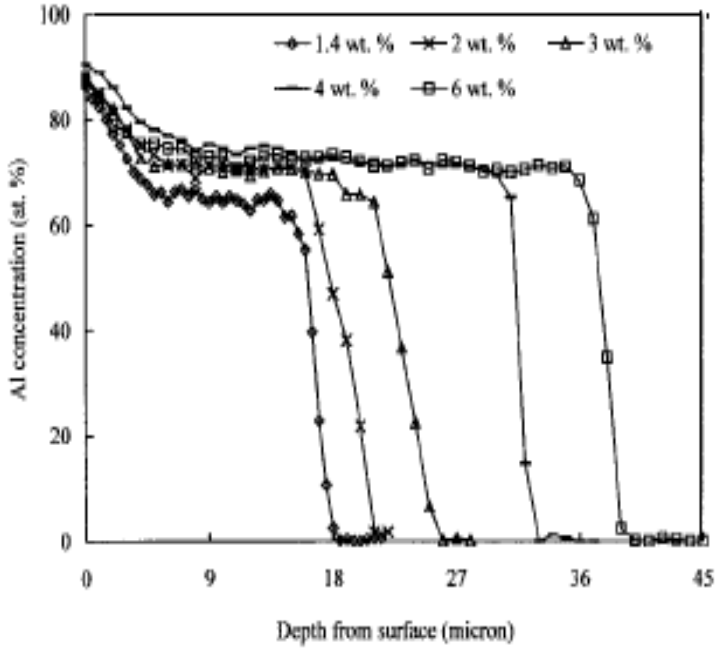

Figure 6.73 Effect of pack Al content on the Al depth profile (deposition condition: 650^{o}C, 8 hours)[76,77]

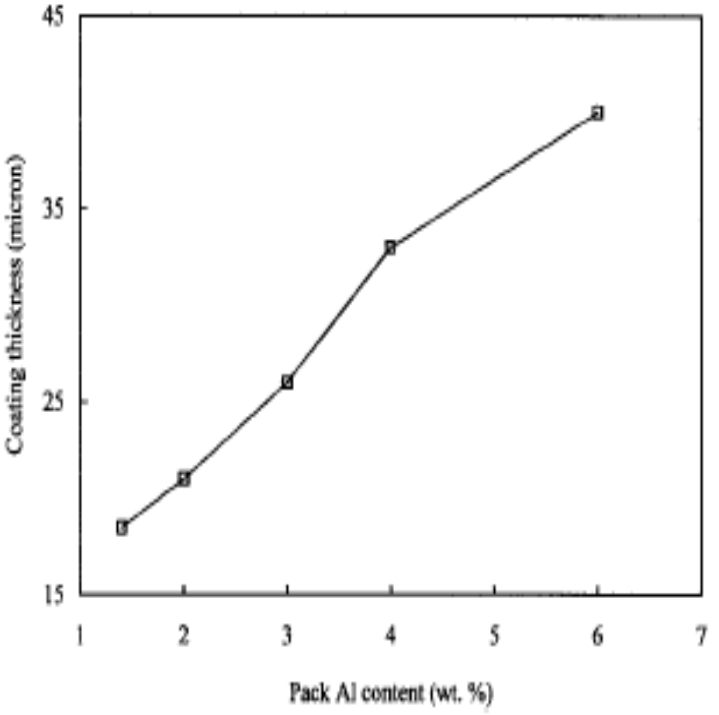

Figure 6.74 Effect of pack Al content on coating thickness with a deposition condition of 650^{o}C, 8 hours

6.7.3. The Effect of Heat Treatments Applied and their Effects and Observed Diffusional Processes Involved: Microstructural Description of the Diffusion Processes Involved

The coatings formed under the deposition conditions, at 650°C on the $9Cr-1Mo$ alloy steel using $AlCl_3$ as an activator and elemental Al powder, used in this study consisted of an outer $Fe_{14}Al_{86}$ phase layer and an inner $FeAl_3$ phase layer. These phases are brittle [82]. To improve the ductility, a series of heat treatment experiments were applied to the coatings for changing $Fe_{14}Al_{86}$ and $FeAl_3$ phases through solid-state diffusion to the ductile $FeAl$ phase at 650°C under an argon atmosphere. The specimen studied had an initial coating thickness of $\sim 33\mu m$. The specimen was taken out of the diffusion furnace and a portion of the specimen analysed periodically. Figures 6.75 (a) and 6.75 (b) present respectively Al and Fe depth profiles in the coating layer at dissimilar diffusion intervals. Figures 6.76 (a – h) illustrate the corresponding cross-sectional SEM images. Figure 6.77 plots the coating thickness, (which measures the thickness of all the phase layers including the diffusion zone) against diffusion time. These results show the change of $Fe_{14}Al_{86}$ and $FeAl_3$ to $FeAl$. However, this process at 650°C, required 1132 hours in total for an initial coating layer thickness of $33\mu m$ to develop. From the results presented in Figures 6.75 – 6.77, it can be assumed that the overall change process was influenced by two different diffusion mechanisms dominating during two different stages.

The following observations were made:

- After 26 hours the $FeAl_3$ layer became thinner shown in Figures 6.75 a and 6.76 (a-c);

- The coating thickness decreased slightly with diffusion time;
- There was a formation of $FeAl$ and a diffusion zone between $FeAl_3$ layer and substrate;
- The appearance of Kirkendall voids at the interface between $FeAl$ and diffusion zone (Figure 6.76 (a-c));
- There was outward diffusion of *Fe*;
- At about 122 hours of diffusion the thickness of $FeAl$ and diffusion started to increase and the thickness of $FeAl_3$ stated to decrease;
- There was increase in coating thickness indicating inward diffusion of *Al* as the main diffusion mechanism;
- At about 554 hours, the Kirkendall voids were eliminated and coating thickness increased to 46 μm (Figures 6.76 (f) and 6.72);
- At about 1132 hours $FeAl_3$ completely changed to $FeAl$ and a diffusion zone formed below $FeAl$ layer as shown in Figure 6.76 (h)
- The coating thickness increased from $33\mu m$ to $48\mu m$;
- After 1132 hours (shown in Figure 6.75 (b)) Fe concentration remained at 50 at% showing a $FeAl$ phase (confirmed by XRD).

These systems have allowed us to obtain information on the microstructural description of the diffusion processes involved. The numerical modelling of the diffusion processes (discussed in chapter seven) has allowed an insight into the coating processes used. The Gas method technique has been used to optimise the diffusion coefficients for Al and Fe when the diagonal terms in the diffusion matrix were constant and also the whole diffusion matrix was constant and variable (see section 6.6).

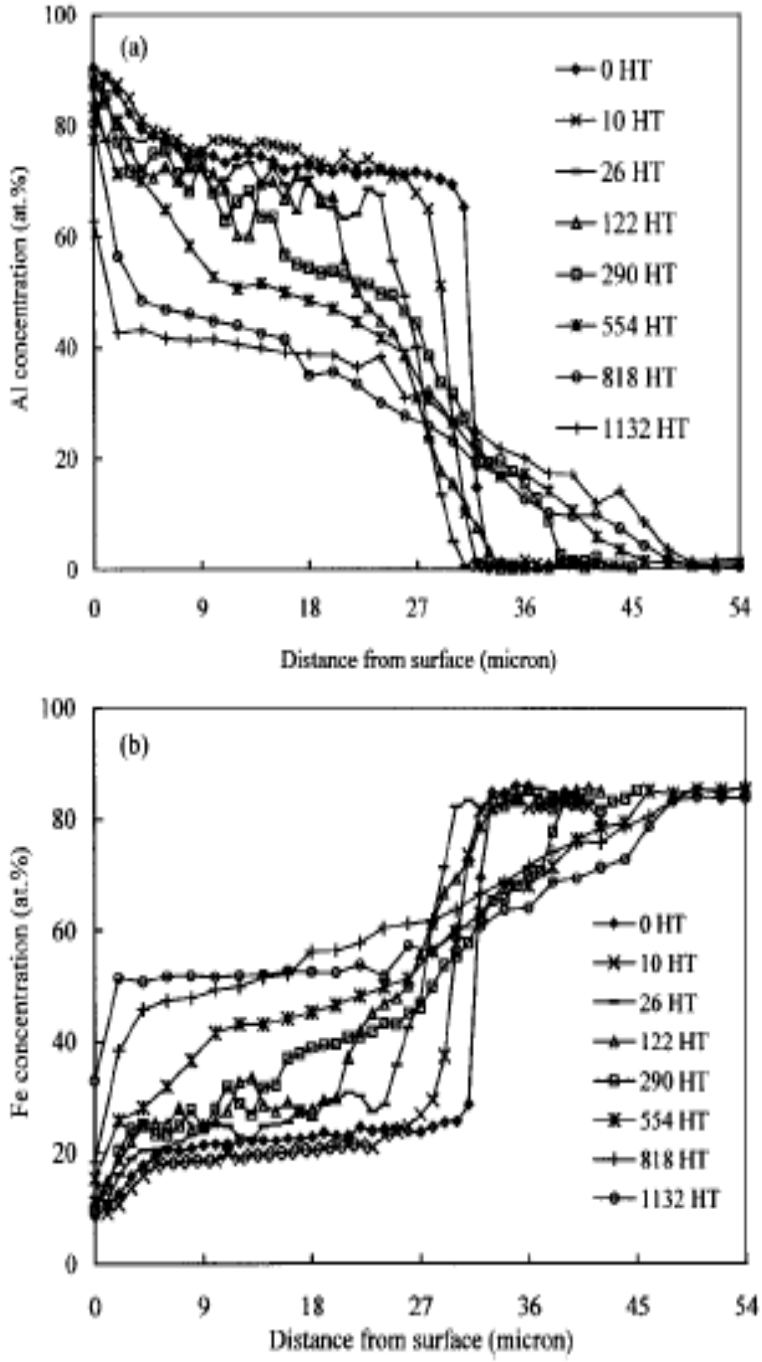

Figure 6.75 Depth profiles of Al and Fe in the coating layer at different diffusion intervals [76, 77]

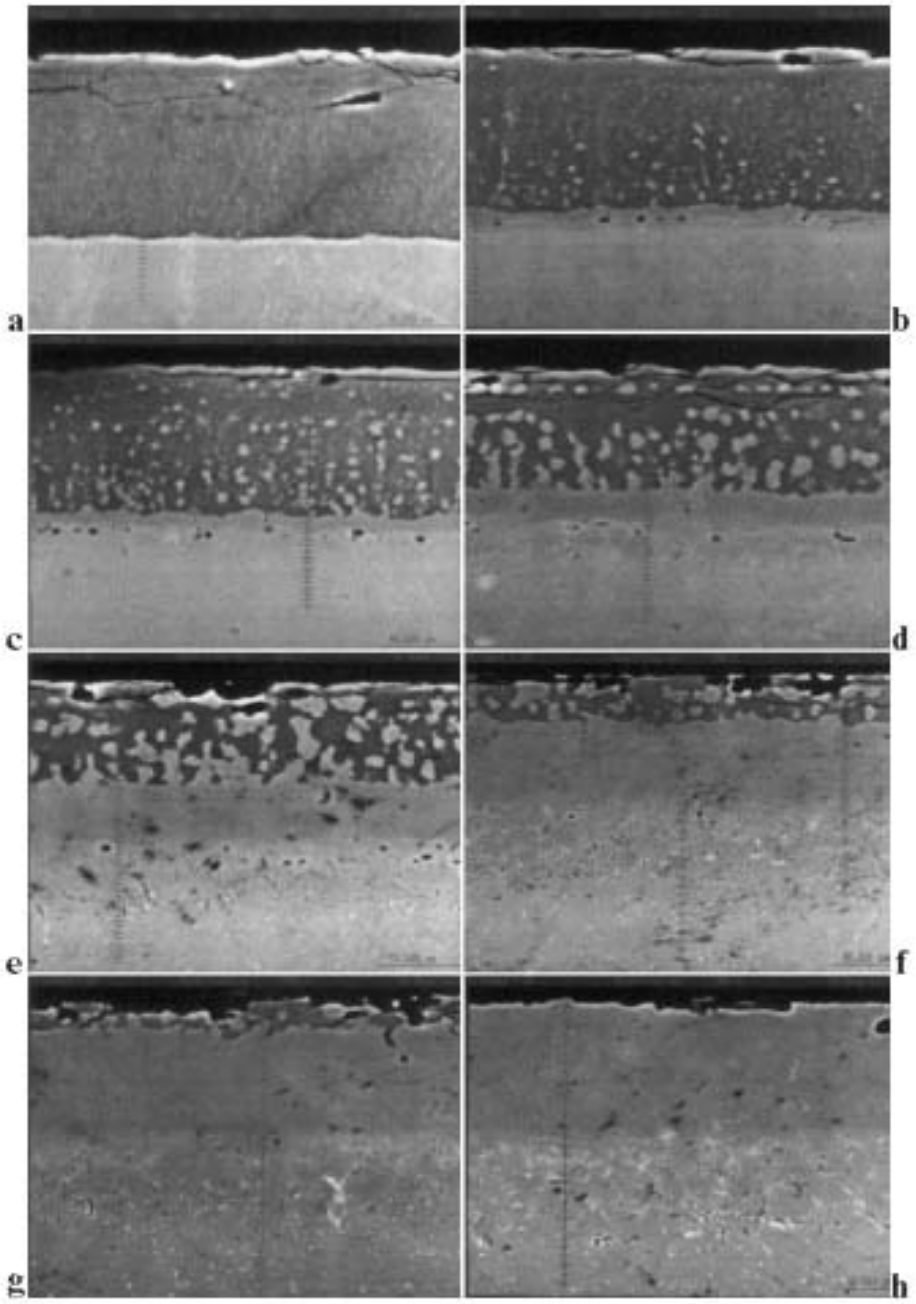

Figure 6.76 Cross-sectional SEM images at different diffusion intervals, a) as-coated; b) 10 hours; c) 26 hours; d) 122 hours; e) 290 hours; f) 554 hours; g) 818 hours; h) 1132 hours [76, 77]

This section reports and discusses the numerical work carried out in determining the diffusion coefficients and calculating the concentration profiles for aluminise coatings deposited on low alloy steels at 650^{o}C.

As mentioned in chapter 4 the coated samples were subjected to diffusion treatments for various times (10, 26, 122, 290 and 554 hours).

Crucially, modelling was used to optimise the process parameters. Varied deposition parameters were used to produce various coatings with various composition profiles. Numerical modelling was used to ascertain the composition parameters and finally the desired profile and hence appropriate process parameters. The full methodology for numerical modelling has been given in chapter 4, and is summarised as follows.

6.7.4. Numerical Techniques to Determine Diffusion Coefficients using GAs Method with the Numerical Methods

The Genetic Algorithms optimization method was used to calculate the diffusion coefficient of aluminum and iron components (*Al*, *Fe*) of the samples. The diffusion coefficients of each component determined were then used to calculate their numerical concentration. The numerical concentration of each component was calculated by using the numerical method (Rung-Kutta of order four). This numerical method (Rung-Kutta of order four) was applied to Ficks second law:

$$\frac{\partial C}{\partial t} = D\frac{\partial^2 C}{\partial x^2}$$

where D is the diffusion coefficient calculated from Genetic Algorithms optimization method.

Rung-Kutta method of order four can be written as:

$$
\begin{aligned}
&C_{n+1} = \frac{1}{6}\left(k_1 + 2k_2 + 2k_3 + k_4\right), \\
&k_1 = hf\left(x_n, y_n\right), \\
&k_2 = hf\left(x_n + \frac{1}{2}h, y_n + \frac{1}{2}k_1\right), \\
&k_3 = hf\left(x_n + \frac{1}{2}h, y_n + \frac{1}{2}k_2\right), \\
&k_4 = hf\left(x_n + h, y_n + k_3\right).
\end{aligned}
$$

The error between the experimental and numerical concentration was calculated using the least squares approximation:

$$Error = \sum_{i=1}^{n} (E_i - N_i)^2$$

where E_i and Ni are the experimental and numerical concentration profiles for each component respectively.

So Fick's second law for multi-component system can be written as:

$$\frac{\partial C_i}{\partial t} = \sum_{j=1}^{n-1} \tilde{D}_{ij}^{n} \frac{\partial^2 C_j}{\partial x^2}$$

$$\Rightarrow \begin{bmatrix} \frac{\partial C_1}{\partial t} \\ \frac{\partial C_2}{\partial t} \end{bmatrix} = \begin{bmatrix} \tilde{D}_{11}^{3} & \tilde{D}_{12}^{3} \\ \tilde{D}_{21}^{3} & \tilde{D}_{22}^{3} \end{bmatrix} \begin{bmatrix} \frac{\partial C_1}{\partial x^2} \\ \frac{\partial C_2}{\partial x^2} \end{bmatrix}$$

$$
\begin{aligned}
&\frac{\partial C_1}{\partial t} = \tilde{D}_{11}^{3} \frac{\partial^2 C_1}{\partial x^2} + \tilde{D}_{12}^{3} \frac{\partial^2 C_2}{\partial x^2} \\
&\frac{\partial C_2}{\partial t} = \tilde{D}_{21}^{3} \frac{\partial^2 C_1}{\partial x^2} + \tilde{D}_{22}^{3} \frac{\partial^2 C_2}{\partial x^2} \qquad (1 = Al, \quad 2 = Fe, \quad 3 = Cr)
\end{aligned}
\tag{6.55}
$$

Thus the diffusion coefficients matrix can be written as:

$$\begin{bmatrix} D_{11} & D_{12} \\ D_{21} & D_{22} \end{bmatrix}$$

6.7.5. Diffusion Analysis Using Constant Diagonal Diffusion Coefficients and Without the Cross Terms

In this analysis only the diagonal diffusion coefficients were considered, and were assumed to be independent of composition.

The aluminum diffusion coefficient ($0.1001 \times 10^{-11} cm^2/s$) was calculated using Genetic Algorithms method after 10 hours of diffusion treatment. Using this diffusion coefficient the aluminum concentration as shown in Figure 6.77 was then calculated using Runge-Kutta method of order four.

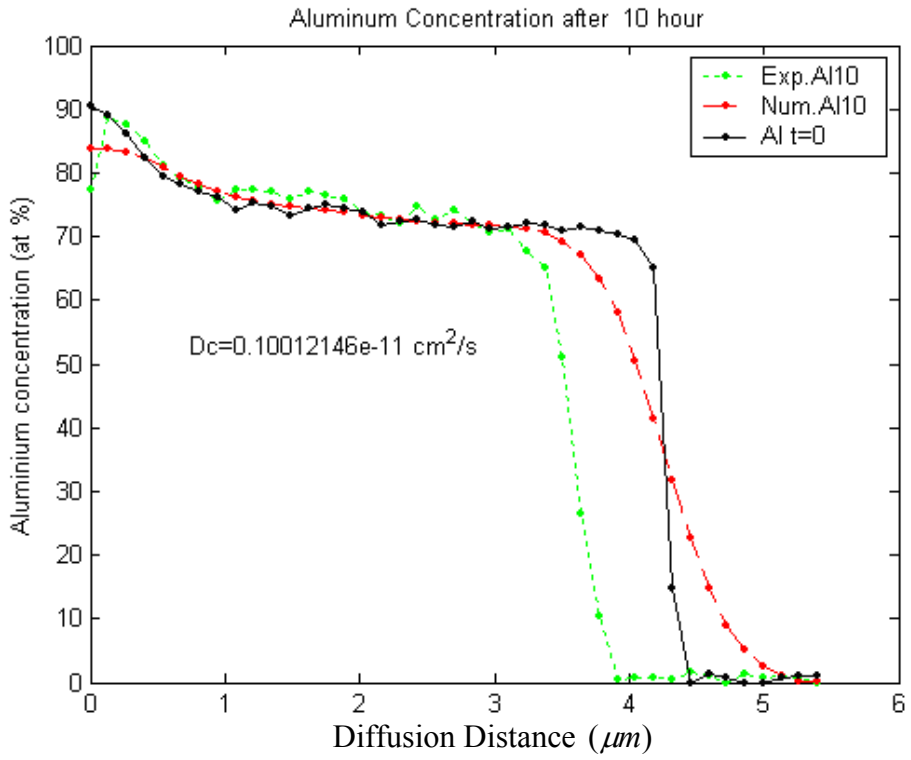

Figure 6.77 Aluminum concentration profiles considering constant diagonal diffusion coefficients after 10 hours diffusion treatment

The experimentally determined concentration profile together with the initial profile (at *t=0*) are also included in this Figure. As shown in the Figure the green concentration profile corresponds to the aluminum experimental concentration after 10 hours diffusion treatment, and the red concentration profile corresponds to the numerical concentration profile of aluminum calculated from the Runge-Kutta method. It is clear that in the range (0- 3.5) μm diffusion distance there is good agreement between the experimental and numerical concentration values of *Al*. However between (3.6-5.5) μm diffusion distance there is some divergence between the experimental and numerical concentration.

In Figure (6.78) the numerical and experimental concentration values for aluminium have been presented after 26 hours diffusion treatment. The aluminum diffusion coefficient calculated from Genetic Algorithms method was ($0.1003x10^{-11} cm^2/s$).

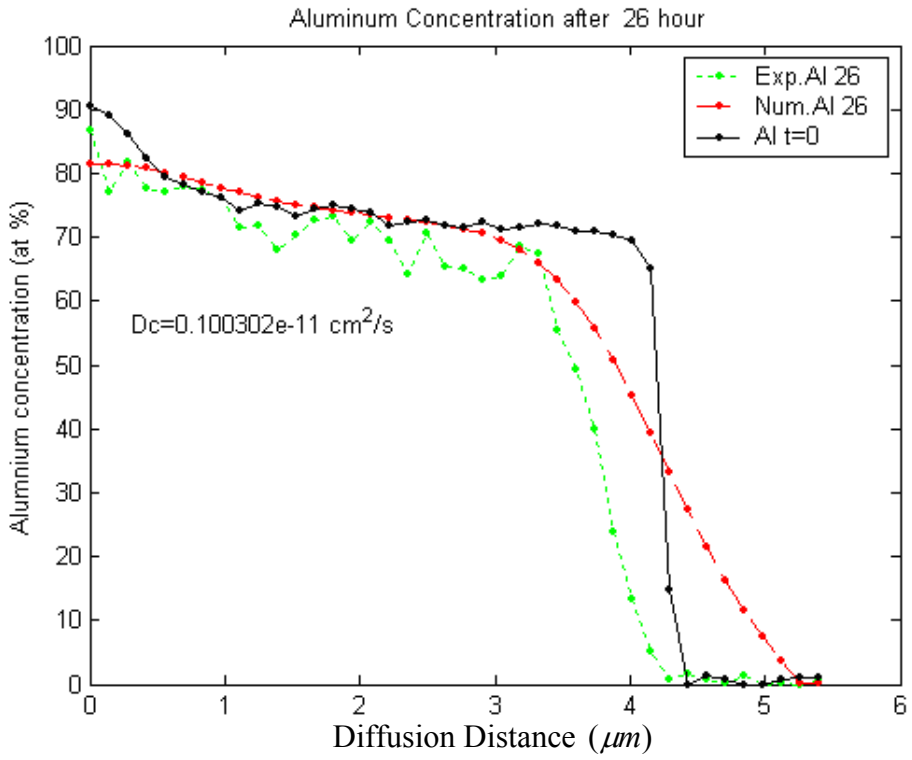

Figure 6.78 Aluminum concentration profiles considering constant diagonal diffusion coefficients after 26 hours diffusion treatment

These results are similar to those in Figure 6.78 at a smaller diffusion distance. There is good agreement followed by disagreement at larger than $4x10^{-3}$cm diffusion distance.

In the following Figures (6.79 - 6.81), the concentration profiles of aluminum have been presented after 122 hours, 290 hours and 554 hours of diffusion treatments.

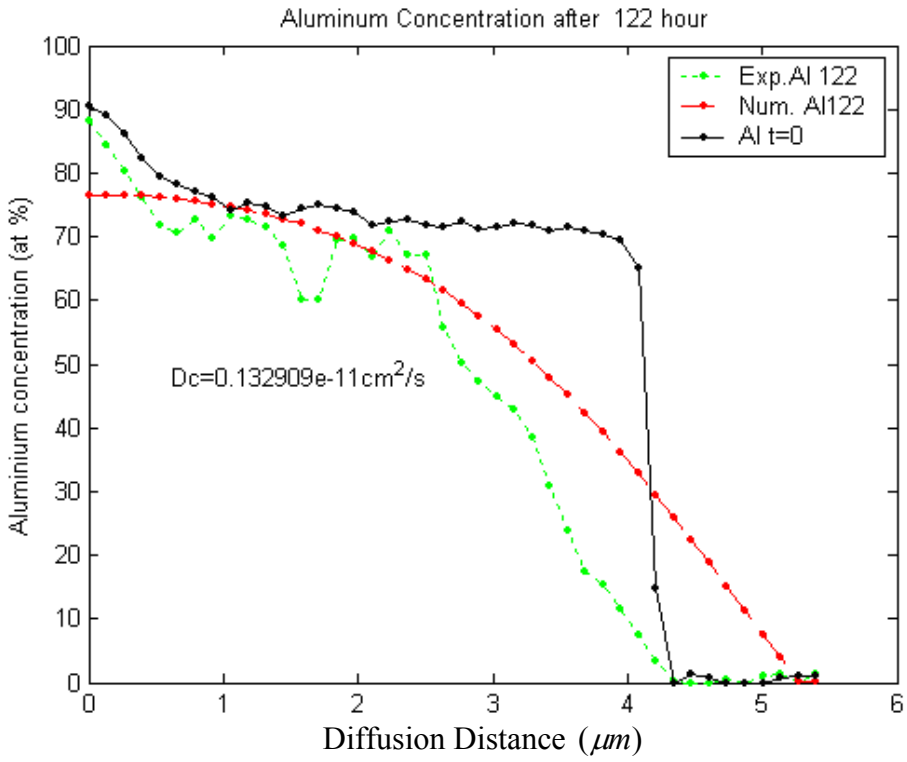

Figure 6.79 Aluminum concentration profiles considering constant diagonal diffusion coefficients after 122 hours diffusion treatment

The diffusion coefficients used at various times were calculated using GAs method:

$D\ (Al) = 0.132 \times 10^{-11}\ cm^2/s$ after 122 hours diffusion treatment

$D\ (Al) = 0.123 \times 10^{-11}\ cm^2/s$ after 290 hours diffusion treatment

$D\ (Al) = 0.130 \times 10^{-11}\ cm^2/s$ after 554 hours diffusion treatment

The initial concentration profile of *Al* used in Figure 6.79 has been taken from the experimental value of concentration at *t=0*. There is good agreement between the numerical concentration and experimental concentration in the range (0-3.0 x 10^{-3}) *cm* diffusion distance and from (3.5 x 10^{-3} to5.0 x 10^{-3}) *cm* diffusion distance the experimental and the numerical concentration profiles diverged.

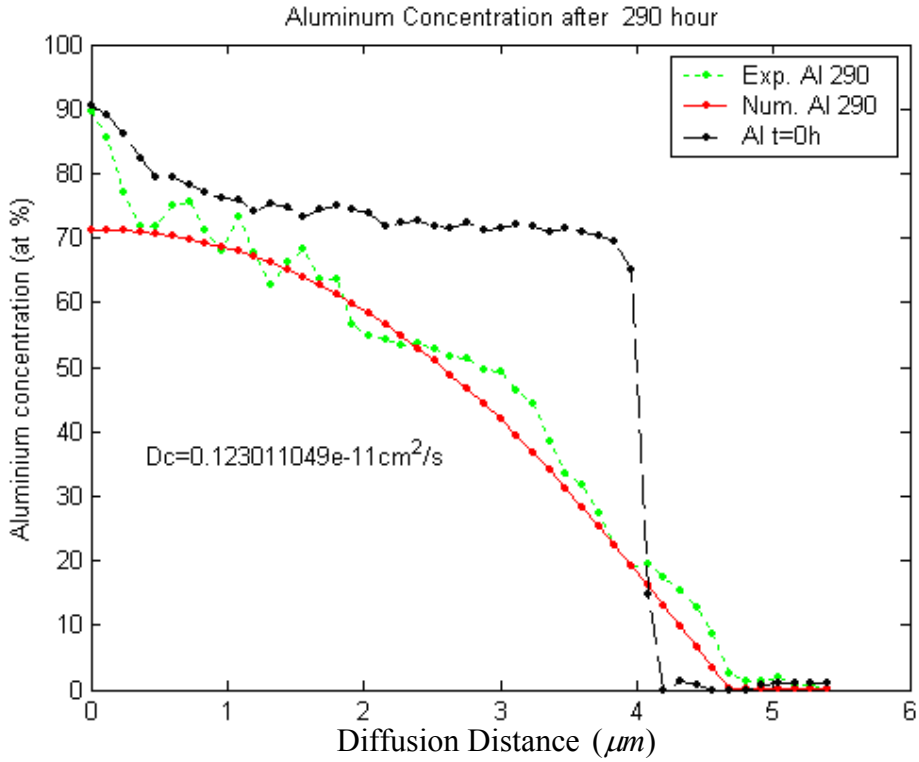

Figure 6.80 Aluminum concentration profiles considering constant diagonal diffusion coefficients after 290 hours diffusion treatment

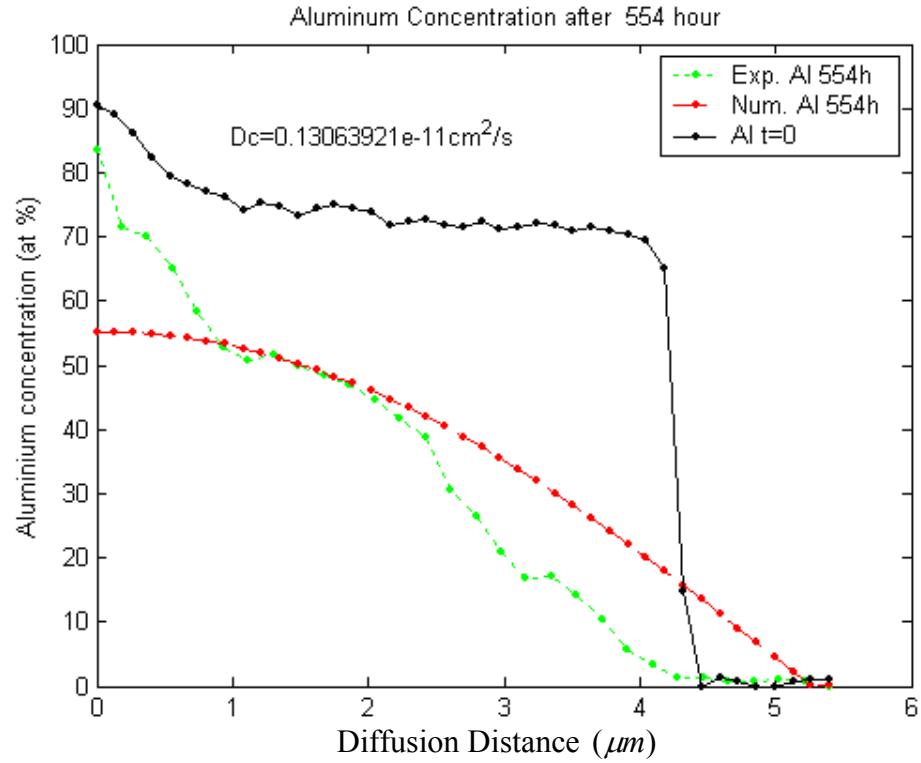

Figure 6.81 Aluminum concentration profiles considering constant diagonal diffusion coefficients after 554 hours diffusion treatment

Again in Figure 6.80 and 6.81 there is good agreement between the aluminum numerical concentration and experimental concentration profiles through the entire range of diffusion distance after 290 hours diffusion treatment.

The following Figure shows the diffusion coefficients with the diffusion time for the aluminum component.

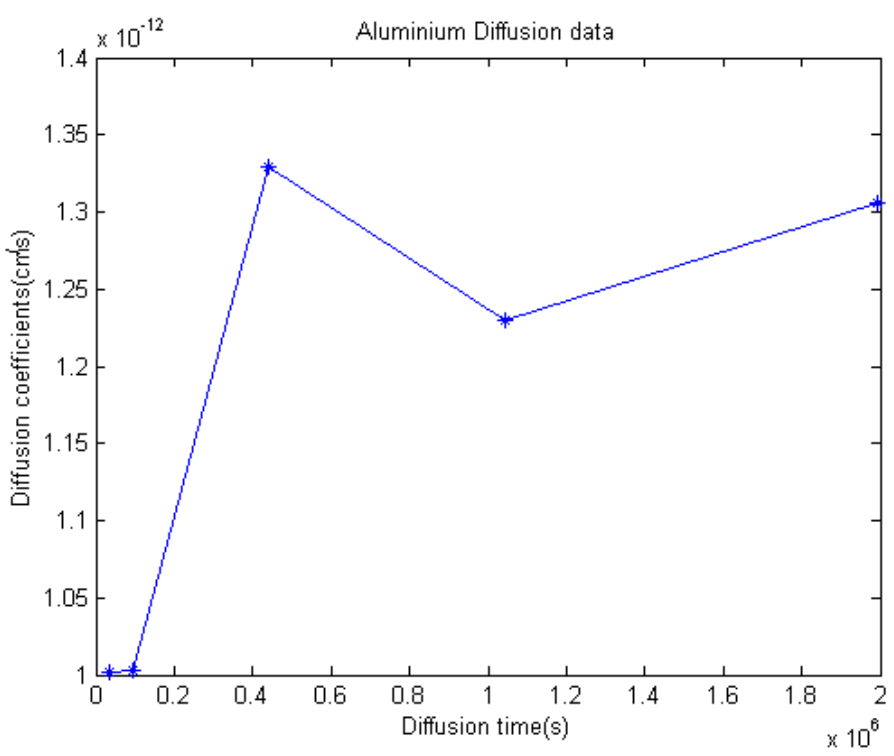

Figure 6.82 Aluminum diffusion coefficients with the diffusion time

Figure 6.82 shows the aluminum diffusion coefficients- (0.10012146, 0.100302, 0.132909, 0.123011049, and 0.13063921) x10^{-11} cm^2/s determined at various times (10, 26, 122, 290, and 554 hours) respectively.

Now applying the procedure used for *Al*, the diffusion coefficients and concentration profiles of *Fe* after 10, 26, and 122 hours of diffusion treatment have been determined.

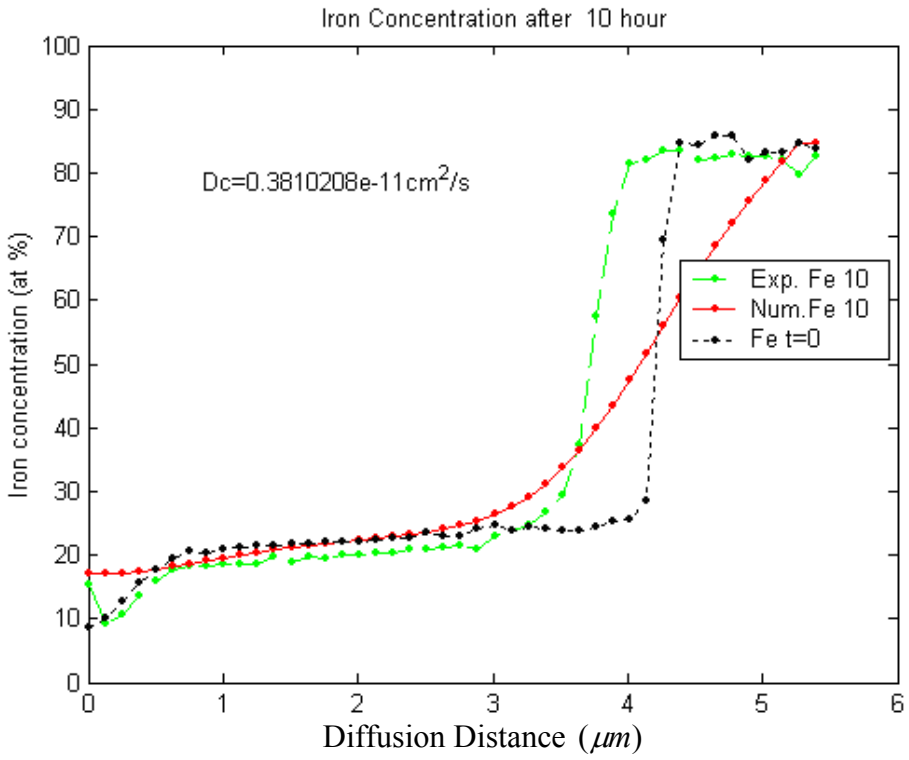

Figure 6.83 Iron concentration profiles considering constant diagonal diffusion coefficients after 10 hours diffusion treatment

Figures (6.83 – 6.85) show the concentration profiles for *Fe* after 10, 26, and 122 hours of diffusion treatments using the following GAs method determined diffusion coefficients:

D (*Fe*) =0.381 x10^{-11} cm^2/s after 10 hours diffusion treatment

D (*Fe*) =0.402x10^{-11} cm^2/s after 26 hours diffusion treatment

D (*Fe*) =0.305 x10^{-11} cm^2/s after 122 hours diffusion treatment

These Figures show that for 10 *h* and 26 *h* diffusion treatments the agreement between the calculated and experimental values did not cover the whole range of diffusion distance. For the case of 122 *h* the calculated and experimental values show an agreement through the entire range of diffusion distance.

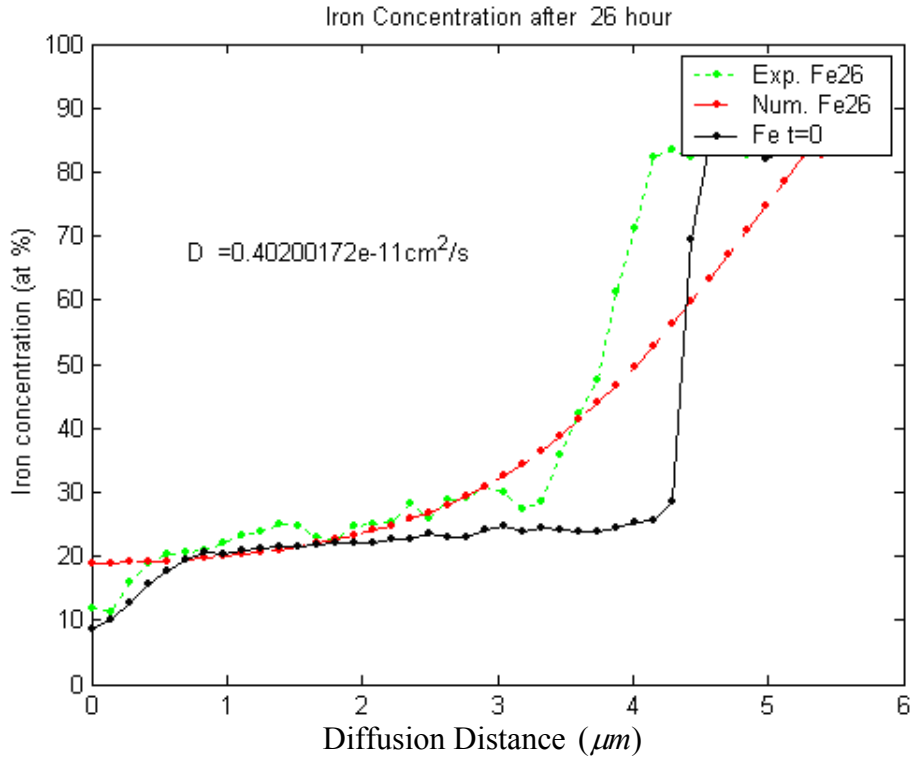

Figure 6.84 Iron concentration Profiles considering constant diagonal diffusion coefficients after 26 hours diffusion treatment

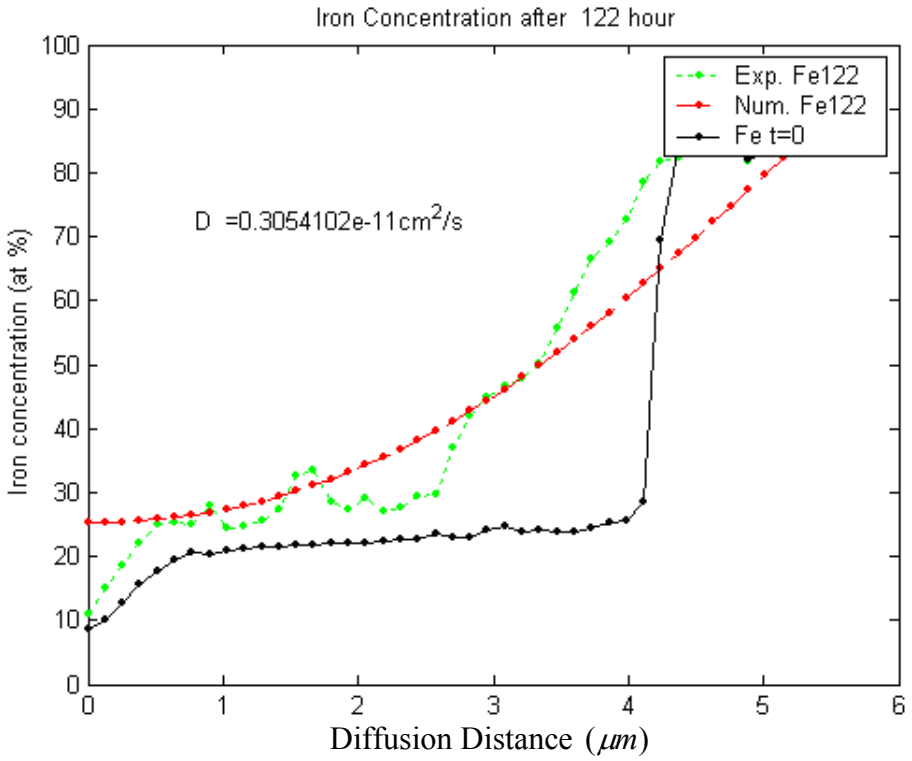

Figure 6.85 Iron concentration profiles considering constant diagonal diffusion coefficients after 122 hours diffusion treatment

In the same way as aluminum in Figure 6.82, the following Figure for iron shows the diffusion coefficients with the diffusion time.

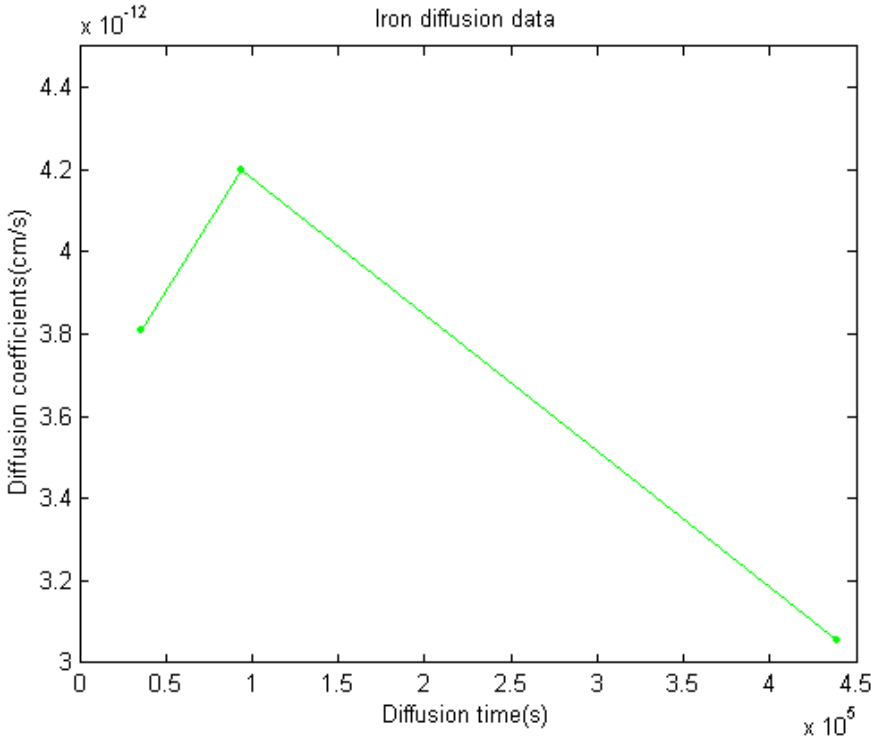

Figure 6.86 Iron diffusion coefficients with the diffusion time

Figure 6.86 shows the iron diffusion coefficients against the diffusion time. The diffusion coefficients for the diffusion time are 10, 26, and 122 hours are (0.3810208, 0.40200172, and 0.3054102) x10^{-11} cm^2/s respectively.

6.7.5.1. Conclusions of Aluminise Coating on low Alloy Steels at 650^{o}C (Constant Diagonal Terms)

The numerical concentration profile for each component (*Al, Fe*) has been calculated considering only the diagonal terms from the diffusion matrix. These numerical concentration profiles have been compared with the experimental data using

Least squares method. There is good agreement between the iron numerical concentration and experimental concentration through the entire range of diffusion distance after 122 hours diffusion treatment. For aluminum component there is good agreement between the numerical concentration and experimental concentration through the entire range of diffusion distance after 122, 290, and 554 hours of diffusion treatment.

6.7.6. Calculation Considering Constant Cross and Diagonal Terms Diffusion Coefficients

Equation 6.56 shows the diagonal and cross terms diffusion coefficients are constants:

$$\Rightarrow \begin{bmatrix} \frac{\partial C_1}{\partial t} \\ \frac{\partial C_2}{\partial t} \end{bmatrix} = \begin{bmatrix} \tilde{D}_{11}^{3} & \tilde{D}_{12}^{3} \\ \tilde{D}_{21}^{3} & \tilde{D}_{22}^{3} \end{bmatrix} \begin{bmatrix} \frac{\partial C_1}{\partial x^2} \\ \frac{\partial C_2}{\partial x^2} \end{bmatrix} \tag{6.56}$$

$$\Rightarrow \frac{\partial C_1}{\partial t} = \tilde{D}_{11}^{3} \frac{\partial^2 C_1}{\partial x^2} + \tilde{D}_{12}^{3} \frac{\partial^2 C_2}{\partial x^2}$$

$$\frac{\partial C_2}{\partial t} = \tilde{D}_{21}^{3} \frac{\partial^2 C_1}{\partial x^2} + \tilde{D}_{22}^{3} \frac{\partial^2 C_2}{\partial x^2} \tag{6.57}$$

So the diffusion matrix is:

$$\begin{bmatrix} D_{11} & D_{12} \\ D_{21} & D_{22} \end{bmatrix}$$

In this matrix the diagonal and cross terms have been considered to be constant.

In Figure 6.87 the experimental and numerical concentration for the components (aluminum and iron), have been presented with the interdiffusion coefficients calculated from Genetic Algorithms method and using equation 6.56, Fick's second law. That is to say the cross terms have been taken into account.

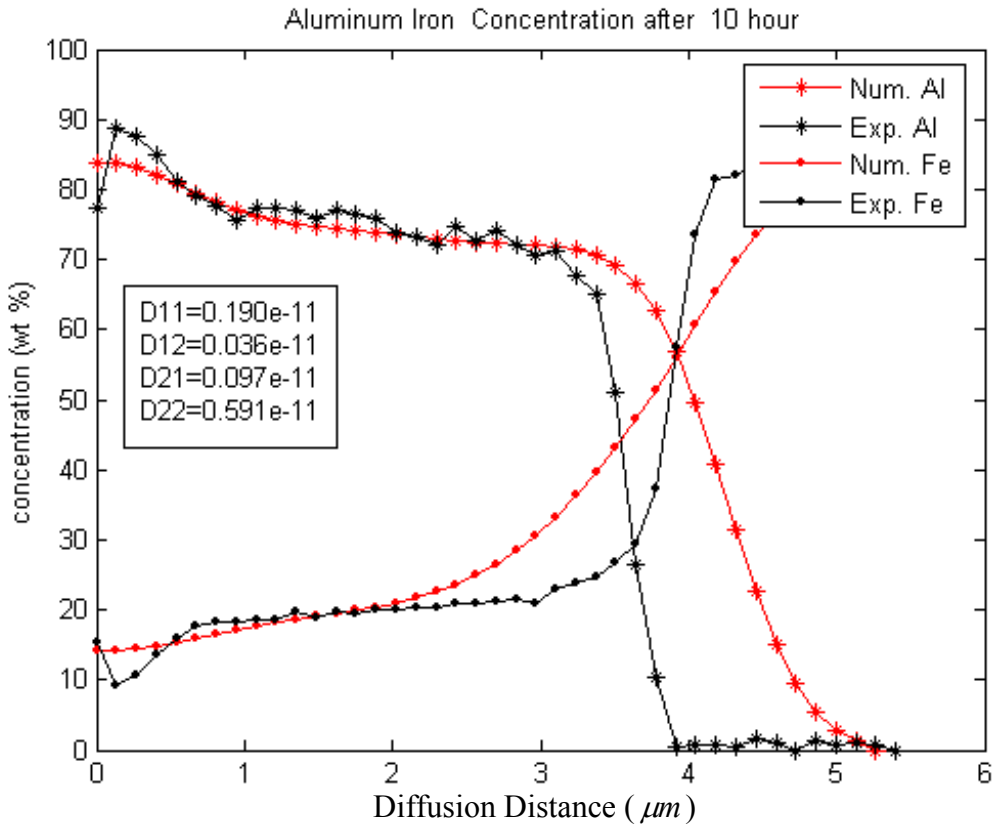

Figure 6.87 Aluminum and iron concentration profiles considering constant diagonal and cross terms diffusion coefficients after 10 hours diffusion treatments

Figure 6.87 shows iron and aluminum concentration (numerical and experimental) using constant diffusion coefficients $D_{11}, D_{12}, D_{21}, D_{22}$ determined from Genetic Algorithms optimization method:

$$D_{11} = 0.190 \times 10^{-11} cm^2 / s$$
$$D_{12} = 0.036 \times 10^{-11} cm^2 / s$$
$$D_{21} = 0.097 \times 10^{-11} cm^2 / s$$
$$D_{22} = 0.591 \times 10^{-11} cm^2 / s$$

Reasonable agreement between the experimental and numerical concentration for iron component is shown. For the aluminum component, the divergence between the experimental and numerical concentration occurs after the diffusion distance of 4 μm. The experimental concentration profile shows a sharp fall – this can not be produced by numerical method; the numerical concentration profile shows gradual change. The other reason for the divergence beyond 4 μm diffusion distance is probably due to the fact that the coefficients in the diffusion matrix have been considered constant. In the following Figure the numerical and experimental concentration profiles for Al and Fe have been presented after 26 hours.

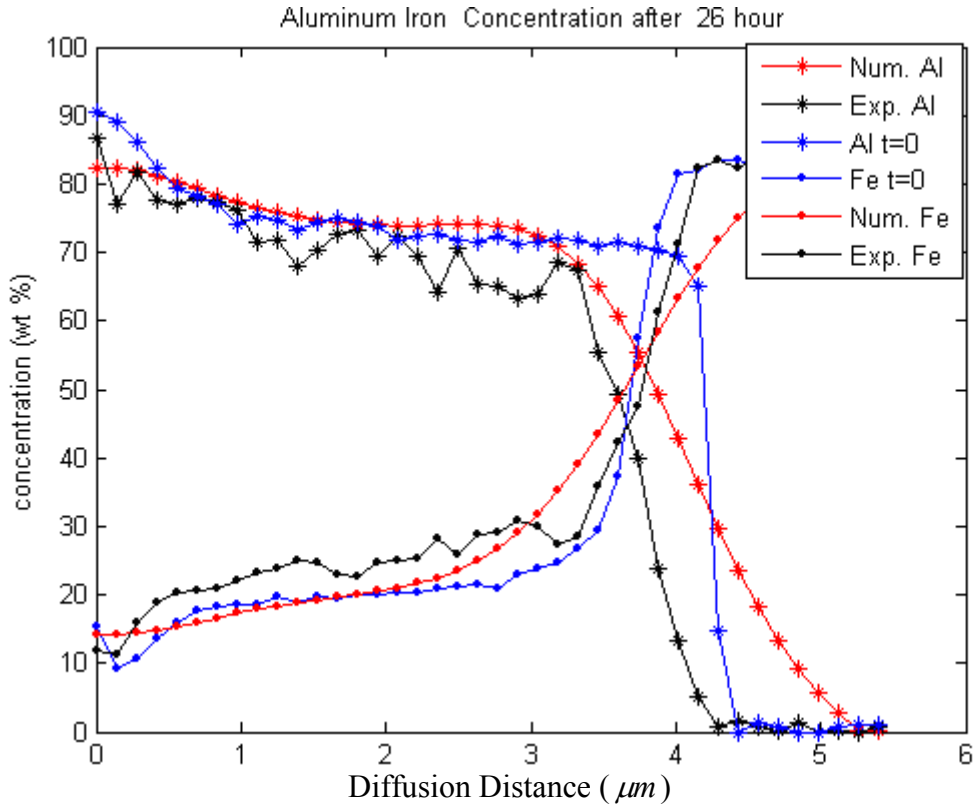

Figure 6.88 Aluminum and iron concentration profiles considering constant diagonal and cross terms diffusion coefficients after 26 hours diffusion treatments

Figure 6.88 shows experimental and numerical concentration profiles for the components iron and aluminum after 26 hours. This Figure includes the initial concentration profile at *t=0* from the experimental value. The diffusion coefficients considered to be constant (concentration independent). Genetic Algorithms optimization method has been used to calculate these coefficients D_{11}, D_{12}, D_{21}, D_{22} :

$$D_{11} = 0.110 \times 10^{-11} cm^2 / s$$
$$D_{12} = 0.056 \times 10^{-11} cm^2 / s$$
$$D_{21} = 0.012 \times 10^{-11} cm^2 / s$$
$$D_{22} = 0.110 \times 10^{-11} cm^2 / s$$

This Figure shows deviation between the numerical and experimental concentration profile after 26 hours for the diffusion distances (3.5-5.0) μm for the aluminum component. There is good agreement between the iron numerical and experimental concentration profiles through the entire range of diffusion distance. Figure 6.89 described the numerical and experimental concentration profiles for Al and Fe after 122 hours.

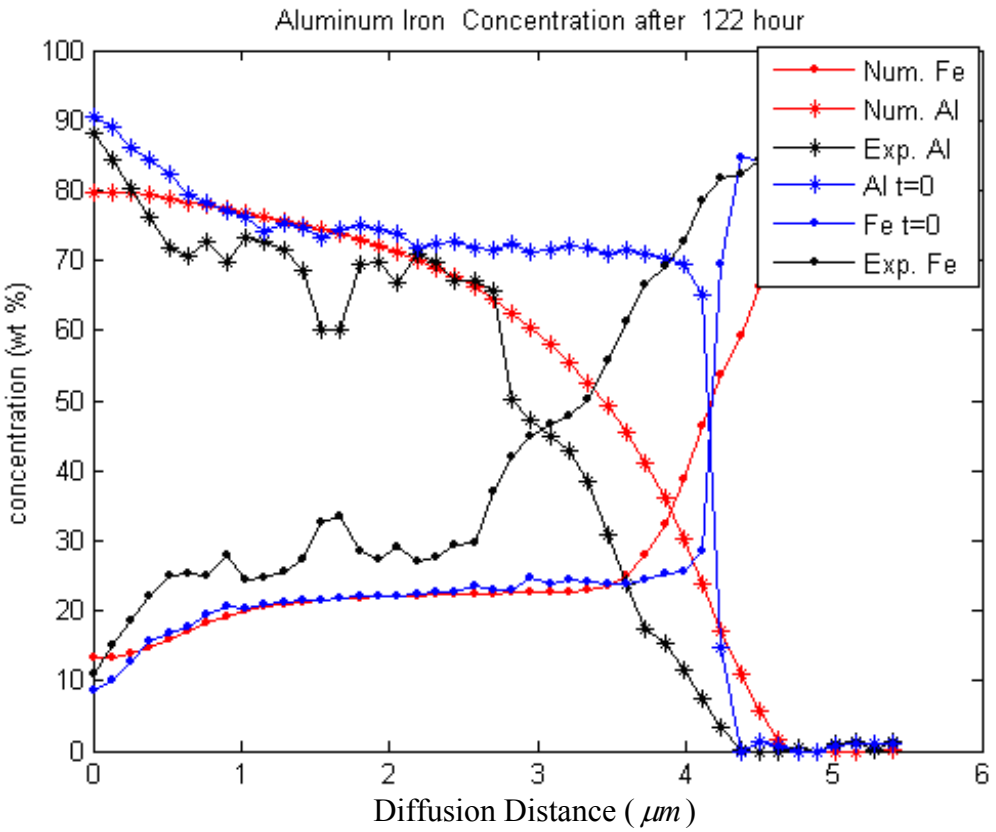

Figure 6.89 Aluminum and iron concentration profiles considering constant diagonal and cross terms diffusion coefficients after 122 hours diffusion treatments

Similar to Figure 6.89 the diffusion coefficients were considered to be constant (concentration independent) after 122 hours diffusion treatment. Genetic Algorithms optimization method has been used to calculate these diffusion coefficients D_{11}, D_{12}, D_{21}, D_{22}:

$$D_{11} = 0.102 \times 10^{-11} cm^2 / s$$
$$D_{12} = 0.024 \times 10^{-11} cm^2 / s$$
$$D_{21} = 0.010 \times 10^{-11} cm^2 / s$$
$$D_{22} = 0.010 \times 10^{-11} cm^2 / s$$

Good agreement has been found between the aluminum experimental and numerical concentration after 122 hours diffusion treatment. For the iron component, the

divergence between the experimental and numerical concentration occurs after the diffusion distance of ($2.9\ \mu m$).

6.7.6.1. Conclusions Considering Constant Cross and Diagonal Terms Diffusion Coefficients

Fick's second law has been used to find the concentration profile for each component (*Al, Fe*) using Rung-Kutta method of order four. The Genetic Algorithms method permits optimization of the values of diffusion coefficients, in the diffusion matrix. The calculated concentration profiles have been compared with the experimental data using Least squares method. There is good agreement between the iron numerical concentration and experimental concentration through the entire range of diffusion distance after 26 hours. While for the aluminum component there is good agreement between the numerical concentration and experimental concentration through the entire range of diffusion distance after 122 hours.

6.7.7. Calculation Considering Variable Cross and Diagonal Terms Diffusion Coefficients

In the earlier sections the diffusion coefficients (diagonal and cross terms) for the both components (*Al, Fe*) were considered to be constant. In this section the diffusion coefficients are considered to be concentration dependent (a function of concentration). First order polynomial has been used for concentration dependence diffusion coefficients for the iron and aluminum (Figure 6.90).

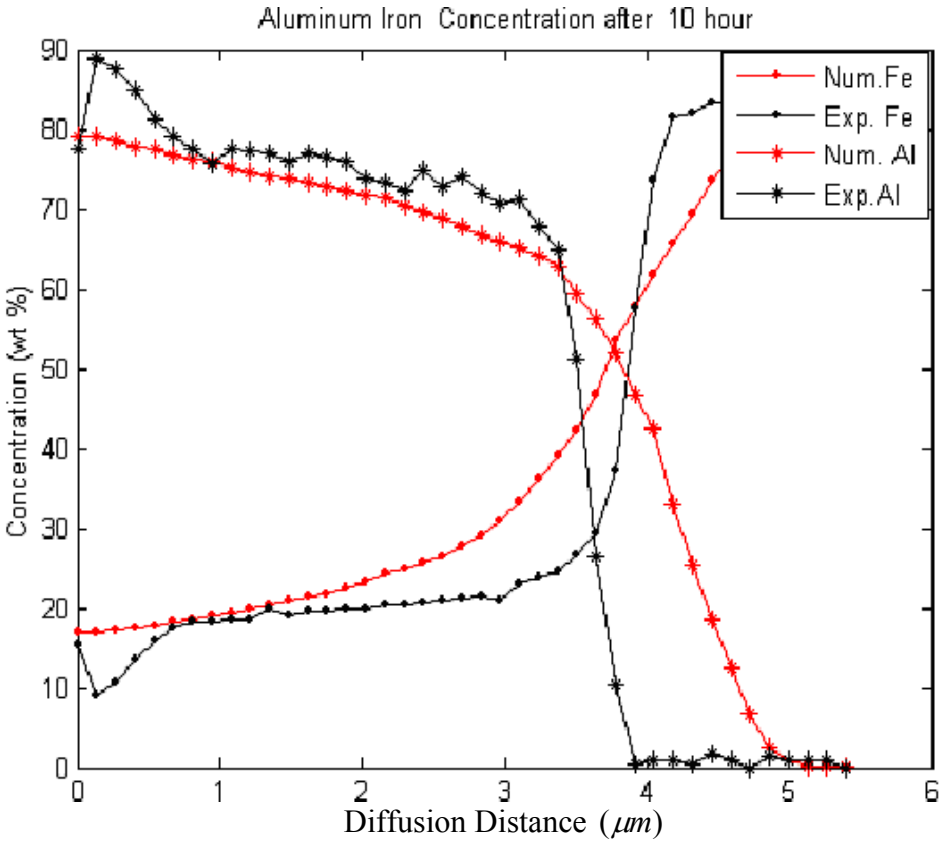

Figure 6.90 Aluminum and iron concentration profiles considering variable diagonal and cross terms diffusion coefficients after 10 hours diffusion treatment (concentration dependent, first order polynomial)

Figure 6.90 shows the numerical and experimental concentrations for iron and aluminum with concentration dependent diffusion coefficients $D_{11}, D_{12}, D_{21}, D_{22}$ (first order polynomial) after 10 hours diffusion treatment:

$$\begin{aligned} D_{11} &= x_1 + x_2 C_1 \\ D_{12} &= y_1 + y_2 C_1 \\ D_{21} &= z_1 C_2 \\ D_{22} &= v_1 + v_2 C_2 \end{aligned} \tag{6.58}$$

$$D_{11} = 0.318 \times 10^{-11}\ cm^2/s$$
$$D_{12} = 0.017 \times 10^{-11}\ cm^2/s$$
$$D_{21} = 0.009 \times 10^{-11}\ cm^2/s$$
$$D_{22} = 0.043 \times 10^{-11}\ cm^2/s$$

where C_1 and C_2 are the initial concentration profiles for aluminum and iron respectively. $x_1, x_2, y_1, y_2, z_1, v_1, v_2$ are the polynomial coefficients calculated by using Genetic Algorithms optimization method. There is good agreement between the iron numerical and experimental concentration profiles for the entire range of the diffusion distance, while for the aluminum component (Figure 6.90) shows deviation between the numerical and experimental concentration profiles after 26 hours for the diffusion distances for the range (3.8-5.0) μm.

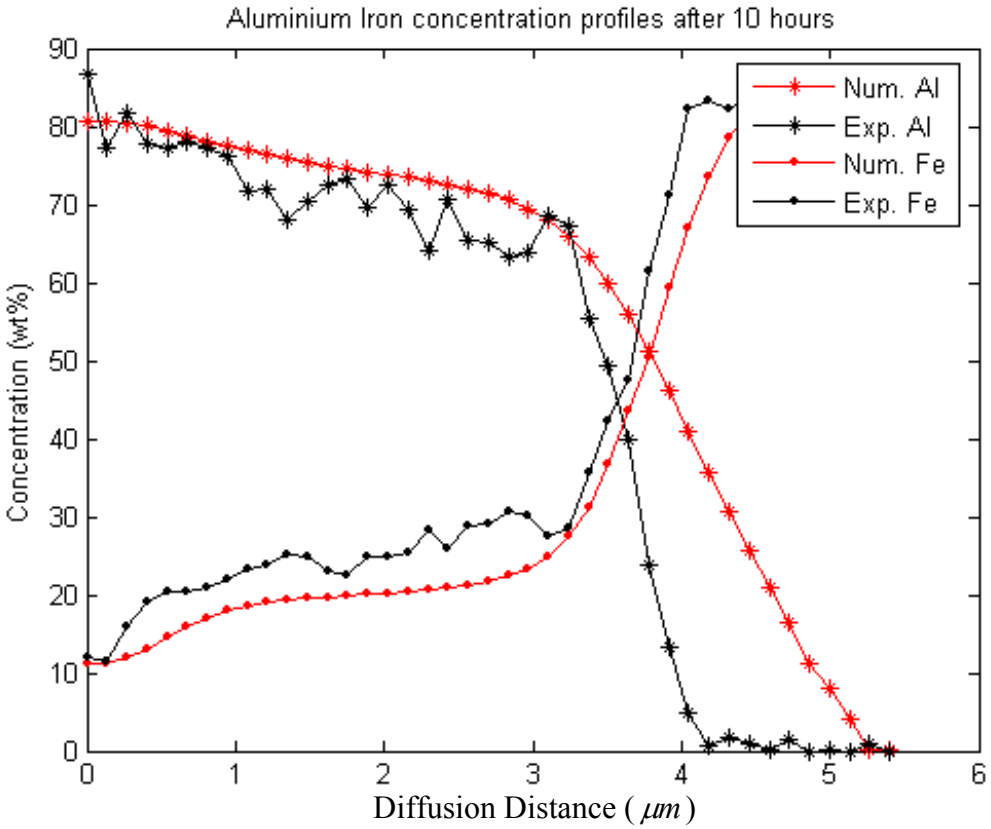

Figure 6.91 Aluminum and iron concentration profiles considering variable diagonal and cross terms diffusion coefficients after 10 hours (second order polynomial)

Figure 6.91 shows the numerical and experimental concentrations profiles for iron and aluminum with concentration dependent diffusion coefficients $D_{11}, D_{12}, D_{21}, D_{22}$ (second order polynomial)

$$\begin{aligned} D_{11} &= x_1 + x_2 C_1 + x_3 C_1^{\,2} \\ D_{12} &= y_1 + y_2 C_1 C_2 + y_3 C_2 \\ D_{21} &= z_1 C_2 + z_2 C_2^{\,2} \\ D_{22} &= v_1 + v_2 C_2 + v_3 C_2^{\,2} \end{aligned} \tag{6.59}$$

$$\begin{aligned} D_{11} &= 0.291 \times 10^{-11}\ cm^2 / s \\ D_{12} &= 0.038 \times 10^{-11}\ cm^2 / s \\ D_{21} &= 0.037 \times 10^{-11}\ cm^2 / s \\ D_{22} &= 0.015 \times 10^{-11}\ cm^2 / s \end{aligned}$$

Where C_1 and C_2 are the initial concentration for aluminum and iron respectively. $x_1, x_2, x_3, \cdots, v_1, v_2, v_3$ are the polynomial coefficients calculated using Genetic Algorithms optimization method. Again there is good agreement in the numerical and experimental concentration values for *Fe* for the entire range of the diffusion distance. For the *Al* component, there is a deviation between the numerical and experimental *Al* concentration for the diffusion distances for the range (3.8-5.0) μm.

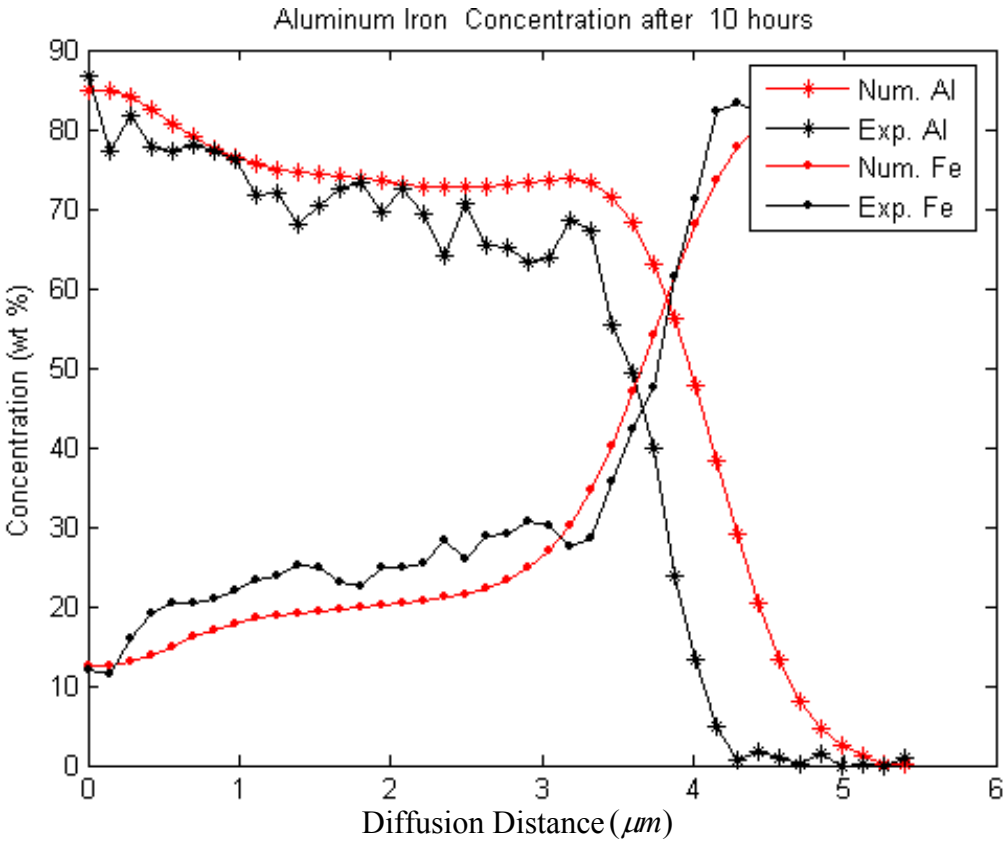

Figure 6.92 Aluminum and iron concentration profiles considering variable diagonal and cross terms diffusion coefficients after 10 hours diffusion treatment (third order polynomial)

Figure 6.92 shows the numerical and experimental concentrations for iron and aluminum with concentration dependent diffusion coefficients $D_{11}, D_{12}, D_{21}, D_{22}$ (third order polynomial):

$$
\begin{aligned}
D_{11} &= x_1 + x_2 C_1 + x_3 C_1^{\,2} + x_4 C_2^{\,3} \\
D_{12} &= y_1 C_2 + y_2 C_1^{\,2} C_2 + y_3 C_1 \\
D_{21} &= z_1 C_1^{\,3} + z_2 C_1^{\,2} \\
D_{22} &= v_1 C_2 \; + v_2 C_2 + v_3 C_2
\end{aligned}
\qquad (6.60)
$$

$$
\begin{aligned}
D_{11} &= 0.2910561 \times 10^{-11}\, cm^2/s \\
D_{12} &= 0.13865 \times 10^{-11}\, cm^2/s \\
D_{21} &= 0.237175 \times 10^{-11}\, cm^2/s \\
D_{22} &= 0.7605034 \times 10^{-11}\, cm^2/s
\end{aligned}
$$

using Genetic Algorithms optimization method. There is an agreement in the numerical and experimental concentration values for *Fe* for the entire range of the diffusion distance, while for *Al* there is good agreement in the numerical and experimental values between (0-3.5) $x10^{-3}$ *cm* diffusion distance, followed by divergence between the numerical and experimental values from $(3.8\ x10^{-3})$ cm diffusion distance.

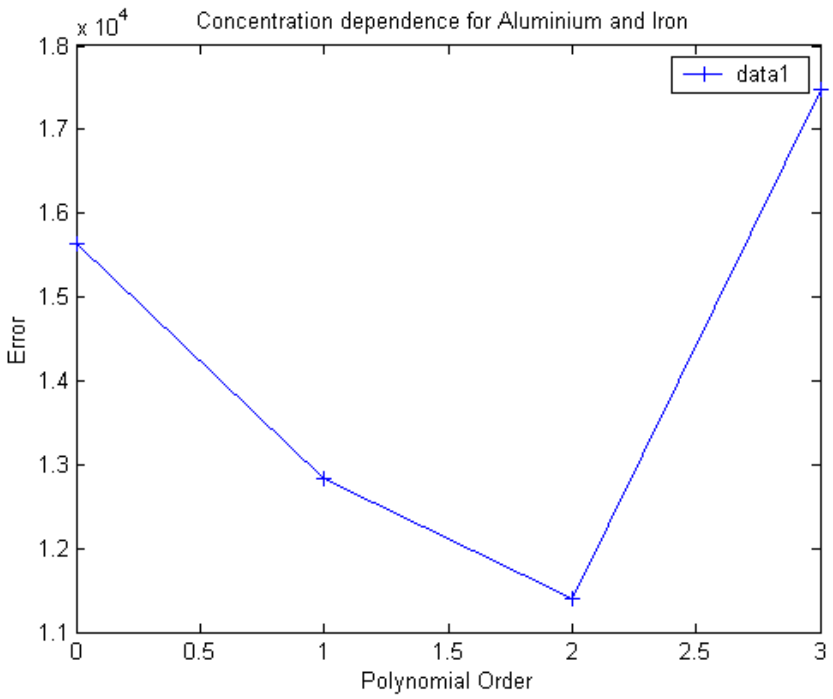

Figure 6.93 Aluminum and iron diffusion coefficient's polynomial order with the absolute error

Figure 6.93 shows the order of the polynomial plotted against the absolute error between the experimental and numerical concentration for the components aluminum and iron. The x-axis corresponds to the order of the polynomial, and the y-axis represents the sum of the absolute error between the experimental and the numerical concentration for the components (*Al, Fe*). The minimum error between the experimental and numerical concentration is (1.1391e+4) when the order of the polynomial is second order (equation 6.59), where 0, 1, 2, and 3 correspond to the constant, first, second, and the third order polynomial respectively.

In the next section another structure of second order polynomial has been applied to calculate the diffusion coefficients for the components (*Al, Fe*).

$$
\begin{aligned}
D_{11} &= x_1 C_2 C_1 + x_2 C_1^{\,2} \\
D_{12} &= y_1 C_1 C_2 + y_2 C_2 \\
D_{21} &= z_1 C_2 C_1 + z_2 C_1^{\,2} \\
D_{22} &= v_1 C_2^{\,2} + v_3 C_2^{\,2}
\end{aligned}
\qquad (6.61)
$$

The coefficients $x_1, x_2, \ldots, v_3$ have been calculated using Genetic Algorithm optimization method.

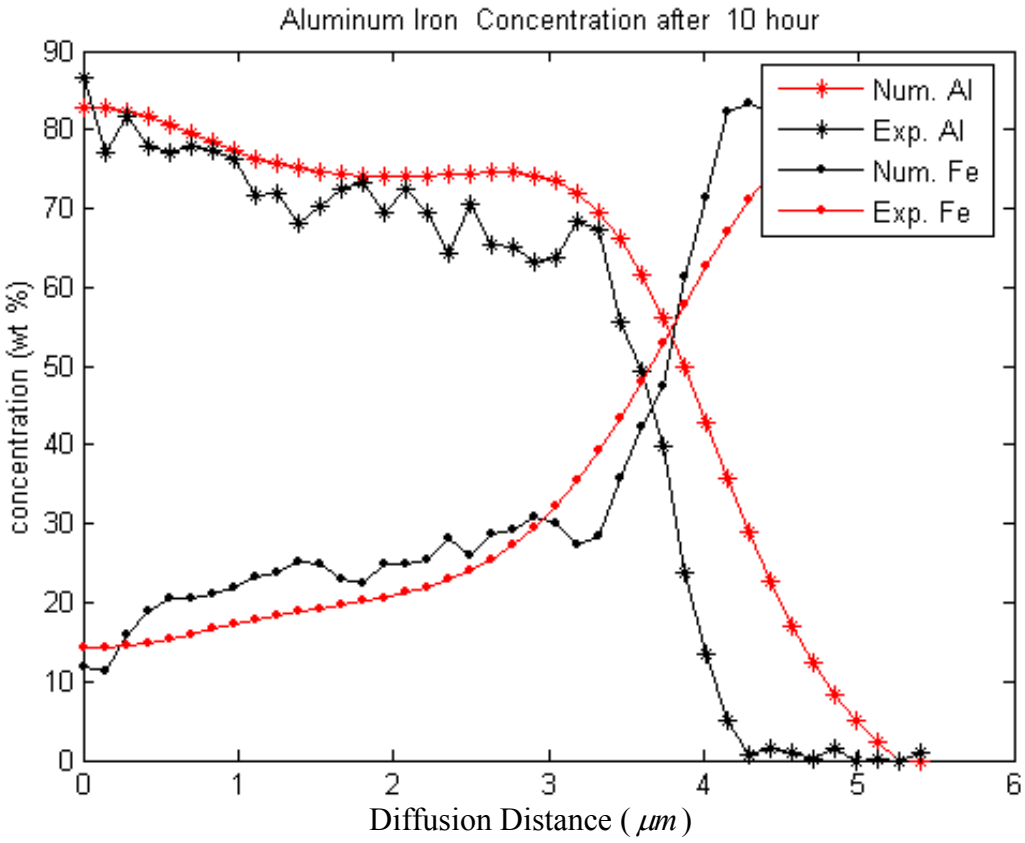

Figure 6.94 Aluminum and iron concentration profiles considering variable diagonal and cross terms diffusion coefficients after 10 hours diffusion treatment (second order polynomial)

Figure 6.94 shows the numerical and experimental concentration profiles values for aluminum and iron after 10 hours. The initial concentrations for (*Al, Fe*) have been taken from the experimental concentration at *t=0*. Genetic Algorithms optimization method was used to optimise the diffusion coefficients $D_{11}, D_{12}, D_{21}, D_{22}$ (equation 6.61). For the entire range of the diffusion distance, there is reasonable agreement between the numerical and experimental concentration profiles for (*Al, Fe*). Figure 6.95 shows the experimental and numerical concentration profiles for both components after 26 hours.

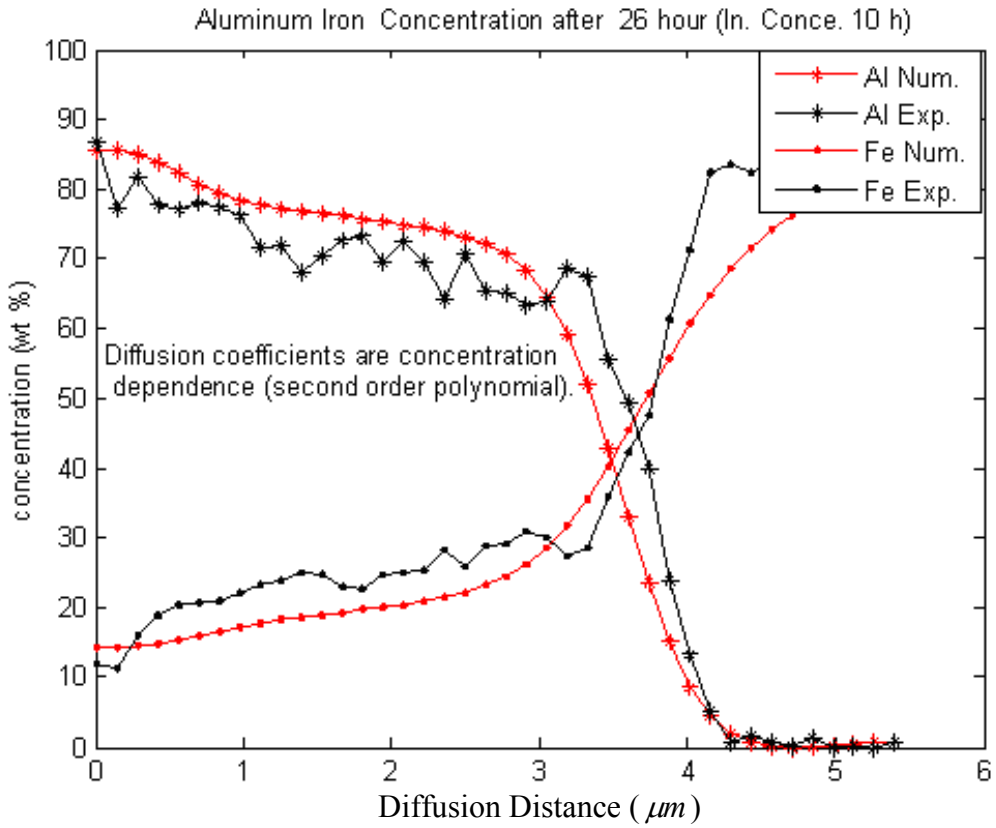

Figure 6.95 Aluminum and iron concentration profiles considering variable diagonal and cross terms diffusion coefficients after 26 hours (second order polynomial)

Figure 6.95 shows the numerical and experimental concentration values for aluminum and iron after 26 hours when the diffusion coefficients are concentration dependent (equation 6.59). Here the initial concentrations for (*Al, Fe*) have been taken from the experimental concentration at *t*=10 hours instead at *t=0*. Again good

agreement between the experimental concentration and numerical concentration for the components (*Al, Fe*), through the entire range of diffusion distance.

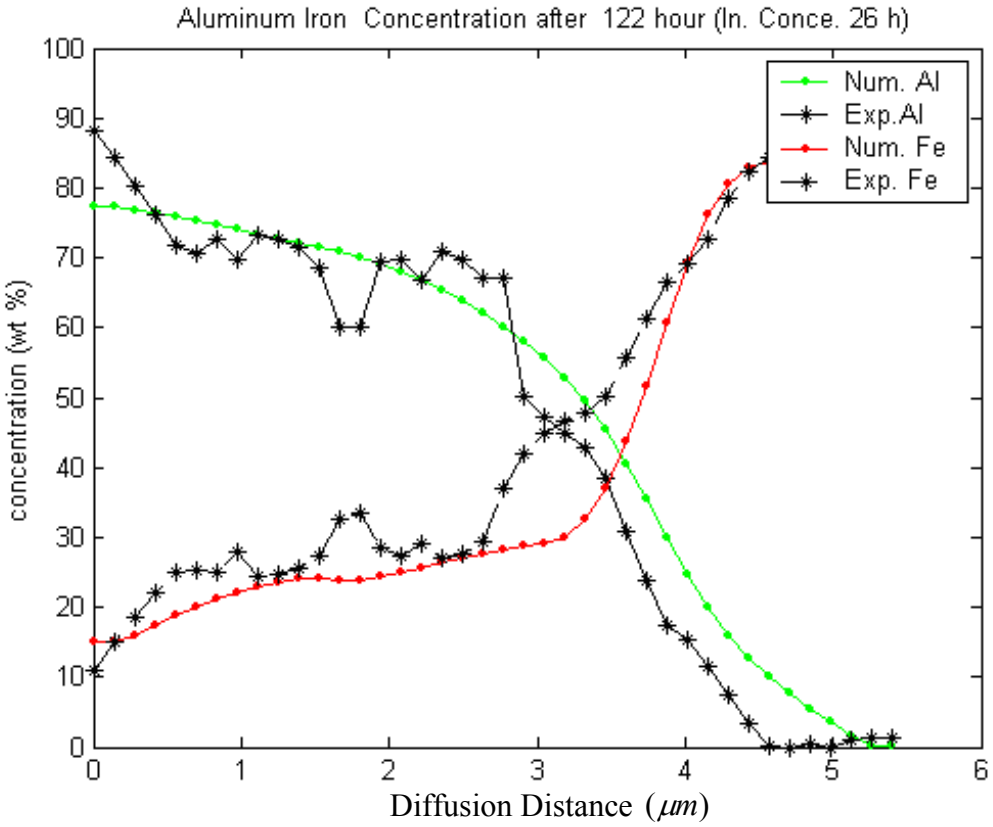

Figure 6.96 Aluminum and iron concentration profiles considering variable diagonal and cross terms diffusion coefficients after 122 hours (second order polynomial)

Figure 6.96 shows the numerical and experimental concentration values for aluminum and iron after 122 hours when the diffusion coefficients are concentration dependent (second order polynomial, equation 6.59). The initial concentrations for (*Al, Fe*) have been taken from the experimental concentration at t=26 hours. There is very good agreement between the experimental concentration and numerical concentration for the components (*Al, Fe*), through the entire range of diffusion distance.

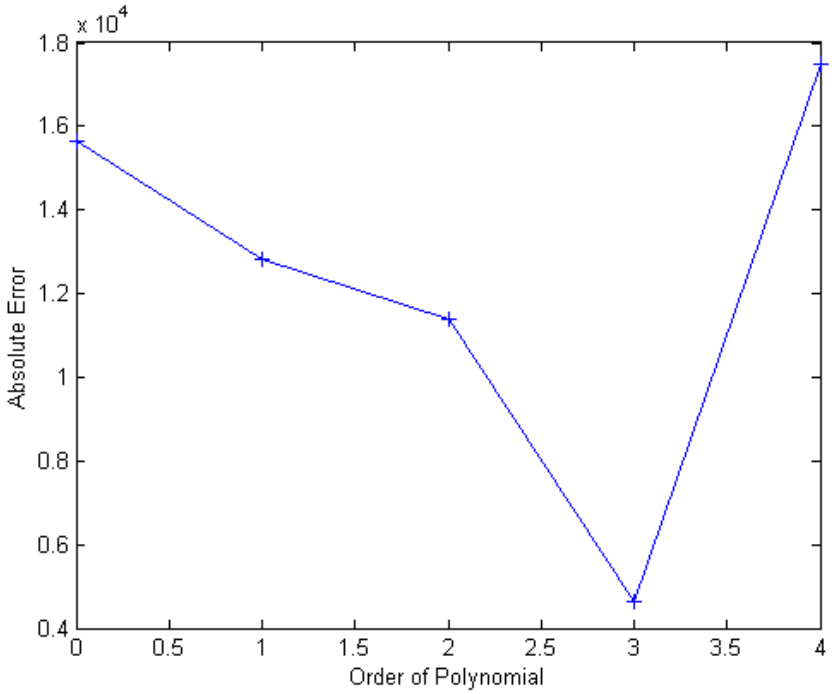

Figure 6.97 Aluminum and iron diffusion coefficients' polynomial order with the absolute error

Figure 6.97 shows that the minimum absolute error between the experimental and numerical concentration for the components aluminum and iron, (0.4639e+4), when the order of the polynomial is second order polynomial (equation 6.59). The x-axis corresponds to the order of the polynomial, and the y-axis corresponds to the sum of the absolute error between the experimental and the numerical concentration for the components (*Al, Fe*). 0, 1, 2, 3 and 4 correspond to the constant, first, second, (equation 6.59), and third order. There is good convergence between the experimental and numerical concentration for the components (*Al, Fe*) when equation 6.61 was used to calculate the diffusion coefficients (concentration dependent diffusion coefficients).

6.7.7.1. Conclusions

In this section variable cross and diagonal (concentration dependent) terms in the diffusion matrix have been taken into account. In Figures 6.90, 6.91 and 6.92, first, second and third order polynomials respectively have been used to calculate the diffusion matrix after 10 hours diffusion treatment. Figure 6.93 shows the minimum error between the experimental and numerical concentration for (*Al, Fe*) when second order polynomial (equation 6.59) has been used. In Figure 6.94 another type of second order polynomial (equation 6.61) has been used to estimate the diffusion matrix. There is improved agreement between the experimental and experimental concentration for both components for the entire range of diffusion distance after 10 hours diffusion treatments. Figure 6.95 and 6.96 demonstrate superior agreement between the numerical and experimental concentration values for *Al, Fe* after 26, 122 hours diffusion treatment respectively for the reason that the initial concentration was at t=10 hours instead of t=0*, and* t=26 hours instead of t=0 respectively. So it means there is an additional improvement when the initial concentration has been transformed. Therefore when we change the initial concentration from step to step, (initial concentration for 26 hours is the concentration profile at t =0 and for 122 hours is the concentration profile at t =26), the agreement has been improved.

6.8. Ti45Al8Nb Coated with Al_2Au Subjected to Air Oxidation at 750°C for 1000 Hours - Microstructural Aspects/Microstructure Modelling of Diffusion Process -Results and Discussion

Background information on Al_2Au coatings including the rationales for the development of these coatings and their methods of production has been presented in sections 3.7.1 and 3.7.2.

6.8.1 The Results from SEM/EDS Investigations of Al_2Au Coated Ti-45Al8Nb after Oxidation at 750°C for 1000 Hours

Figure 6.98 shows a cross section SEM image after 1000 hours of oxidation at 750°C. The numbers on the image are defined at the end of the section. The image shows scale formation in various layers. The EDS concentration profiles have been presented in Figure 6.99.

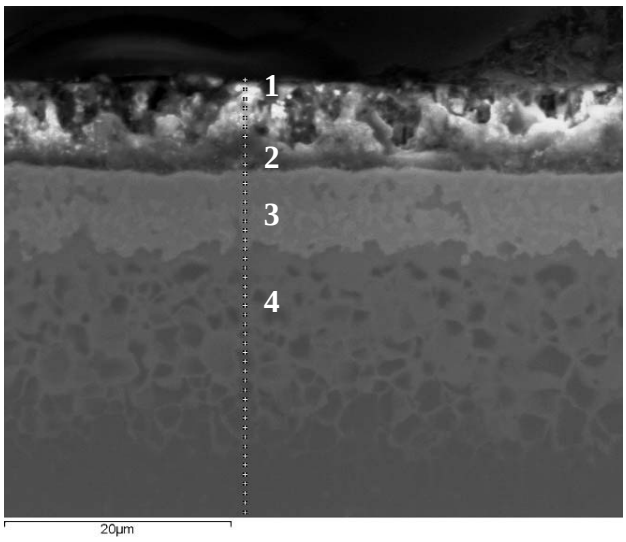

Figure 6.98 SEM cross section image with mag. 5000x of the sample (*Al_2Au* coated *Ti*45*Al*8*Nb*) after 1000 hours of oxidation at 750°C (1023 K)

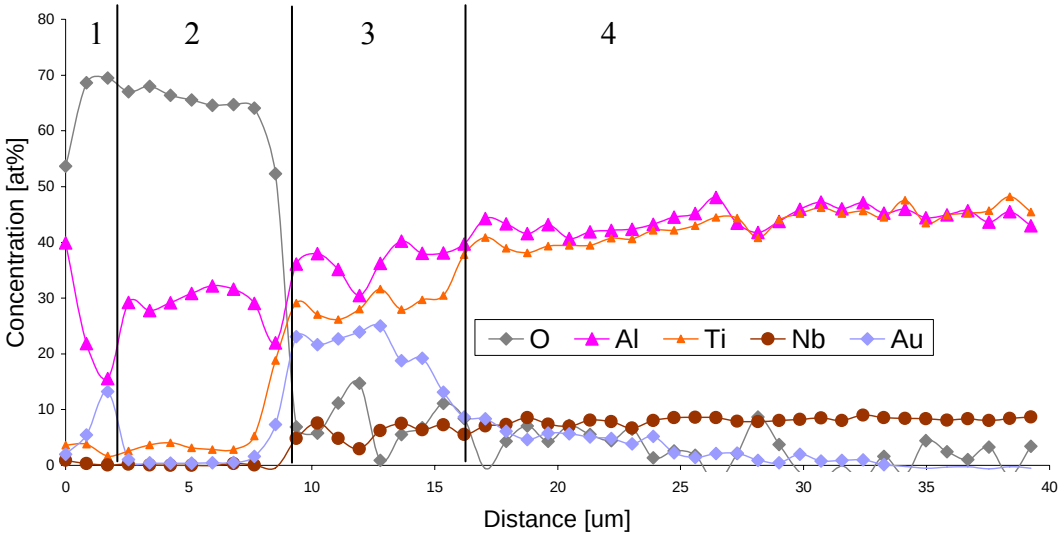

Figure 6.99 EDS concentration profiles obtained from Al_2Au coated *Ti*45*Al*8*Nb* alloy after 1000 hours of oxidation at 750°C (1023 K)

The EDS cross–section concentration profiles presented in Figure 6.99 shows that a relatively thin (2 μm) outer Al_2O_3 scale with *Au* inclusions developed, underneath this scale pure Al_2O_3 without inclusions of *Au* formed, and a little amount of *Ti* was detected. Both these layers were extremely porous and brittle (Figure 6.98). Beneath two Al_2O_3 layers the modified coating (Al_2Au) was found. At the scale/substrate interface a large diffusion zone of *Al*, *Au*, and *Ti* was formed. The EDS concentration profiles identified the following regions:

- Al_2O_3 oxide with Au inclusions;
- Al_2O_3 oxide layer;
- Modified coating (Al_2Au);
- Scale/substrate interface with *Au*, *Ti*, and *Al* diffusion zone.

6.8.2. Microstructural Description of the Diffusion Processes Involved in Al_2Au Coated Ti-45Al8Nb after Oxidation at 750°C for 1000 Hours: Consideration of Thermodynamic and Kinetic Factors

The scale formed after 1000 hours oxidation (pO_2 = 0.21 atm) at 750°C consisted of Al_2O_3 with small amount of TiO_2 and Au oxide.

The mechanism of the scale formation can be described as follows:

A large amount of Al in the deposited coating (66 at% of Al) has developed Al_2O_3 oxide scale, due to outward Al^{3+} diffusion from the coating, and inward O^{2-} diffusion from the ambient atmosphere. The produced scale was thick and had porous structure. The porous structure formed due to the fact that Al_2Au is a solid solution only up to 650°C [83]. Beyond this temperature Al_2Au phase is transformed into a liquid state. Thus the porous structure developed during the heating up and cooling down processes.

The reason for the presence of small amounts of TiO_2 in the top scale was that because Ti ions were only in the substrate, and the diffusion distance for Ti ions to reach the top layers was large.

A schematic model of the scale development at 750°C for the Al2Au coated alloy is presented in Figure 6.100. Al has high affinity for oxygen. The thermodynamic factor ΔG^o for the oxidation of Al is $\Delta G^o_{Al2O3,T} = -1676.000 + 320T$. The diffusion coefficients of Al is (D_{Al}=1.972x10^{-12}). Both thermodynamic and kinetic factors favour the formation of Al_2O_3. The outward diffusion of Al caused depletion of Al in the modified coating. Below the modified coating the diffusion zone of Al and Ti developed.

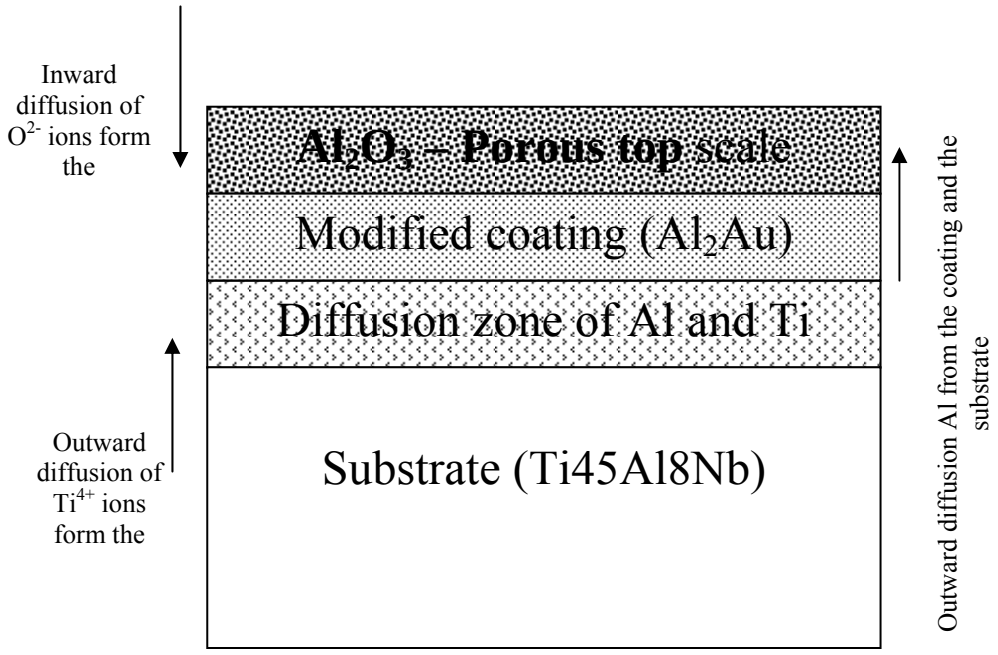

Figure 6.100 Al_2Au exposed to oxidation at 750C after 1000 hours (final stage)

In the following sections the numerical modelling for interdiffusion for this system has been presented.

6.8.3. Modelling Interdiffusion Using Genetic Algorithms Method (GAs) with the Numerical Method

As in other cases the interdiffusion coefficient for each component was optimised from a range of possible values. The Genetic Algorithms method allows optimisation of the values of the interdiffusion coefficients. Using this technique the results obtained are shown below where we have assumed constant diffusion coefficient and ignored the cross terms. D_{Al}=3.10x10^{-12} cm^2/s

In the following Figure the aluminum concentration has been presented:

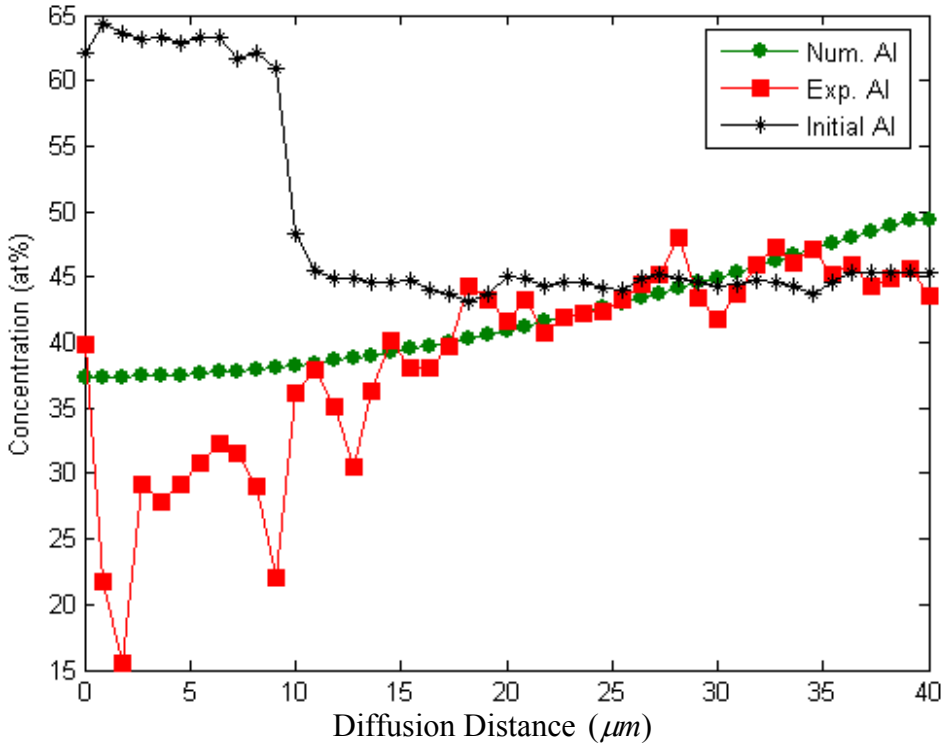

Figure 6.101 Interdiffusion studies GAs in *TiAlNb* – Al_2Au after 1000 hours (*Al* concentration profiles)

Figure 6.101 shows the numerical and experimental concentration after 1000 hours of diffusion treatment. The black diamond curve represents the initial EDX aluminum profile, the red square curve represents the numerical concentration profile for aluminum after 1000 hours of diffusion treatment, and the green triangle curve represents the EDX aluminium profile after 1000 hours. There is good agreement between the aluminum numerical and EDX concentration profiles from (9-45) μm diffusion distance after 1000 hours diffusion treatment, while some divergence can be seen from (0-8) μm diffusion distance.

In the following Figure 6.102 the titanium concentration has been presented:

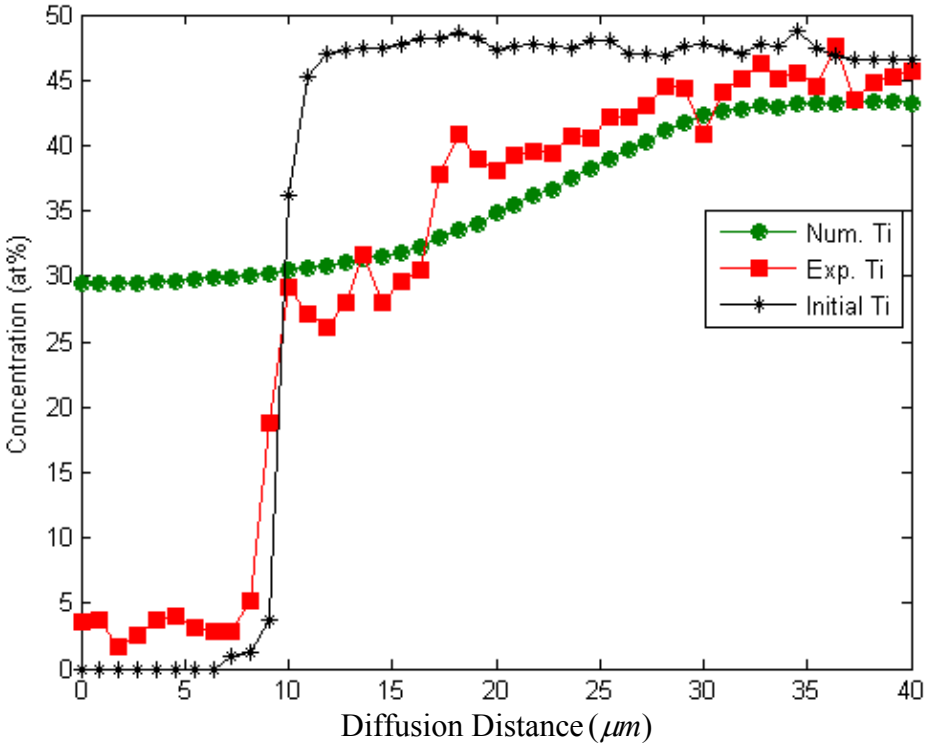

Figure 6.102 Interdiffusion studies (GAs) in *TiAlNb – Al_2Au* after 1000 hours (titanium concentration profiles)

Figure 6.102 shows the titanium numerical and experimental concentration after 1000 hours of diffusion treatment. Using the GAs method determined $D_{Ti} = 2.6 \times 10^{-12}\, cm^2/s$ The black diamond curve represents the initial EDX titanium profile, the red square curve represents the numerical concentration profile for titanium after 1000 hours diffusion treatment, and the green triangle curve represents the EDX titanium profile after1000 hours. There is good agreement between the titanium numerical and EDX (experimental) profiles from (10-45) μm diffusion distance after 1000 hours diffusion treatment, while some divergence can be seen from (0-9) μm diffusion distance.

In the following Figure 6.103 the gold concentration has been presented:

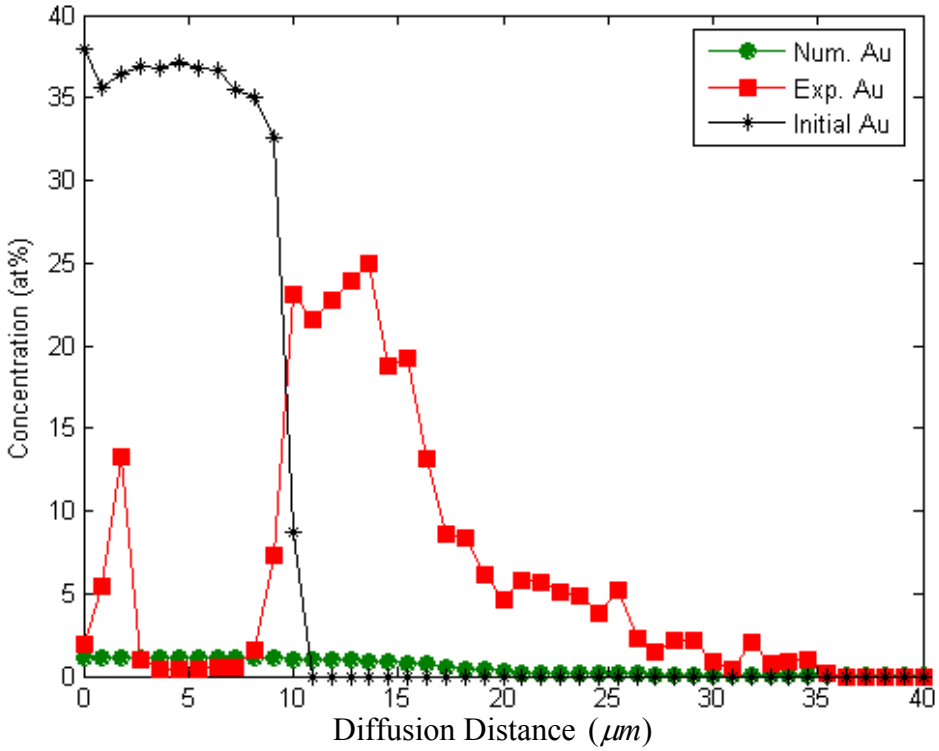

Figure 6.103 Interdiffusion studies (GAs) in $TiAlNb - Al_2Au$ after 1000 hours (gold concentration profiles)

Figure 6.103 shows the numerical and experimental concentration profiles after 1000 hours of diffusion treatment. The optimum value of the gold diffusion coefficient used was $1.01\times10^{-11}\,cm^2/s$.

For the niobium the concentration profile can be calculated by using the equation:

$$C_1 + C_2 + C_3 + C_4 = 100\%$$
$$C_4 = 100\% - (C_1 + C_2 + C_3) \qquad (6.62)$$

where: C_1 is the aluminum concentration.

C_2 is the titanium concentration.

C_3 is the gold concentration.

C_4 is the niobium concentration.

Therefore equation 6.62 has been applied and the niobium concentration profiles have been presented as follows:

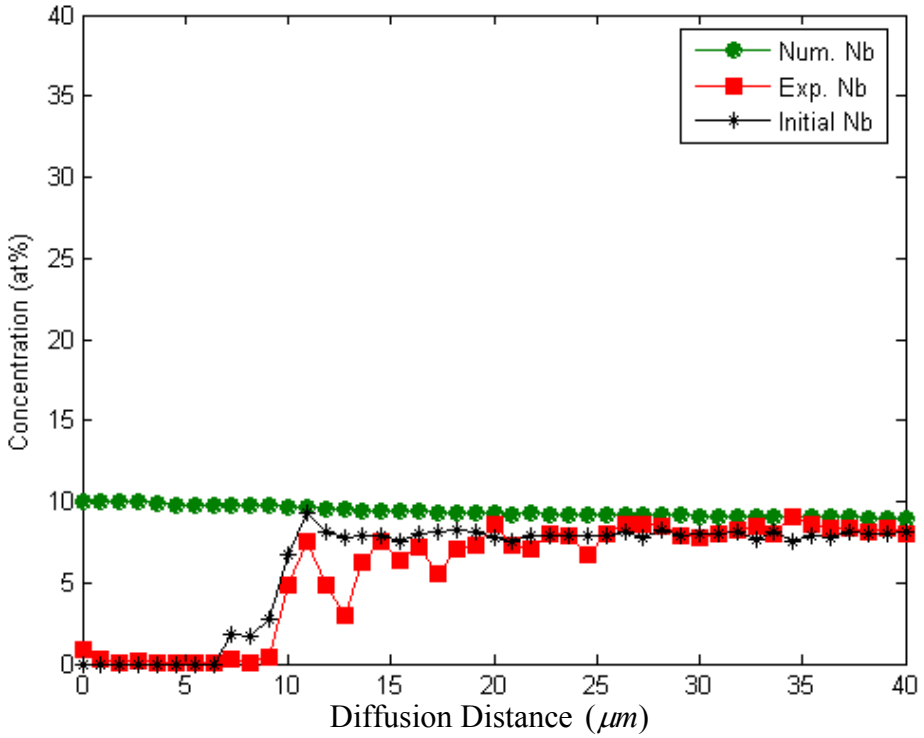

Figure 6.104 Interdiffusion studies (GAs) in *TiAlNb – Al_2Au* after 1000 hours (niobium concentration profiles)

6.8.3.1. Conclusions for Ti45Al8Nb Coated with *Al_2Au* Subjected to Air Oxidation at 750°C for 1000 Hours (Constant Diagonal Terms)

The Genetic Algorithms optimization method (GAs) has been used to optimise the diffusion coefficients for the components (Al, Ti, Au, and Nb), and the results clarify practical agreement between the numerical and experimental concentration profiles for these components. Additional improvement can be achieved by taking into account the cross terms in the diffusion matrix and introducing composition dependent diffusion coefficients.

6.8.4. Diffusion Analysis Using Constant Diagonal and Cross Terms Diffusion Coefficients

In this section the whole 3x3 diffusion matrix has been considered, Fick's second law for multicomponent systems (three independent components (Al, Ti, Au)) can be written as:

$$\begin{bmatrix} \frac{\partial C_1}{\partial t} \\ \frac{\partial C_2}{\partial t} \\ \frac{\partial C_3}{\partial t} \end{bmatrix} = \begin{bmatrix} \tilde{D}_{11}^4 & \tilde{D}_{12}^4 & \tilde{D}_{13}^4 \\ \tilde{D}_{21}^4 & \tilde{D}_{22}^4 & \tilde{D}_{23}^4 \\ \tilde{D}_{31}^4 & \tilde{D}_{32}^4 & \tilde{D}_{33}^4 \end{bmatrix} \begin{bmatrix} \frac{\partial C_1}{\partial x^2} \\ \frac{\partial C_2}{\partial x^2} \\ \frac{\partial C_3}{\partial x^2} \end{bmatrix}$$

$$\begin{aligned} \Rightarrow \frac{\partial C_1}{\partial t} &= \tilde{D}_{11}^4 \frac{\partial^2 C_1}{\partial x^2} + \tilde{D}_{12}^4 \frac{\partial^2 C_2}{\partial x^2} + \tilde{D}_{13}^4 \frac{\partial^2 C_3}{\partial x^2} \\ \frac{\partial C_2}{\partial t} &= \tilde{D}_{21}^4 \frac{\partial^2 C_1}{\partial x^2} + \tilde{D}_{22}^4 \frac{\partial^2 C_2}{\partial x^2} + \tilde{D}_{23}^4 \frac{\partial^2 C_3}{\partial x^2} \\ \frac{\partial C_3}{\partial t} &= \tilde{D}_{31}^4 \frac{\partial^2 C_1}{\partial x^2} + \tilde{D}_{32}^4 \frac{\partial^2 C_2}{\partial x^2} + \tilde{D}_{33}^4 \frac{\partial^2 C_3}{\partial x^2} \end{aligned} \qquad (6.63)$$

So the diffusion matrix is as follows:

$$\begin{bmatrix} D_{11} & D_{12} & D_{13} \\ D_{21} & D_{22} & D_{23} \\ D_{31} & D_{32} & D_{33} \end{bmatrix}$$

considered to be all constant terms.

In Figure 6.105 the experimental and numerical concentration for the components (aluminum, gold and titanium) have been presented with the interdiffusion coefficients

calculated from Genetic Algorithms method and using equation 6.63, Fick's second law. Here the cross terms have been taken into account.

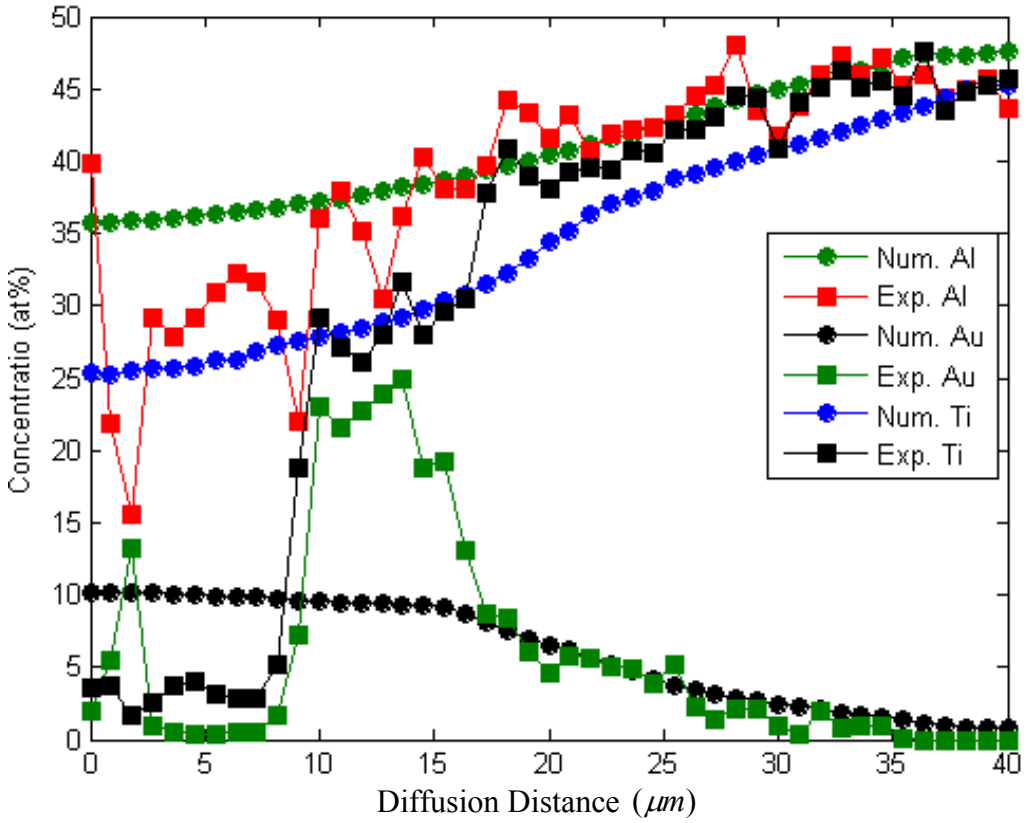

Figure 6.105 Numerical and experimental concentration profiles in *TiAlNb – Al_2Au* after 1000 hours diffusion treatment (constant diagonal and cross terms)

Figure 6.105 shows aluminum, gold and titanium numerical and experimental concentrations profiles using constant diffusion coefficients $D_{11}, D_{12}, D_{13}, D_{21}, D_{22}, D_{23}, D_{31}, D_{32}, D_{33}$ calculated from Genetic Algorithms optimization method chapter (5) as:

$$
\begin{aligned}
D_{11} &= 0.6191\times10^{-11}\,cm^2/s \\
D_{12} &= 1.9426\times10^{-12}\,cm^2/s \\
D_{13} &= 0.4326\times10^{-11}\,cm^2/s \\
D_{21} &= 0.7384\times10^{-12}\,cm^2/s \\
D_{22} &= 0.9191\times10^{-12}\,cm^2/s \\
D_{23} &= 0.5026\times10^{-11}\,cm^2/s \\
D_{31} &= 0.028\times10^{-11}\,cm^2/s \\
D_{32} &= 0.1351\times10^{-11}\,cm^2/s \\
D_{33} &= 1.2910\times10^{-11}\,cm^2/s
\end{aligned}
\tag{6.64}
$$

Figure 6.106 shows the concentration profiles for niobium after 1000 hours diffusion treatments using the equation 6.62.

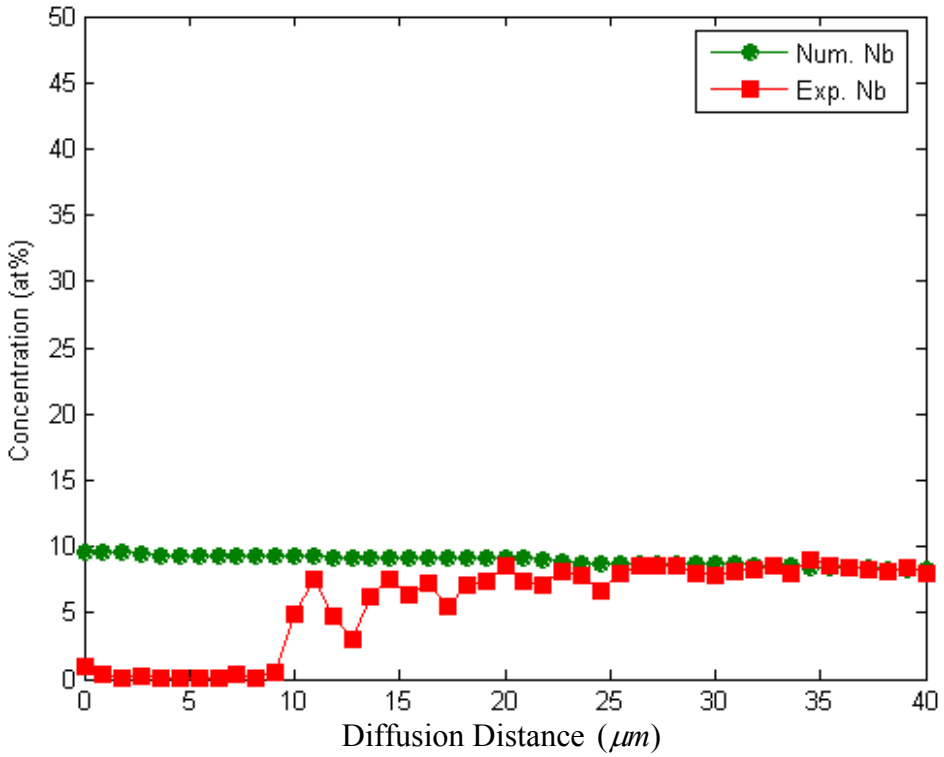

Figure 6.106 Niobium concentration profiles in *TiAlNb – Al_2Au* after 1000 hours diffusion treatment (constant cross and diagonal terms)

6.8.4.1. Conclusions for Considering Constant Diagonal and Cross Terms Diffusion Coefficients

The GAs technique has been used to optimise *D* (diffusion coefficients). The agreement has been enhanced between the experimental and numerical concentration for the components (*Al, Au*, and *Ti*) when equation 6.63 was used to calculate the diffusion coefficients, including the cross terms. The agreement between the experimental and numerical concentration profiles for the components (*Al, Au*, and *Ti*) has been improved compared to those formed by using diagonal terms only. This mean that the numerical concentration profiles for aluminum, gold and titanium demonstrate much improvement compared to the numerical concentration profiles when the cross terms considered to be zero. The following Figures 6.107 and 6.108 illustrate the absolute error for the components aluminum, gold, titanium and niobium against the number of the components when 1, 2 3, and 4 belong to the aluminum, gold, titanium and niobium respectively.

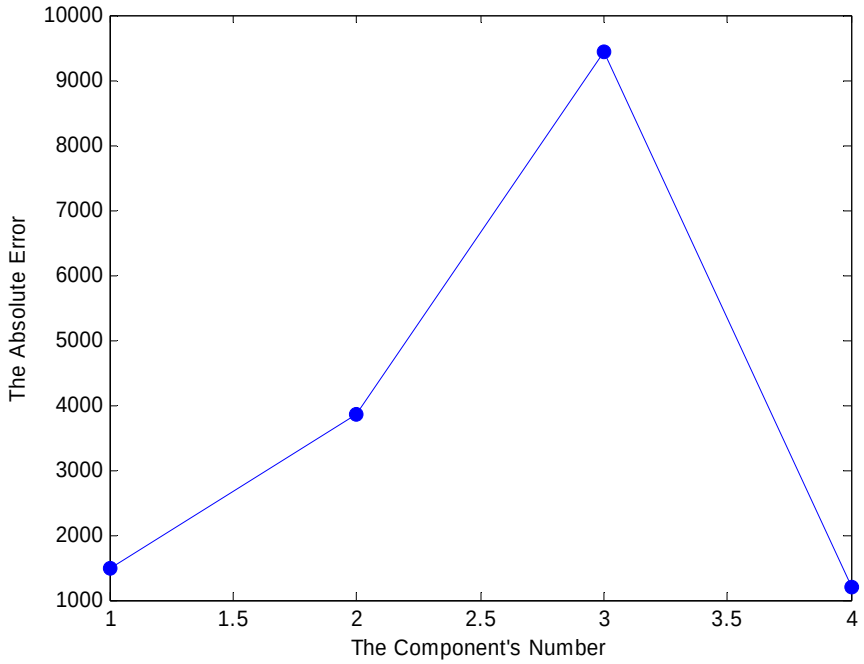

Figure 6.107 The absolute error for the components aluminum, gold, titanium and niobium with the constant diagonal terms diffusion coefficients

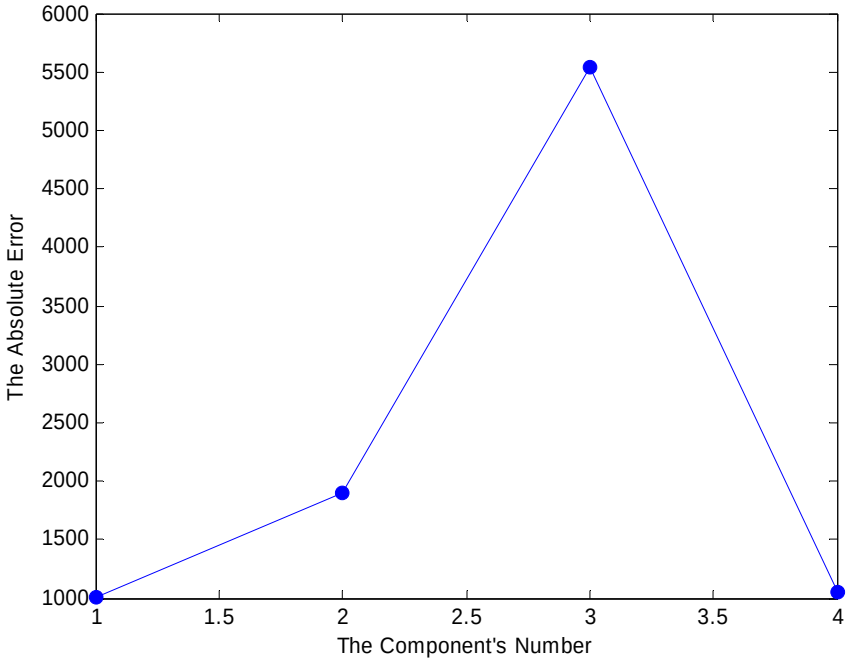

Figure 6.108 The absolute error for the components aluminum, gold, titanium and niobium with the constant diagonal and cross terms diffusion coefficients

The above two Figures 6.107 and 6.108 show the absolute errors between the experimental and numerical concentration profiles for all the components. From these Figures, it can be noticed that the error has been decreased significantly.

6.8.5. Diffusion Analysis Using Variable Diagonal and Cross Terms Diffusion Coefficients

In the earlier part 6.7.4 the diffusion coefficients (diagonal and cross terms) for the components Al, Au, Ti were considered to be constant. Here the diffusion coefficients are considered to be concentration dependent (a function of concentration). This function will be second order polynomial. Figure 6.109 shows the concentration profiles for the three components (Al, Au, Ti) .

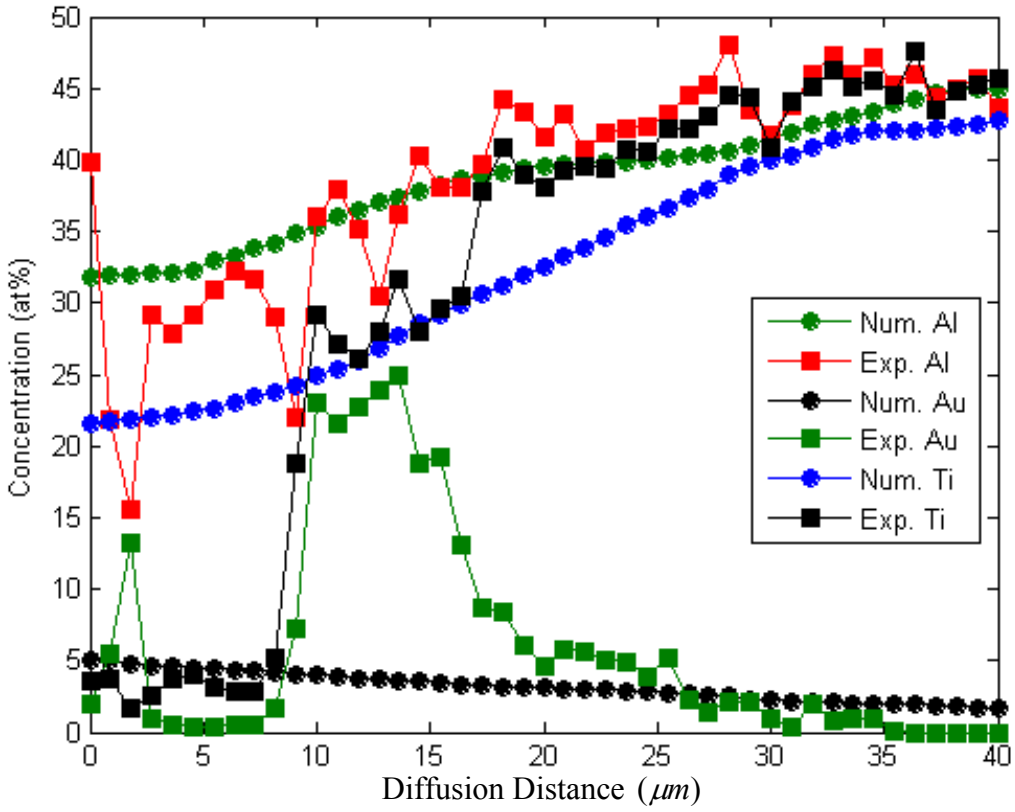

Figure 6.109 The numerical and experimental concentration profiles in $TiAlNb - Al_2Au$ after 1000 hours diffusion treatment (variable diagonal and cross terms)

Figure 6.109 describes the numerical and experimental concentrations for aluminum, gold and titanium with concentration dependent diffusion coefficients $D_{11}, D_{12}, D_{13}, D_{21}, D_{22}, D_{23}, D_{31}, D_{32}, D_{33}$ (second order polynomial) after 1000 hours diffusion treatment:

$$
\begin{aligned}
D_{11} &= x_1 + x_2 C_1 + x_3 C_1^{\,2} + x_4 C_3^2 \\
D_{12} &= y_1 + y_2 C_1 C_2 + y_3 C_2 \\
D_{13} &= z_1 C_2 + z_2 C_2^{\,2} \\
D_{21} &= v_1 C_1 + v_2 C_2 + v_3 C_2^{\,2} \\
D_{22} &= u_1 C_3 + u_2 C_2^2 + u_3 C_2 C_3 \\
D_{23} &= w_1 C_1^2 + w_2 C_3^2 \\
D_{31} &= e_1 C_1 C_3 + e_2 C_3 \\
D_{32} &= f_1 C_3 + f_2 + f_3 C_3 + f_4 C_3 C_1 \\
D_{33} &= g_1 C_1 C_2 + g_2 C_3^2
\end{aligned}
\qquad (6.65)
$$

where the values of *D*'s are as follows:

$$
\begin{aligned}
D_{11} &= 4.0003 \times 10^{-11}\, cm^2 / s \\
D_{12} &= 1.41710 \times 10^{-12}\, cm^2 / s \\
D_{13} &= 0.2318 \times 10^{-11}\, cm^2 / s \\
D_{21} &= 0.1015 \times 10^{-12}\, cm^2 / s \\
D_{22} &= 0.0921 \times 10^{-12}\, cm^2 / s \\
D_{23} &= 0.0747 \times 10^{-11}\, cm^2 / s \\
D_{31} &= 0.0471 \times 10^{-11}\, cm^2 / s \\
D_{32} &= 0.6742 \times 10^{-11}\, cm^2 / s \\
D_{33} &= 1.6567 \times 10^{-11}\, cm^2 / s
\end{aligned}
$$

where $C_1, C_2, and\ C_3$ are the initial concentrations for aluminum, gold and titanium respectively. $x_1, x_2, x_3, \cdots, \cdots, g_1, g_2$ are the polynomial coefficients calculated using Genetic Algorithms optimization method. There were improved agreements in the numerical and experimental concentration values for aluminum, gold and titanium for the entire range of the diffusion distance.

In the following Figure niobium concentration profiles have been presented.

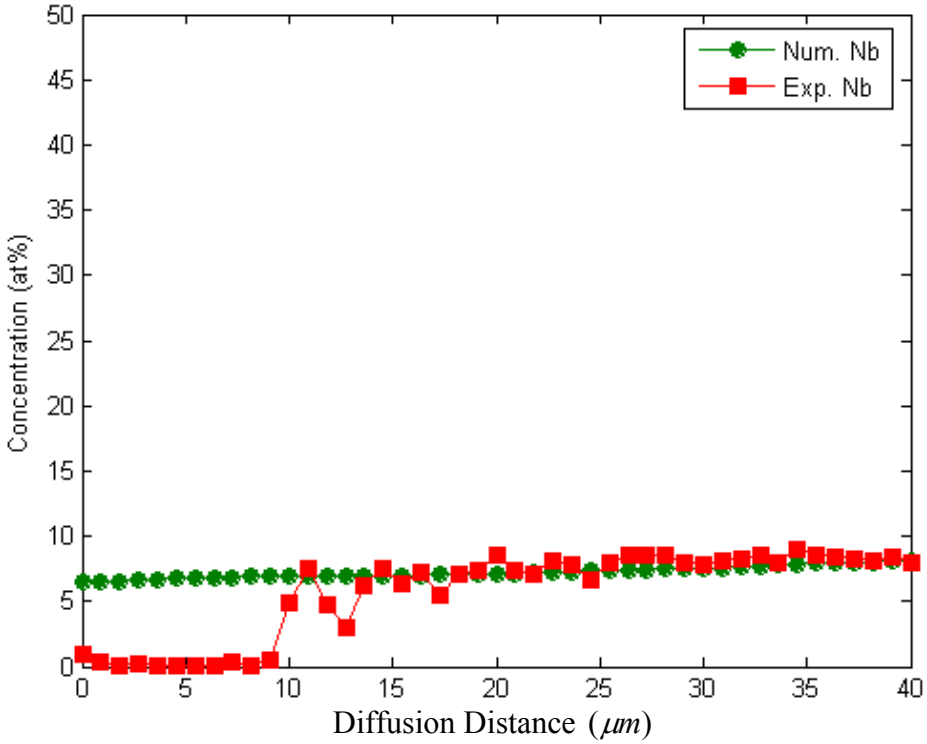

Figure 6.110 Niobium concentration profiles in *TiAlNb – Al_2Au* after 1000 hours diffusion treatment (constant cross and diagonal terms)

In the following Figure 6.111 the absolute error for the components aluminum, gold, titanium and niobium have been plotted against the number of the components as 1, 2, 3 and 4 refer to the aluminum, gold, titanium and niobium respectively,

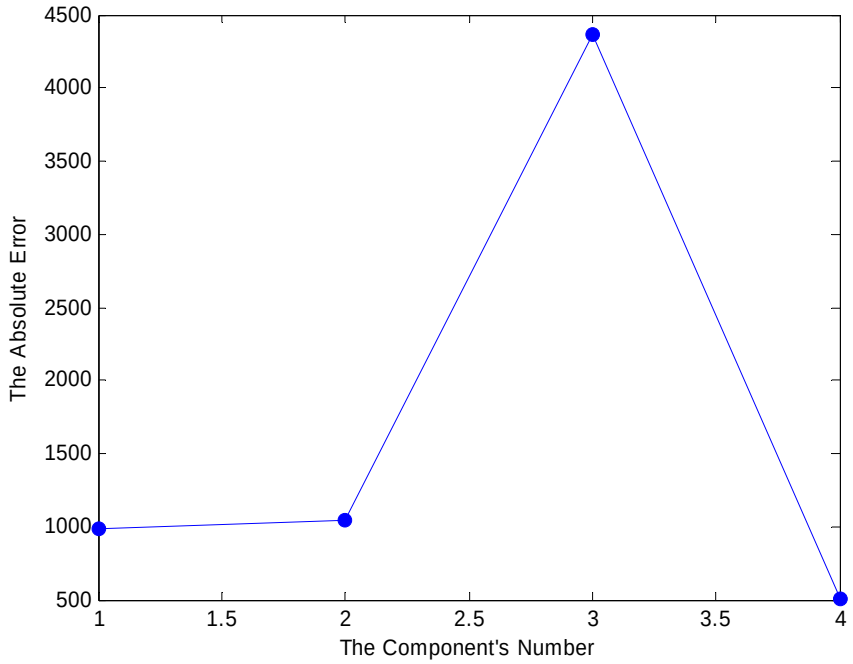

Figure 6.111 the absolute error for the components aluminum, gold, titanium and niobium with the variable diagonal and cross terms diffusion coefficients

6.8.5.1. Conclusions

The agreement between the numerical and experimental concentration profiles has been improved when the diffusion coefficients were concentration dependent and the cross terms were considered.

Genetic Algorithms method optimizes the values of the coefficients in the second order polynomial (equation 6.65) of diffusion coefficients, in the diffusion matrix. There is good convergence between the experimental and numerical concentration for the components *Al*, *Au*, *Ti* when equation 6.65 was used to compute the diffusion coefficients, (taking into account the cross terms). The variation between the experimental and numerical concentration profiles for the components (*Al*, *Au*, *Ti*) has been reduced considerably. Therefore there is an improvement for the numerical concentration profiles for aluminum, gold and titanium compared with the numerical

concentration profiles when the cross terms are considered to be constant. Figures 6.107, 6.108, and 6.111 show the errors between the numerical concentration profiles and the experimental concentration profiles using Least squares method.

6.9. Ti45Al8Nb Coated with TiAlCrY Subjected to Air Oxidation at 750^{o}C for 500 Hours -Microstructural Aspects/Microstructure Modelling of Diffusion Process -Results and Discussion

Background information on TiAlCrY coatings including the rationales for the development of these coatings and their methods of production have been presented in sections 3.8.1 and 3.8.3.

6.9.1. The Results from SEM/EDS Investigations of TiAlCrY Coated Ti45Al8Nb after Oxidation at 750^{o}C for 500 Hours

Figure 6.112 shows the digimaps of TiAlCrY coated Ti45Al8Nb after 500 hours oxidation at 750^{o}C (1023 K).The cross–sectioned SEM image of TiAlCrY coated Ti45Al8Nb alloy after 500 hours oxidation at 750^{o}C (1023 K) in static air is shown in Figure 6.113. The scale shows good protection against high temperature in an oxidising environment: there was no spallation or cracks formation. The different areas shown by Figures 6.113 and 6.114 with different magnifications illustrate that the whole sample oxidized at a similar rate. The detailed analysis was performed and is presented by the EDS concentration profiles in Figure 6.114.

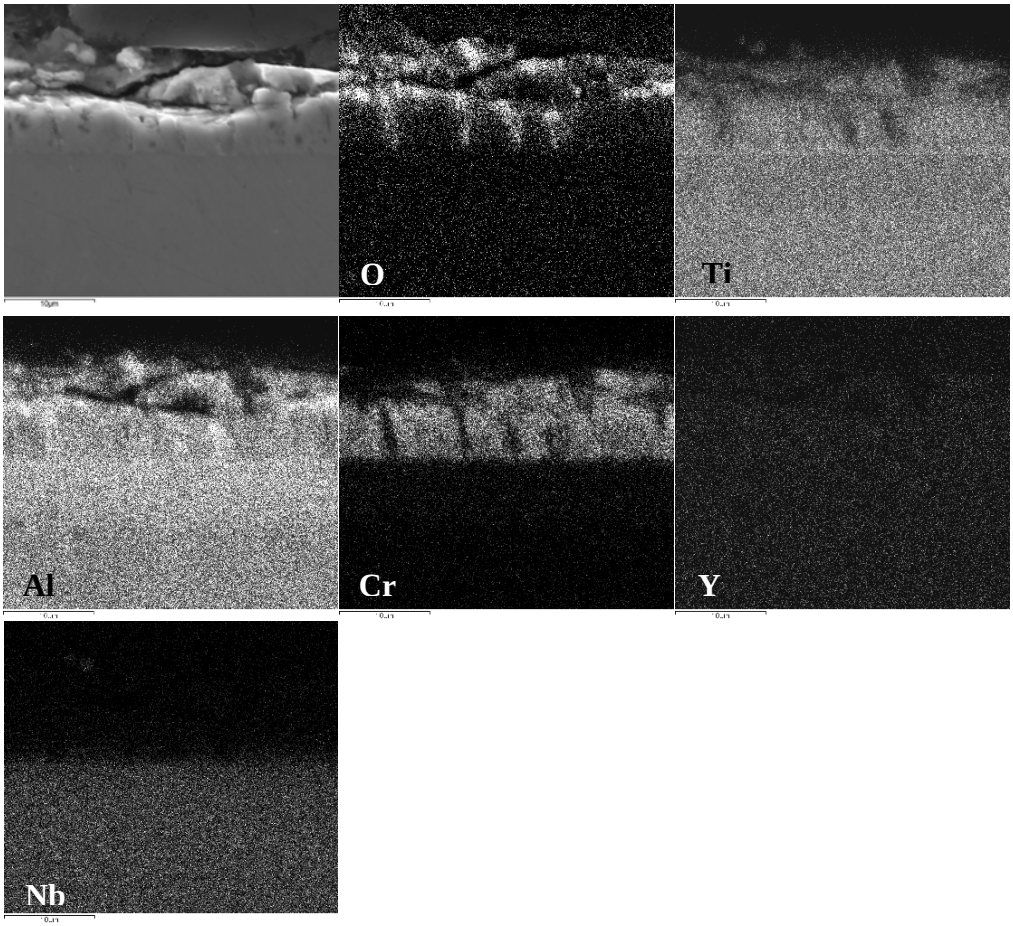

Figure 6.112 Digimaps of TiAlCrY coated Ti45Al8Nb after 500 hours oxidation at 750^{o}C (1023 K)

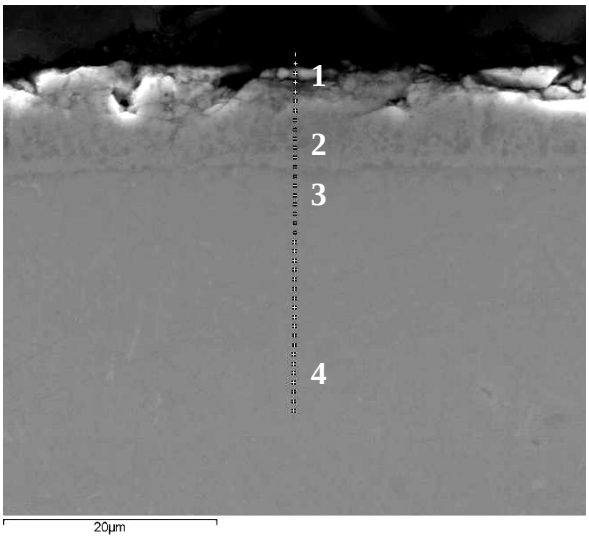

Figure 6.113 Cross – section SEM image (mag. 5000x) of TiAlCrY coated Ti45Al8Nb alloy after 500 hours of oxidation at 750°C (1023 K)

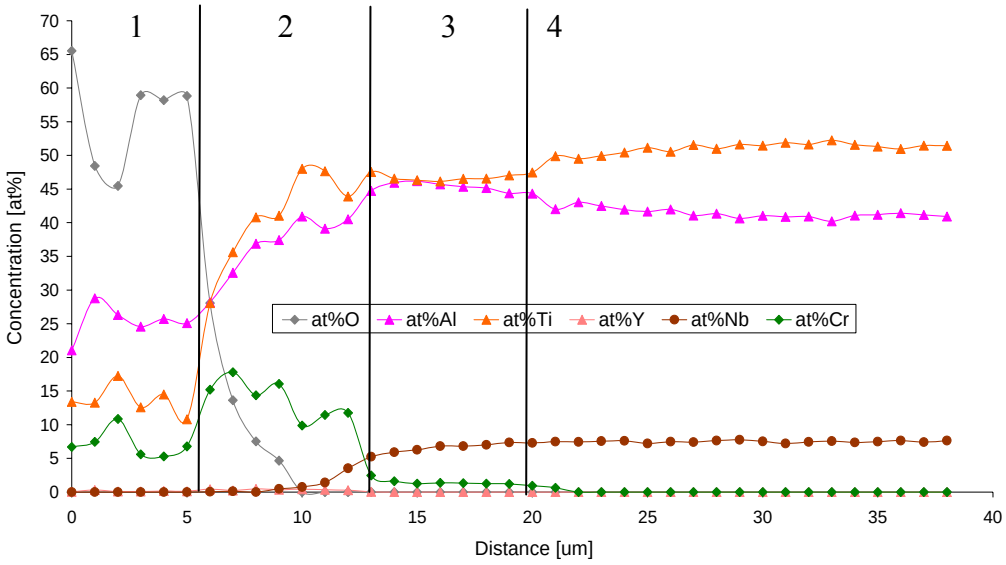

Figure 6.114 EDS Concentration profiles obtained from *TiAlCrY* coated Ti45Al8Nb alloy after 500 hours of oxidation at 750°C (1023 K)

Figure 6.114 shows the cross–sectional EDS concentration profiles of the TiAlCrY coated alloy which had been exposed for 500 hours at 750°C (1023 K). A thick (5 µm) oxide scale consisting of Al, Cr, and Ti oxides was observed to form at the top. Below the top scale we observed the modified coating TiAlCrY. The modified

coating/substrate interface shows a depletion zone of Al and Ti. Beneath the depletion zone is a zone depleted in Ti (pre-depletion zone); where Al concentration increased due to the faster outward diffusion of Ti ions from the bulk material. The straight line in the EDS concentration profiles indicate the different regions formed after exposure. The numbers in the EDS profiles correlate with the SEM image shown in Figure 6.113. An oxide scale of Al, Cr, and Ti is seen to be the same as outer scale and Nb remains in the substrate TiAl45Al8Nb. The EDS X-ray mapping detects the increased concentration of Al in the area where depletion zone of Ti formed. The EDS concentration profiles are indicated by the following regions:

- Al/Ti/Cr oxide scale;
- Modified coating (TiAlCrY) and depletion zone;
- Pre-depletion zone;
- Substrate (Ti45Al8Nb alloy).

6.9.2. Microstructural Description of the Diffusion Processes Involved in TiAlCrY Coated Ti45Al8Nb after Oxidation at 750^{o}C for 500 Hours: Consideration of Thermodynamic and Kinetic Factors

The degradation of the TiAlCrY coated Ti45Al8Nb alloy during high temperature oxidation at 750^{o}C (1023 K) after 500 hours oxidation was associated with the formation of the mixed, Al, Ti, and Cr oxide. The formation of the top scale was caused by the outward diffusion of Al, Ti, and Cr from the modified coating and inward diffusion of O^{2-} from the atmosphere.

The oxidation of TiAlCrY coated alloy at 750^{o}C (1023 K) in the initial stage was related to the formation of non protective TiO_2 scale. The formation of TiO_2 scale was associated with high partial pressure of oxygen (pO_2 = 0.21 atm) in oxidising

atmosphere and with Ti having a high affinity for oxygen [88]. The calculated values of Gibbs Free Energy Formation (ΔG_T^o) [J/mole] for Al_2O_3, Cr_2O_3, and TiO_2 are given in Table 6.4.

ΔG_T^o [J/mole]	750°C (1023 K)
TiO_2	-733021
Al_2O_3	-1348640
Cr_2O_3	-728470

Table 6.4 Calculated free energies of formation (ΔG_T^o) of developed oxides at temperature 750°C

The development of TiO_2 outer scale is given by reaction 1:

Reaction 1 $$Ti(s) + O_2(g) \rightarrow TiO_2(s)$$

The formation of Al_2O_3 and Cr_2O_3 develops according to the reactions 2 and 3

Reaction 2 $$2Al(l) + \frac{3}{2}O_2(g) \rightarrow Al_2O_3(s)$$

Reaction 3 $$2Cr(s) + \frac{3}{2}O_2(g) \rightarrow Cr_2O_3(s)$$

A schematic model of the scale development at 750°C of TiAlCrY coated alloy is presented in Figure 6.115.

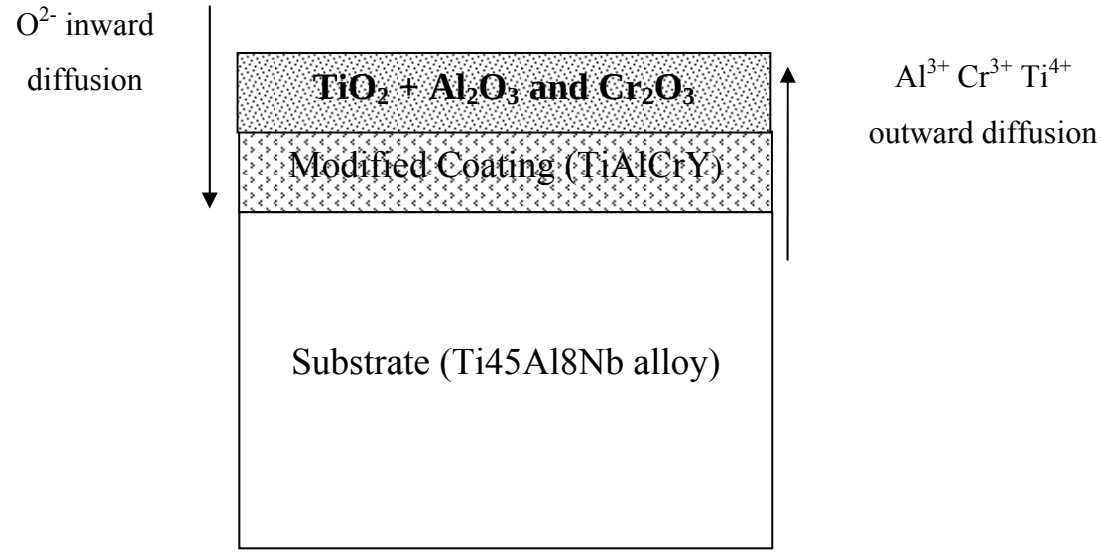

Figure 6.115 The scale formation at 750°C (1023 K) on TiAlCrY coated Ti45Al8Nb alloy with formation of the final scale after 500 hours of oxidation

In the following section 6.8.3, the interdiffusion has been modeled in this multi-component system consisting of *TiAlCrY* coating on *TiAl* materials using the Genetic algorithms (GAs) method.

6.9.3. Modelling Interdiffusion Using Genetic Algorithms Method (GAs) with the Numerical Method

As previously shown the GAs method has been used to optimise the diffusion coefficient. With this technique the results found are shown below where we have supposed constant diffusion coefficient in the diffusion matrix:

$$\begin{bmatrix} D_{11} & D_{12} & D_{13} \\ D_{21} & D_{22} & D_{23} \\ D_{31} & D_{32} & D_{33} \end{bmatrix}$$

Where the diagonal terms (D_{11}, D_{22}, D_{33}) have been taken into account and the cross terms ignored.

In the following Figure 6.116 the aluminum concentration profiles have been presented:

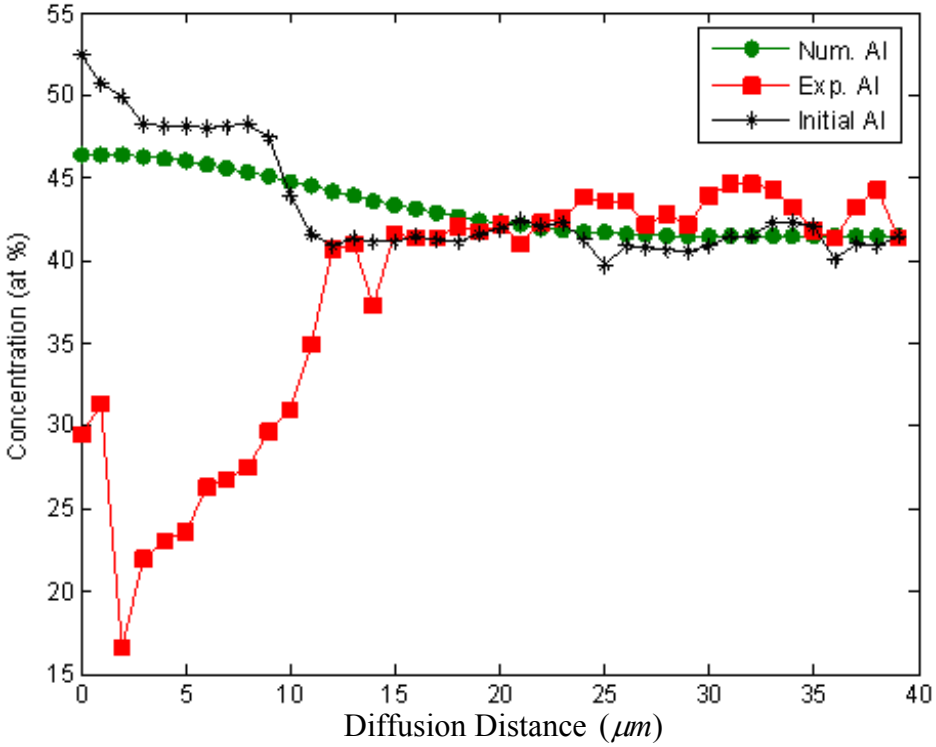

Figure 6.116 Interdiffusion studies GAs in $TiAl - TiAlCrY$ after 500 hours (aluminum concentration profiles)

Figure 6.116 shows the numerical and experimental concentration after 500 hours of diffusion treatment. The optimum value of aluminum diffusion coefficient is $0.1247 \times 10^{-11} cm^2 / s$. The red solid square curve (represents the EDS aluminum profile after 500 hours), the green solid circle curve represents the numerical concentration profile for aluminum after 500 hours of diffusion treatment, and the black star curve represents the initial EDS aluminum profile. There is good agreement between the aluminum numerical and EDS concentration profiles from (9-40) μm diffusion distance after 500 hours diffusion treatment, while some divergence can be seen from (0-8) μ m diffusion distance.

Figure 6.117 and 6.118 show the modelling concentration profile results for *Cr* and *Ti* using GAs optimised D_{Cr} =5.61301201x10^{-12} cm^2/s , D_{Ti} =0.156171x10^{-11} cm^2/s

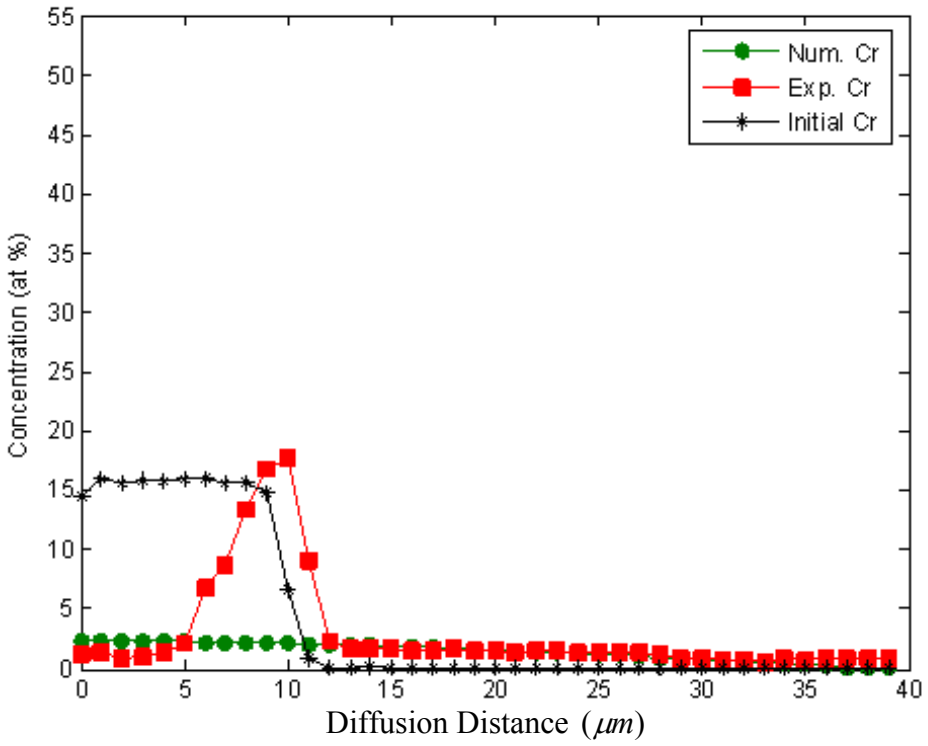

Figure 6.117 Interdiffusion studies GAs in $TiAl - TiAlCrY$ after 500 hours (chromium concentration profiles)

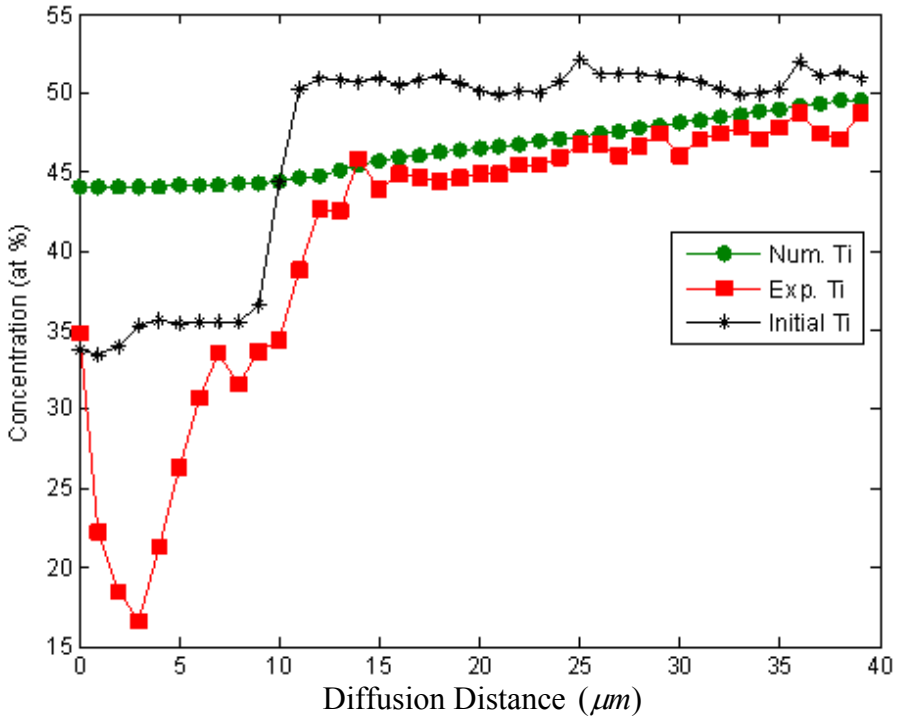

Figure 6.118 Interdiffusion studies GAs in $TiAl - TiAlCrY$ after 500 hours (titanium concentration Profiles)

For the niobium concentration can be calculated by using the equation:

$$C_1 + C_2 + C_3 + C_4 = 100\%$$
$$C_4 = 100\% - (C_1 + C_2 + C_3)$$

Where: C_1 is the aluminum concentration.

C_2 is the chromium concentration.

C_3 is the titanium concentration.

and C_4 is the niobium concentration, is presented as follows:

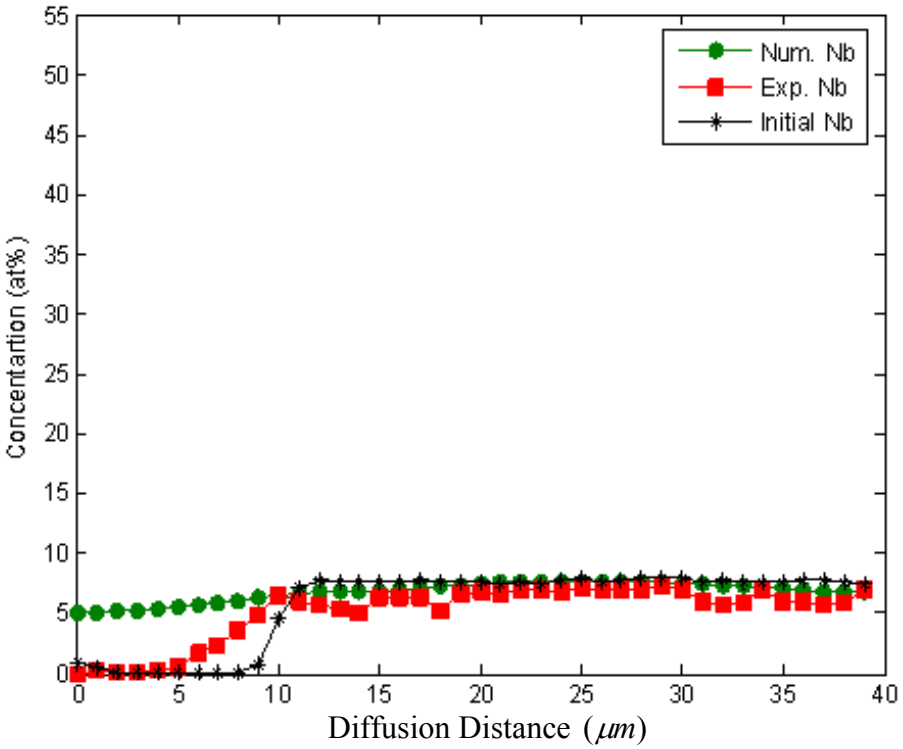

Figure 6.119 Interdiffusion studies GAs in $TiAl - TiAlCrY$ after 500 hours (niobium concentration profiles)

6.9.3.1. Conclusions for Ti45Al8Nb Coated with TiAlCrY Subjected to Air Oxidation at 750°C for 500 Hours (Constant Diagonal Terms)

The results using Genetic Algorithms optimization method (GAs) show reasonable agreement between the theoretical and experimental concentration profiles for these components. Further improvement can be attained by initiating composition dependent diffusion coefficients and including the cross terms in the diffusion matrix.

6.9.4. Calculation Considering Constant Cross and Diagonal Terms Diffusion Coefficients

Fick's second law for multicomponent system can be written as:

$$\frac{\partial C_i}{\partial t} = \sum_{j=1}^{n-1} \tilde{D}_{ij}^{n} \frac{\partial^2 C_j}{\partial x^2} \quad i = 1,2,3 \quad n = 4 \tag{6.66}$$

$$\Rightarrow \begin{bmatrix} \frac{\partial C_1}{\partial t} \\ \frac{\partial C_2}{\partial t} \\ \frac{\partial C_3}{\partial t} \end{bmatrix} = \begin{bmatrix} D_{11}^4 & D_{12}^4 & D_{13}^4 \\ D_{21}^4 & D_{22}^4 & D_{23}^4 \\ D_{31}^4 & D_{32}^4 & D_{33}^4 \end{bmatrix} \begin{bmatrix} \frac{\partial C_1}{\partial x^2} \\ \frac{\partial C_2}{\partial x^2} \\ \frac{\partial C_3}{\partial x^2} \end{bmatrix} \tag{6.67}$$

Where the number 1 means aluminum, 2 means chromium, 3 means titanium, and 4 means yttrium

So the diffusion matrix is as follows:

$$\begin{bmatrix} D_{11}^4 & D_{12}^4 & D_{13}^4 \\ D_{21}^4 & D_{22}^4 & D_{23}^4 \\ D_{31}^4 & D_{32}^4 & D_{33}^4 \end{bmatrix} \tag{6.68}$$

In this matrix the diagonal and cross terms have been considered to be constant.

In Figure 6.120 the experimental and numerical concentration for the components aluminum, chromium and titanium have been presented with the interdiffusion coefficients calculated from Genetic Algorithms method and using equation 6.67, Fick's second law. Here the cross terms have been taken into account.

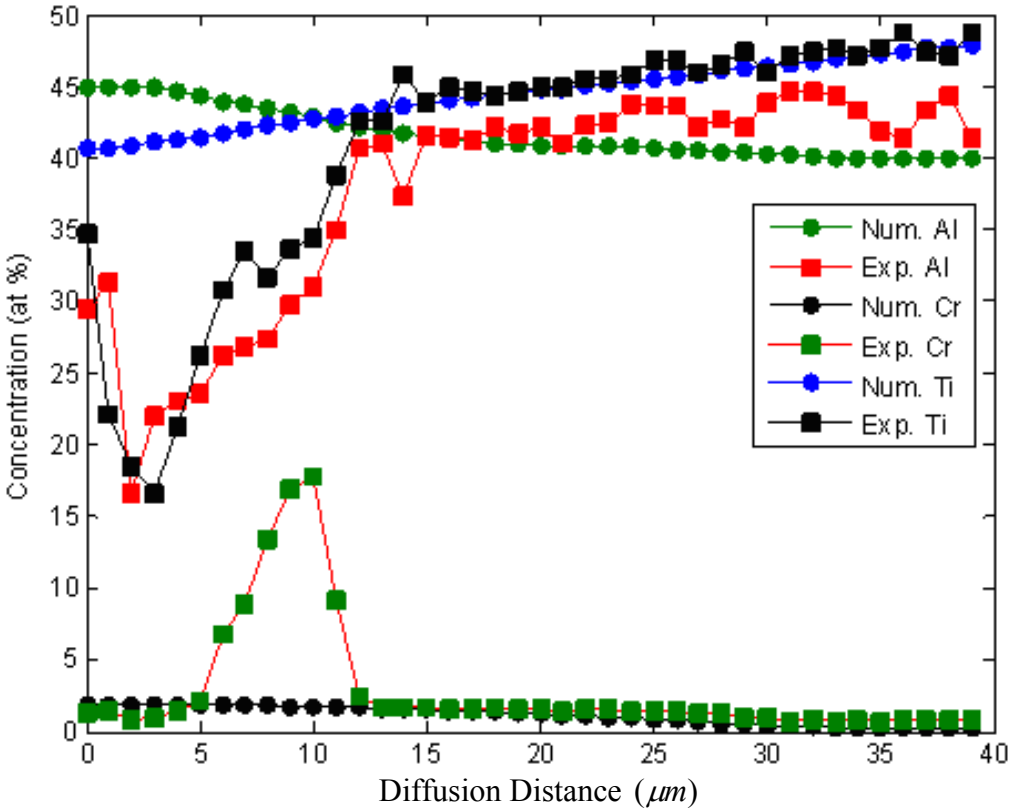

Figure 6.120 The numerical and experimental concentration profiles in $TiAl-TiAlCrY$ after 500 hours diffusion treatment for *Al, Ti*, and *Cr*

Figure 6.120 demonstrates aluminum, chromium and titanium concentrations (numerical and experimental) using constant diffusion coefficients $D_{11}, D_{12}, D_{13}, D_{21}, D_{22}, D_{23}, D_{31}, D_{32}, D_{33}$ determined from Genetic Algorithms optimization method chapter 5 as:

$$
\begin{aligned}
D_{11} &= 0.3119 \times 10^{-11} cm^2 / s \\
D_{12} &= 2.494231 \times 10^{-12} cm^2 / s \\
D_{13} &= 0.7215 \times 10^{-11} cm^2 / s \\
D_{21} &= 0.700810 \times 10^{-12} cm^2 / s \\
D_{22} &= 1.29180 \times 10^{-12} cm^2 / s \\
D_{23} &= 0.0348 \times 10^{-11} cm^2 / s \\
D_{31} &= 0.026 \times 10^{-11} cm^2 / s \\
D_{32} &= 0.0167 \times 10^{-11} cm^2 / s \\
D_{33} &= 0.4317 \times 10^{-11} cm^2 / s
\end{aligned}
\qquad (6.69)
$$

In the above Figure 6.120 the numerical concentration profiles for the components aluminum, chromium and titanium have been calculated considering constant cross terms and diagonal terms, in a diffusion matrix. There is reasonable agreement between the experimental and numerical concentration for all the components shown.

6.9.4.1. Conclusions for Considering Constant Cross and Diagonal Terms Diffusion Coefficients

Fick's second law has been solved using Runge-Kutta method of order four with GAs method for diffusion coefficient *D* optimisation. There is good convergence between the experimental and numerical concentration for the components (*Al, Cr*, and *Ti*) when equation 6.67 was used to calculate the diffusion coefficients, taking into account the cross terms. The difference between the experimental and numerical concentration profiles for the components (*Al, Cr*, and *Ti*) has been reduced compared to those produced by using diagonal terms only. It means the results (the numerical concentration profiles for aluminum, chromium and titanium) show much improvement compared to the numerical concentration profiles when the cross terms was considered to be zero. In the following Figure 6.121 the absolute error for the components aluminum, chromium and titanium have been plotted against the number of the

components where 1, 2 and 3 refer to the aluminum, chromium and titanium respectively.

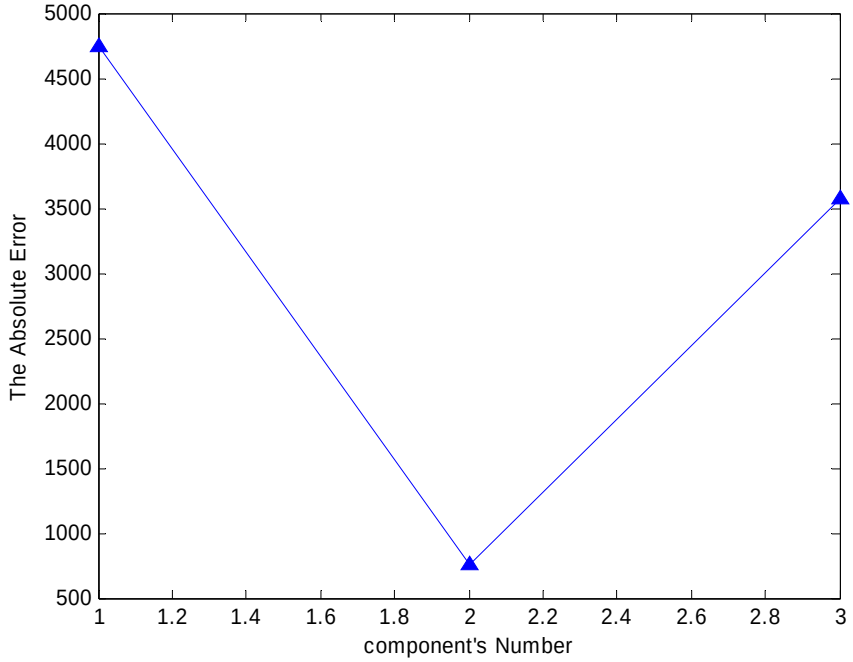

Figure 6.121 The absolute error for the components aluminum, chromium and titanium with the constant diagonal diffusion coefficients

As shown in Figure 6.121 the error for aluminum is more than 4500, and more than 3500 for titanium, while if we look at the following Figure 6.122 the absolute error for aluminum is just more than 4000, and more than 2500 for titanium.

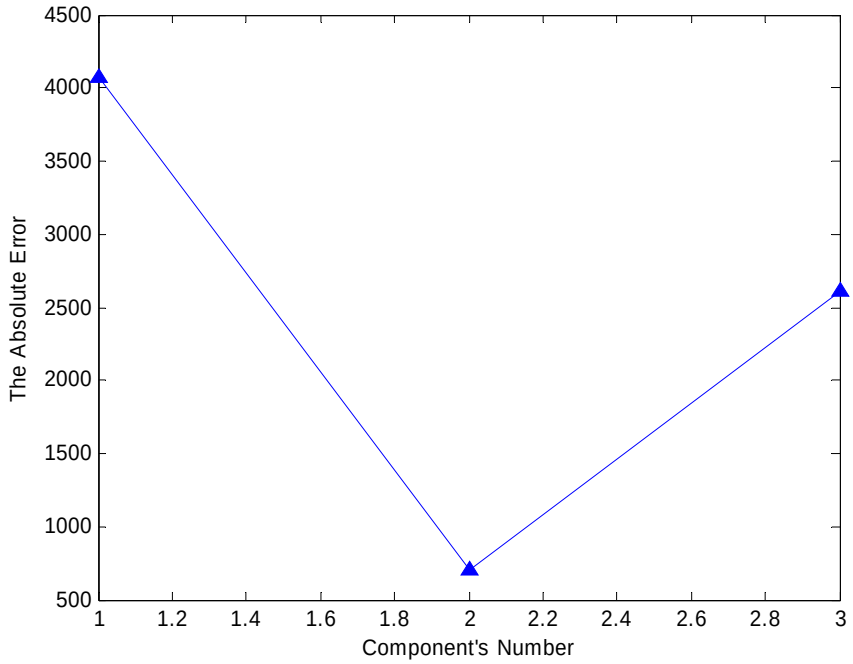

Figure 6.122 The absolute error for the components aluminum, chromium and titanium (whole constant diffusion coefficient matrix, equation 7.68)

6.9.5. Calculation Considering Variable Cross and Diagonal Terms Diffusion Coefficients

In the previous part 6.8.4, the diffusion coefficients (diagonal and cross terms) for the both components (*Al*, *Cr*, *Ti*) were considered to be constant. In the present part all the diffusion coefficients are considered to be concentration dependent (a function of concentration). Second order polynomial has been used to represent the concentration dependence diffusion coefficients for the aluminum, chromium and titanium:

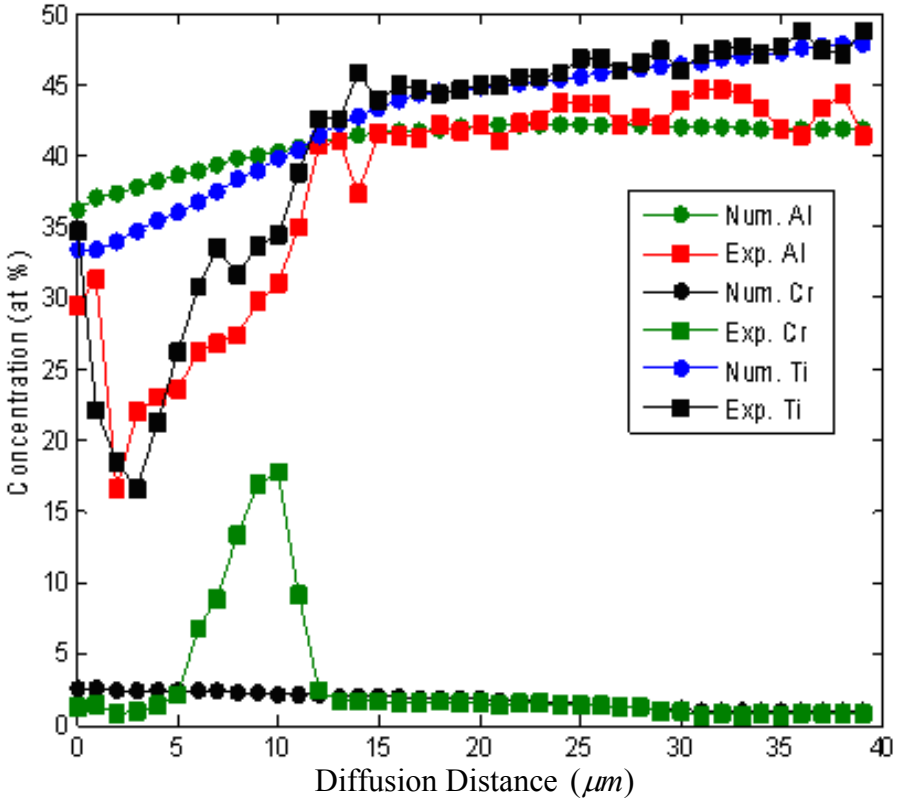

Figure 6.123 The numerical and experimental concentration profiles in $TiAl-TiAlCrY$ after 500 hours diffusion treatment for *Al, Ti*, and *Cr* considering variable cross terms

Figure 6.123 illustrates the numerical and experimental concentrations for aluminum, chromium and titanium with concentration dependent diffusion coefficients $D_{11}, D_{12}, D_{13}, D_{21}, D_{22}, D_{23}, D_{31}, D_{32}, D_{33}$ (second order polynomial) after 500 hours diffusion treatment as shown below:

$$
\begin{aligned}
D_{11} &= x_1 + x_2 C_1 + x_3 C_1^{\,2} + x_4 C_3^2 \\
D_{12} &= y_1 + y_2 C_1 C_2 + y_3 C_2 \\
D_{13} &= z_1 C_2 + z_2 C_2^{\,2} \\
D_{21} &= v_1 C_1 + v_2 C_2 + v_3 C_2^{\,2} \\
D_{22} &= u_1 C_3 + u_2 C_2^2 + u_3 C_2 C_3 \\
D_{23} &= w_1 C_1^2 + w_2 C_3^2 \\
D_{31} &= e_1 C_1 C_3 + e_2 C_3 \\
D_{32} &= f_1 C_3 + f_2 + f_3 C_3 + f_4 C_3 C_1 \\
D_{33} &= g_1 C_1 C_2 + g_2 C_3^2
\end{aligned}
\tag{6.70}
$$

where the values of *D*'s are as follows:

$$
\begin{aligned}
D_{11} &= 2.09332 \times 10^{-11}\, cm^2 / s \\
D_{12} &= 2.494231 \times 10^{-12}\, cm^2 / s \\
D_{13} &= 1.03745 \times 10^{-11}\, cm^2 / s \\
D_{21} &= 0.311910 \times 10^{-12}\, cm^2 / s \\
D_{22} &= 0.03654 \times 10^{-12}\, cm^2 / s \\
D_{23} &= 0.09261 \times 10^{-11}\, cm^2 / s \\
D_{31} &= 0.1924 \times 10^{-11}\, cm^2 / s \\
D_{32} &= 0.9121 \times 10^{-11}\, cm^2 / s \\
D_{33} &= 3.91754 \times 10^{-11}\, cm^2 / s
\end{aligned}
$$

where $C_1, C_2, and\ C_3$ are the initial concentrations for aluminum, chromium and titanium respectively. $x_1, x_2, x_3, \cdots, \cdots, g_1, g_2$ are the polynomial coefficients calculated using Genetic Algorithms optimization method. There were better agreements in the numerical and experimental concentration values for aluminum, chromium and titanium for the entire range of the diffusion distance.

In the following Figure 6.124 the absolute error for the components aluminum, chromium and titanium have been plotted against the number of the components where 1, 2 and 3 belong to the aluminum, chromium and titanium respectively, exactly like we did in Figure 6.121 and 6.122. In this Figure the diffusion coefficient in the whole

diffusion matrix, equation 6.70, has been considered a concentration dependence (second order polynomial).

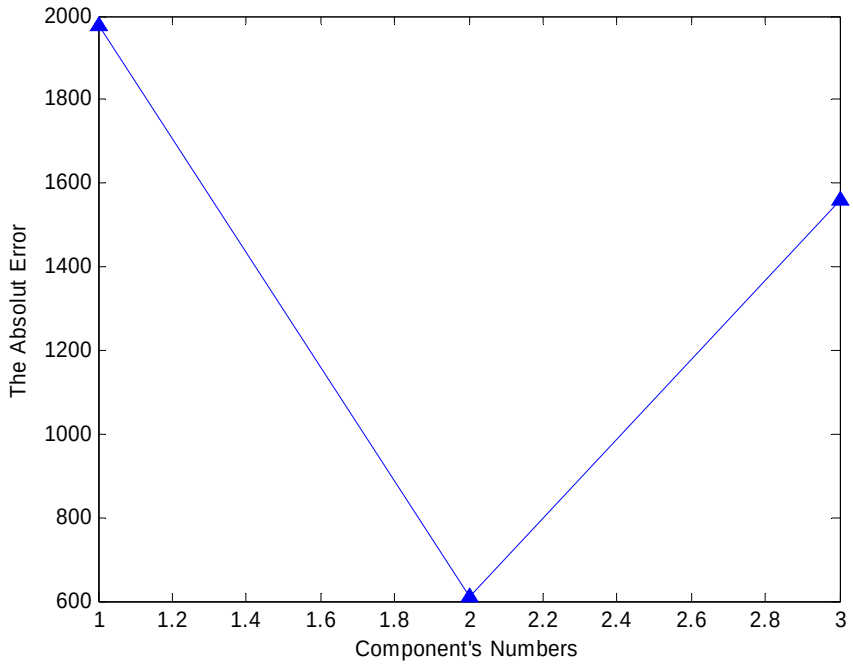

Figure 6.124 The absolute error for the components aluminum, chromium and titanium (whole concentration dependent diffusion coefficient matrix, equation 6.70)

6.9.5.1. Conclusions

The agreement between the numerical and experimental concentration profiles improved when composition dependent diffusion coefficients including the cross terms.

Genetic Algorithms method permits optimization of the values of the coefficients in the second order polynomial (equation 6.70) of diffusion coefficients, in diffusion matrix (equation 6.68). There is good convergence between the experimental and numerical concentration for the components (*Al*, *Cr*, *Ti*) when equation 7.70 was used to calculate the diffusion coefficients, (taking into account the cross terms). The difference between the experimental and numerical concentration profiles for the components (*Al*, *Cr*, *Ti*) has been reduced significantly. It means that the numerical concentration

profiles for aluminum, chromium and titanium) were improved compared with the numerical concentration profiles when the cross terms are considered to be constant. The minimum absolute error was (611.02) in Figure 6.124 while it was (704.97) in Figure 6.123. Therefore there is good convergence between the experimental and numerical concentration for the components (*Al*, *Cr*, *Ti*) when equation 6.70 was used to calculate the diffusion coefficients (concentration dependent diffusion coefficients).

CHAPTER SEVEN

Analysis and Discussion

CHAPTER SEVEN

7. Discussion

7.1. Introduction

Interdiffusion modelling has been the main focus of this thesis. Interdiffusion processes, in selected high performance coatings systems, occurring at elevated temperature during the preparation of the coatings or during subsequent property enhancing heat treatments have been studied and modelled in terms of microstructure evolution (chapter 3 and 6) and using numerical methods (chapter 6). Information on microstructural description / microstructural modelling of the diffusion processes involved in the deposition and heat treatment of coatings has been discussed along with the results on microstructural evolution in chapter 6. This chapter (chapter 7) only present discussion of the results obtained from numerical modelling.

At the outset it is important to note that we are dealing with binary and multicomponent systems. The difficulties in modelling of interdiffusion in multicomponent complex systems cannot be over emphasized.

Numerical modelling of interdiffusion in the systems studied (chapter 3) has been studied using the technique of Genetic Algorithms method combined with the numerical modelling. In addition the fminbnd method combined with the numerical modelling and Simplex search method combined with the numerical modelling have been used to solve and understand the diffusion processes in the Pt-Ni-Al solid alloy ternary system.

Runge-Kutta method of order four is the numerical method which has been used to solve Fick's second law.

In numerical modelling of interdiffusion the first step is to optimise the diffusion coefficient for each component from a range of possible values. Genetic Algorithms

method has been used (for all systems) to optimize the values of the interdiffusion coefficients from these range values. Fick's second law has been used to find the concentration profile for each component using Runge-Kutta method of order four. Then least squares method has been used to compare between these profiles with the experimental data.

Fminbnd method (used only in Pt-Ni-Al solid alloy ternary system) is a combination of the Golden section search method and a polynomial interpolation. The Golden section search is a technique for finding the minimum or maximum of a unimodal function by successively narrowing the range of values. The Polynomial interpolation is the interpolation of a given data set by a polynomial. Given some data points {xi, yi}, the aim is to find a polynomial which goes exactly through these points.

Simplex search method (again used only in Pt-Ni-Al solid alloy ternary system) is described for the minimization of a function of n variables, which depends on the comparison of function values at the (n+1) vertices of a general simplex, followed by the replacement of the vertex with the highest value by another point.

7.2. Nonsteady State Diffusion in Iron Carburized at 950^{o} C, 7.1 Hours

The results presented in Figure 6.5 in chapter 6, section 6.1.4 show carbon concentration wt %, against diffusion distance, obtained using the modified Euler method (Runge-Katta method of order two RK2) (Num. carbon (MEm)), the Runge-Kutta method of order four RK4 (Num. carbon (RKm), and analytically calculated carbon concentration in iron.

From Figure 6.5 giving carbon concentration profiles against diffusion distance after 7.1 hours at 950^{o}C, the following carbon concentrations at 0.5 x10^{-3} m diffusion distance; by different methods have been obtained;

0.8002 wt % C at 0.5×10^{-3} m analytical

0.7832 wt % C at 0.5×10^{-3} m Runge-Katta method of order four

0.6878 wt % C at 0.5×10^{-3} m Modified Euler method

The numerical concentration profiles for carbon derived using Runge-Kutta method of order two and four and analytical method are given in Table 7.1. The agreement between the results obtained from Runge-Kutta method of order four, RK4, and the analytical solution results (concentration profile) validates the numerical method (Runge-Kutta method of order four). This means that the RK4 can be used when the analytical solution is not available.

Least squares method as shown in chapter 4 section 4.5 has been used to calculate the absolute error between the numerical and the analytical concentration profiles. The absolute error between the analytical solution and the numerical solution using modified Euler's method was (0.158) whereas the absolute error between the analytical solution and the numerical solution using Runge-Kutta method of order four was 0.005 (see Table 7.1). The accuracy of the numerical concentration profile has been given as better than $\pm$ 0.1 wt% C using RK4 and $\pm$ 0.3 wt% C using RK2. Therefore there is a clear difference between the results using Runge-Kutta method of order four (RK4) and Runge-Kutta method of order two (RK2). It can be concluded that Runge-Kutta method of order four is more reliable to solve Fick's second law in the carburizing system to calculate the concentration profile for carbon.

Diffusion Distance	Analytical C D(C) =1.61e-11	Numerical C RK2	Numerical C RK4
0.0001	1.1161	1.0886	1.1121
0.0002	1.0332	0.9795	1.0254
0.0003	0.9524	0.8751	0.941
0.0004	0.8744	0.7774	0.86
0.0005	**0.8002**	**0.6878**	**0.7832**
0.0006	0.7304	0.6075	0.7114
0.0007	0.6656	0.537	0.6452
0.0008	0.6061	0.4765	0.585
0.0009	0.5522	0.4256	0.531
0.001	0.504	0.3838	0.483
0.0011	0.4613	0.3501	0.4411
0.0012	0.424	0.3236	0.4049
0.0013	0.3918	0.3031	0.374
0.0014	0.3644	0.2876	0.3479
0.0015	0.3413	0.2761	0.326
0.0016	0.3221	0.2677	0.3078
0.0017	0.3064	0.2617	0.2926
0.0018	0.2936	0.2574	0.2799
0.0019	0.2833	0.2544	0.2689
0.002	0.2752	0.2524	0.2592
		err=0.1587	**err=0.0055**

Table 7.1 Carbon numerical (Runge-Kutta of order 2, RK2, and Runge-Kutta of order 4, RK4), and analytical concentration profiles at 950^{o}C after 7.1 hours diffusion treatments

Table 7.1 shows the absolute errors between the analytical concentration and numerical concentration profiles for carbon using MEm and RKm and they were (0.158), and (0.005) respectively.

7.3. Copper Nickel System after 300 Hours Diffusion Treatment

In this section the nickel diffusion coefficient has been calculated using GAs technique, whereas in chapter 6 section 6.2.4 the Cu diffusion coefficient was calculated using GAs method. $D_{Ni} = 3.715 \times 10^{-10} cm^2 / s$ obtained using GAs method, and in the following Figure 7.2, the nickel numerical and experimental concentration profiles have

been presented. The Ni experimental concentration profile has been calculated from Cu experimental concentration given in Table 6.1 and Figure 6.11 using the equation;

$$C_{Ni} = 100 - C_{Cu} \tag{7.1}$$

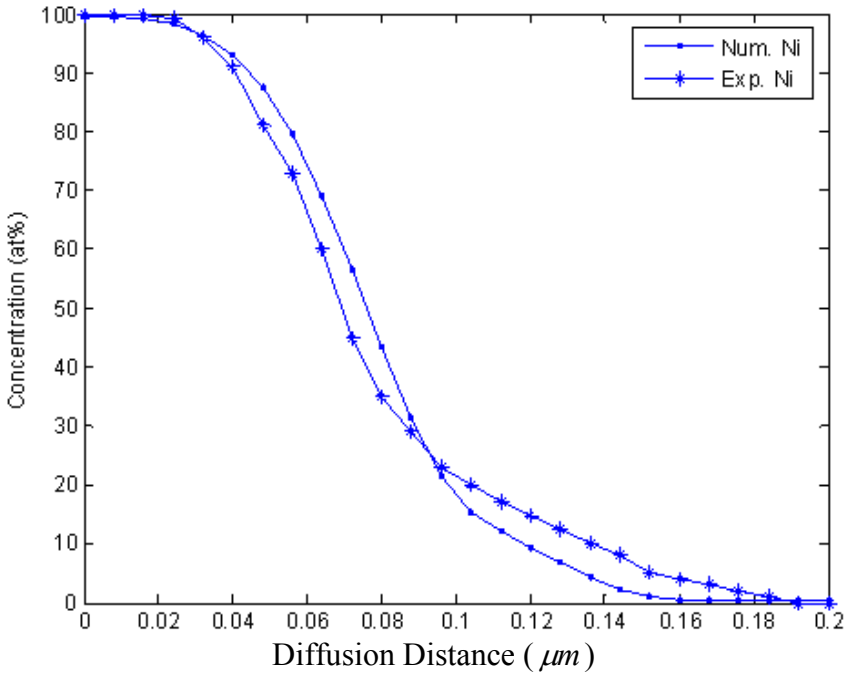

Figure 7.1 Nickel numerical and experimental concentration profiles after 300 h diffusion treatment

Figure 7.1 presents nickel numerical concentration profile after 300 hours diffusion treatments along with the Ni experimental concentration profile. The Cu concentration profile determined experimentally and given in literature [91] has been presented in chapter 6 section 6.3.4.

There is good agreement between nickel experimental and numerical concentration profiles when the diffusion coefficient for nickel has been optimised using GAs technique.

In the next section we will discuss the numerical result for copper component.

One of the uncertainties associated with the techniques that have been used in calculating the diffusion coefficients in this study is the assumption of constant diffusion coefficient.

The maximum difference between the numerical concentration profile using analytical copper diffusion coefficient value $8.35 \times 10^{-10} cm^2/s$ and the experimental concentration profile was 22.5 at% as shown in Figure 7.13, while the greatest difference was 18.60 at% using the GAs optimum diffusion coefficient value (1.54×10^{-10} cm^2/s) for copper given in Figure 7.15. This indicates that the diffusion coefficient value from GAs technique produced improved results.

It is interesting to examine the concentration dependence diffusion coefficient as a function of copper concentration, because the error between the copper experimental and numerical concentration is still obvious. To take into account the concentration dependence of diffusion coefficients, second order polynomial equations with the independent variables (equation 7.23) have been used to calculate the copper diffusion coefficient (given in Figure 7.16) as shown again below for clarification.

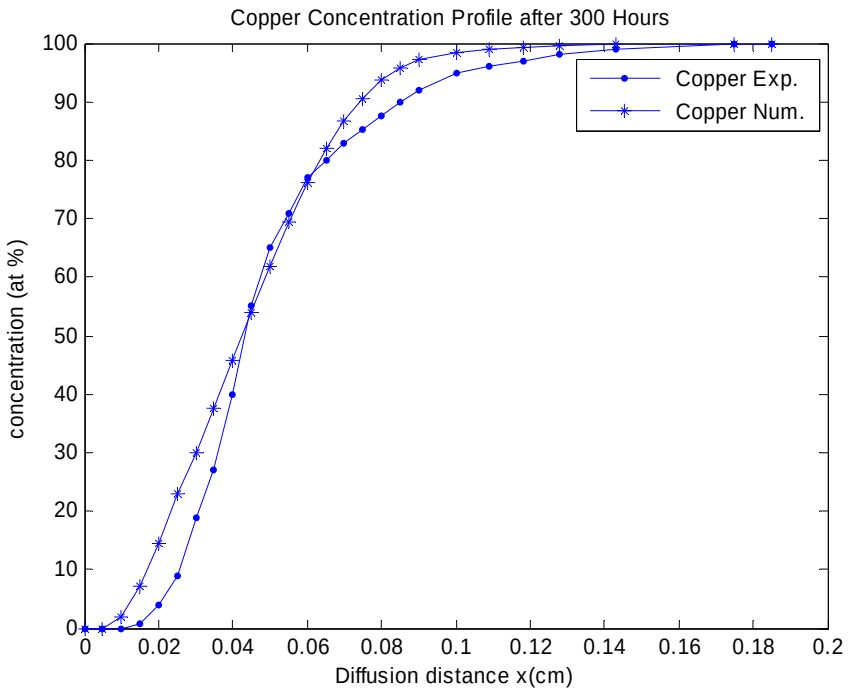

Figure 7.16 Copper numerical and experimental concentration profiles

The highest difference between copper numerical and experimental concentration profiles after 300 hours diffusion treatment at 1054^{o}C was 10.6 at% as shown in Figure 6.17. Therefore using variable diffusion coefficients had decreased the absolute error. Table 7.2 presents the absolute error between the experimental concentration profile and numerical concentration profile for copper component.

	Copper Experimental and Numerical Concentration using $D_{Cu}=8.35x10^{-10}cm^2/s$ (eq. 7.18)	Copper Experimental and Numerical Concentration using $D_{Cu}=1.54x10^{-10}cm^2/s$	Copper Experimental and Numerical Concentration using Variable diffusion coefficient (eq. 7.23)
Maximum Error	22.5	18.6	10.6

Table 7.2 The maximum error values for different diffusion coefficients

To conclude the discussion in this section it is instructive to examine the inverse method of calculation the diffusion coefficient from the concentration profile described in chapter 6 section 6.3.6.

The copper diffusion coefficient which was calculated in section 7.2.6 using inverse method was ($3.3021x10^{-10}cm^2/s$), and the GAs optimum diffusion coefficient was ($1.54x10^{-10}$ cm^2/s) given in chapter 6 section 6.2.4. It is clear that the GAs method is the most suitable method to calculate the diffusion coefficient for each component in the system, as the use of GAs method ensures minimum error.

7.4. *Pt-Ni-Al* Solid Alloy System Containing Three Elements

The first part investigation for this system (three component system) was trial and error technique, and the second part was using Genetic Algorithms method. Figures 6.21 and 6.22 show the numerical and experimental concentration profiles for nickel

and platinum respectively using trial and error technique. There is a divergence between the numerical and experimental concentration profiles for the both components (Ni, Pt) as presented in these Figures, probably because the diagonal terms in the diffusion matrix $\begin{bmatrix} D_{11} & D_{12} \\ D_{21} & D_{22} \end{bmatrix}$ have been considered and the cross terms have been considered to be zero. The other reason because the diffusion coefficients were not optimised using GAs technique. The numerical and experimental concentration profiles using GAs technique for nickel and platinum have been presented in Figures 6.24 and 6.25 respectively. There is an improvement in the numerical concentration profiles using GAs technique for both (Ni and Pt) given in Figures 6.24 and 6.25 compared with the numerical concentration profiles for (Ni and Pt) shown in Figures 6.21 and 6.22 using trial and error technique. Although there is a divergence between the numerical concentration profiles for both components since the cross terms in the diffusion matrix have not been considered so far. In Figure 6.27 the agreement between the experimental concentration and numerical concentration profiles for both the components (Ni and Pt) have been improved compared with Figures 6.24 and 6.25 considering only the diagonal terms in the diffusion matrix , because the cross terms have been taken into account. However small divergence between the experimental and numerical concentration profiles for nickel, (Figure 6.27), in the diffusion distance ranges (0.4-0.9) $x10^{-3}\ \mu m$ and (1.5-2) $x10^{-3}\ \mu m$ because of the smoothness of the nickel numerical concentration profile. The absolute errors between the numerical and experimental concentration for Ni and Pt have been presented in Table 7.3.

The results obtained using variable cross and diagonal terms have been considered in Figure 6.29. Significant enhancement can be seen in the agreement between the experimental and numerical concentration profiles for Ni and Pt using concentration dependence diffusion coefficients (equation 6.37) as shown in Table 7.3.

	Absolute error for nickel	Absolute error for platinum
Trial and Error(const. diago. terms)	2.20E+02	1.75E+02
GAs (const. diago. terms)	2.05E+02	1.68E+02
GAs (const. diago. and cross terms)	1.98E+02	1.53E+02
GAs (variab. diago. and cross terms)	1.75E+02	1.40E+02

Table 7.3 The absolute error between the experimental and numerical concentration profiles for nickel and platinum

Now let us consider the use of fminbnd method to optimise the diffusion coefficient for nickel component, details of this method are given in chapter 5 section 5.6.1. The observed disagreement between the nickel numerical and experimental concentration profiles as shown in Figures 6.31 and 6.32 using the diffusion coefficient calculated from fminbnd can be ascribed to the fact that the initial guess in the diffusion coefficient range was not close to the optimum values. In GAs method the diffusion coefficient range are arbitrarily large range, that is, GAs method has a big advantage to reach the optimum diffusion coefficient whatever was the diffusion coefficient range. In Figures 6.33 and 6.34 the agreement between the numerical concentration profiles for nickel using GAs and fminbnd methods was good because the diffusion range used in fminbnd was very close to the diffusion coefficient value , (accurate range), therefore reaching the optimum diffusion coefficient was possible with very strict condition (perfect range).

The same system has also been modelled using the simplex search method to determine the nickel and platinum diffusion coefficients. The same problem appears in this method Figure 6.35, when the diffusion coefficient range was not the right range,

the disagreement between the experimental concentration profile and numerical concentration profile for nickel and platinum can be clearly seen. Therefore the concord between the experimental concentration profile and numerical concentration profile for nickel can be achieved only when the diffusion coefficient range (initial guess) is close to the optimum diffusion coefficient value.

Table 7.4 compares the values of diffusion coefficients of the components (Pt, Ni, and Al) previously determined by Darken's method in our laboratory [41] with the values determined using GAs with the numerical modelling.

Temperature [K]	D_{Al}	D_{Ni}	D_{Pt}
1273 K Experimental Darken's method [41]	4.19×10^{-10} cm^2/s	2.60×10^{-11} cm^2/s	7.81×10^{-11} cm^2/s
1273 K Numerical	3.001×10^{-10} cm^2/s	4.724×10^{-11} cm^2/s	6.973×10^{-11} cm^2/s

Table 7.4 Calculated and numerical intrinsic diffusivities in the PtNiAl system

The above Table (7.4) shows that D_{Al} calculated by Darken's and GAs methods are about four orders of magnitude larger than the diffusion coefficient in binary system Ni-Al (without platinum).

It is important now to consider the influence of temperature on the diffusion coefficients of the components in solid Pt-NiAl system. The effect of temperature on diffusion coefficients presents valuable information. This effect has been calculated using the following equation:

$$D = D_o \exp\left(-\frac{Q}{RT}\right) \qquad (7.2)$$

where

Q = the activation energy for Diffusion (J/mol)

D_o =a temperature – independent pre-exponential cm^2/s

R =the gas constant 8.314J/mol-K

T =absolute temperature (K)

It has been assumed that Q and D_o do not change with temperature, and the values are in the following Table 8.5;

Element	Q[$kJmol^{-1}$]	Do[cm^2s^{-1}]
Al	223	0.48
Ni	297	50.97
Pt	351	$9.95*10^5$

Table 7.5 The activation energy Q and pre-exponential factor D_o for the diffusion in Pt/β-NiAl system at 1073-1273 K [41]

Table 7.6 presents the calculated diffusion coefficients for the components (Pt, Ni, and Al) using the equation 7.2 for different temperature:

Temperature (K)	D_{Al}	D_{Ni}	D_{Pt}
1073	$6.6903x10^{-12}$	$1.7747x10^{-13}$	$8.1451x10^{-12}$
1123	$2.0360x10^{-11}$	$7.814x10^{-13}$	$4.6953x10^{-11}$
1173	$5.6353x10^{-11}$	$3.031x10^{-12}$	$2.3312x10^{-11}$
1223	$1.4351x10^{-10}$	$1.053x10^{-11}$	$1.015x10^{-10}$
1273	$3.396x10^{-10}$	$3.316x10^{-11}$	$3.9392x10^{-10}$

Table 7.6 Calculated diffusion coefficients for the three components (Al, Ni, and Pt) according to equation 8.2 for various temperatures

Table 7.7 gives the diffusion coefficients for (Al, Ni, and Pt) calculated previously by Datta Fillipek, *et al*. [41]:

Temperature (K)	D_{Al}	D_{Ni}	D_{Pt}
1073	$6.23x10^{-12}$	$2.12x10^{-13}$	$1.48x10^{-13}$
1123	$2.48\ x10^{-11}$	$3.29x10^{-13}$	$1.07x10^{-12}$
1173	$4.64x10^{-11}$	$4.94x10^{-12}$	$6.44x10^{-12}$
1223	$1.04x10^{-10}$	$1.07x10^{-11}$	$1.78x10^{-11}$
1273	$4.19x10^{-10}$	$2.60x10^{-11}$	$7.81x10^{-11}$

Table 7.7 Calculated diffusion coefficients for the three components (Al, Ni, and Pt) for various temperatures

The values in the Tables 7.6 and 7.7 have the same order of magnitude for both aluminum and nickel. For platinum the values in Table 7.7 are smaller than in Table 7.6 one order of magnitude. In spite of differences and limitations improved by assumptions of constant Do and Q, these results are very important.

7.5. Pt-aluminide Multicomponent Coatings on MAR M002 Superalloys

The results on this system presented in chapter 6 section 6.4, are now discussed. As mentioned before this is the most complex multicomponent system studied in this project. In this system the optimum diffusion coefficients have been calculated for the elements in the coating/alloy system using GAs technique. In Figures (6.39- 6.42) the concentration profiles for Ni, Al, Co, and Pt respectively have been presented. There is some deviation between the experimental and numerical concentration profiles for Ni,

Al, and Co in Figures (6.39, 6.40, and 6.41). Attempts have been made to minimize the deviations by inclusion of the cross terms in the diffusion matrix with the two options:

- constant cross and diagonal terms
- variable cross and diagonal terms (second order polynomial has been used for concentration dependent diffusion coefficient calculation)

Figures 6.43 and 6.44 present the concentration profiles for all the components (Ni, Al, Co, and Pt) using constant and variable diffusion coefficients respectively. The absolute error in Figure 6.44 has been improved compared with the absolute error in Figure 6.43 as shown in Table 7.8. It is clear that the agreement between the experimental and numerical concentration profiles for Ni, Al, Co and Pt has been obviously improved using variable diffusion coefficients for the whole diffusion matrix;

$$\begin{bmatrix} D_{11} & D_{12} & D_{13} & D_{14} \\ D_{21} & D_{22} & D_{23} & D_{24} \\ D_{31} & D_{32} & D_{33} & D_{34} \\ D_{41} & D_{42} & D_{43} & D_{44} \end{bmatrix}$$

and this diffusion matrix considered to be concentration dependence (equation 6.43).

	Constant diagonal and cross terms	Variable diagonal and cross terms
Absolute Error	1.208 e+003	860.17

Table 7.8 The absolute errors using constant and variable diffusion coefficients for the components Ni, Al, Pt, and Co

7.6. Discussion of a Critical Issue in Pt - Modified Ni-Al Systems

The critical issue surrounding interdiffusion in Pt-modified Ni-aluminide coating is to examine the influence of Pt on the transport property of Al in Ni-aluminide coatings systems. As stated in section 4.4 the main rationale for incorporating Pt in the Ni-aluminide coating system is to enhance Al diffusion leading to the formation of protective Al_2O_3.

The results obtained in this work can be used to resolve this long standing issue. The first point is to note that in the simple solid Pt-βNiAl ternary system the diffusivity of Al is one order of magnitude higher than those of Ni and Pt in the temperature range (1073-1273K) studied [41], (see Table 7.9 below). To resolve further this issue of enhanced diffusion coefficient of Al through the incorporation of Pt. Table 7.9 giving D_{Al} values obtained from various sources has been completed.

Table 7.9 clearly shows the enhancement of D_{Al} in Pt containing systems. This enhanced Al diffusion can be a factor that is responsible for the protective properties of Pt modified Ni-Al system.

It is also important to note that the diffusivities of Al in Pt-modified β-NiAl coating on MAR M002 and in solid Pt-βNiAl ternary systems are different. These differences probably arose because of the differences in microstructures in the two systems.

Diffusivities (cm^2/s)	Binary system NiAl	Solid system Ni-Al-Pt	Pt-aluminide coating on MAR M002	CrAl2%YN
Al	2.96×10^{-14} [116]	4.19×10^{-10} [41]	2.49×10^{-11}	5.93×10^{-11}

Table 7.9 The diffusion coefficient values for aluminum obtained in various systems

7.7. Discussion on Numerical Results obtained for of Ir and Ir/Pt Low-Activity Aluminid / MAR M002 System

Both the Ir-aluminide and IrPt-aluminide coatings on MAR M002 system have been considered for modelling interdiffusion using GAs technique after 100 hours at 1100^{o}C. Figures 6.51 and 6.52 presented the aluminium numerical and experimental concentration profiles after 100 hours at 1100^{o}C in Ir-aliminide and IrPt-aluminide coatings respectively. In these Figures the diagonal terms have been considered constant and the cross terms have been considered zero. Similarly Figures (6.53-6.58) demonstrated the concentration profiles for Cr, Ir, and Ni in both coatings Ir-aluminide and IrPt-aluminide respectively considering constant diagonal terms. However the results (numerical concentration profiles) were still not satisfactory because the cross terms considered to be zero. In the next parts diffusion modelling was performed using constant terms in the whole diffusion matrixes;

$$\begin{bmatrix} D_{11} & D_{12} & D_{13} & D_{14} \\ D_{21} & D_{22} & D_{23} & D_{24} \\ D_{31} & D_{32} & D_{33} & D_{34} \\ D_{41} & D_{42} & D_{43} & D_{44} \end{bmatrix}, \begin{bmatrix} D_{11} & D_{12} & D_{13} & D_{14} & D_{15} \\ D_{21} & D_{22} & D_{23} & D_{24} & D_{25} \\ D_{31} & D_{32} & D_{33} & D_{34} & D_{35} \\ D_{41} & D_{42} & D_{43} & D_{44} & D_{45} \\ D_{51} & D_{52} & D_{53} & D_{54} & D_{55} \end{bmatrix}$$

for the two coatings Ir and Ir-Pt low activity aluminide on MAR M002 system respectively (Figures 6.60 and 6.63). In Figures 6.66 and 6.68 the whole diffusion matrixes for the two coatings have been considered to be concentration dependent respectively. Considering concentration dependence of D_s the agreement between the experimental and numerical concentration profiles in Figure 6.66 for Ir low-activity aluminide on MAR M002 system has improved compared with the agreement in Figure 6.60, (considering constant diagonal and cross terms). Similarly for Ir/Pt-low activity aluminide on MAR M002 system the agreement has been improved from Figure 6.63 to Figure 6.68. These improvements are explained in the Tables 6.10 and 6.11.

Absolute error	Al	Cr	Ir	Ni
Constant Diagonal terms	1945.3	385.8	544.6	752.1
Constant Diagonal and Cross terms	1680.3	197.6	355.8	327
Variable Diagonal and Cross terms	1383.2	116.7	219.2	94.2

Table 7.10 The absolute error for the components in Ir/aluminide coating on MAR M002 system at 1100^{o}C after 100 hours

Absolute Error	Al	Cr	Ir	Ni	Pt
Constant Diagonal terms	1945.3	385.8	544.6	752.1	351.1
Constant Diagonal and Cross terms	1680.3	197.6	355.8	327	256.7
Variable Diagonal and Cross terms	1383.2	116.7	219.2	94.2	198.3

Table 7.11 The absolute error for the components in IrPt/aluminide coating on MAR M002 system at 1100^{o}C after 100 hours

In Tables 7.10 and 7.11 the absolute errors between the experimental and numerical concentration profiles for the components (Al, Cr, Ir, and Ni), and (Al, Cr, Ir, Ni, and Pt), in Ir/aluminide and IrPt/aluminide coatings respectively have been presented. Therefore when the whole diffusion coefficient matrix considered to be variable (concentration dependent), comprehensible convergence between the experimental and predicted value can be noticed. It can be concluded that the diffusion coefficient of certain component depends on the concentration of the component at each point in the material.

7.8. Aluminise Coating on Low Alloy Steels at 650^{o}C

The diffusion coefficients for aluminum and iron have been calculated using GAs technique. Figures (6.77-6.81) demonstrate Al concentration profiles (numerical and experimental) after 10, 26, 122, 290, and 554 hours diffusion treatments respectively. Similarly Figures 6.83, 6.84 and 6.85 present Fe numerical and experimental concentration profiles after 10, 26, and 122 hours diffusion treatments. However in these Figures only the diagonal terms from the diffusion matrix;

$$\begin{bmatrix} D_{11} & D_{12} \\ D_{21} & D_{22} \end{bmatrix}$$

have been considered constant and the cross terms considered to be zero. Therefore the divergence between the experimental and numerical concentration profiles for both (Al, Fe) can be seen for some diffusion distance in Figures (6.77-6.79) and (6.83-6.85) respectively.

In the second part of modelling interdiffusion for this system (section 6.6.6) the whole diffusion matrix has been considered to be constant, and in Figures (6.87,6.88, and 6.89) the concentration profiles for (Al, Fe) have been shown after 10, 26, and 122

hours diffusion treatment respectively. The numerical concentration profiles for Al and Fe have been converging to the experimental concentration profile since the cross terms have been taken into account. Although some divergence can still been seen in the ranges (3.5-5.5) μm diffusion distance for Al in Figures 6.87 and 6.88, and in (2.5-5) μm diffusion distance for Fe in Figure 6.87 because of considering constant terms in the diffusion matrix.

The last part of this investigation was to look upon the composition dependence diffusion coefficient. First, second and third order polynomial (equations 6.58, 6.59, and 6.60 respectively) for concentration dependence diffusion coefficients have been considered. The results (concentration profiles for Al and Fe) have been presented in Figures 6.90, 6.91, and 6.92 respectively after 10 hours diffusion treatment. The numerical concentration profile for Fe after 10 hours diffusion treatment have shown good convergence and small divergence for Al in the range (3.8-5) μm diffusion distance when the second order polynomial (equation 6.59) has used, since the order two can be considered as a standard number to use, and maybe the accumulative error could be smaller with the second order polynomial.

7.9. Al_2Au and TiAlCrY Coated Ti45Al8Nb Subjected to Air Oxidation at 750°C for 1000 Hours (Al_2Au Coatings) and 500 Hours (TiAlCrY Coatings)

From the results (the numerical concentration profiles for aluminum) obtained in sections 6.7.3 and 6.8.3, the optimum diffusion coefficients for aluminum are (determined by GAs method):

$D_{Al}=3.10\times10^{-12}\,cm^2/s$ and $D_{Al}=0.12\times10^{-11}\,cm^2/s$

in the Al_2Au and TiAlCrY respectively coated Ti45Al8Nb, considering only diagonal constant terms in the diffusion matrix (Figures 6.101 and 6.116).

There were good agreements between the experimental and numerical concentration profiles for aluminum in the substrate for both coatings (due to the aluminum outward diffusion).

For (titanium, gold) and (titanium, chromium) components in both (Al_2Au and TiAlCrY) coated Ti45Al8Nb respectively the following Table 7.12 includes the diffusion coefficients for all the components in both coatings:

Al_2Au coating	D_{Al}	D_{Ti}	D_{Au}
Constant Diagonal terms	$3.10\text{x}10^{-12}$ cm^2/s	2.6×10^{-12} cm^2/s	1.01×10^{-11} cm^2/s
TiAlCrY coating	D_{Al}	D_{Ti}	D_{Cr}
Constant Diagonal terms	0.12×10^{-11} cm^2/s	$0.16\text{x}10^{-11}$ cm^2/s	$5.61\text{x}10^{-12}$ cm^2/s

Table 7.12 Calculated diffusion coefficients for the components in both coatings Al_2Au and TiAlCrY

Figures 6.107, 6.108 and 6.111, (the absolute error against the component's number), show the development of the agreement between the experimental and numerical concentration profiles for the components Al, Au, Ti, and Nb in Al_2Au coated Ti45Al8Nb. The maximum error in Figure 6.107 was over 9000 for titanium while in Figure 6.108 was just over 5500 for the same component (Ti) when the whole diffusion matrix;

$$\begin{bmatrix} D_{11} & D_{12} & D_{13} \\ D_{21} & D_{22} & D_{23} \\ D_{31} & D_{32} & D_{33} \end{bmatrix}$$

was considered to be constant, and in Figure 6.111 the maximum error was just above 4000 when the whole diffusion matrix considered to be variable (concentration dependence diffusion coefficients). The same improvement of the agreement between the experimental and numerical concentration profiles for the components Al, Cr, and Ti can be seen for the other coating TiAlCrY on Ti45Al8Nb in Figures 6.121, 6.122, and 6.124 for constant diagonal terms, constant diffusion matrix, and variable diffusion matrix (concentration dependent) respectively.

Therefore the significant point has been observed from studying the above systems (Al_2Au and TiAlCrY coated Ti45Al8Nb**)** using GAs technique to optimise the diffusion coefficients for each component as follows:

The agreement between the experimental and numerical concentration profiles was the most substantial when the complete diffusion matrix with concentration dependent diffusion coefficients (second order polynomial) have been considered. The second order polynomials are the equations 6.65 and 6.70 in sections 6.7.5 and 6.8.5 for the coatings Al_2Au and TiAlCrY on Ti45Al8Nb respectively.

7.10. Examination of the Feasibility of Applying A Transfer Matrix Method for the Solution of Interdiffusion and Calculation of Concentration Profiles in the Present Work

This section discusses the solution of diffusion problems and calculation of concentration profiles using an alternative technique. It is considered appropriate to include this method in the discussion chapter.

A transfer matrix method was presented for the development of solutions for multi-component diffusion couples containing number of components by Ram-Mohan *et al*

[117]. Expressions were derived for the transfer matrix and its integral; consequently the interdiffusion fluxes and concentrations of all components can be determined at any section in the diffusion zone from the initial values of either interdiffusion fluxes or concentration gradients available at some other section. This method used interdiffusion coefficients evaluated as average values over various regions of the diffusion zone.

The efficacy of this method has been examined in this work.

In the following section 7.8.1 the concentration profiles for the independent components (Ni and Pt) in the ternary system (NiPtAl) have been explained using the diagonalization technique for the diffusion matrix.

7.10.1. Diagonalization the Diffusion Matrix (Transfer Matrix)

In this section the diffusion matrix for the ternary system (NiPtAl) has been considered to be a 2x2 matrix, as nickel and platinum components have been considered to be independent components and the third component (aluminum) has been considered to be the dependent component (see section 6.3). So the diffusion matrix becomes a 2x2 matrix:

$$\begin{bmatrix} D_{11} & D_{12} \\ D_{21} & D_{22} \end{bmatrix} \tag{7.4}$$

Using the GAs method in section 6.3.4 equation 6.36, all the D terms have been determined as given below:

$$\begin{aligned} D_{11} &= 4.594001\times10^{-11} cm^2/s \\ D_{12} &= 2.494231\times10^{-11} cm^2/s \\ D_{21} &= 0.700810\times10^{-11} cm^2/s \\ D_{22} &= 3.193216\times10^{-11} cm^2/s \end{aligned} \tag{7.5}$$

The diagonalization of the above matrix led to:

$$\begin{bmatrix} D^*_{11} & \\ & D^*_{22} \end{bmatrix} \tag{7.6}$$

Where D^*_{11} and D^*_{22} have been calculated analytically using the eigenvalues and eigenvectors as follows:

$$\begin{aligned} D^*_{11} &= 9.3886 \times 10^{-11} cm^2/s \\ D^*_{22} &= 2.3989 \times 10^{-11} cm^2/s \end{aligned} \tag{7.7}$$

In the following Figure 7.2 the numerical and the experimental concentration profiles for the components nickel and platinum have been presented:

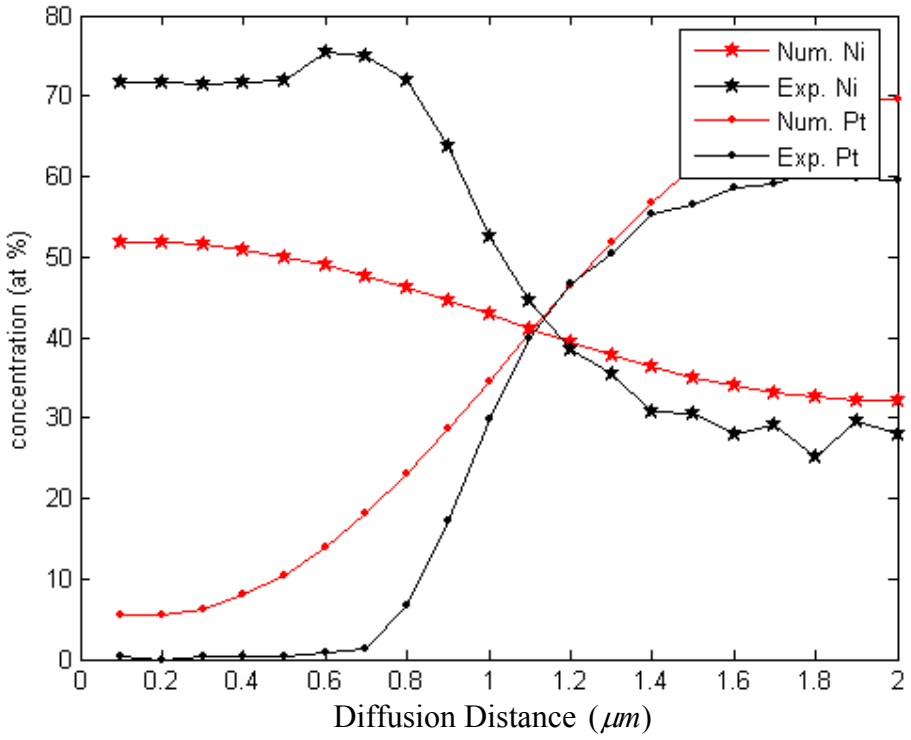

Figure 7.2 Nickel & platinum concentration profiles after 1 hour diffusion treatment at 1273 K with diagonalizable the diffusion matrix

In Figure 7.2 the diffusion matrix (equation 7.4) has been diagonalized to obtain the diagonal terms D^*_{11} and D^*_{22}, (equation 7.6, which represents the diffusion coefficients for nickel and platinum respectively).

The red stars show the calculated concentration profile for nickel and the black stars give the experimental concentration profile for nickel. The red and the black points show the calculated and experimental concentration profiles for platinum respectively. Disagreement exists between the nickel numerical concentration profile using equation 7.6 and the experimental concentration profile, although there is an agreement between the platinum numerical concentration profiles calculated using equation 7.6 and the experimental concentration profile. This agreement is for (1-1.4) $\times 10^{-3}\,\mu m$ diffusion distance.

Figure 7.3 presents the aluminum concentration profile calculated from the equation;

$$C_1+C_2+C_3=100\% \qquad (7.8)$$

where C_1, C_2, C_3 are the numerical nickel, platinum, and aluminium concentration profiles respectively, So the numerical Al concentration ;

$$C_3=100\% - (C_1+C_2) \qquad (7.9)$$

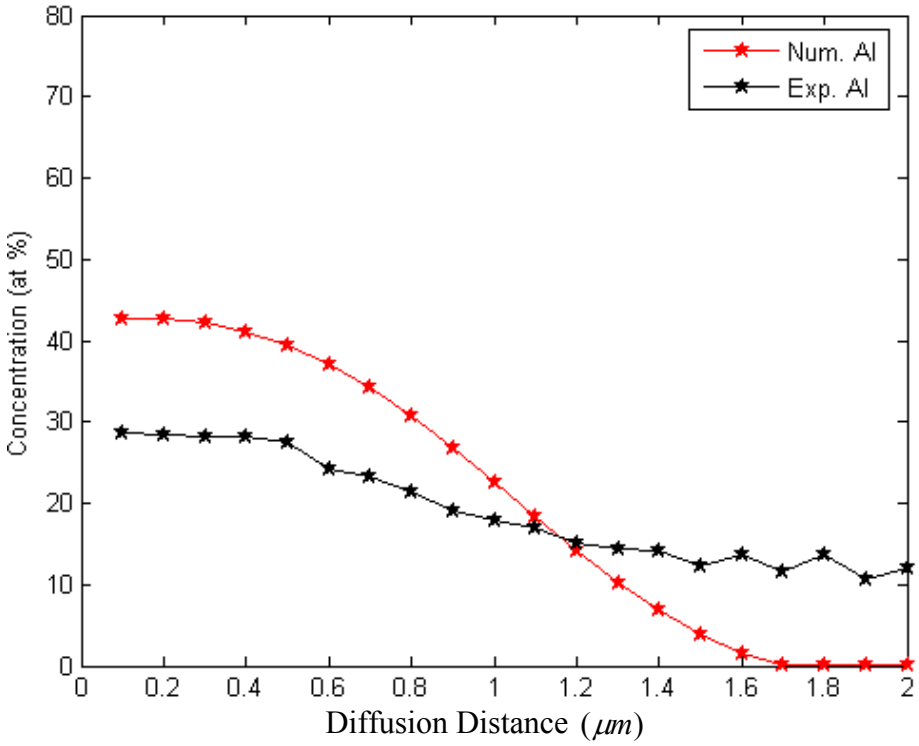

Figure 7.3 Aluminum concentration profiles after 1 hour diffusion treatment at 1273 K

Figure 7.3 shows the aluminum concentration profiles after 1 hour diffusion treatment. Again a divergence between the aluminum experimental concentration and the calculated concentration profiles using equation 7.9 is seen.

7.10.1.1. Conclusions

The diffusion matrix (equation 7.4) has been transferred into diagonal matrix (equation 7.6), using the mathematical method. Figure 7.4 shows the concentration profiles for nickel and platinum using equation 7.6. There is a divergence between the experimental concentration profiles and numerical concentration profiles for both nickel and platinum; while in Figure 6.27 better agreement can be observed between the numerical concentration profiles and experimental concentration profiles for both nickel

and platinum using the constant whole diffusion matrix D values calculated from GAs method (equation 7.5). Figure 6.27 is presented below for clarification. Thus the Genetic Algorithms optimization method until now is the superior way to optimize the diffusion coefficients for the components in any system. Consequently the transfer matrix method [117] is not suitable to determine the numerical concentration profiles for nickel and platinum compared with the Genetic Algorithms method.

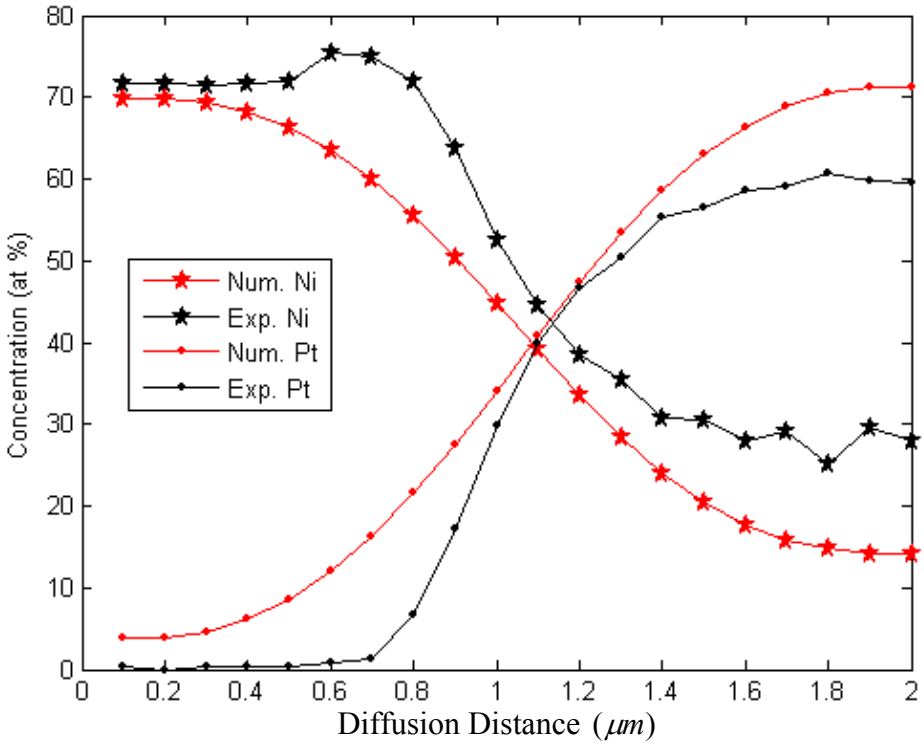

Figure 6.27 Nickel and platinum concentration profiles after 1 hour diffusion treatment (constant cross and diagonal terms) using equation 7.5

7.11. Life Time Modelling

7.11.1. Calculation of Life-time of (TiAlCrY) Coating Deposition on Ti45Al8Nb using Concentration Profiles Simulation of Critical Elements by Interdiffusion Modelling

This subsection presents the results on life-time calculation of TiAlCrY coating studied in this research. In calculating the life-time of this coating it has been assumed that only high temperature oxidation controls the life-time and the most important factor in governing the life-time is the formation of Al_2O_3 from the oxidation of Al. Thus Al is the critical element and its concentration profile determines its ability to form Al_2O_3.

Regarding the formation Al_2O_3 the following observation has been made:

The lifetime modelling was performed on the basis of Interdiffusion modelling which used a numerical optimisation method as discussed in chapter 4.

Briefly the concentration profiles of the critical elements have been calculated using Runge – Kutta method with Genetic Algorithms technique. In calculating the life–time of TiAlCrY coating, it has been assumed that the critical element in this coating is Al, and between 0 and 20 at% there is no possibility to form protective Al_2O_3 oxide scale. When the concentration of aluminium is around 25 at% the formation of Al_2O_3 is possible [118]. Therefore the higher concentration of Al (over 25 at %) reflects formation of an alumina sub layer in the oxide scale, which protects against high temperature oxidation.

7.11.2. Background Information Underpinning the Life-time Calculation

In the formation of Al_2O_3 further assumptions have been made:

1. Oxidation and diffusion mechanism and model parameters do not vary with time.
2. The oxide scale formation occurs at the boundary x_1.
3. The diffusion coefficients of the Al alloying element D_{Al} are constant.

Figure 7.4 shows a cross – sectional image of as deposited TiAlCrY coated Ti45Al8Nb

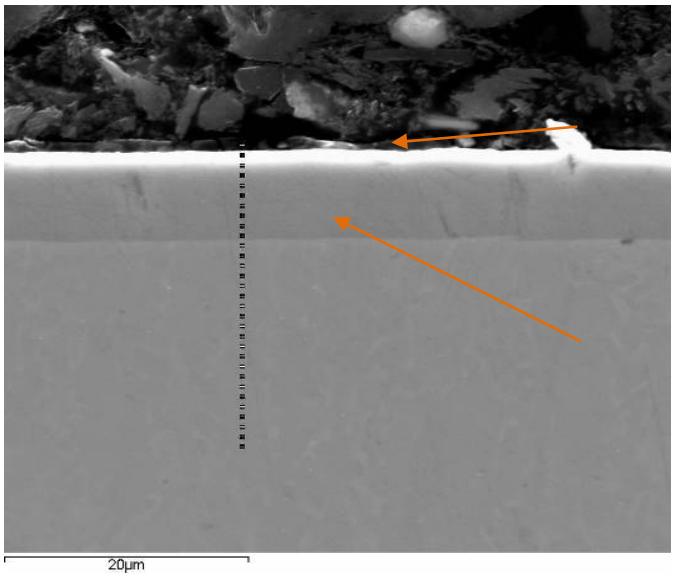

Figure 7.4 as deposited TiAlCrY coated Ti45Al8Nb alloy

Figure 7.5 shows a cross – sectional EDS concentration profiles performed on oxidised TiAlCrY coated Ti45Al8Nb alloy after 500 hours oxidation at 750^{o}C

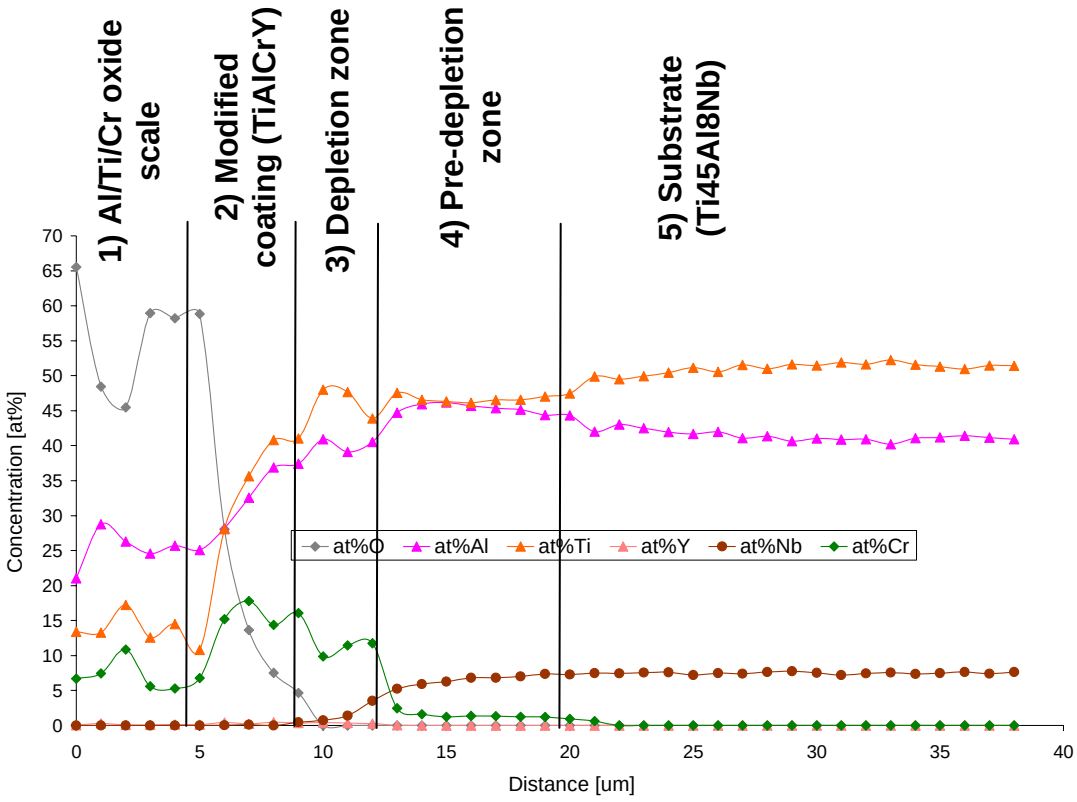

Figure 7.5 EDS concentration profiles obtained from TiAlCrY coated Ti45Al8Nb alloy after 500 hours of oxidation at 750^{o}C (1023 K)

The model of the material degradation after 500 hours at 750^{o}C is shown below:

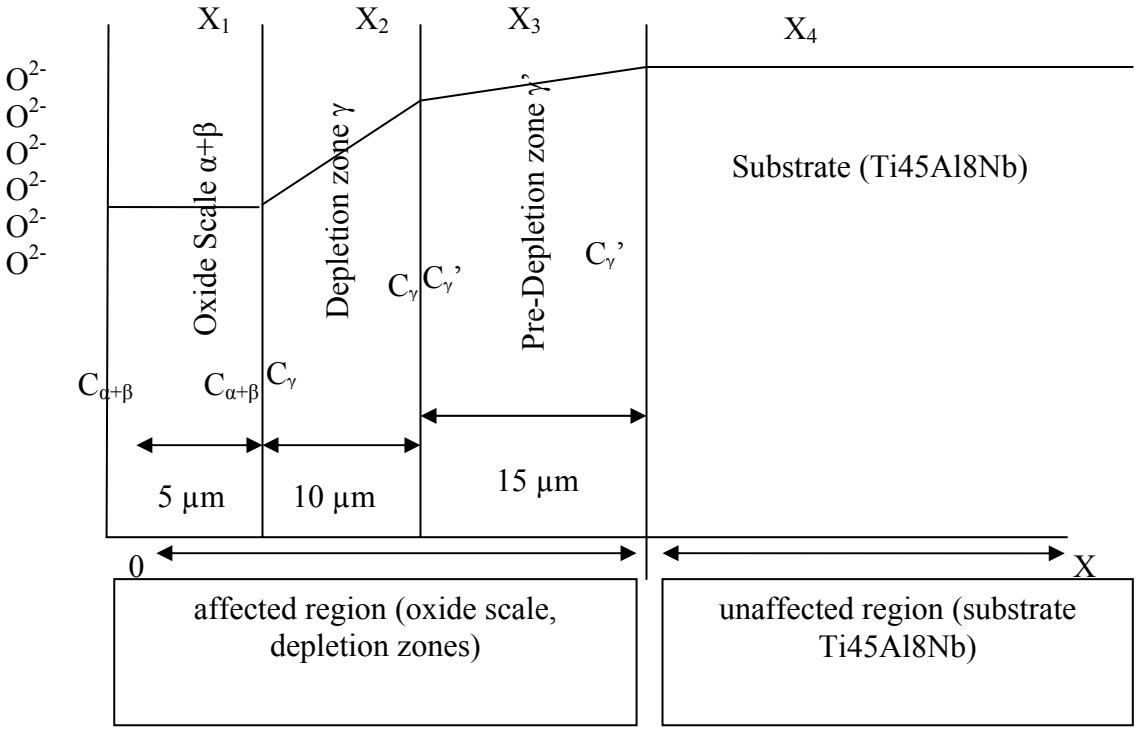

Where:

α – Al_2O_3 phase

β – TiO_2 phase

γ - depletion zone of Al and Ti

γ' – pre-depleted zone of in the substrate near to the scale/alloy interface, the pre-depleted zone of Ti ions is related to the faster diffusion of Ti ions in the bulk material, an increase of Al concentration in pre-depleted zone.

$C_{\alpha+\beta}$ – average concentration of phase α and β

X_1, X_2, X_3 and X_4 – regions of different concentration and different mass transport in the system

Figure 7.6 shows a cross – sectional EDS concentration profiles performed on oxidised TiAlCr coated Ti45Al8Nb alloy after 5000 hours oxidation at 750^{o}C

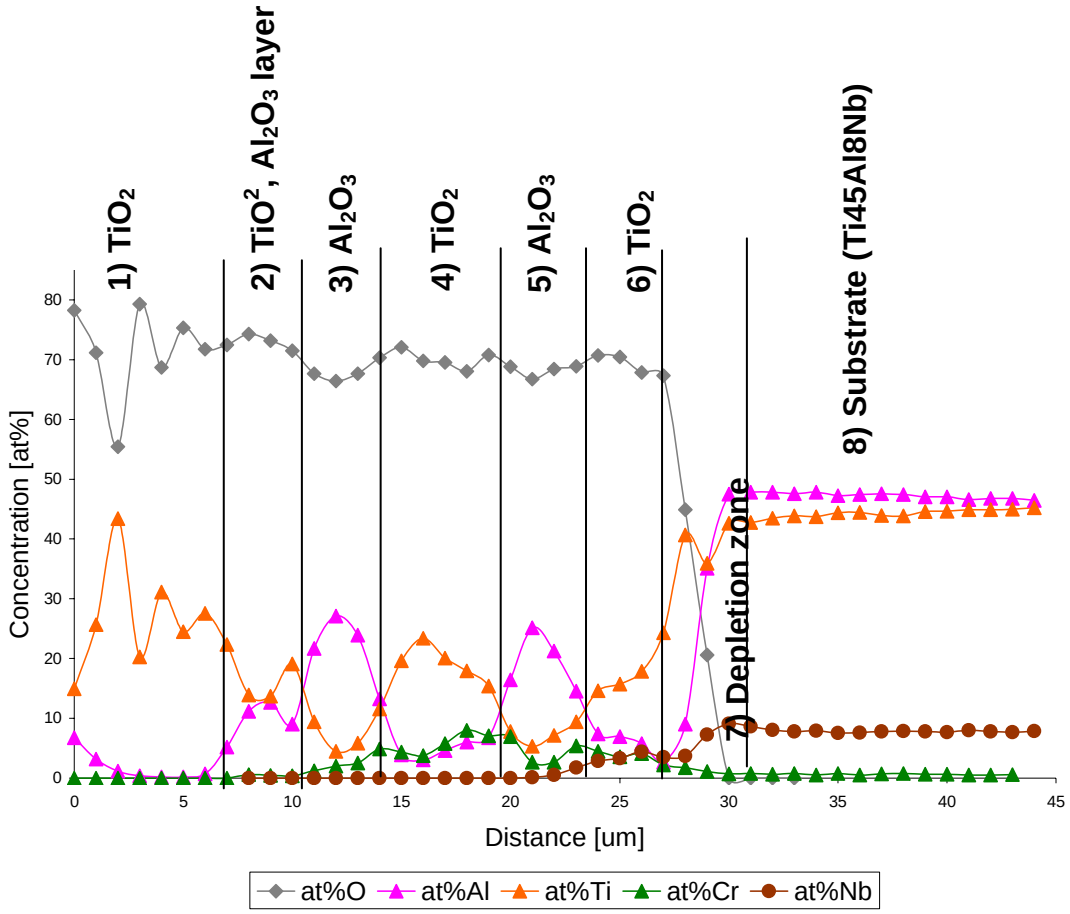

Figure 7.6 EDS concentration profiles obtained from TiAlCr coated Ti45Al8Nb alloy after 5000 hours of oxidation at 750°C (1023 K)

Figure 7.7 shows a mass transport diagram through the oxide scale developed on TiAlCrY –coated Ti45Al8Nb alloy after 5000 hours of oxidation at 750°C

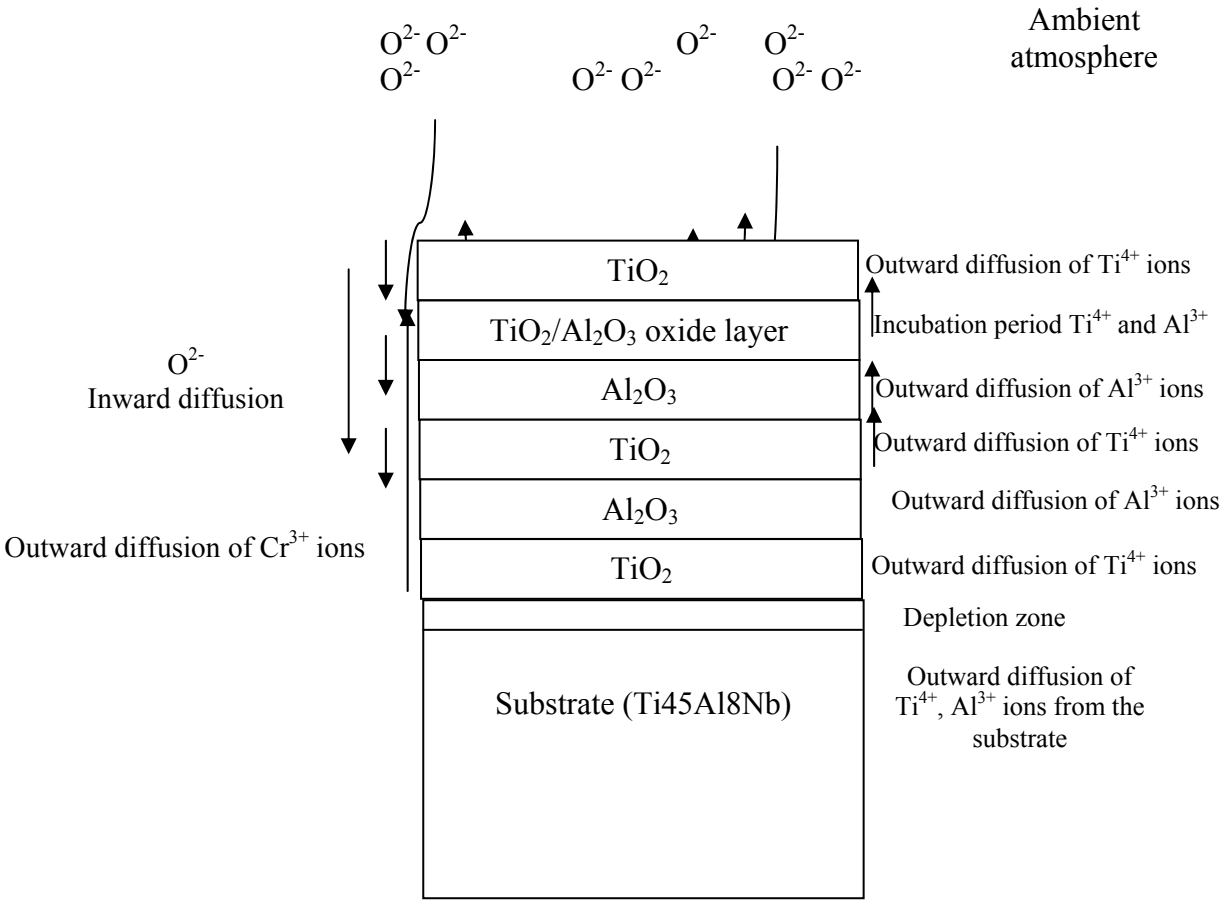

Figure 7.7 Schematic diagram of the oxidation mechanism and scale development on TiAlCr coated Ti45Al8Nb after 5000 hours oxidation at 750^{o}C

Schematic model of the degradation of TiAlCr coated Ti45Al8Nb after 5000 hours oxidation at 750^{o}C is presented:

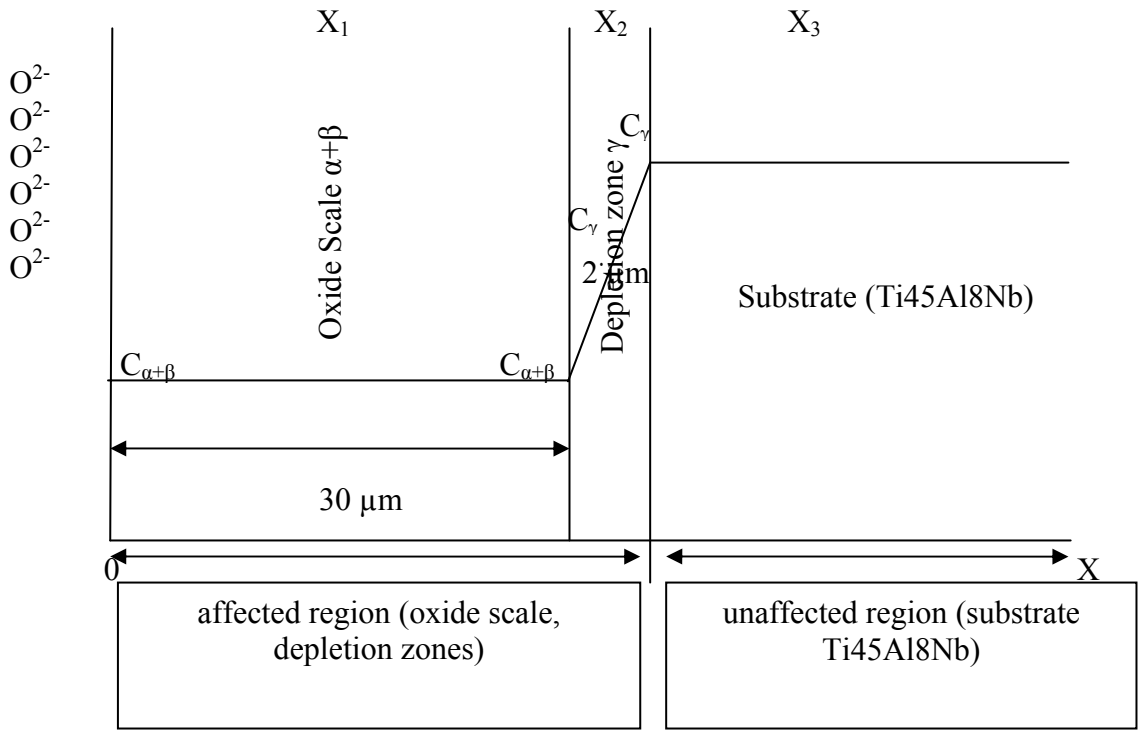

Figure 7.8 Schematic model of degradation of TiAlCrY after 5000 hours of oxidation at 750^{o}C

Where:

α – Al_2O_3 phase

β – TiO_2 phase

γ - depletion zone of Al and Ti

γ' – pre-depleted zone of in the substrate near to the scale/alloy interface, the pre-depleted zone of Ti ions is related to the faster diffusion of Ti ions in the bulk material, an increase of Al concentration in pre-depleted zone.

$C_{\alpha+\beta}$ – average concentration of phase α and β

X_1, X_2, and X_3, – regions are different concentration and different mass transport in the system.

7.12. Lifetime Prediction by Interdiffusion Modelling

Figure 7.9 shows interdiffusion modelling of Al concentration after 5000 hours oxidation at 750°C

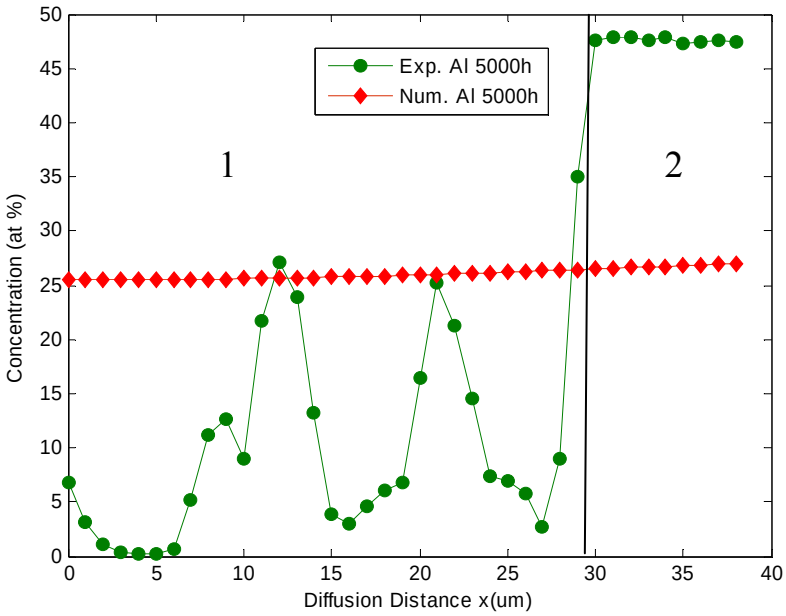

Figure 7.9 Aluminum concentration profiles of interdiffusion modelling performed on TiAlCrY coated Ti45Al8Nb alloy after 5000 hours of oxidation at 750C

Modelling curve (red line) shows good agreement with experimental data obtained for oxidised sample at 750°C, at the atmosphere/oxide scale interface and scale/substrate interface. The following regions are:

1) Oxide scale

2) Substrate

However the numerical concentration profiles of Al decreased to 26 at% which is near to the critical concentration which allows the development of Al_2O_3 oxide. Figure 8.10 shows Al numerical concentration profiles after 5000, 8500 and 10000 hours oxidation at 750°C.

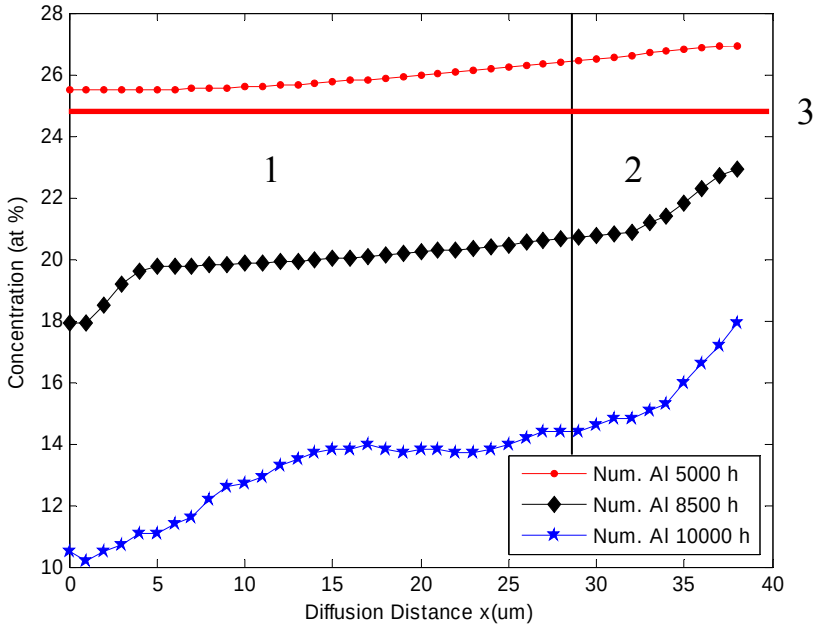

Figure 7.10 The concentration profiles of interdiffusion modelling performed on TiAlCrY coated Ti45Al8Nb alloy after 5000, 8500 and 10000 hours of oxidation at 750^{o}C

The following regions indicate:

1) Oxide scale

2) Substrate

3) Critical level of Al

Figure 7.10 shows Aluminium numerical concentration profiles and prediction of development Al_2O_3, the red thick line designates the critical concentration of Al which allows formation of Al_2O_3 protective scale according to Welsch [118]. Under this level as modelling curves indicate (8500 and 1000 hours) that the concentration profile of Al is not enough to develop protective Al_2O_3 oxide scale. Thus life-time modelling performed for TiAlCrY coated Ti45Al8Nb alloy shows that the life-time of this coating is correspondent to 5000 hours at 750^{o}C. At higher temperatures 800, 850^{o}C the life-time will be reduced, due to the faster diffusion processes.

7.12.1. Conclusions

The life time of the deposited coatings on Ti45Al8Nb with modelling studies was studied. The following remarks are postulated:

1) TiAlCrY coating after 5000 hours oxidation developed multilayered scale consisted of TiO2 and Al_2O_3 alternative layers

2) Life-time predication for TiAlCr coating was estimated using Interdiffusion Modelling Studies performed by Genetic Algorithm Method.

3) Life-time of TiAlCrY coating is equivalent to 5000 hours at 750^oC.

CHAPTER EIGHT

Conclusions and Suggestions for Further Work

CHAPTER EIGHT

8.1. Conclusions and Suggestions for Future Work

This chapter summarises the main conclusions from the work undertaken in this thesis. Additionally some suggestions for future work are included.

8.2. Conclusions

8.2.1. Some General Points

The systems considered for (microstructural and numerical) diffusion modelling included:

1. Iron carburized at 950^{o}C for 7.1 hours;
2. A copper-nickel diffusion couple subjected to 300 hours of treatment at temperature 1054^{o}C;
3. Three component $Pt-Ni$ - aluminide system subjected to diffusion anneal at 1273K for 1 hour;
4. Multicomponent $Pt-Ni$ -aluminide coatings on MAR M002 subjected to 150 hours of diffusion treatment at temperature 1273K;
5. *Ir* and *IrPt* low-activity aluminide / MAR M002 system subjected to 100 hours of diffusion treatment at temperature 1100^{o}C;
6. Four component $TiAlCrY/TiAl$ system (subjected to oxidation at 750^{o}C for 500 hours), $Al_2Au/TiAl$ (subjected to oxidation at 750^{o}C for 1000 hours),
7. Formation of aluminised coatings on low alloy steels at 650^{o}C.

Numerical technique with Genetic Algorithms (GAs) for optimising diffusion coefficients Ds has been used. The GAs method has been applied to optimise the diffusion coefficients for each component in each system studied. The numerical technique used was Runge-Kutta method of order four to solve Fick's second law to find the concentration profile for each component in each system studied. The experimental and numerical concentration profiles have been compared using the Least squares method.

The strategy used in the numerical technique involved the following steps:

- constant diagonal terms;
- all constant terms (diagonal and cross terms in the diffusion matrix);
- all variable terms (diagonal and cross terms in the diffusion matrix).

First second and third order polynomial have been considered for concentration dependence diffusion coefficient.

Where possible microstructural description of the diffusion processes involved has been considered, explained and discussed constituting the microstructural modelling.

8.2.2. Iron Carburized at 950^{o}C for 7.1 Hours

The numerical methods that have been used in this system were Runge-Kutta method of order four and order two using the carbon diffusion coefficient ($1.6\times10^{-11} m^2/s$) determined analytically. Very good agreement between carbon analytical and numerical concentration profiles using Runge-Kutta method of order four as shown in Figure 6.5 (carbon numerical and analytical concentration profiles after 7.1 hours diffusion treatment at 950^{o}C). RK method of order two did not yield the desired agreement. As shown in Figure 6.5 the carbon concentrations at 0.5 x10^{-3} m diffusion distance that have been obtained by different methods are given below:

0.8002 wt % C at 0.5 x10^{-3} m analytical

0.7832 wt % C at 0.5 x10^{-3} m RK method of order four

0.6878 wt % C at 0.5 x10^{-3} m RK method of order two

8.2.3. Copper-Nickel Diffusion Couple after 300 Hours Diffusion Annealing

Darken's equations (equations 6.11 and 6.14) have been used to calculate copper and nickel diffusion coefficients. The copper analytical diffusion coefficient (8.35x10^{-10} cm^2/s) has been used to calculate the copper concentration profiles using Runge-Kutta method of order four. However some divergence between the numerical and experimental concentration profiles for copper occurred. In order to decrease the maximum error (22.514) between the experimental and numerical concentration profiles for copper, GAs method has been used to optimize the copper constant diffusion coefficient. The maximum error (18.61) has been decreased but still there remained some divergence between the copper experimental and numerical concentration profiles. Therefore variable diffusion coefficients were considered in this step as shown in equation 6.23. The agreement between the experimental and numerical concentration profiles for copper was very good (the maximum error was 10.61) for the entire range of diffusion distance (0-0.2cm) when second order polynomial has been used for the copper concentration dependence diffusion coefficient.

8.2.4. Pt-*Ni-Al* Solid Alloy System Containing Three Elements Subjected to Diffusion Annealing at 1273K for 1 Hour

Trial and error technique was used to calculate the diffusion coefficients of nickel and platinum components ((D_{Ni}=4.7241x10^{-11}, D_{Pt}=6.973241x10^{-11}) *cm2/s*) of the

sample. Figures 6.21 and 6.22 show reasonable agreement (see Table 7.3) between the experimental and numerical concentration profiles for nickel and platinum respectively; Table 7.3 gives the absolute error between the experimental and numerical concentration profiles for nickel and platinum). In Figures 6.24 and 6.25 for nickel and platinum respectively the differences between the experimental and numerical concentration profiles were reduced using the optimum constant diagonal diffusion coefficients (D_{11}, D_{22}) for nickel and platinum determined using GAs method, D_{11}, D_{22} are as follows:

$D_{Ni} = 6.7619 \times 10^{-11} cm^2 / s$, D_{Pt}=3.38712x$10^{-11} cm^2/s$

Further good agreement was obtain between the numerical and experimental concentration profiles for nickel and platinum when all the terms (though constant) in the entire diffusion matrix $\begin{bmatrix} D_{11} & D_{12} \\ D_{21} & D_{22} \end{bmatrix}$ were considered. This diffusion matrix has given below:

$D_{11} = 4.5940 \times 10^{-11} cm^2 / s, D_{12} = 2.49423 \times 10^{-11} cm^2 / s, D_{21} = 0.7008 \times 10^{-11} cm^2 / s$
$D_{22} = 3.193216 \times 10^{-11} cm^2 / s.$

Further improved agreement was achieved using variable diffusion coefficient (second order polynomial equation 6.37) for the whole diffusion matrix;

$D_{11} = 1.3497 \times 10^{-11} cm^2 / s, D_{12} = 1.0013 \times 10^{-11} cm^2 / s, D_{21} = 0.1451 \times 10^{-11} cm^2 / s$
$D_{22} = 4.3519 \times 10^{-11} cm^2 / s$

In the whole range of temperature 1073-1273 K the aluminum diffusion coefficient determined using GAs and Darken's methods (Table 7.4) is approximately one order if magnitude higher than the diffusion coefficients of nickel and platinum. These results show that the fast diffusion of aluminum in PtNiAl alloy system can be a factor that is responsible for the very good protective properties of the platinum-aluminde coatings on superalloys.

8.2.5. Nickel-Aluminide and Platinum-Aluminide Coatings on MAR M002 Subjected to 150 Hours of Diffusion Treatment at Temperature 1273K

The Genetic Algorithms method allowed optimization of the values of diffusion coefficients, in the diffusion matrix. Only the constant diagonal terms in the diffusion matrix were used to calculate the concentration profiles for Ni, Al, Co, and Pt. These D values were as follows:

$D_{Ni} = 12.368 \times 10^{-13} cm^2 / s,\ D_{Al} = 5.9181x10^{-13} cm^2 / s, D_{Co} = 3.6412 \times 10^{-13} cm^2 / s$

$D_{Pt} = 8.0297 \times 10^{-13} cm^2 / s$

As expected there was a divergence between the experimental and numerical concentration profiles for these components. Further improvements occurred considering the cross terms in the diffusion matrix as shown in Figure 6.43 (the numerical and experimental concentration profiles after 150 hours of diffusion annealing for all the components Co, Ni, Al, and Pt with constant diffusion coefficients). The absolute error for the entire components was 1.2089e+003 when the whole diffusion matrix was constant.

Still better agreements were found when the diffusion matrix was considered concentration dependent as shown in Figure 6.44 (the numerical and experimental concentrations after 150 hours of diffusion annealing for all the components Co, Ni, Al, and Pt with variable diffusion coefficients(equation 6.43). The absolute error for these entire components was 860.1731.

8.2.6. Ir and Ir/Pt Low-Activity Aluminide / MAR M002 System Subjected to 100 Hours of Diffusion Treatment at Temperature 1100^{o}C

The agreements between the experimental and numerical concentration profiles for Al, Cr, Ir and Al, Cr, Ir, Pt in Ir and Ir/Pt low-activity aluminide coatings respectively on MAR M002 were improved from considering constant diagonal terms in the diffusion matrix to include constant cross terms in the diffusion matrix and finally considering the variable diffusion matrix. Therefore when the whole diffusion matrix was considered concentration dependent the agreements between the numerical and experimental concentration profiles for these components considerably improved.

For the *Ir*-aluminide coating, the *Ir*-rich layer was contained the substrate elements-*W*, *Ta*. While for the *Ir-Pt* aluminide coatings the substrate elements were excluded from the coating. The XRD analysis showed that the outer layers of the systems had a structure similar to that of β-NiAl.

8.2.7. Four Component Systems – TiAlCrY/TiAl System (Subjected to Oxidation at 750^{o}C), Al_2Au/TiAl (Subjected to Oxidation at 750^{o}C) and Formation of Aluminised Coatings on Low Alloy Steels at 650^{o}C

The agreement between the experimental and numerical concentration profiles improved progressively using the following conditions:

- constant diagonal terms;
- constant diagonal and cross terms;
- variable diagonal and cross terms.

The D values for these coatings (TiAlCrY, Al_2Au) on Ti45Al8Nb have been shown in Table 7.12 (chapter 7 section 7.9). As expected the agreement between the numerical and experimental concentration profiles was the best when all terms in the diffusion matrix were considered concentration dependent as shown in Figures 6.123 (the numerical and experimental concentration profiles in $TiAl - TiAlCrY$ after 500 hours diffusion treatment for *Al, Ti*, and *Cr* considering variable cross terms) and 6.109 (the numerical and experimental concentration profiles in $TiAlNb - Al_2Au$ after 1000 hours diffusion treatment considering variable diagonal and cross terms) for TiAlCrY and Al_2Au coatings respectively. Second order polynomial has been considered to be the best function for the concentration dependence diffusion coefficient (equations 6.70 and 6.65 for TiAlCrY and Al_2Au coatings respectively).

The conclusions from the microstrructural model indicated that for the TiAlCrY coating a thick oxide scale consisting of Al, Cr, and Ti oxides was observed to form at the top. Below the top scale we developed a modified coating TiAlCrY. The modified coating/substrate interface showed a depletion zone of Al and Ti. Beneath the depletion zone was a zone depleted in Ti (pre-depletion zone); where Al concentration increased due to the faster outward diffusion of Ti ions from the bulk material. For the Al_2Au coating a thin outer Al_2O_3 scale with *Au* inclusions was developed, underneath this scale pure Al_2O_3 without inclusions of *Au* was formed, and a little amount of *Ti* was detected. Both these layers were extremely porous and brittle (Figure 6.98). Beneath two Al_2O_3 layers were existed the modified coating (Al_2Au). At the scale/substrate interface a large diffusion zone of *Al*, *Au*, and *Ti* was formed.

8.2.8. Simplex Search and fminbnd Optimisation Methods Applying on *NiPtAl* Alloy Subjected to Diffusion Annealing at 1273K for 1 Hour

Simplex search and fminbnd optimisation methods were also used to optimize the diffusion coefficients for nickel in three component system *NiPtAl*. These diffusion coefficients for nickel have been compared with the diffusion coefficient calculated from Genetic Algorithms method ($D_{Ni} = 6.7619 \times 10^{-11} cm^2 / s$) by calculating the numerical concentration profile for this component and use least squares method to compare between the numerical and experimental concentration profiles. The numerical concentration profiles obtained using GAs diffusion coefficients ($D_{Ni} = 6.7619 \times 10^{-11} cm^2 / s$) showed better agreement with the experimental concentration profile than the numerical concentration profiles relating with the diffusion coefficients calculated from Simplex search and fminbnd methods. Therefore the calculated errors between the experimental and numerical concentration profiles for nickel show the efficiency of using Genetic Algorithms technique. Therefore using the other two methods (Simplex search and fminbnd optimisation methods) we need to be careful when choosing the diffusion range while GAs method does not need this consideration.

8.3. Suggestions for Further Work

One of the principal reasons for the disagreement between the experimental and numerically predicted concentration profiles is that numerical technique cannot take into account the local perturbation in compositions in the system. This violates the assumption of the existence of single phase/homogeneous compositions. It is suggest that some ideal systems consisting of a single phase need to be considered.

2. In the present work considered no definitive identification of the formation of second phases was carried out. Clearly the formation of second phases / precipitation formation need to be identified.
3. If the second phase formations are extensive then knowing the temperature range of the phase formation separate modelling can be performed for each phase.
4. Low temperature homogenization heat treatment can be considered to apply.
5. Many diffusion anneal experiments need to be performed. This would allow modelling of the close system. Diffusion treatment can also eliminate oxide phase formation.
6. GAs method needs to be improved (to optimize the order of the polynomial, concentration dependence diffusion coefficients).
7. Improved numerical procedure needs to be formed to describe the composition dependence of the terms in the diffusion matrix.
8. Improved microstructural description of the diffusion processes involved need to be achieved.

APPENDIX A

Nernst-Einstein Relation

Suppose that an external driving force F proceeds on diffusing particles. After a short transition period, a steady state particle flux develops. The drift velocity $\tilde{v}$ of the particles under the action of the driving force is,

$$\tilde{v} = uF \tag{A1}$$

where u is called the mobility. The mobility is the drift velocity for a unit driving force, i.e. for $F = 1$. The particle flux is $C\tilde{v} = C\,u\,F$. The total flux due to diffusion plus the action of the driving force is:

$$j = -D\frac{\partial C}{\partial x} + \tilde{v}C \tag{A2}$$

The first term is the well-known Fickian term and the second term is the drift term.

We consider a system with one mobile component, where the flux resulting from an external driving force exactly balances the diffusion flux. The shared effect of a concentration gradient and of a driving force can lead to a steady state, if the corresponding fluxes are equal and opposite in sign, that is means if the total flux vanishes. Then, we get from equation (A2):

$$0 = -\tilde{D}\frac{\partial C}{\partial x} + \tilde{v}C \tag{A3}$$

The diffusion coefficient $\tilde{D}$ in equation (A3) refers to a chemical composition gradient as will become evident below. It is definitely conceived as a chemical diffusion coefficient not as a tracer diffusion coefficient.

Let the diffusing substance be contained in a cylinder and let us suppose that $\tilde{v} = uF$ is the stationary velocity in negative *x*-direction due to an external field. Then, the solution of equation (A3) is:

$$C = C_o \exp\left(-\frac{\tilde{v}}{\tilde{D}}x\right) \tag{A4}$$

where C_o denotes the initial concentration at $x = 0$. Let us further assume that the external force is the derivative of a potential U :

$$F = -\frac{\partial U}{\partial x} \tag{A5}$$

At thermodynamic equilibrium, the distribution of non-interacting particles must also follow the Boltzmann distribution,

$$C(x) = \alpha \exp\left(-\frac{U}{k_B T}\right) \tag{A6}$$

where k_B indicates the Boltzmann constant, T absolute temperature, and α a constant. Differentiation with respect to x gives up:

$$\frac{\partial C}{\partial x} = -\frac{C}{k_B T}\frac{\partial U}{\partial x} = \frac{CF}{k_B T} \tag{A7}$$

Substituting this equation in equation (A3), we obtain:

$$\tilde{D} = \frac{\tilde{v}}{F}k_B T = uk_B T = u\frac{RT}{N_A} \tag{A8}$$

$R = k_B N_A$ denotes the gas constant and N_A the Avogadro number. Equation (A8) relates the chemical coefficient $\tilde{D}$ and the mobility u of the diffusing particles. This relation is called the Nernst-Einstein relation.

APPENDIX B

Application of Runge-Kutta Method on Fick's Second law

Runge-Kutta method of order four;

$$
\begin{aligned}
K_1 &= hf(t_n, C_n), \\
K_2 &= hf\left(t_n + \frac{1}{2}h, C_n + \frac{1}{2}K_1\right), \\
K_3 &= hf\left(t_n + \frac{1}{2}h, C_n + \frac{1}{2}K_2\right), \\
K_4 &= hf\left(t_n + h, C_n + K_3\right) \\
C_{(x,t+h)} &= C_{(x,t)} + \frac{1}{6}\left(K_1 + 2K_2 + 2K_3 + K_4\right)
\end{aligned}
\tag{B1}
$$

where

$$f\left(t_n, C_n\right) = \left(\frac{\partial C}{\partial t}\right)_{(x,t)}$$

From Euler method:

$$C_{(x_o+h,t_o+h)} = C_{(x_o,t_o)} + hC'_{(x_o,t_o)} \tag{B2}$$

Where $C_{(x_o,t_o)}$ is the initial concentration at $t = 0$, h is the step size and

$$C'_{(x_o,t_o)} = \left(\frac{\partial C}{\partial t}\right)_{(x_o,t_o)} = \frac{D}{(\Delta x)^2}\left[C_{i+1} - 2C_i + C_{i-1}\right] \quad (i = 1,2,\cdots,n) \tag{B3}$$

K_1 is the equation (B2), to find K_2 as follows the steps:

$C'_{(x_o+h,t_o+h)}$ has to be calculated in order to apply the following equation:

$$C_{(x_o+h,t_o+h)} = C_{(x_o,t_o)} + h\frac{C'_{(x_o,t_o)} + C'_{(x_o+h,t_o+h)}}{2} \tag{B4}$$

Equation (B4) is modified Euler method, (K_2). We cannot calculate $C'_{(x_o+h,t_o+h)}$ with $C_{(x_o+h,t_o+h)}$ unknown, so applying equation (B2) using the new concentration from equation (B1) instead of initial concentration at $t=0$.

$$C'_{(x_o+h,t_o+h)}=\left(\frac{\partial C}{\partial t}\right)_{(x_o+h,t_o+h)}=\frac{D}{(\Delta x)^2}\left[C_{i+1}-2C_i+C_{i-1}\right] \quad (i=1,2,\cdots,n) \quad \text{(B5)}$$

while $C_i \quad (i=1,2,\ldots,n)$ is the new concentration from equation (B1).

So K_2 can be calculated because each term in equation (B3) is become known.

The same procedure can be followed to calculate K_3 and K_4.

APPENDIX C

Flowchart for Determine Optimum D and Calculating Concentration Profiles

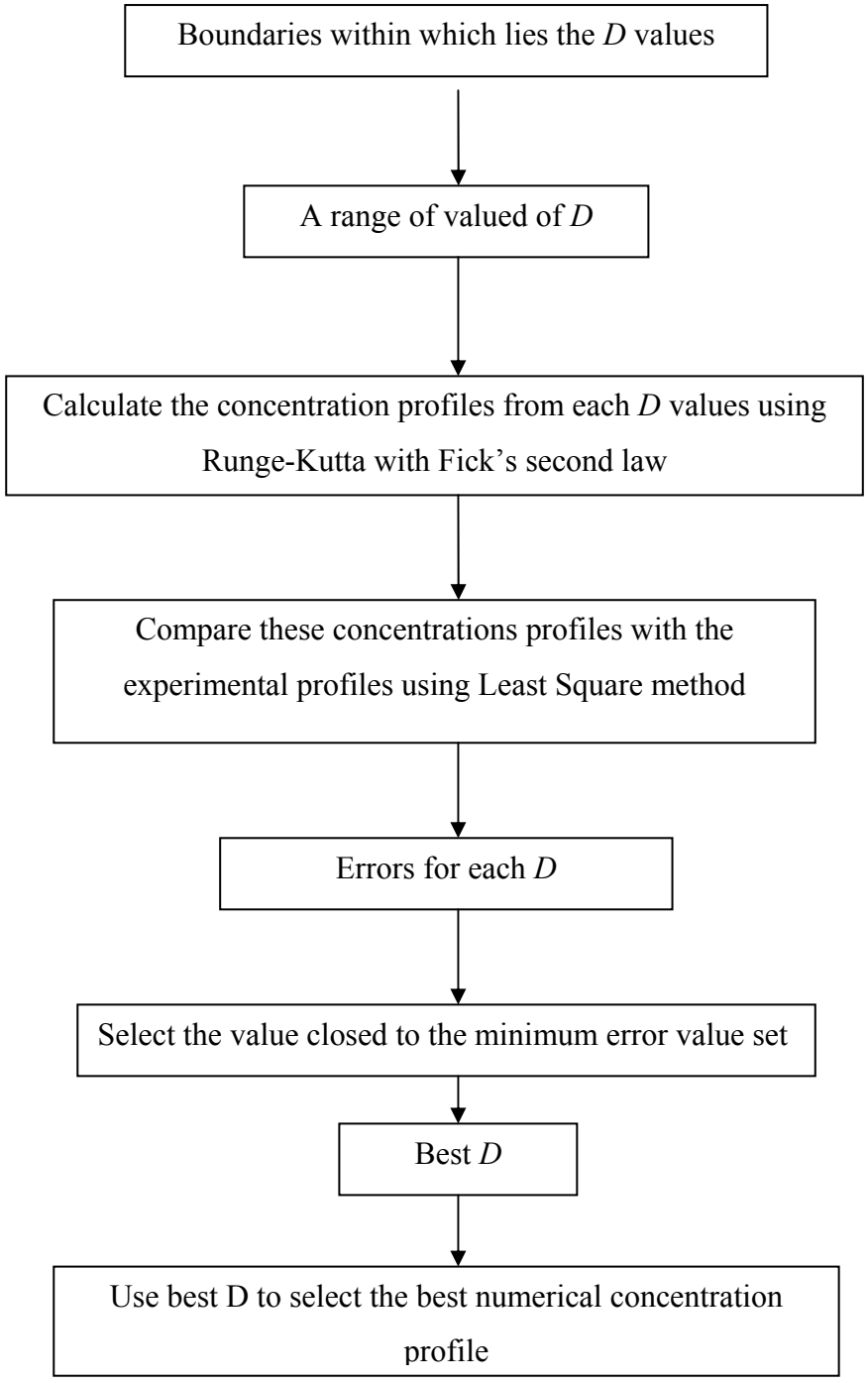

APPENDIX D

Calculating the Interdiffusion Coefficient in Cu-Ni Diffusion Couple

$$\tilde{D}(N_{Cu}) = -\frac{1}{2t}\frac{\partial x}{\partial N_{Cu}}\int_{C_R}^{N_{Cu}}(x - X_M)dN_{Cu} \quad [91]$$

where $N_{Cu} = 0.71$, $X_M = 0$, Matano interface, and $\frac{\partial N_{Cu}}{\partial x} = 12.69$, so the diffusivity at the composition 0.71 is,

$$\tilde{D}(0.71) = -\frac{1}{2t}\frac{1}{12.69}\left(x(0.71 - C_R)\right)$$

If the diffusion time is assumed to be 300 hour (1080000s), the result of applying the above analysis at Matano interface is that,

$$\tilde{D}(0.71) = 3.16x10^{-10} cm^2/s.$$

REFERENCES

1. Diffusion in Solids, Springer Series in Solid State science 155 (2007).
2. T. Graham, Philos. Trans. of the Roy. Soc. of London 140, 1 (1950).
3. A. Fick, Annalen der Phyik und Chemie 94, (1855) 59; Philos. Mag. 10, (1855) 30.
4. J.B.J. Fourier, The Analytical Theory of Heat, translated by A. Freeman, University Press, Cambridge, 1978.
5. C. Matano, Japan. J. Phys., 8 (1933) 109.
6. A. D. Smigelskas, E.O. Kirkendall, Trans. AIME 171 (1947) 130.
7. R. E. Reed-Hill, Physical Metallurgy Principles, Third Edition, PWS Publishing Company, 1973.
8. L.S. Darken, Transactions AIME 175 (1948) 184.
9. S. Prager, J. Chem. Phys., 21 (1953) 1344–1347 References 177.
10. A. R. Allnatt, A.B. Lidiard, Atomic Transport in Solids, Cambridge University Press, 1993.
11. J. Philibert, Atom Movements – Diffusion and Mass Transport in Solids, Les Editions de Physique, Les Ulis, 1991.
12. J. E. Reynolds, B. L. Averbach, and M. Cohen, Acta Met., 5 (1957) 29.
13. R. Nakamura, K. Fujita, Y. Iijima, and M. Okada, Acat Materialia 51 (2003) 3861-3870.
14. H. Mehrer, N. Stolica, Landolt-Börnstein new series group III, Crystal and Solid State Physics. Diffusion in Solid Metals and Alloys, 26.Berlin:Springer Verlag, (1990).
15. P. C. Tortorici, and M. A. Dayananda, Metall. and Mater. Trans., 30A (1999) 545.
16. M. A. Dayananda and C. W. Kim, Metall. Trans. A, 10A (1979) 1333-39.

17. M. A. Dayananda, Metall. Trans., A, 14A (1983) 1851-58.

18. C. Wagner, Acta Metall., 17 (1969) 99-107.

19. M. A. Dayananda, Defect Diffusion Forum, 27A (1993) 521-36.

20. M. A. Dayananda, Metall. Mater. Trans. A, 27A (1996) 2504-09.

21. P. C. Tortorici and M. A. Dayananda, Scripta Mater.38 (1998) 1863-69.

22. J. A. Nesbitt and R. W. Heckel, Metall. Trans. A,18A (1987) 2075.

23. J. S. Kirkaldy, in Advances in Materials Research, H. Herman, ed. Wiley, New York, NY, 4 (1970) 55-100.

24. D. P. Whittle and A. Green, Scripta Metall., 8 (1974) 883-84.

25. M. S. A. Karunaratne, P. Carter and R. C. Reed, Acta Mater. 49 (2001) 861-875.

26. L. Onsager, Ann. N. Y. Acad. Sci., 46 (1945) 241.

27. J. S. Kirkaldy and D. J. Young, Diffusion in the Condensed State, The Institute of Metals, London, 1987.

28. J. S. Kirkaldy, Adv. Mater. Res., 4 (1970) 55.

29. P. C. Tortorici and M. A. Dayananda, Materials Science and Engineering A261 (1999) 64-77.

30. V. I. Ivanov, E. P. Nicparenko, and V. I. Zmii, Phys. Metall. Et. Metallov. 17 (1964) 94.

31. V. I. Zmii, A. S. Seryugina, Isv. Akad. Nauk. SSSR, Neorg. Mater. 7(10) (1971) 1730.

32. R. W. Bartlett, P. R. Gage, P. A. Larssen, Trans. Metall. Soc. AIME 230 (1964) 1528.

33. P. R. Gage, R. W. Bartlett, Trans. Metall. Soc. AIME 233 (1965) 832.

34. P. C. Tortorici and M. A. Dayananda, Scr. Mater. 38 (1998) 1863-1869.

35. P. C. Tortorici and M. A. Dayananda, Metall. Mater. Trans. A (1998).

36. P. K. Datta and J. S. Burnell-Gray, Intermetallic Compounds, Principles and Practice, 3, Chapter 27, (2002) 564-566.
37. L. S. Darken, L. S., Trans. AIME, 174 (1948) 184.
38. R. Filipek, Interdiffusion in non-ideal systems, AGH University of Science and Technology Faculty of Materials Science and Ceramics Department of Solid State Chemistry.
39. S. Datta, R. Filipek and M. Danielewski, Defect and Diffusion Forum, Scientific Publications, Switzerland, 203-205 (2002) 47-51.
40. S. Datta, R. Filipek and M. Danielewski, Defect and Diffusion Forum, 203-205 (2002) 47-60.
41. R. Filipek, P. K. Datta, M. Danielewski, L. Bednarz, R. Best and A. Rakowska, Defect and Diffusion Forum, 194-199 (2001) 571-576.
42. R. Filipek, Journal of Molecular Liquids 86 (2000) 69-76.
43. Demonstration version of the software is available at the web site http://ceramrtr.ceramika.agh.edu.pl/~rof/demo.html.
44. R. Bachorczyk, M. Danielewski and R. Filipek, Defect and Diffusion Forum, 141 (2003) 216-217.
45. R. Felipek, M. Danielewski and R. Bachorczyk, Defect and Diffusion Forum, 237-240 (2005) 408-413.
46. M. Danielewski and K. Holly, W. Krzyżański, Polish J. Chem., 68 (1994) 2031.
47. R. Filipek, Archives of Metallurgy and Materials, 49 No. 2 (2004) 201.
48. P. E. Gill, W. Murray and N.H. Wyight, Practical optimalization, Academic Press, (1981) 247.
49. J. A. Nelder and L. Mad, Computer Journal, 7 (1965) 308.

50. S. N. Ghani, Performance of Global Optimization Algorithm for non-linear non-differentiable Constraint Objective Functions, IEEE International Conference on Evolutionary Computations, Perth Western Australia, (1995) 320.
51. A. Vignes and J.P. Sabatier, Trans. AIME, 245 (1969) 1795.
52. E. Walsöe de Reca and C. Pampillo, Acta Metall., 15 (1967) 1263.
53. Yu.E. Ugaste, A.A. Kodentsov and F. van Loo, Phys. Met. Metallogr., 88 (6) (1999) 598.
54. A. Kohn, J. Levasseur, J. Philibert and M. Wanin, Acta Metall., 18 (1970) 163.
55. Ken-ichi Hirano, R.P. Agarwala, B.L. Averbach, Morris Cohen, J. Appl. Phys., 33 (10) (1962) 3049.
56. B. Million and J. Kucera, Acta Metall., 17 (1969) 339.
57. J. I. Goldstein, R. E. Hanneman and R.E. Ogilvie, Trans. Metall. Soc. AIME, 233 (1965) 812.
58. T. Ustad and H. Sorum, Phys. Stat. Sol. (a), 20 (1973) 285.
59. J. G. Guh and M. A. Dayananda, in Diffusion and Defect Data, Trans Tech Publications, Switzerland, 39 (1985) 1.
60. J. E. Reynolds, B. L. Averbach and M. Cohen, Acta Met., 5 (1957) 29.
61. M. Danielewski and R. Filipek, J. Comp. Chem., 17, No. 13 (1996) 1497.
62. H. Hindman and W. Smeltzer, Oxidation of Metals, 14 (4) (1980).
63. L. R. Streiff. , Joiurnal de Physique IV. Colloque C9, 3 (1993) 17.
64. G. Fisher, P. K. Datta, and J. S. Burnell-Gray: An Assesment of the Oxidation Resistance of an Iridium and Iridium/Platinum Low Activity Aluminide /MAR M002 System at 1100oC (Conf. Proc., 5th International Conference on Advances in Surface Engineering, Sao Paulo, Brazil, 11-13th November 1998).
65. P. K. Datta, G. Fisher and J. S. Burnell-Gray, High Performance Diffusion Coatings: A Review of the current status and future development of noble metal

diffusion coatings (Key note talk; Conf. Proc. International Conference on Surface Engineering, Sao Paulo, Brazil, 1998).

66. P. K. Datta, K. Natesan and J. S. Burnell-Gray: Invited book chapters in Intermetallic Compounds: Principles and Practice Vol. 3, Progress (Ed J. H. Westbrook and R. L. Fleischer, John Wiley 2001).
67. R. Prescott and M. J. Graham: Oxidation of Metals, 38 (3/4) (1992) 233.
68. J. Jedlinski and S. Mrowec: Materials Science & Engineering, 87 (1987) 281.
69. W. Y. Chan, and P. K. Datta et al, Environmental Effects on High Technology materials (Proc. Polish-Japanese Symposium, polish academy of Science, (1997) 81.
70. R. Prescot, D. Mitchell and M. Graham, Corrosion Science, 50 (1) (1994) 64.
71. J. Schaffer, G.M. Kim, G.H. Meier and F.S. Pettit, The Role of Active Elements in the Oxidation Behaviour of High Temperature Metals and Alloys, Elsevier, Amsterdam, (1991) 231.
72. H. M. Tawancey, N. M. Abbas and T. N. Rhys-Jones, Surf. Coat. Technol. 49 (1991) 1.
73. P. C. Patnaik, Advances in High Temperature Structural Materials and Protective Coatings, NRC Canada, (1994) 164.
74. G. Fisher, P. K. Datta, J.S. Burnell-Gray and W.Y. Chan, Surf. Coat. Technol. 110 (1998) 24.
75. G. Fisher, P.K. Datta, J.S. Burnell-Gray and W.Y. Chan, High Temperature Surface Engineering, Edinburgh, 23–25 September (1997) Institute of Materials, submitted.
76. Z. D. Xiang and P. K. Datta, Surf. Coat. Technol., 179 (2004) 95 – 102.
77. Z. D. Xiang, S. R. Rose, J. S. Burnellgray and P. K. Datta, J. Mater. Sci., 38 (2003) 19 – 28.

78. T. H. Wang and L. L. Seigle, Mater. Sci. Eng., A108 (1989) 253 –263.

79. L. Levin, A. Ginzburge, L. Klinger, T. Werber, A. Katsman and P. Schaaf, Surf. Coat. Technol., 106 (1998) 209 – 213.

80. Z. D. Xiang and P. K. Datta, Surf. Coat. Technol., 184 (2004) 108 – 115.

81. Z. D. Xiang and P. K. Datta, J. Mater. Sci., 38 (2003) 3721 –3728.

82. H. M. Soliman, K. E. Mohamed, M. E. Abd El-azim and H. F. Hammad, J. Mater. Sci. Technol., 13 (1997) 383 – 388.

83. Journal of Phase Equilibria and Diffusion, 26(4) / October (2005) 391-393.

84. C. Mitterer, H. Helmut, P. H. Mayrhofer and Sputtered, Sputtered Coatings Based on the Al_2Au Phase , Materials Research Society, 842 (2005) S5.38.1.

85. A. Gil, B. Rajchel, N. Zheng, W. J. Quadakkers and H. Nickel, the Influence of implanted Chromium and Yttrium on the Oxidation Behaviour of TiAl Based Intermetallics.

86. RA. Perkins, KT. Chiag and GH. Meier, Scripta Metall., 1505 (1987) 21.

87. Z. Tang, F. Wang and W. Wu, Effect of a Sputtered TiAlCr Coating on Hot Corrosion Resistance of γ-TiAl, Intermetallics,7 (1999) 1271-1274.

88. ASM Handbook, Corrosion Materials, 13B (2005) 490 – 510.

89. W. D. Callister, Jr., Materials Science and Engineering An Introduction, Third Edition, John Wiley & Sons, INC., 1994.

90. J. Grank, the Mathematics of Diffusion, 1975.

91. M. E. Glicksman, Diffusion in Solids, John Wiley & Sons, INC., 2000.

92. R. E. Reed-Hill, Physical Metallurgy Principles, PWS Publishing Company, 1992.

93. C. F. Gerald, Applied Numerical Analysis Second Edition, Addition-Wesley Publishing Company, 1980.

94. L. Boltzmann, Ann. Phys., 53 (1894) 960.

95. C. Matano, Japan physics, 8 (1933) 109.

96. W. Seith, Diffusion in Metallen, 1955, Berlin, Springer.

97. J. S. Kirkaldy, Acta Met., 4 (1956) 92.

98. Cheney, Ward and Kincaid, David, Numerical Mathematics and Computing Fifth Edition, Belmont, Thomson Learning, 2004.

99. Chapra, Steven and Canale, Raymond, Numerical Method for Engineers: With Software and Programming Applications Fourth Edition, McGraw-Hill, 2005.

100. Keller, Gerald, Statistics for Management and Economics Seventh Edition, Thomson Higher Education, 2005.

101. H. Holland, Adaptation in Natural and Artificial Systems, university of Michigan Press, Ann Arbor 1975.

102. K. A. De Jong, An Analysis of Behaviour of a Class of Genetic Adaptive Systems' Doctoral Dissertation , University of Michigan, Ann Arbor, 1975.

103. D. E. Goldberg, Genetic Algorithms in Search, Optimisation and Machine learning, Addison-Wesley, Reading ,MA,1989.

104. Z. Michalewicz, Genetic Algorithms +data Structure=Evolution Programs, Springer-Verlag, 1992.

105. P. E. Gill, W. Murray, and H. M. Wright, Practical Optimisation, Academic Press, London 1981.

106. R. E. Steuer, Multiple Criteria Optimisation: Theory, Computation, and Application, John Wiley, Canada, 1986.

107. B. L. Miller, D. E. Goldberg, Genetic Algorithms, Tournament Selection, and the Effect of Noise, 1995.

108. W. Cheney and D. Kincaid, Numerical Mathematics and Computing, Third Edition, Brooks/Cole Publishing Company, 1994.

109. J. A. Nelder and R. Mead, A Simplex Method for Function Minimization, Computer Journal 7 (1995) 303-313.

110. Avriel, Mordecai (2003). Nonlinear Programming: Analysis and Methods. Dover Publishing. ISBN 0-486-43227-0.

111. F. S. Hillier and G. J. Lieberman, Introduction to Operations Research, 8th edition. McGraw-Hill. ISBN 0-07-123828-X.

112.T. H. Cormen, C. E. Leiserson, R. L. Rivest, and C. Stein, Introduction to Algorithms, Second Edition. MIT Press and McGraw-Hill, 2001. ISBN 0-262-03293-7.

113. C. F. Gerald and P. O. Wheatley Applied Numerical Analysis. Seventh Edition, Addison-Wesley, 2004.

114. Floyd Hanson, MCS 471 Class Optimization Notes, Method of Golden Section Search. Available at http://www.math.uic.edu/»hanson/mcs471/classnotes.html.

115. J. C. Lagarias, J. A. Reeds, M. H. Wright, and P. E. Wright, Convergence Properties of the Nelder-Mead Simplex Method in Low Dimensions, SIAM Journal of Optimization, 9 (1998) 112–147.

116. S. P. Garg, G. B. Kale, R. V. Patil, and T. Kundu, Intermetallics 7 (1999) 901-908.

117. L. R. Ram-Mohan, and M. A. Dayananda, Acta Materialia 54 (2006) 2325-2334.

118. G. Welsch and A. I. Kahveci, Oxidation Behaviour of Titanium Aluminide Alloys, Oxidation of High-Temperature Intermetallics, eds: T. Grobstein and J. Doychak, TMS Warendale, PA, (1989) 207−212.

LIST OF FIGURES

LIST OF TABLES